Pontifícia Universidade Católica do Rio de Janeiro

Luis Fhernando Mendonça da Silva

Study of the chemical composition of atmospheric particulate matter in urban, burned, and natural areas of the State of Rio de Janeiro

Tese de Doutorado

Thesis presented to the Programa de Pós-graduação em Química of PUC-Rio in partial fulfillment of the requirements for the degree of Doutor em Química.

Advisor: Prof. Adriana Gioda

Rio de Janeiro

March 2025

Luis Fhernando Mendonça da Silva

Study of the chemical composition of atmospheric particulate matter in urban, burned, and natural areas of the State of Rio de Janeiro

Thesis presented to the Programa de Pós-graduação em Química of PUC-Rio in partial fulfillment of the requirements for the degree of Doutor em Química.

Prof. Adriana Gioda
Advisor
Departamento de Química – PUC-Rio

Prof. Giovana Anceski Bataglion
Departamento de Química – UFAM

Prof. Pérola de Castro Vasconcellos
Instituto de Química – USP

Prof. Ricardo Jorgensen Cassella
Departamento de Química – UFF

Prof. Graciela Arbilla de Klachquin
Instituto de Química – UFRJ

Prof. Ricardo Queiroz Aucélio
Departamento de Química – PUC-Rio

Rio de Janeiro, March 14th, 2025

Luis Fhernando Mendonça da Silva

Chemistry degree in Chemistry from Federal Institute of Education, Science and Technology of Amazonas – IFAM (2019) and M.Sc. Degree in Chemistry from the Federal University of Amazonas - UFAM (2021).

Bibliographic data

Silva, Luis Fhernando Mendonça da

Study of the chemical composition of atmospheric particulate matter in urban, burned, and natural areas of the State of Rio de Janeiro / Luis Fhernando Mendonça da Silva ; advisor: Adriana Gioda. – 2025.

284 f. : il. color. ; 30 cm

Tese (doutorado)–Pontifícia Universidade Católica do Rio de Janeiro, Departamento de Química, 2025.

Inclui bibliografia

1. Química – Teses. 2. Material particulado. 3. Composição química. 4. Modelagem atmosférica. 5. Sensor. I. Gioda, Adriana. II. Pontifícia Universidade Católica do Rio de Janeiro. Departamento de Química. III. Título.

Acknowledgements

I would like to express my deepest gratitude to everyone who has contributed to my journey as a researcher. Completing this stage has been a long-held dream, and I am immensely grateful for the support and encouragement I have received along the way.

First and foremost, I thank my family, especially my parents, Elcimar Ramos and Marta Mendonça, and my siblings, Marcielen, Mylenna, and Daniel. Even from a distance, they have always been there for me, offering unwavering love and support. This achievement is not mine alone - it belongs to my entire family. I hope they feel as proud of me as I am of myself.

To my nephews and nieces - you may not realize it, but you are my greatest motivation. Everything I do is always with you in mind.

To my lifelong friends and my best friends, Vitória Moreira, Beatriz Moreira, Fernanda Pacheco, Adrya Ariel, Andrei Talison, Wyllow Assunção, Thália Phedra, Isabele Moraes and Caroline Borges - thank you for always being by my side, offering support, advice, and friendship through every challenge and triumph.

A special thank you to my psychologist, Carolina, who has been with me since the beginning of my doctorate and my move to Rio de Janeiro. Your guidance has been invaluable.

To Alexander Minor - thank you for your love, patience, and unwavering support. Your kindness and encouragement have meant the world to me.

To my advisor, Adriana Gioda, and mentors, Adrien Deroubaix and Guy Brasseur - thank you for your invaluable guidance, knowledge, and support throughout this journey.

To my friends from Rio de Janeiro and PUC-Rio and to those I met along the way in the city - Kaio Rodrigues, Miguel Ferreira, Victor Matamala, Rafaela Santiago, João Meirelles, Kamila Gramlich, Dayanne Martins, Franccesca Fornasier, Annielle Mendes, Jéssica Fonseca, Carolina Vesga,

Jennifer Matilde, Samuel Bento and Pamela Subirana - thank you for making my time in Rio de Janeiro so much more enjoyable. Without you, this experience would not have been the same.

To my friends from Europe - Sancy Wang, Hugo Pasa, Sylvia Perez and Pamela Vidal - you made my time in Germany unforgettable, and I am so grateful for the memories we created together.

To LQA, LabMAM and LABSPECTRO, especially Leonny Fragoso, Marllon Campos, Guilherme Lopes, Bruno Siciliano, Allan Vinicius, Gabriel Barros, Judith Cardoso. Thank you for all your contributions and companionship over the years.

To all the institutions involved in this thesis, Max Planck Institute for Meteorology (MPI-M), Federal University of Rio de Janeiro (UFRJ), Federal University of Bahia (UFBA), SENAI-CIMATEC University, Darcy Ribeiro State University of Norte Fluminense (UENF), Federal University of Fluminense (UFF), Federal University of Paraná (UFPR), ZANE.

To PUC-Rio, for all the structure and support.

This study was financed in part by the Coordenação de Aperfeiçoamento de Pessoal de Nível Superior - Brasil (CAPES) - Finance Code 001. to CNPq, and FAPERJ for financial support.

Abstract

Silva, Luis Fhernando Mendonça da; Gioda, Adriana (Advisor). **Study of the chemical composition of atmospheric particulate matter in urban, burned, and natural areas of the State of Rio de Janeiro.** Rio de Janeiro, 2025. 284p. Tese de Doutorado – Departamento de Química. Pontifícia Universidade Católica do Rio de Janeiro.

Air pollution remains a major environmental challenge, impacting air quality and human health. This study analyzes fine particulate matter ($PM_{2.5}$) and its chemical composition in three regions of Rio de Janeiro: Gávea (urban area), Parque Nacional da Serra dos Órgãos (PARNASO, protected environmental area) e Campos dos Goytacazes (urban with biomass burning) focusing on BC, trace elements, soluble ions, PAH, *n*-alkanes and saccharides. In addition, modeling of ozone concentrations and other pollutants, and real-time monitoring of NO_x emissions from heavy vehicles in the Metropolitan Region of Rio de Janeiro were performed. Samples were collected from February 2022 to June 2023 using glass fiber and quartz filters. $PM_{2.5}$ concentrations varied spatially and seasonally, with the highest levels in PARNASO and the lowest in Campos. BC was more abundant in PARNASO, likely from fossil fuels and wildfire, while biomass burning dominated in Campos. SO_4^{2-}, NO_3^-, Cl^-, and Na^+ were the main ions, with sulphate of anthropogenic origin. Hg levels were higher in the dry season, possibly linked to sugarcane burning. PAH and *n*-alkanes indicated contributions from fossil fuel combustion, with saccharides serving as tracers of biomass burning. NO_x emissions from heavy vehicles varied due to weight, engine power, age, and maintenance. Atmospheric modeling showed discrepancies between simulated and observed O_3 and NO_2 levels, highlighting the need for improved emission profiles and VOC representation. The results emphasize the importance of monitoring, public policies, and emission control to mitigate air pollution.

Keywords

Particulate matter, chemical composition, atmospheric modeling, sensor

Resumo

Silva, Luis Fhernando Mendonça da; Gioda, Adriana (Orientador). **Estudo da composição química do material particulado atmosférico em áreas urbanas, com queimadas e naturais do Estado do Rio de Janeiro**. Rio de Janeiro, 2025. 284p. Tese de Doutorado - Departamento de Química. Pontifícia Universidade Católica do Rio de Janeiro.

.

A poluição do ar continua a ser um grande desafio ambiental, afetando a qualidade do ar e a saúde humana em escala global. Este estudo integra os resultados de várias análises realizadas em diferentes regiões do Rio de Janeiro, com foco no material particulado fino ($PM_{2,5}$) e sua composição química. Foram analisados carbono negro (BC), elementos traços, íons solúveis, hidrocarbonetos policíclicos aromáticos (HPA) e hidrocarbonetos alifáticos, sacarídeos, nitro e oxi-HPA e mercúrio. Além disso, foram estudadas as emissões de NO_x de veículos pesados e aplicada a modelagem atmosférica às reações fotoquímicas na região metropolitana do Rio de Janeiro. As coletas foram realizadas de fevereiro de 2022 a junho de 2023 usando filtros de fibra de vidro e de quartzo em três locais com diferentes níveis de urbanização: Gávea (área urbana), Parque Nacional da Serra dos Órgãos (PARNASO, área de proteção ambiental) e Campos dos Goytacazes (urbano com queima de biomassa).

Foram observadas variações espaciais e sazonais significativas nas concentrações de $PM_{2,5}$, com os níveis mais altos registrados no PARNASO e os mais baixos em Campos. Os níveis de BC também foram altos no PARNASO, provavelmente devido à queima de combustíveis fósseis e biomassa, enquanto em Campos a queima de biomassa teve um papel predominante. A análise de íons solúveis identificou Cl^-, Na^+, SO_4^{2-} e NO_3^- como os principais constituintes, sendo o sulfato principalmente de origem antropogênica. As concentrações de Hg apresentaram variação sazonal, sendo mais elevadas na estação seca e em áreas influenciadas pela queima de cana-de-açúcar. A distribuição do HPA e seus derivados, e *n*-alcanos indicaram forte contribuição da combustão de gasolina e diesel, enquanto os sacarídeos serviram como traçadores da queima de

biomassa.

O estudo também analisou as emissões de NO_x de veículos pesados, destacando uma grande variabilidade nos fatores de emissão entre os diferentes veículos avaliados. As emissões foram influenciadas por características como peso do veículo, potência do motor, idade e condições de manutenção, refletindo o impacto das especificidades da frota na qualidade do ar urbano. Além disso, a relação entre a velocidade média e os fatores de emissão indicou que certas faixas de operação dos veículos podem contribuir para um aumento na liberação de NO_x, o que pode ter implicações na formação de ozônio (O_3) na região metropolitana do Rio de Janeiro A modelagem atmosférica foi utilizada para avaliar a distribuição espacial e temporal dos poluentes, revelando discrepâncias entre as concentrações simuladas e observadas de O_3 e NO_2. Esses desvios sugerem a necessidade de refinamento dos perfis de emissão e uma melhor representação dos compostos orgânicos voláteis (VOCs) nos modelos, especialmente em áreas industriais e de tráfego intenso.

Os resultados reforçam a necessidade de políticas públicas voltadas à melhoria da qualidade do ar, monitoramento contínuo e estratégias eficazes de controle de emissões para mitigar a poluição atmosférica em áreas urbanas e preservadas. A integração de dados observacionais com técnicas avançadas de modelagem atmosférica é essencial para aprimorar as avaliações da qualidade do ar e implementar medidas eficazes de mitigação.

Palavras-chave:

Material particulado, composição química, modelagem atmosférica, sensor.

Summary

List of Figures

List of Tables

Abbreviations

ABNT Associação Brasileira de Normas Técnicas

ANOVA Analysis of Variance

ATN Attenuation

BC Black Carbon

BSTFA N,O-bis-(trimetilsilil)-trifluoroacetamida

CAMS Copernicus Atmosphere Monitoring Service

CAN Controller Area Network

CONAMA Conselho Nacional do Meio Ambiente

CPI Carbon Preference Index

CRM Certified Reference Material

DETRAN-RJ Departamento de Trânsito do Estado do Rio de Janeiro

EGR Exhaust Gas Recirculation

EI Electron Impact Ionization

GC-MS Gas Chromatography-Mass Spectrometry

HDDV Heavy-Duty Diesel Vehicle

HYSPLIT Hybrid Single-Particle Lagrangian Integrated Trajectory Model

IBGE Instituto Brasileiro de Geografia e Estatística

IC Ion Chromatography

ICMBIO Instituto Chico Mendes de Conservação da Biodiversidade

ICP-MS Inductively Coupled Plasma Mass Spectrometry

INEA Instituto Estadual do Ambiente

IoT Internet of Things

LOQ Limit of Quantification

LOD Limit of Detection

m/z Mass-to-Charge Ratio

NIST National Institute of Standards and Technology

NO_x Nitrogen Oxides (abreviação química para NO + NO_2)

nss Non-Sea-Salt

OBD On-Board Diagnostics

PAH Polycyclic Aromatic Hydrocarbons

PCA Principal Component Analysis

PM Particulate Matter

$PM_{2.5}$ Particulate Matter ≤ 2.5 μm

ppm Partes por milhão

QA/QC – Quality Assurance and Quality Control

SCR Selective Catalytic Reduction

SenML Sensor Markup Language

SIM Selected Ion Monitoring

SRM Standard Reference Material

σATN Specific Attenuation Coefficient

T Transmitted Light Intensity through the Sample Filter

T_0 Transmitted Light Intensity through the Blank Filter

US EPA United States Environmental Protection Agency

VOC Volatile Organic Compounds

WRF-Chem Weather Research and Forecasting Model with Chemistry

WHO World Health Organization

"'Cause there were pages turned with the bridges burned

Everything you lose is a step you take. So make the friendship bracelets, take the moment and taste it. You've got no reason to be afraid. You're on your own, kid. Yeah, you can face this.

You're on your own, kid

You always have been."

- *Taylor Swift*

1. Introduction

1.1. Air Pollution

Air pollution is monitored in several cities around the world. The main pollutants have regulated maximum limits, whose values are used to diagnose air quality and guide resolutions and atmospheric emission standards.

The World Health Organization (WHO, 2022a) classifies air pollution contamination of internal or external environments by any chemical, physical or biological agent that modifies the natural characteristics of the atmosphere.

According to article 2 of the Resolution of the National Environmental Council (CONAMA, in Portuguese, Conselho Nacional do Meio Ambiente) n. 491/2018, an air pollutant is defined as

> any form of material in quantity, concentration, time or other characteristics, which renders or may render air inappropriate or harmful to health, inconvenient to public well-being, harmful to materials, fauna, and flora or harmful to safety, the use and enjoyment of the property or the normal activities of the community (BRASIL, 2018).

Air pollution has natural sources such as forest fires or anthropogenic activities such as vehicular and industrial emissions, which release various substances into the atmosphere (BRITO; SODRE; ALMEIDA, 2018; ROCHA MARTINS; BITTENCOURT DE ANDRADE, 2002). However, due to the dynamics and chemical reactivity of the compounds in the atmosphere, there are still uncertainties regarding the pollutants' sources, reactions, and fate. Some examples are presented below.

The set of potentially toxic pollutants that are now legislated refers to what we call air pollution. This group of pollutants is composed of carbon monoxide (CO), sulfur dioxide (SO_2), nitrogen dioxide (NO_2), ozone (O_3), particulate matter (PM), and lead (Pb) in PM. Among these pollutants,

particulate emissions stand out since the effects on human health and ecosystems are proven (BRITO; SODRE; ALMEIDA, 2018). A "mixture of gases and particulates" exists in the atmosphere; however, the concentration level may not be adequate for maintaining life in ideal conditions, which occurs when the air is polluted.

The atmosphere functions as a means of transport, where interactions occur physically and chemically. Detection is established by determining the concentration of the pollutant in the receptors. The exposure of receptors can be from humans, animals, plants, or materials (SEINFELD; PANDIS, 2016).

Due to this, several studies have been carried out in Brazil. In Rio de Janeiro, studies on air quality have been dated since the 1990s. The highest PM concentrations were observed in places with a strong influence of anthropogenic activities, such as vehicular traffic and industries. Lower concentrations are in areas further away from large urban centers, with few anthropogenic sources (BERINGUI et al., 2021).

Increased emissions of pollutants into the atmosphere and their diversity result from increased fossil fuel burning, industrial development, increased vehicle circulation, and population growth.

1.2. Atmospheric Particulate Matter (PM)

The term particulate matter is a complex mixture of liquid and solid particles (aerosols) suspended in the air, with a diameter up to one hundred micrometers, and can be classified as its size and its formation (primary and secondary particles) (LENZI; FAVERO, 2019; WHO, 2022a)

Aerosol particle sizes can range from a few nanometers to tens of micrometers in diameter. Among them, the most studied are $PM_{2.5}$ and PM_{10}.

Particulates with a diameter of less than 2.5 µm are known as $PM_{2.5}$ and remain in the air for days or weeks and can reach great distances, reaching other countries and continents. These particles have a large surface per unit mass, making them excellent carriers of inorganic and

organic compounds (SEINFELD; PANDIS, 2016; SHALTOUT et al., 2014; US EPA, 2022b)

PM_{10} has a diameter of up to 10 µm and rapidly deposits due to its weight and size. They come mostly from mechanical processes, such as the soil resuspension by the action of winds, and are retained in the upper tract of the respiratory system ((ALVES et al., 2014; LENZI; FAVERO, 2019; SEINFELD; PANDIS, 2016; US EPA, 2022b).

PM can have natural or anthropogenic sources and is emitted as particles of primary origin. Those are directly expelled into the atmosphere or formed by secondary processes, that is, by transforming precursor gases (FUZZI et al., 2015). The primary particles tend to constitute the $PM_{2.5}$ and PM_{10} fraction of the particulate matter, and the secondary, the $PM_{2.5}$ fraction. PM_{10} is usually produced mechanically by the fragmentation of larger particles and transferred to the atmosphere by the action of winds, such as soot, pollen, and volcanic ash.

$PM_{2.5}$ are formed in the atmosphere by physical (condensation, nucleation, and evaporation) and chemical (oxidation and photochemical) processes, mainly by the gas-particle conversion process (SEINFELD; PANDIS, 2016)

The permanence of PM in the atmosphere is influenced by meteorological elements (radiation, relative humidity, wind direction, and speed) and climatic phenomena (El Niño, thermal inversion). Such factors can lead to the imprisonment of PM in a given location, consequently increasing its concentration or influencing the dispersion of these particles, taking them to distant areas of their source (SANTOS et al., 2016a; US EPA, 2022b).

The polluting gases and particulate matter present in the atmosphere can cause various health problems in the population, depending on the concentration level. In 2019, the World Health Organization (WHO) disclosed that about 4.2 million deaths are related to ambient (external) air pollution, and this mortality is due to exposure to $PM_{2.5}$, which cause cardiovascular and respiratory diseases and cancers (WHO, 2022b).

In general, studies indicate that particulate matter affects health,

including cancer, arteriosclerosis, inflammation in the lung, increased hospitalization, and death. There is evidence that SO_2 aggravates pre-existing respiratory symptoms due to its significant solubility, such as asthma. In contrast, NO_2, due to its low solubility, can penetrate the respiratory system and give rise to carcinogenic substances. CO decreases the ability to transport oxygen in the bloodstream, at low concentrations, causes fatigue and chest pain, and at high concentrations, can lead to asphyxiation and death. Long O_3 exposure can cause a reduction in lung capacity, the development of asthma, and a decrease in life expectancy (GREENBERG et al., 2017; KAMAREHIE et al., 2017; US EPA, 2022a; VERONESI et al., 2017).

About particles when inhaled, they can reach several organs. Particle size is the leading cause of health problems; the smaller the particle, the deeper it will penetrate the respiratory tract.

In the body, the nasal eyelashes and the body act as filters for particles exceeding 10 µm in diameter. In this way, this particle size will be collected in the nose and throat or can be housed in the trachea or bronchi. However, particles that have an impact on the effects of human health are those that have a diameter of less than 10 µm. Particles between 5 and 10 µm are quickly deposited in the tracheobronchial tree, while 1 to 5 µm are deposited in respiratory bronchioles and alveoli and may affect gas exchange within the lungs. In general, particles smaller than 1 m will penetrate the alveoli and can move more to the cellular tissue and/or circulatory (ATKINSON et al., 2010; KIM; KABIR; KABIR, 2015; LÖNDAHL et al., 2007). Because of these health impacts, reduced levels of air pollutants can save lives and significantly reduce state costs, as well as ensuring the health of animals, vegetation, conservation of monuments, among others. That is why it is necessary to manage air quality effectively.

1.3. Source and composition

The chemical composition of particulate matter is primarily defined by its emitting sources. The particles of atmospheric aerosols can comprise

several elements, such as sulfates, nitrates, ammonia, materials containing carbon, marine salts, minerals, metals, and water. In a complementary way, the particulates arise of anthropogenic or natural origin, and depending on their source, they can be found in $PM_{2.5}$ or PM_{10} (ALVES, 2005; SEINFELD; PANDIS, 2016). Figure 1.1 represents the various mechanisms that assist in forming atmospheric PM.

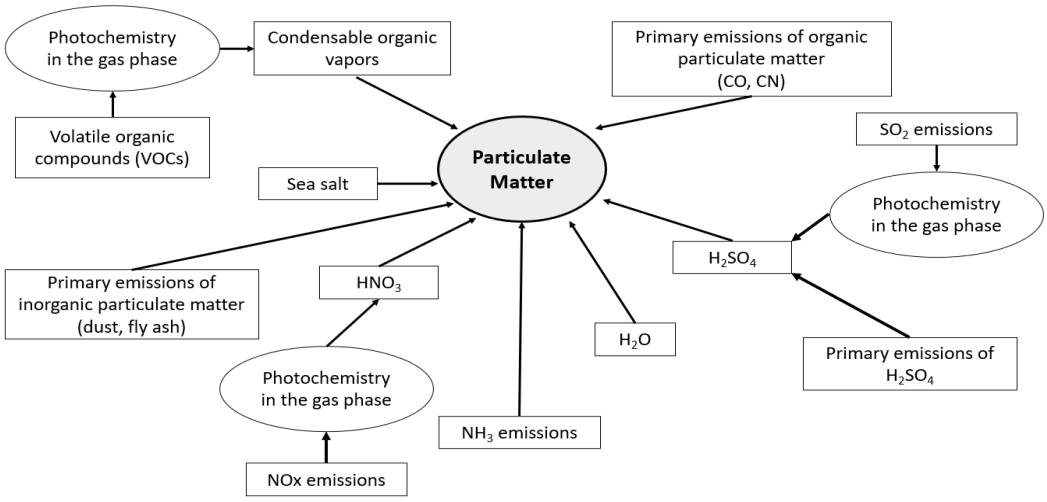

Figure 1.1. Schematic representation of the mechanisms of formation of particulate matter. (ALVES, 2005).

1.3.1 Soluble ions and elements

Among the inorganic compounds that can make up the mass of PM, sulfate, nitrate, and ammonium are the predominant. The PM composed of these ions are formed in the atmosphere through the oxidation of their gas precursors, namely: sulfur dioxide (SO_2), nitrogen oxides ($NO_x = NO + NO_2$), and ammonia (NH_3) (WANG et al., 2013). Primarily, sulfate and nitrate can be produced by natural sources (leaf respiration, soil emission) or by the combustion of fossil fuels (FREITAS; SOLCI, 2009; XU; PENNER, 2012).

Ammonium nitrate is one of the leading products of the NO_x gas oxidation reaction. After the emission of these NO_x to the atmosphere, its oxidation process occurs and subsequently, the formation of nitric acid

(HNO_3), which is considered an atmospheric gas highly soluble in water (KHEZRI et al., 2013; SEINFELD; PANDIS, 2016; SLEZAKOVA et al., 2011; XU; PENNER, 2012). From HNO_3, the formation of nitrate aerosol occurs in two ways different. First, by the reaction of HNO_3, which dissociates directly into an aqueous solution, due to its high solubility, as shown below:

$$NO\ (g) + O_3\ (g) \rightleftharpoons NO_2\ (g) + O_2\ (g) \quad (1)$$

$$NO_2\ (g) + HO\bullet \rightleftharpoons HNO_3\ (g) \quad (2)$$

$$HNO_3\ (g) \rightleftharpoons HNO_3\ \text{(aqueous or particulate)} \quad (3)$$

$$HNO_3\ \text{(aqueous)} \rightleftharpoons H^+ + NO_3^- \quad (4)$$

In addition, it can react with ammonia gas (NH_3) to form ammonium nitrate aerosol (NH_4NO_3). However, in this case, the formation of the nitrate aerosol will depend on a greater availability of ammonia than usually is necessary to neutralize the sulfate. This is because the sulfate aerosol is neutralized by ammonia to become ammonium sulfate. Thus, excess ammonia will help in the nitrate formation process (KHEZRI et al., 2013; SLEZAKOVA et al., 2011; XU; PENNER, 2012).

$$HNO_3\ \text{(aqueous or particulate)} + NH_3\ (g) \rightleftharpoons NH_4NO_3\ \text{(aqueous or particulate)} \quad (5)$$

Nitrate aerosols can be found in $PM_{2.5}$ and PM_{10} fractions. Usually, the $PM_{2.5}$ fraction is formed by the reaction of nitric acid with pre-existing $PM_{2.5}$ particles, such as ammonium nitrate. The PM_{10} is derived from the reaction of HNO_3 with PM_{10} particles, such as sodium chloride, that form sodium nitrate (SEINFELD; PANDIS, 2016; ZHUANG et al., 1999). Regarding the lifetime, such particles have four days in the atmosphere on average (XU; PENNER, 2012).

Sulfate aerosols are produced by chemical reactions in the aqueous phase, which occur within the clouds by condensation of pre-existing particles or by oxidation of sulfur gases in the gas phase. The chemical reactions of sulfur compounds will depend on the oxidation state, so the lower the degree of oxidation of sulfur, the response will occur faster

(SEINFELD; PANDIS, 2016).

The main precursors of sulfate aerosols in the atmosphere are formed from the oxidation of SO_2 from volcanoes and anthropogenic sources (burning of fossil fuels and biomass) and dimethylsulfide (DMS) from biogenic sources from marine phytoplankton, leading to submicrometric aerosols (JACKSON et al., 2020; LIU; CHAN; ABBATT, 2021).

The optical properties of this aerosol will depend on its size and are radiation scattering particles that act in the radiative cooling of the atmosphere and surface; but with a small degree of absorption in the near-infrared (LI et al., 2022a; LIU; CHAN; ABBATT, 2021). They are also considered predominantly hygroscopic particles and are, therefore, water-soluble.

The chemical composition of the particulate matter may vary accordingly to its size. Generally, the PM_{10} fraction consists mainly of SO_4^{2-}, Na^+, Ca^{2+}, Mg^{2+}, Cl^-, and K^+, presenting an essential contribution of marine salts in coastal regions (TEGEN et al., 1997). $PM_{2.5}$ is mainly composed of inorganic compounds derived from SO_2, NO_x, NH_3, volatile organic compounds (VOCs) derivatives, and elements such as Pb, Cd, V, Ni, Cu, and Zn (FUZZI et al., 2015).

1.3.2. Polycyclic aromatic hydrocarbon (PAH)

Polycyclic aromatic hydrocarbons (PAH) are a class of persistent organic chemicals emitted directly due to the incomplete combustion of organic materials, including natural and anthropogenic sources (BAEK et al., 1991; YANG et al., 2021; ZHANG; TAO, 2009).

PAHs are non-polar and hydrophobic molecules. Its physical and chemical properties vary with molar mass, such as vapor pressure, hydrophobicity, and water solubility. PAHs with two to three aromatic rings are commonly considered low molecular weight (LMW), and those with four or more rings are considered high molecular weight (HMW). The United States Environmental Protection Agency (US EPA) has classified 16 PAH

species in a priority control pollutant list (Table 1.1). The most carcinogenic compounds are benzo[a]anthracene, chrysene, benzo[b]fluoranthene, benzo[j]fluoranthene, benzo[k]fluoranthene, benzo[a]pyrene, indene[1,2,3-cd]pyrene and dibenzo[a,h]anthracene (TOBISZEWSKI; NAMIEŚNIK, 2012).

PAHs can usually be grouped according to their origin: petrogenic (petroleum derivatives), pyrogenic (incomplete combustion of organic substances), biogenic (biological processes), and diagenetic (geological processes). The diagnostic reasons can qualitatively identify the sources of PAHs since the distributions of the compounds are strongly related to the formation mechanisms. Table 1.1 shows the typical reasons reported in the literature.

Table 1.1. Main diagnostic reasons used to evaluate anthropogenic sources in the environment. (ABREU-MOTA et al., 2014; DAVIS et al., 2019; PEREIRA et al., 2017; TOBISZEWSKI; NAMIEŚNIK, 2012).

Ration	Range of values	Source
IndP/(IndP+BghiP)	< 0.02 0.2 – 0.5 > 0.5	Petrogenic, Combustion of petrol, Combustion of coal, wood, and vegetation.
Σ COMB/Σ PAHs	~ 1	Combustion.
Ant/(Ant+Phe)	< 0.1 > 0.1	Petrogenic, Pirogenic.
Flt/(Flt+Pyt)	< 0.4 0.4 – 0.5 > 0.5	Petrogenic, Fossil fuel combustion, Combustion of wood, coal, and vegetation.

BaA/(BaA+Chr)	0.2 – 0.35 > 0.35 < 0.2 < 0.35	Coal combustion, vehicular emissions, Petrogenic, The mix of sources.

IndP: Indeno[1,2,3-cd]pyrene; BghiP: Benzo[ghi]perylene; ∑ COMB (Flt, Pyr, BaA, Chr, BbF, BkF, BaP, IndP e BghiP); ∑PAH: Total sum of non-alkylated PAH; Ant: Anthracene; Phe: Phenanthrene; Flt: Fluoranthene; Pyr: pyrene; BaA: Benz[a]anthracene; Chr: Chrysene.

Identifying PAH sources is based on the different conditions of the processes that generate the PAH. Thus, low molar mass PAHs are generally formed during low-temperature combustion processes (e.g., wood burning), while in high-temperature combustion processes such as burning fuels in vehicular engines, high molar mass compounds (MOSTERT; AYOKO; KOKOT, 2010; YANG et al., 2021). Diagnostic reasons are still essential in identifying the source of PAHs, mainly distinguishing the emission from the pyrogenic or petrogenic origin, particularly a qualitative analysis (RAVINDRA; SOKHI; VAN GRIEKEN, 2008; TOBISZEWSKI; NAMIEŚNIK, 2012).

1.3.3. Black Carbon, levoglucosan, and retene

Black carbon (BC) is a significant component of $PM_{2.5}$, primarily emitted by combustion sources. As the main constituent of soot, BC is formed through incomplete combustion, with most emissions originating from anthropogenic activities. It is considered a primary aerosol due to its direct release from biomass and fossil fuel burning (LI et al., 2019b).

BC is a unique carbonaceous material formed in flames and emitted directly into the atmosphere (BOND et al., 2013; BUSECK et al., 2012; ZHANG et al., 2015). Its main sources include diesel combustion from vehicular and industrial engines, as well as the burning of coal and biomass (LONG; NASCARELLA; VALBERG, 2013). BC aerosols play a crucial role

in the Earth's climate system, affecting cloud properties on regional and global scales and impacting air quality, visibility, and public health. As a marker of anthropogenic pollution, BC also contributes to the long-range transport of polluted air masses (BOND et al., 2013; BUSECK et al., 2012; LONG; NASCARELLA; VALBERG, 2013; ZHANG et al., 2015).

Since BC and PM share common urban sources, BC significantly contributes to urban PM mass, reducing visibility and warming the atmosphere due to its strong interaction with visible light (LONG; NASCARELLA; VALBERG, 2013; ZHANG et al., 2015)

Another key tracer of biomass burning is levoglucosan (LEV), a monosaccharide formed by the pyrolysis of cellulose at temperatures above 300°C (FRASER; LAKSHMANAN, 2000; SIMONEIT et al., 1999; URBAN et al., 2012). Emitted in relatively high concentrations (40–1200 mg kg^{-1} of burnt wood), LEV remains stable in the atmosphere for up to ten days, allowing long-range transport (LARSEN; SCHANTZ; WISE, 2007).

Additionally, retene (1-methyl-7-isopropylphenanthrene) is a methylated tricyclic aromatic compound derived from the thermal alteration of resin diterpenoids in wood. It serves as a key indicator for distinguishing softwood combustion from hardwood combustion (LI et al., 2019a; RAMDAHL, 1983; SHEN et al., 2012).

1.4. Legislation

The air quality standard is one of the air quality management tools, determined as the concentration value of a specific pollutant in the atmosphere, associated with an exposure time interval so that the environment and the health of the population are preserved from the risks of damage caused by air pollution (CONAMA, 2024).

Given the importance of pollutants and their effects on human health and the environment, some international institutions establish limits for their daily and average annual concentration of them. The WHO, based on epidemiological studies, provide guidelines on air quality standards for pollutants that pose a risk to the population’s health, aiming to reduce their

impact (US EPA, 2023; WHO, 2022a).

In the 1960s, the United States established air quality standards after acute episodes of air pollution in urban centers. The US EPA was created in 1970 and had the attributions to define air quality standards, detailed studies, and collect and systematize data. Such assignments gained reinforcement with the approval by the US Congress of the Clean Air Act (CAA), marking the beginning of efforts to control air pollution in the US (SANTANA et al., 2012).

National air quality standards ("National Ambient Air Quality Standards" - NAAQS) were approved in 1971. Currently, the legislated pollutants ("criteria air pollutants") are carbon monoxide (CO), lead (Pb), nitrogen dioxide (NO_2), ozone (O_3), particulate matter ($PM_{2.5}$ and PM_{10}), and sulfur dioxide (SO_2). The values with the year of the last update are shown in Table 1.2.

Table 1.2. National air quality standards exist in the U.S. (US EPA, 2023).

Pollutant	Primary/ Secondary	Averaging Time	Level	Form
CO	Primary	8 h	9 ppm	Not to be exceeded more than once per year
		1 h	35 ppm	
Pb	Primary and Secondary	Rolling 3 month average	0.15 μg m^{-3}	Not to be exceeded
NO_2	Primary	1 h	100 ppb	98th percentile of 1-hour daily maximum concentrations averaged over 3 years
	Primary and Secondary	1 year	53 ppb	Annual Mean

O_3	Primary and Secondary	8 h	0.070 ppm	Annual fourth-highest daily maximum 8-hour concentration averaged over 3 years.
$PM_{2.5}$	Primary	1 year	12 μg m^{-3}	Annual mean averaged over 3 years
	Secondary	1 year	15 μg m^{-3}	
	Primary and Secondary	24 h	35 μg m^{-3}	98th percentile averaged over 3 years
PM_{10}	Primary and Secondary	24 h	150 μg m^{-3}	Not to be exceeded more than once per year on average over 3 years
SO_2	Primary	1 h	75 ppb	99th percentile of 1-hour daily maximum concentrations averaged over 3 years
	Secondary	3 h	0.5 ppm	Not to be exceeded more than once per year

Primary air quality standards refer to concentrations of pollutants that, when exceeded, may affect the population's health and can be understood as maximum tolerable levels of concentration of air pollutants. Medium-term goals, that is, protect public health, including protecting the health of "sensitive" populations, such as asthmatics, children, and the elderly (BRASIL, 1989; US EPA, 2023).

Secondary standards refer to concentrations of air pollutants below

which the minimum adverse effect on the well-being of the population is expected, as well as the minimum damage to fauna and flora, materials, and the environment in general, which can be understood as desired levels of concentration of pollutants, constituting a long-term goal, that is, they protect public welfare, including protection against reduced visibility and damage to animals, crops, vegetation and building (BRASIL, 1989; US EPA, 2023).

In 2021, the WHO released updates on air quality standards for five types of air pollutants applicable in all regions based on their effects on human health. Although the WHO recommendations have global application, it is up to each country to establish its air quality standards, considering its circumstances. Variations may occur due to the country's development, health risks, technological feasibility, and other social and political factors (WHO, 2021a). (Table 1.3).

Table 1.3. WHO recommendations for environmental concentrations of air pollutants (WHO, 2021a).

Pollutant	Averaging time	Level
$PM_{2.5}$	24 h	15 μg m^{-3}
	Annual	5 μg m^{-3}
PM_{10}	24 h	45 μg m^{-3}
	Annual	15 μg m^{-3}
O_3	Peak season	60 μg m^{-3}
	8 h	100 μg m^{-3}
CO	24 h	4 mg m^{-3}
NO_2	24 h	25 μg m^{-3}
	Annual	10 μg m^{-3}
SO_2	24 h	40 μg m^{-3}

In Brazil, the enactment of Law 14.850/24 marks a breakthrough in Brazilian environmental management by establishing the National Air Quality Policy (PNQAr). The law provides mechanisms for monitoring air

quality and widely disseminating this data to the population, making information more accessible and transparent. This index will be incorporated into the National Air Quality Management System (MonitoAr), consolidating a national database on atmospheric pollutants. In addition, the implementation of a National Air Quality Monitoring Network, under the responsibility of environmental agencies, will strengthen the capacity to monitor and analyze air pollution in different regions of the country.

The updating of air quality standards by CONAMA Resolution 506/2024 aligns Brazil with international goals, especially the UN's 2030 Agenda. This new legislation is based on the WHO guideline of 2021. National air quality standards are divided into two categories:

I - intermediate air quality standards - IS: standards established as temporary values to be met in stages;

II - final air quality standard - FS: guide values defined by the World Health Organization - WHO in 2021.

The parameters regulated by environmental legislation are total suspended particles (TSP), smoke, inhalable particles (PM_{10} and $PM_{2.5}$), sulfur dioxide (SO_2), carbon monoxide (CO), ozone (O_3), nitrogen dioxide (NO_2), and lead (Pb). The exact resolution also sets out the criteria for acute air pollution episodes. It should be noted that the declaration of the states of Attention, Alert, and Emergency requires, in addition to the levels of concentration reached, the forecast of unfavorable weather conditions to the dispersion of pollutants (CONAMA, 2024) (Table 1.4).

Table 1.4. Air quality standards of Brazilian legislation (CONAMA). (CONAMA, 2024).

Pollutant	Averaging time	IS-1 (μg m^{-3})	IS-2 (μg m^{-3})	IS-3 (μg m^{-3})	IS-4 (μg m^{-3})	FS (μg m^{-3})
TSP	24 h	-	-	-	-	240
	Annual	-	-	-	-	80
PM_{10}	24 h	120	100	75	50	45
	Annual	40	35	30	20	15

$PM_{2.5}$	24 h	60	50	37	25	15
	Annual	20	17	15	10	5
NO2	24 h	260	240	220	200	200
	Annual	60	50	45	40	10
SO_2	24 h	125	50	40	40	40
	Annual	40	30	20	20	20
CO	24 h	-	-	-	-	9 (ppm)
O_3	8 h	140	130	120	100	100
Smoke	24 h	120	100	75	50	45
	Annual	40	35	30	20	15
Pb	Annual	-	-	-		0.5

With the implementation of the National Air Quality Policy (PNQAr) and the revision of CONAMA Resolution 506/2024 by the National Environmental Council (CONAMA), Brazil is making progress in adopting stricter regulations aligned with the UN's goals. However, despite this advancement, concerns remain about meeting the established deadlines, particularly the final target set for 2044. This is because the World Health Organization (WHO) may update its guidelines by then, suggesting that shorter timelines would be more effective in ensuring the country aligns with international air quality (BERINGUI et al., 2021; CONAMA, 2024; TAVELLA et al., 2024).

In Brazil, the transport of passengers and cargo is carried out mostly by road, having significant dependence on fossil fuels. Thus, this sector has contributed decisively to the increase of emissions of air pollutants (LOPES et al., 2018).

For the control of vehicular pollution in Brazil, the National Environmental Council (CONAMA) created the Air Pollution Control Program for Automotive Vehicles (PROCONVE) in 1986 (Resolution 18/1986). In 2022, the last phases of the L-7 for light vehicles and the P-8 for heavy vehicles came into force. The transition from P7 to P8 occurred. Currently, the maximum NO_x emission value is 2.0 g kWh^{-1} (BRASIL, 2018;

BRASIL, 1986).

1.5. Thesis presentation and organization

The Laboratório de Química Atmosférica (LQA) has been conducting research on PM since 2009. Over the years, the primary analyses have focused on ions and elements present in all samples, in addition to specific studies PAH. Various types of PM, such as TSP, PM_{10}, and $PM_{2.5}$, have been analyzed in multiple locations, including Rio de Janeiro, Santa Cruz, Seropédica, Resende, Itatiaia, Barra Mansa, Volta Redonda, Porto Real, Quatis, Ilha Grande, Queimados, Japeri, Itaguaí, Nova Iguaçu, Belford Roxo, São João de Meriti, Nilópolis, Duque de Caxias, Magé, Guapimirim, Niterói, São Gonçalo, Itaboraí, and Teresópolis (BERINGUI et al., 2021; GIODA et al., 2016; JUSTO et al., 2020; MATEUS; GIODA, 2017; QUIJANO et al., 2019)**.**

In my doctoral thesis, I analyzed the ionic, elemental, black carbon, and organic composition (PAH, nitro- and oxy-PAH, aliphatic hydrocarbons, and saccharides) of PM. Nitro-PAH, known for their high mutagenic and carcinogenic potential, originate primarily from the incomplete combustion of organic matter, such as diesel and gasoline engines, fossil fuel burning, and industrial processes like aluminum smelting. Oxy-PAH, which are toxicological intermediates, were measured for their potential impacts, including cytotoxicity, immunotoxicity, and carcinogenicity. Despite challenges related to the low concentration and instability of these compounds, consistent atmospheric measurements were achieved.

Biomass burning markers, including black carbon, saccharides (levoglucosan, mannosan, and galactosan), and retene, were evaluated to identify sources through their "chemical fingerprints." Mercury levels were analyzed using a Direct Mercury Analyzer (DMA-80, Milestone), highlighting the role of the atmosphere as a receptor of both natural and anthropogenic emissions in the state of Rio de Janeiro.

During my sandwich Ph.D. program at the Max Planck Institute for Meteorology (MPI-M, Hamburg, Germany), I applied atmospheric modeling

to understand the photochemical formation of compounds in the metropolitan region of Rio de Janeiro. To complement my thesis, I incorporated data from NO_x sensors in heavy vehicles to evaluate the effectiveness of PROCONVE legislation in reducing pollutant emissions, particularly NO_x. The results contribute to a better understanding of pollution sources and their impact on health and the environment.

The present PhD thesis is presented in an article-based format, in which the "Results and Discussion" section comprises an adaptation of articles that have been published, submitted, or are in the process of being written (Chapters 4–11).In order to adhere to the standard for final papers, the "Materials and Methods" section is described in Chapter 3 and includes the methodology employed for all written articles. Consequently, in chapters where the results are described, readers will find the corresponding methodology section in Chapter 3.

2. Research Objectives

2.1. General objective

To monitor air quality and chemically characterize particulate matter samples in three locations in the State of Rio de Janeiro, aiming to identify the anthropogenic influence and regional impacts. In addition, modeling of ozone concentrations and other atmospheric pollutants, and the use of sensors to monitor in real time NO_x emissions from heavy-duty diesel vehicles, both in the Metropolitan Region of Rio de Janeiro, to support the development of air quality management strategies in the region.

2.2. Specific objectives

- To evaluate the variation in the concentration of $PM_{2.5}$, elements, soluble ions, black carbon and organic compounds in three regions with different levels of urbanization in the state of Rio de Janeiro, considering the meteorological influence.
- To install NO_x sensors in heavy vehicles and analyze the factors that influence NO_x emissions, including engine power, vehicle weight, speed, and age, to assess their impact on emission levels.
- To carry out an atmospheric modeling study using pollutant concentrations from forecasts and real-time data obtained at monitoring stations in the metropolitan region of Rio de Janeiro, to understand the formation of photochemical organic compounds in the region.

3. Material and Methods

As this thesis follows an article format for the presentation of the "Results and Discussion" section, the material and methods will be presented here and omitted from the respective articles. All the articles were studied in the same locations with the same collection and conditioning methods. Therefore, this information will be commented on below and will not be repeated in their respective articles.

3.1. Study Area

The state of Rio de Janeiro (22.84 S, 43.15 W), the third most populous in Brazil, with 16.1 million inhabitants with a density of 366.97 inh/km^2, is characterized by a high concentration of vehicles in its capital and metropolitan region. It is recognized as the country's second-largest industrial hub and the third most significant area in South America, according to the Brazilian Institute of Geography and Statistics (IBGE) (IBGE, 2021a).

The MRRJ encompasses 21 municipalities, including the capital city, Rio de Janeiro. According to the latest census, its population has reached 17 million inhabitants. The capital has approximately 7 million residents, making it the second-largest urban center in Brazil, with 71 % of its territory urbanized (IBGE, 2021b). Approximately 36 % of the metropolitan area is covered by remnants of tropical forest vegetation (BRAGA et al., 2019). The state of Rio de Janeiro has the second-largest Gross Domestic Product (GDP) in Brazil (IBGE, 2021c). Furthermore, the MRRJ has 5 million vehicles, of which 38 % are light gasoline vehicles (GVs), and 4 % are heavy-duty diesel vehicles (HDDVs) (DETRAN-RJ, 2022).

The MRRJ covers a total of 4,930 km^2. It was consolidated on a site characterized by mountain and lowland topographic domains. To the north, the Serra do Mar borders the Guanabara Bay Basin and reaches altitudes of up to 2,000 meters. To the south, the terrain is made up of lowland areas that do not exceed altitudes of 100 meters. The portion that falls to the

Municipality of Rio de Janeiro covers 1,224 km^2, where detachments from the Serra do Mar form the chain of mountain massifs that define the city's striking natural profile. The Tijuca and Pedra Branca massifs form a physical barrier between the seafront and the north of the municipal territory and thus create the boundary references, albeit unofficial, for the North and South zones, while the proximity of the Pedra Branca and Gericinó massifs define the West Zone and the Baixada de Jacarepaguá. The North, South and West zones and the Baixada de Jacarepaguá, although not regions with formally defined boundaries, are the compartmentalization references traditionally used by the carioca population (IBGE, 2021b; MATEUS et al., 2020; PREFEITURA DO RIO DE JANEIRO, 2013).

The main industrial activities in the RMRJ are the chemical and pharmaceutical sectors, with companies of considerable national prominence that extend across the municipalities of Duque de Caxias, Belford Roxo, São João de Meriti and São Gonçalo. Also, the naval hub, shared between the municipalities of Niterói, São Gonçalo and Rio de Janeiro, which represents 85% of the national installed capacity, between small, medium and large units; the considerable participation of the state's oil hub, in which the Duque de Caxias Refinery - REDUC stands out, one of the most important refineries in the country, as well as the gathering of more than 700 companies in the oil sector (DANTAS et al., 2019; IBGE, 2021b; PREFEITURA DO RIO DE JANEIRO, 2013). It also boasts a few national preservation parks, such as the Serra dos Órgãos National Park (PARNASO).

PARNASO is located in the Atlantic Forest, the most devastated of Brazil's ecosystems, and is the third largest national park in the country. It covers an area of 20,024 hectares with altitudes ranging from 200 m to 2,263 m above sea level. Currently, the Serra dos Órgãos National Park represents one of the few remaining areas of biodiversity in the state of Rio de Janeiro and is notable for protecting important water sources that feed two major drainage basins, namely Paraíba do Sul and Guanabara Bay (CRONEMBERGER; VIVEIROS DE CASTRO, 2007; ICMBIO, 2008).

Gávea is a neighborhood in the south of the city of Rio de Janeiro. It

is located near the Pontifical Catholic University of Rio de Janeiro (PUC-Rio), a few meters from the subway line 4, 8.5 km from the André Rebouças Tunnel, and close to the sea.

Campos dos Goytacazes is a city located in the interior of Rio de Janeiro, Brazil, and is a key city in the northern region of the State. With a population of over 500,000, it is the seventh most populous city in the state's interior (IBGE, 2022). Covering an area of 4,032.5 square kilometers, Campos is known for its industrial and economic activities, especially as the location of Brazil's largest oil platform, the P-51, in the Campos Basin, earning it the title of National Petroleum Capital (FERREIRA et al., 2021; LIMA et al., 2020). It also serves as a residential center for workers at Porto do Açu, Latin America's largest industrial port complex. In agriculture, sugarcane dominates, occupying 56 % of the cultivated area and contributing to 53.5 % of the state's production in 2018. Despite laws aimed at eliminating sugar cane burning, the practice remains widespread in the region (GIODA et al., 2016; LIMA et al., 2020).

3.2. Sampling strategy

Samples of $PM_{2.5}$ were collected from three monitoring sites situated at Gávea, in the south region of Rio de Janeiro city (GÁVEA, 22º58'50" S and 43º13'58" W), Campos dos Goytacazes (CAMPOS, 21º45'39.1''S 41º17'31.1'' W), and the Serra dos Órgãos National Park (PARNASO, 22º29'47.5'' S and 43º00'05.2'' W) (Figure 3.1).

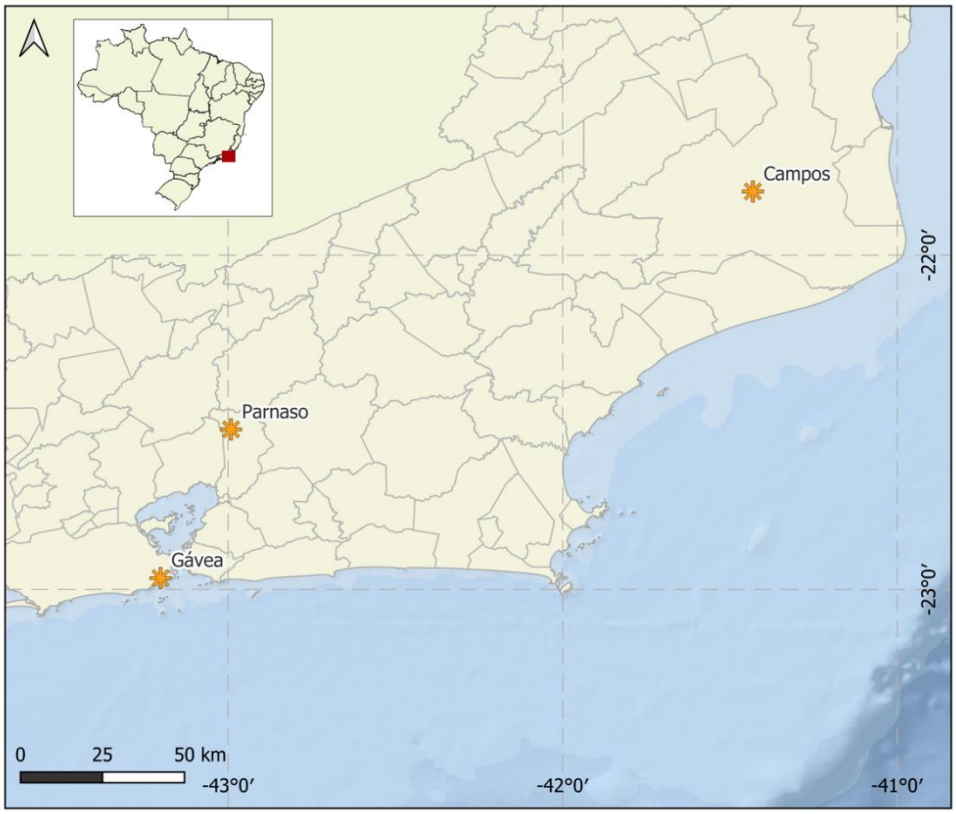

Figure 3.1. $PM_{2.5}$ monitoring stations in the state of Rio de Janeiro, South-eastern Brazil. GAVEA: Gávea, PARNASO: Serra dos Órgãos National Park, and CAMPOS: Campos dos Goytacazes. QGIS 3.26.3.

3.3. Measurements of $PM_{2.5}$ concentration

$PM_{2.5}$ samples were collected using microfiber filters (Whatman, Fisher Scientific, Maidstone, United Kingdom) every two weeks in all locations, alternating between fiberglass and quartz filters from February 2022 to June 2023. The monitoring adhered to Brazilian standards (ABNT-NBR 129 9547/86) and methods outlined by the United States Environmental Protection Agency (US EPA) under Method 130 (Method IO – 2.1). A high-volume air sampler (Hi-Vol 3000, Energética, São Paulo, Brazil) was employed, operating at an average airflow rate of 1.07 m^3 per minute, during 24h. The filters were conditioned in a desiccator for 24 hours. They underwent gravimetric analysis before and after sampling sessions using an analytical balance (Gehaka AG200 ± 0.0001, Marte Científica, Brazil) to ensure precise measurement of particulate mass. The system

maintained the relative humidity between 20 % and 30 %, and the temperatures ranged from 20 °C to 25 °C throughout the weighing process. This study analyzed all available $PM_{2.5}$ samples to evaluate their particulate mass content.

Samples collected on fiberglass filters were used for inorganic analysis, while samples collected on quartz filters were used for organic analysis. In this study, for organic analysis, 18 (eighteen) samples were collected in Gávea, 14 (fourteen) in PARNASO and 16 (sixteen) in Campos (quartz filters). For inorganic analysis, 17 (seventeen) samples were collected in Gávea, 14 (fourteen) in PARNASO and 16 (sixteen) in Campos dos Goytacazes. The collections carried out in Gávea and PARNASO were carried out by LQA, while the samples from Campos de Goytacazes were carried out by UENF. Details of the sampling periods are available in the Supplementary Material 1 (Fiberglass filters) and 2 (Fiberquartz filters).

In PARNASO, the collection was challenging due to the lack of electricity. The samples were collected with the Hi-vol in places close to the road, less than 100 meters away, and in the surroundings of the parking lot and the park entrance. Therefore, it is likely that the results that will be presented reflect the anthropogenic impact at the park's access points, and not the conditions deeper within the park.

3.4 Research Article 1 – Spatial Variability and Source Apportionment of Particulate Matter ($PM_{2.5}$) in Rio de Janeiro: Insights from Urban, Preserved, and Biomass Burning Areas.

The following description of methods refers to chapter 4, page 67.

3.4.1. Measurement of Black Carbon concentration

The determination of BC in selected $PM_{2.5}$ samples was performed using a portable optical transmissometer (SootScan, OT-21, Berkeley, Florida, USA) equipped with an infrared beam (λ = 880 nm). This non-destructive technique allows for rapid BC analysis, with a processing time of less than one minute, and is compatible with various filter types. The

device features a movable tray with two filter holder slots: one for the sample filter (external holder) and another for the reference blank (internal holder), which are measured simultaneously (FERNANDES et al., 2021). The instrument determines light attenuation at 370 nm and 880 nm by comparing the transmission intensities of the sample and reference filters. Attenuation (ATN) is calculated using the formula below:

$$ATN = -ln(\frac{T}{T_0}) \qquad \textbf{(Equation 3.1)}$$

where T represents the transmitted light intensity through the sample filter and T_0 corresponds to the blank filter.

The BC density is calculated by dividing the relative ATN by the specific attenuation coefficient σATN in units of $m^2\ g^{-1}$, using the formula:

$$BC = \frac{ATN}{\sigma ATN} \qquad \textbf{(Equation 3.2)}$$

This value is then converted into a BC concentration (µg m^{-3}) using a conversion factor (AHMED et al., 2009).

3.4.3. Measurement of ion concentration

With the assistance of Teflon scissors, a rectangular strip of filter with a sample, measuring approximately 86 cm^2 in area, was excised. For the blanks, a strip of approximately 43 cm^2 was cut. The weight of each strip was then measured on an analytical balance (Gehaka, AG200, ± 0.0005 g) and transferred to 50 mL polyethylene tubes (Techno Plastic Products AG, graduated and with a conical bottom). Subsequently, 20 mL of ultrapure water (Millipore, USA) was added to each tube using a dispenser. To facilitate the extraction process, the tubes were subjected to mechanical agitation in a vortex (Biomixer, Brazil) for one minute and subsequently subjected to centrifugation (Kindly, KC5) at a speed of 2000 rpm for four minutes. The resulting extract was then filtered through a cellulose acetate

membrane (Filtrilo, Paraná, Brazil) with a porosity of 0.22 µm (Filtrilo, Brazil) using a syringe without a needle, to remove all insoluble material.

The aqueous extract was analyzed by ion chromatography (Dionex, ICS 5000, Thermo Scientific, USA) which allows the simultaneous determination of cations (Li^+, Na^+, Ca^{2+}, $NH4^+$, K^+ and Mg^{2+}), inorganic anions (F^-, Br^-, Cl^-, NO_2^-, NO_3^-, PO_4^{3-}, and SO_4^{2-}) and anions of carboxylic acids ($HCOO^-$, CH_3COO^-, $(C_2O_4)^{2-}$ e $CH_2(COO)_2^{2-}$) (JUSTO et al., 2020).

The ion chromatography had an isochronic cationic component, an anionic gradient, and an autosampler AS-AP. The cations were analyzed using a Dionex IonPac CS12A (Thermo Scientific Dionex, USA), while the anions were examined on a Dionex IonPac AS19 (Thermo Scientific Dionex, USA). Analytical curves were prepared for both anions and cations, using standard solutions (Sigma Aldrich, Missouri, USA) at a concentration of 1000 mg L^{-1}. The analytical curves ranged from 0.20 to 40 mg L^{-1} for anions and from 0.75 to 40 mg L^{-1} for cations. A calibration check with external standards was performed to ensure an accuracy of ± 10 % on ANOVA. The LOD for the analyzed water-soluble ions in $PM_{2.5}$ samples was classified as follows: 0.001 – 0.01 µg m^{-3}: Li^+, K^+; 0.01 – 0.05 µg m^{-3}: Na^+, NH_4^+, Mg^{2+}, NO_2^-, Br^-, NO_3^-, PO_4^{3-}, $(C_2O_4)^{2-}$; 0.05 – 0.10 µg m^{-3}: SO_4^{2-}, CH_3COO^-, $HCOO^-$; 0.10 – 0.30 µg m^{-3}: Cl^-, Ca^{2+}, F^- and $CH_2(COO)_2^{2-}$.

Table 3.1. Operational Conditions Used for Ion Analysis by Ion Chromatography (Thermo Scientific Dionex, ICS 5000).

Parameter	**Cation**	**Anion**
Column	Dionex IonPac CS12A	Dionex IonPac AS19
Pre-column	Dionex IonPac CG12A	Dionex IonPac AG19
Eluent	Methanesulfonic Acid (CH_3SO_2OH) 18.0 mmol L^{-1}	Potassium Hydroxide (KOH) 3.0 mmol L^{-1}
Flow Rate (max)	0.300 mL min^{-1}	0.300 mL min^{-1}
Injection Volume	250 µL	100 µL
System Pressure	200 – 3000 psi	200 – 3000 psi

Detector	Conductivity	Conductivity
	Suppressor	Suppressor
Conductivity	< 1 µS	< 1 µS
Sampler	Autosampler AS-AP	Autosampler AS-AP

For the quantification of the ions present in the samples, two analytical curves were prepared using the external calibration method: one for cations and another for anions. To prepare these curves, individual standards of each inorganic ion with a concentration of 1000 mg L^{-1} (Sigma Aldrich, USA) were used, while the standards for organic ions were prepared at the same concentration, using formic acid and acetic acid (Sigma Aldrich, USA), malonic acid (TCI America, USA), and dihydrate oxalic acid (Spectrum, USA).

For the anion system, the analytical curve preparation was divided into two groups: minority ions (F^-, NO_2^-, Br^-, PO_4^{3-}, $CHOO^-$, CH_3COO^-, and $CH_2(COO)_2^{2}$) and major ions (Cl^-, SO_4^{2-}, NO_3^-, and $C_2O_4^{2}$). Standard solutions of 100 mg L^{-1} were prepared for the minority ions, while the major ions were maintained at a concentration of 1000 mg L^{-1}. From these solutions, a mixed solution containing all the ions was prepared, with a final concentration of 100 mg L^{-1} for the major anions and 7.5 mg L^{-1} for the minority ones, which was used to prepare the last three points of the analytical curve. Subsequently, the 100 mg L^{-1} solution was diluted to 25 mg L^{-1} for the major ions and 1.9 mg L^{-1} for the minority ions, which was used to prepare the first five points of the curve. All solutions were prepared using variable-volume micropipettes and a volume dispenser for adding water.

For the cation system, individual standards of 1000 mg L^{-1} concentration were used for Na^+, K^+, and Ca^{2+} (major ions), and for Mg^{2+}, NH_4^+, and Li^+ (minor ions). From these standards, a mixed solution was prepared containing all the ions, with a final concentration of 250 mg L^{-1} for the major ions and 33.4 mg L^{-1} for the minor ions, which was used to prepare the last three points of the analytical curve. To prepare the first five points of the curve, the 250 mg L^{-1} solution was diluted to a final concentration of

50 mg L^{-1} for the major ions and 6.7 mg L^{-1} for the minor ions. For both systems, the analytical curves ranged from 0.1 to 5 mg L^{-1} for the minor ions and from 0.75 to 40 mg L^{-1} for the major ions. A calibration check with external standards was performed to ensure an accuracy of ± 10 % on ANOVA.

The detection limits of the chromatographic technique (LODInstrumental) were calculated by considering the standard deviations (S_{y1}) and the mean values (y_m) obtained from the lowest concentration of the analytical curve (X_1), applying equation 3.3. Meanwhile, the instrumental quantification limits ($LOQ_{Instrumental}$) were calculated using equation 3.4. Next, the detection and quantification limits of the sample were evaluated by using the blank filters (LOD_{Sample} and LOQ_{Sample}). LOD_{Sample} was calculated based on the concentrations obtained from the analysis of ten blank filter strips, the same ones used in the sampling. For each blank filter, the values were normalized to the total mass of the filter. LOD_{Sample} was determined from the mean and standard deviation calculated after applying the Grubbs test with a significance level of $\alpha = 0.05$, using equation 3.5. The sample quantification limits (LOQ_{Sample}) were calculated using equation 3.6.

$$LOD_{Instrumental} = 3.3\ (S_{y1}\ X_1)/y_m \quad \textbf{(Equation 3.3)}$$

$$LOQ_{Instrumental} = 3\ LOD_{Instrumental} \quad \textbf{(Equation 3.4)}$$

$$LOD_{sample} = \overline{x} + 3\ S \quad \textbf{(Equation 3.5)}$$

$$LOQ_{sample} = \overline{x} + 10\ S \quad \textbf{(Equation 3.6)}$$

The detection and quantification limits used to evaluate the experimental data were the results from the analysis of the blank filters (LOD_{sample} and LOQ_{sample}), but for the undetected analytes, $LOD_{Instrumental}$ and $LOQ_{Instrumental}$ were used.

The LOD for the analyzed water-soluble ions in $PM_{2.5}$ samples was classified as follows: 0.001 – 0.01 µg m^{-3}: Li^+, K^+; 0.01 – 0.05 µg m^{-3}: Na^+, NH_4^+, Mg^{2+}, NO_2^-, Br^-, NO_3^-, PO_4^{3-}, $(C_2O_4)^{2-}$; 0.05 – 0.10 µg m^{-3}: SO_4^{2-}, CH_3COO^-, $HCOO^-$; 0.10 – 0.30 µg m^{-3}: Cl^-, Ca^{2+}, F^- and $CH_2(COO)_2^{2-}$.

3.4.4. Estimation of non-sea-salt particles

To identify the origin of the ions detected in the samples and assess the potential influence of seawater due to the sampling site's proximity to the coast, non-sea-salt (nss) calculations were performed. Using Na^+ as a reference element for sea salt, nss was calculated using the following equation:

$$nss - X = X_i - Na_i^+ \times (\frac{X}{Na^+})_{sea} \quad \textbf{(Equation 3.7)}$$

Where X_i and Na^+_i represent the concentrations of ions and Na^+ (µg m^{-3}) in particulate matter samples, respectively, and $(X/ Na^+)_{sea}$ is the ratio of each ion's concentration to Na^+ in seawater. The $(X / Na^+)_{sea}$ ratios for SO_4^{2-} (0.2516), K^+ (0.0371), Ca^{2+} (0.0385), Cl^- (1.7944), and Mg^{2+} (0.1190) (KONG et al., 2014; MCINNES et al., 1996).

3.4.2. Measurement of elemental concentration

The elemental analysis was performed using Inductively coupled plasma mass spectrometry (ICP-MS) model NexIon 300X (PerkinElmer, USA). First, to determine the elements present in the collected PM, filter strips containing the particulate matter and blank were cut and weighed on an analytical balance (Gehaka, AG200). After weighing, the filter strips were transferred to 50.0 mL polyethylene tubes (Techno Plastic Products AG, graduated and conical bottom), followed by the addition of 5.0 mL of doubly distilled nitric acid, followed by heating for 2 h on a heating plate at about 100 ºC for acid decomposition purposes. Then, the acid extracts were cooled at room temperature and diluted with 45.0 mL of ultrapure water (Millipore, USA) and then centrifuged for 4 min at a speed of 2000 rpm for separation of the insoluble material. The supernatant was transferred to 15.0 mL polyethylene tubes and subsequently analyzed by ICP-MS (NexIon 300 X, PerkinElmer, USA) (BERINGUI et al., 2021; MATEUS et al., 2013).

Calibration solutions N9300235 (Multi-element calibration standard 5 - B, Ge, Mo, Nb, P, Re, S, Si, Ta, Ti, W, Zr), N9300232 (Multi-element calibration standard 2 - Ce, Dy, Er, Eu, Gd, Ho, La, Lu, Nd, Pr, Sm, Sc, Tb,

Th, Tm, Y, Yb) e N9301720 (Multi-element calibration standard 3 - Al, Ag, As, Ba, Be, Bi, Ca, Cd, Co, Cr, Cs, Cu, Fe, Ga, In, K, Li, Mg, Mn, Na, Ni, Pb, Rb, Se, Sr, Tl, V, U, Zn) from PerkinElmer and monoelemental solutions of Br, Sn, Ti, Hg, Sb (Specsol®, São Paulo, Brazil) were prepared in ultrapure water (5 % v/v) and acidified with bi-distilled HNO_3.The analytical curves ranged from 1 to 1000 µg L^{-1}, and Rh (40 µg L^{-1}) was used as the internal standard in an acidified aqueous solution (5 % v/v HNO_3), injected online. The operational conditions were checked through the daily performance process to monitor the signal intensities of In, Mg, U, the CeO^+/Ce^+ ratio for oxide formation, and the Ba^{2+}/Ba ratio for the formation of divalent species. The operational conditions of the equipment are shown in Table 10. All concentrations were checked against quality controls, and the coefficient of variation for this comparison was less than 10 % on analysis of variance (ANOVA).

Parameter	Value
Radio Frequency Power	1100 W
Plasma Argon Flow	15.0 L min^{-1}
Nebulization Argon Flow	1.06 L min^{-1}
Auxiliary Flow	1.0 L min^{-1}
Reading Mode	Peak hopping
Sweep/Readings	1
Readings/Replicas	1
Number of Replicas	5

The detection limits of the spectrometric technique ($LOD_{Instrumental}$) were determined from 10 blank readings of 10 % nitric acid and calculated using equations 8 and 9, where *m* represents the slope of the analytical curve obtained for each element and *S* is the standard deviation of the ratio between the intensities of the standard solutions and the internal standard. The detection and quantification limits (LOD_{Sample} and LOQ_{Sample}) were calculated similarly to those in Ion Chromatography. The calculation was

performed from the analysis of ten blank filter strips, and the results were then normalized to the total mass of the filter. The detection and quantification limits were obtained from the mean and standard deviation calculated after applying the Grubbs test with a significance level of α = 0.05, using equations 3.8 and 3.9.

The detection and quantification limits used to evaluate the experimental data were the results of the analysis of the blank filters (LOD_{Sample} and LOQ_{Sample}), but for the elements not detected, $LD_{Instrumental}$ and $LOQ_{Instrumental}$ were used.

$$LD_{Instrumental} = 3\ S/\alpha \qquad \textbf{(Equation 3.8)}$$

$$LQ_{Instrumental} = 3.3\ LD_{Instrumental} \qquad \textbf{(Equation 3.9)}$$

The limit of detection (LOD) for the analyzed elements in $PM_{2.5}$ samples was classified as follows: 0.01 – 1 ng m^{-3}: Mn, Co, Ti, V, Cr, Ni, Cd, Sb, Pb, Mo, La, Ce, Ti; 1 – 5 ng m^{-3}: Al, Cu, Fe, Zn.

3.4.5. Quality assurance and quality control (QA/QC)

To check for possible contamination in the chemical composition of the filters and in the collection, handling and extraction processes, blank filters (BF) were analyzed in parallel with the samples. Five filters were extracted duplicate, totaling 10 samples of BF. After obtaining the results from the BF, the Grubbs test was applied to eliminate any anomalous values that could interfere with determining the composition of the samples. The average concentration of the species measured on the BF was then calculated and subtracted from the concentrations observed in the PM filter samples.

The ultrapure water used in the extractions and the water filtered through 0.22 µm membranes was monitored in the equipment used to analyze the aqueous extracts to identify possible contaminants. In addition, BF that had not been filtered through 0.22 µm cellulose acetate membranes were analyzed; these samples were centrifuged at 2000 rpm for 10 min to

check for contamination from the cellulose acetate filters.

The nitric acid used in the acid extraction was also analyzed to check for the presence of metals that could contaminate the samples. Another test performed was the pre-treatment of BF to minimize background contamination before analysis. Initially, they were washed with nitric acid and ultrapure water, followed by drying in a muffle furnace at 450 ºC. After cooling in a desiccator, the filters were weighed and subjected to different analytical procedures: acid-washed filters were used for elemental analysis by ICP-MS and ultrapure water-washed filters were analyzed for ion content. This procedure aimed to assess the efficiency of the washing methods in reducing the presence of ions and elements in the BF.

In addition, the extraction efficiency and accuracy of the spectroscopic technique were determined using a standard reference material (SRM) specific for particulate matter (NIST SRM 1648a - Urban Dust).

3.4.6. Statistical Analysis

Statistical analysis was conducted using PyCharm 2023.2.5 for Windows. Parametric and non-parametric statistical tests were conducted for $PM_{2.5}$ and chemical species concentrations over the entire study period. To assess differences in pollutant levels between Gávea, PARNASO, and Campos, analysis of variance (ANOVA) and Student's t-test were employed. When parametric methods were unsuitable, the Kruskal-Wallis test was used to determine differences. Statistical significance was evaluated at a 95 % confidence level.

3.4.7. Principal Component Analysis

Principal Component Analysis (PCA) is a multivariate method used to reduce the dimensionality of the data while preserving the chemical and descriptive information of the samples, thereby facilitating the interpretation of the results. This procedure involves transforming the original variables into new axes, called principal components (PC), which explain most of the

variation in the samples, allowing the data to be represented more compactly without losing relevant information (FERREIRA, 2023; VIEIRA et al., 2023).

In this study, the concentrations of chemical constituents were used as original variables to separate the samples according to the sampling location. Initially, the concentrations were autoscaled, ensuring that the variables had similar weights in the multivariate analysis. The entire chemometric process was carried out using Microsoft Excel® 2007 and the R programming language. Finally, the Hotelling's t^2 test was applied to identify outliers in the analyzed samples.

3.5. Research Article 2 – Characterization of mercury in atmospheric particulate matter in the State of Rio de Janeiro, Brazil.

The following description of methods refers to chapter 5, page 89.

3.5.1. Measurement of Hg concentration

Total Hg concentrations in $PM_{2.5}$ were determined using a Direct Mercury Analyzer - DMA-80 (Milestone, Sorisole (BG), Italy). The DMA-80 operates on the thermal decomposition of the sample, mercury amalgamation, and atomic absorption for mercury detection. Initially, samples were weighed and placed into a nickel boat, which was then subjected to thermal decomposition in a stream of air or oxygen. Mercury, along with other combustion by-products, was directed into the catalyst section after decomposition. Here, a continuous oxygen flow transports the decomposition products through a heated catalyst bed, where mercury gases are captured. Mercury species are converted to elemental mercury (Hg^0), which, along with the reaction gases, is selectively captured to a gold amalgamator, while other gases and decomposition products are expelled from the system. The amalgamator is then heated to release the captured mercury into a single beam, fixed wavelength atomic absorption spectrophotometer for quantification. The amount of mercury released is

measured in an optical cell through atomic absorption spectrometry at a wavelength of 253.65 nm (DE JESUS et al., 2020; SOLA et al., 2022a; WINDMÖLLER et al., 2017). LOD and LOQ were 0.002 pg m^{-3} and 0,006 pg m^{-3}, respectively.

3.5.2. Backward trajectories analysis

The National Oceanic and Atmospheric Administration (NOAA) HYSPLIT model was utilized to perform a 7-day backward trajectory analysis aimed at gaining insights into the origins of air masses affecting the study locations. This analysis is crucial for identifying the sources of pollutants, thus enhancing air quality forecasting. Additionally, forward trajectory analysis was employed to assess pollution dispersion patterns. Trajectories were computed at different altitudes (100 m, 500 m, and 1000 m). In the HYSPLIT model, these altitudes corresponded to different layers of the atmosphere: 100 m representing the ground surface layer, 500 m representing the boundary layer, and 1000 m representing the upper boundary layer (NOAA, 2024).

3.5.3. Statistical analysis

Statistical analysis was conducted using PyCharm 2023.2.5 for Windows. The one-way ANOVA test was utilized to assess the variance in mercury in particulate matter (PHg) concentrations across different locations and seasons.

3.6. Research Article 3 – Tracing Organic Pollutants in Particulate Matter: Source Identification and Implications for Air Quality and Public Health

The following description of methods refers to chapter 6, page 101.

3.6.1. Sample extraction

An aliquot (86.4 cm^2) of the filter was ultrasonically extracted (three times) with dichloromethane:methanol (2:1, v/v), and 20 µL of surrogate

standards were used for analytical control. The extracts were collected and concentrated using a rotary evaporator to a volume of approximately 1 mL. After pre-concentration, the extract was divided into two fractions (500 µL each), one for anhydrous saccharides and another for PAHs and aliphatic hydrocarbons analyses.

The recovery of the analytical protocol was evaluated using a mixture of deuterated *n*-alkanes (*n*-C_{16}d, *n*-C_{20}d, and *n*-C_{30}d) with a concentration of 5 µg mL^{-1} for the aliphatic fraction and *p*-terphenyl-d_{14} (Accustandard, New Haven, EUA) with a concentration of 125 µg mL^{-1} for the PAHs fraction.

The solvents hexane and dichloromethane (pesticide grade or better) were used for extraction and clean-up. Silica (60-230 mesh, Exodo Cientifica, Brazil) and neutral alumina (Sigma Aldrich, India) were cleaned by heating at 400 ºC for four hours and then deactivated with ultra-pure water at a concentration of 5 % (m/m) and 2 % (m/m), respectively.

3.6.2. PAH and AH determination

The bulk extracts were purified, and the AH and PAH fractions were isolated by liquid chromatography in a glass column filled with 2 g of silica gel and 1 g of alumina. 6 mL of hexane was used as the eluent for the AH, and 20 mL of hexane:dichloromethane (1:1, v/v) for the PAHs. The fractions were concentrated using a purified stream of N_2 until a final volume of 1 mL and 20 µL of the internal standards (mix of 5 deuterated compounds: naphthalene-d_8, acenaphthene-d_{10}, phenanthrene-d_{10}, chrysene-d_{12}, and perylene-d_{12}).

The PAHs were determined following the EPA8270D protocol by injecting 1 µL of each extract into a gas chromatography-mass spectrometry system (Thermo Scientific ISQ Single Quad GC-MS with Trace GC Ultra; Bremen, Germany) with electron impact ionization (EI, 70eV), DB5MS column (30 m × 0.25 mm × 0.25 µm), at a constant flow rate of He at 1.2 mL min^{-1}, following the temperature programming: 50 °C for 5 min; 50 °C min^{-1} up to 80 °C; 6 °C min^{-1} up to 280 °C, with a dwell time of 4 min; and 12 °C min^{-1} up to 305 °C with a dwell time of 5 min. The mass spectrometer

operated in Selected Ion Monitoring (SIM) mode, monitoring ions with mass-to-charge ratios (m/z) from 127 to 279 for the determination of 20 monitored PAHs (Supplementary material 2, Table S2): naphthalene, acenaphthene, acenaphthylene, fluorene, dibenzothiophene, phenanthrene, anthracene, fluoranthene, pyrene, chrysene, benzo[a]anthracene, benzo[b]fluoranthene, benzo[k]fluoranthene, benzo[a]pyrene, benzo[e]pyrene, benzo[g,h,i]perylene, perylene, indeno[1,2,3-c,d]pyrene, dibenzo[a,h]anthracene and retene (perylene, benzo[e]pyrene, dibenzothiophene and retene are not considered priorities according to the US Environmental Protection Agency - EPA). In addition, the 18 following alkylated PAHs also were monitored: C1–C4-naphtalenes, C1–C3-fluorenes, C1–C3-dibenzothiophenes, C1–C4-phenanthrenes, C1 and C2-pyrenes, C1 and C2-chrysenes. These 38 PAHs were based on technical opinions and official guidelines of IBAMA following the guidelines of the National Council for the Environment (Conselho Nacional do Meio Ambiente - CONAMA) to assess the impacts of oil and gas exploitation in Brazil. Moreover, retene was quantified as an indicator of combustion.

Alkylated PAHs were quantified based on the parental PAH curve and the corresponding internal standards. The retention time (RT) was corrected, and the peaks were integrated using the ASTM (American Society for Testing Materials) oil standard profile as a reference.

Aliphatic hydrocarbons were analyzed using a gas chromatograph (Thermo Scientific ISQ Single Quad GC-MS with Trace GC Ultra; Bremen, Germany) equipped with a Flame Ionization Detection. An aliquot of 1 µL sample was injected using an AS 3000 automatic injector in splitless mode at 270 °C for 1 min. An AG 122-5532 capillary column (30 m in length, 0.25 mm of internal diameter, and 0.25 µm of film thickness) was used under the following conditions: 50 °C for 2 min up to 320 °C at 6 °C min^{-1}, being held at the final temperature for 26 min. The GC-FID interface was kept at 280 °C. Helium (99.9 % purity) at a flow rate of 30 mL min^{-1} was used as the carrier gas. Aliphatic hydrocarbons were quantified using the full scan mode (mass interval of 50–600 Da). The ion source was operated at 250 °C, with an electron ionization source at 70 eV.

Quality assurance of the method was performed by evaluating the calibration curve (0.5 to 1000 ng mL^{-1}) and recovery (%) of aliphatic hydrocarbons after extraction.

3.6.3. Nitro-PAH and quinone determination

The extraction of particulate matter samples was carried out according to the methodology described and validated by Santos *et al.*, (2016) (SANTOS et al., 2016b) for the simultaneous determination of nitro-PAHs and quinones in particulate matter samples. Briefly, a 4.15 cm^2 circular section of a sampled quartz fiber filter was cut off and transferred to a microextraction device (Whatmann Mini™ UniPrep Filters, Whatmann, USA). Then, 500 µL of the ACN:DCM mixture (18 % acetonitrile in dichloromethane) was added and the entire microextractor system was sonicated for 23 min. After that, the extract was instantly filtered into the microextraction device and injected into a GCMS-QP2010SE (Shimadzu, Japan). This instrument was equipped with an AOC-20i autosampler and an Agilent DB-5MS capillary column (5 % diphenyl, 95 % dimethylpolysiloxane, 30 m × 0.250 mm × 0.25 µm). Ultrapure helium (99.999 %) (White Martins, Brazil) was used as a carrier gas at 1.0 mL min^{-1}. The oven temperature program was started at 70 °C, held for 2 min, then increased to 200 °C at 30 °C min^{-1} and held for 5 min. Finally, the oven temperature was increased to 330 °C at 5 °C min^{-1} and held for 0.67 min. The total run time was 38 min. The injector was operated at 310 °C using split/splitless injection mode with a sampling time of 0.8 min. The mass spectrometer was operated in electron impact (EI) mode at 70 eV. The ion source temperature was maintained at 250 °C, and the GC-MS transfer line temperature was set at 280 °C. Data acquisition was performed in SIM mode. Using this condition, 20 nitro-PAHs were analyzed: 1-Nitronaphthalene, 1-Methyl-3-nitronaphtalene, 2-Nitronaphthalene, 2-Nitrobiphenyl, 1-Methyl-4-nitronaphtalene, 1-Methyl-5-nitronaphtalene, 1-Methyl-6-nitronaphtalene, 2-Methyl-4-nitronaphtalene, 3-Nitrobiphenyl, 4-Nitrobiphenyl, 5-Nitroacenaphthene, 2-Nitrofluorene, 2-Nitrophenanthrene,

3-Nitrophenathrene, 9-Nitrophenanthrene, 2-Nitrofluoranthene, 3-Nitrofluoranthene, 6-Nitrochrysene, 2-Nitrobenzanthrone, and 6-Nitrobenzo[*a*]pyrene. In addition, three oxy-PAH, such as1,4-Naphtoquinone, 9,10-Anthraquinone, and Benzanthrone were investigated The analytical method for nitro-PAHs and oxy-PAHs was validated based on the following parameters: linear range, linearity, limit of detection (LOD), and limit of quantification (LOQ) (see Supplementary material 2, Table S3). The determination coefficients (R^2) for nitro-PAHs ranged from 0.9951 (3-NFLT) to 0.9992 (2-NNAP), while those for oxy-PAHs ranged from 0.9969 (9,10-AQ) to 0.9994 (1,4-NQ). The LOD and LOQ values for nitro-PAHs ranged from 1.9 pg to 5.9 pg and 6.4 pg to 19.6 pg, respectively. For oxy-PAHs, the LOD and LOQ values ranged from 0.81 pg to 2.16 pg and 2.69 pg to 7.20 pg, respectively. In addition, six deuterated compounds (acenaphthene-d_{10} (ACY-d_{10}), fluorene-d_{10} (FLU-d_{10}), pyrene-d_{10} (PYR-d_{10}), fluorene-d_{10} (FLU-d_{10}), phenanthrene-d_{10} (PHE-d_{10}), perylene-d_{12} (PER-d_{12}) were used as surrogate standards. An aliquot 10 µL of a mix working standard solution (1.0 mg L^{-1}) containing these compounds was added to the samples prior to the extraction. The recoveries were calculated in each batch. The recoveries ranged from 70.1 % to 110 % (C_{20}d), 99.1 % to 123 % (C_{24}d), and 72 % to 119 % (C_{30}d) for *n*-alkanes, and from 76 to 124 % (*p*-terphenyl-d_{14}) for PAHs, whereas the calibration curves showed correlation coefficients above 0.99. For nitro-PAHs and quinones, recovery ranged from 88 % to 170 % (ACY-d10), 72.9 % to 105 % (FLU-d10), 71% to 164 % (PHE-d10), 71 % to 107 % (PYR-d10), and 43 % to 138 % (PER-d12).

3.6.4. Anhydro saccharides determination

For the extract intended for anhydrous saccharides analysis, the solution was filtered through a Teflon filter with a pore diameter of 0.22 µm, and then the filtrate was evaporated under a stream of nitrogen. After evaporating the solvent, it was added 40 µL of N,O-bis-(trimethylsilyl)-trifluoroacetamide (BSTFA) containing 1 % trimethylchlorosilane (TMCS, Sigma-Aldrich), 10 µL of internal standard (Levoglucosan-d7) and 10 µL of

pyridine, and heated at 70 °C for 60 min. After derivatization, 940 µL of hexane was added to the derivatized extract, and the mixture was homogenized in a vortex. An aliquot of 1 µL was injected into the GC-MS system.

The saccharides were separated using an inert 5 % phenyl-methyl column, VF - 5 ms (30 m × 0.250 mm, 0.25 µm). For analysis, one µL of the sample was injected into a split/splitless injector, operated in splitless mode (splitless time: 0.5 min) at 250 °C. The flow rate of the carrier gas (He) was 1.3 mL min^{-1}, and the temperature of the transfer line was 300 °C. The furnace temperature ramp was: (i) initial temperature of 120 °C for 2 min, (ii) a gradient of 5 °C min^{-1} up to 200 °C for 2 min, (iii) then 20 °C min^{-1} to 300 °C for 2 min. The total time was ± 20 min. The mass spectrometer was operated at an electron energy of 70 eV and an ion source temperature of 220 °C. Levoglucosan, mannosan and galactosan were identified by GC retention index based on authentic standards and mass spectra (base peak at m/z 204 and 217).

3.6.5. Carbon preference index

The carbon preference index (CPI) for *n*-alkanes was calculated as follows (BRAY; EVANS, 1961; GOGOU et al., 1996):

$$CPI = \frac{\sum Cn\ odd\ (from\ C_{15}\ to\ C_{31})}{\sum Cn\ even\ (from\ C_{16}\ to\ C_{32})} \qquad \textbf{(Equation 3.10)}$$

The *n*-alkanes originating from the epicuticular wax of terrestrial plants exhibit high values of CPI (CPI > 1). Conversely, CPI values for *n*-alkanes originating from vehicular emissions and other anthropogenic activities are close to unity (CPI ≈ 1).

3.6.6. Concentration of Wax *n*-alkanes (WNA)

The concentration of wax *n*-alkanes (WNA) represents proportion of biogenic *n*-alkanes in total *n*-alkanes in $PM_{2.5}$ sample. The WNA was

calculated for each *n*-alkane as follows (GOGOU et al., 1996):

$$WNA\ Cn = Cn - 0.5\ (C_{n-1} + C_{n+1}) \qquad \textbf{(Equation 3.11)}$$

Where C*n* represents the concentration of odd numbered homologues, and C_{n-1} and C_{n+1} are the next lower and higher even homologues concentrations, respectively (KAUSHAL et al., 2020; KAVOURAS et al., 1999; SIMONEIT, 1985; YADAV; TANDON; ATTRI, 2013a). Any negative values of C*n* were set to zero. The percentage of total wax *n*-alkanes to total *n*-alkanes (% WNA) was calculated as follows (GOGOU et al., 1996):

$$\%\ WNA = \frac{\sum WNA\ Cn}{\sum NA} \times 100 \qquad \textbf{(Equation 3.12)}$$

% WNA C*n* is the sum of the concentrations of odd carbon-numbered *n*-alkanes arising from plant waxes and ΣNA is the total concentration of *n*-alkanes in the sample.

Petrogenic *n*-alkane (% PNA) contribution was calculated by subtracting the % WNA from the total *n*-alkane (SIMONEIT, 1985; YADAV; TANDON; ATTRI, 2013a):

$$\%\ PNA = 100 - \%\ WNA \qquad \textbf{(Equation 3.13)}$$

3.6.7. Statistical analysis

Statistical analyses were conducted using PyCharm 2023.2.5 for Windows. ANOVA, Shapiro-Wilk normality test, Wilcoxon test, and Spearman Rank Test Correlation were performed to identify the similarities and differences between the samples and to evaluate the influence of region and season on the PAHs, AHs, and saccharides distribution.

3.7. Research Article 4 – Real-time monitoring of nitrogen oxides emission factors using sensors in the exhaust pipes of

heavy vehicles in the Metropolitan Region of Rio de Janeiro.

The following description of methods refers to chapter 7, page 138.

3.7.1. Sensor

The NO_x sensor used in this study was developed by Continental Automotive Co. (UniNOx model, Hanover, Germany) (Figure 3.2). It consists of a probe and a command module, which are securely connected by a cable harness forming a unit. This sensor unit is installed in the exhaust system and is used to detect NO_x in the exhaust gas flow.

It is an important component of the treatment system for NO_x reduction that is used in diesel vehicles with exhaust gas recirculation (EGR), an emission control technology allowing significant NO_x emission reductions from most types of diesel engine. The NO_x sensor has a Nernst cell and a second cell called pumping cell. The NO_x sensor measuring probe consists of zirconium oxide ceramic and has two chambers, one of which is open to the side of the exhaust, which are located three pairs of electrodes called pumping cells. The operating temperature of the sensor is 800 ºC and to reach this temperature there is a resistance to perform sensor heating (WANG et al., 2022a, 2022b).

The NO_x sensor has its own electronic module that works at voltages of 125 or 250 V. It uses the batteries of vehicles with power source. It works with the J1939 protocol, a network standard used in various vehicles and equipments that are powered by motors with electronic controls. The sensors operate continuously 24 hours a day, 7 days a week; however, measurements are taken only when the vehicles are turned on. Specific concentration ranged from 0 to 1,500 ppm with precision of ± 10 ppm. The sensor comes with factory calibration and a self-correction system. It has a lifespan of 36,000 h and was used during the sample period for less than 1,000 h.

3.7.2. Data Collection

The records were collected using the remote sensing devices provided by Case Zane (Rio de Janeiro, Brazil). The measures are done per minute. The sensor was installed in the exhaust system and measured the gases that passed through its measurement chambers (Figure 3.2). The sensor makes a request for all measurements and stores them until it connects to the mobile network and sends it to the Green-IoT cloud. The Green-IoT database is a database in which the data is stored as object. The stored object follows an agreed data format, called Sensor Markup Language (SenML). SenML includes the name of the sensor responsible for the measurements, the time when the measurements are taken, and a nested object that includes all the measurements.

Figure 3.2. NO_x sensor and control module installed in the vehicles tested for this study.

3.7.3. Test Trucks

The study was performed in MRRJ, Brazil, from July to September 2022. The sensors were placed in 9 heavy-duty diesel vehicles (HDDV) with EGR control technique. Vehicles are used in the delivery of large goods daily within MRRJ and all trucks are in a phase of PROCONVE that will soon be discontinued (P-7) and can be compared shortly with P-8 to assess the gains. Table 3.2 summarizes the main characteristics of the tested vehicles.

Vehicle exhaust emissions are usually measured with a gas analyzer and reported in parts *per* million (ppm). It is crucial to compare these

emissions with the vehicle emission standards. Previous research has shown a correlation between vehicle emission concentration and specific fuel consumption, which is typically reported in grams per kilowatt-hour (g kWh^{-1}) for heavy-duty vehicles (VERGEL-ORTEGA; VALENCIA-OCHOA; DUARTE-FORERO, 2021). For the general conversion of the emission gas concentration (ppm) into specific fuel consumption (g kWh^{-1}) for HDDVs, the following formula was used (PILUSA; MOLLAGEE; MUZENDA, 2012; VERGEL-ORTEGA; VALENCIA-OCHOA; DUARTE-FORERO, 2021):

$$NOx\ \left(\frac{g}{kWh}\right) = 6.636\ x10^{-3}\ x\ NOx\ (ppm) \qquad \textbf{(Equation 3.14)}$$

Empirical constants were obtained and reported in the literature comprising the molecular mass of the exhaust gases on a wet basis (in g mol^{-1}), the power (in kW), and the molecular mass of the components (in g mol^{-1}) (VERGEL-ORTEGA; VALENCIA-OCHOA; DUARTE-FORERO, 2021).

Table 3.2. Summary of vehicles tested with NO_x sensor.

Truck ID	Type	Year	Maximum Net Power - hp (kW) @rpm (*)	Measured data
445	TOCO	2013	186 (137) @ 2.400	17,318
456	TOCO	2013	186 (137) @ 2.400	19,907
160	TRUCK	2014	277 (204) @ 2.300	24,160
457	TRUCK	2019	277 (204) @ 2.300	7,932
595	TRUCK	2014	277 (204) @ 2.300	25,004
905	TRUCK	2013	277 (204) @ 2.300	29,386
931	TRUCK	2013	277 (204) @ 2.300	20,633

932	TRUCK	2013	277 (204) @ 2.300	16,303
951	TRUCK	2013	277 (204) @ 2.300	12,299

3.8. Research Article 5 – Real-Time Analysis of NO_x Emissions in Heavy-Duty Diesel Vehicles: Impact of Speed and Variations Across Vehicle Groups.

The following description of methods refers to chapter 8, page 147.

3.8.1. NO_x monitoring

This study monitored NO_x emissions using the Smart UniNOx sensor (Model Ger 2.8 - 24V) developed by Continental Automotive (Hannover, Germany). This sensor comprises a detection unit and a control module, which are tightly coupled by a cable. It operates using the J1939 protocol, a widely adopted communication standard for electronically controlled vehicle engines. The sensor operates continuously 24/7 and measures NO_x concentrations from 0 to 1,500 ppm with an accuracy of ±10 ppm and is factory-calibrated with an integrated self-calibration system. The sensor's expected lifetime is 36,000 h, with less than 1,000 h measured during this study. No public OBD/CAN data were used in this study. A data collection and analysis scheme can be seen in Figure 3.3.

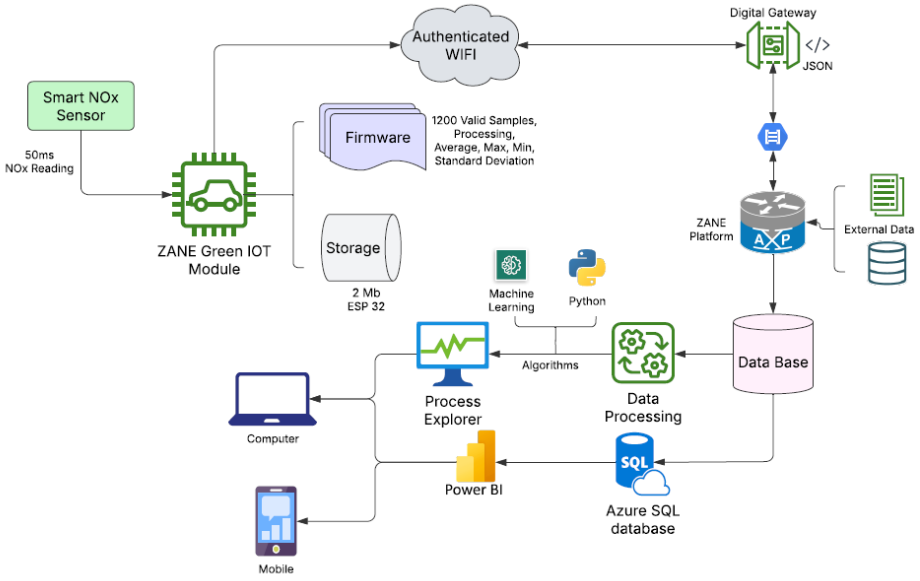

Figure 3.3. NO_x scheme of the data collection process.

Data acquisition was performed using a remote sensing system developed by Zane (Rio de Janeiro, Brazil). The system collected NO_x emission data every 50 milliseconds, storing 1,200 measurements *per* min. These measurements were processed to calculate the mean, maximum, minimum, and standard deviation for NO_x concentrations, along with the mean O_2 percentage. Only data collected while the vehicle was in motion were considered for further analysis.

The processed data were transmitted via a Green IoT module to a cloud database, where additional validation was performed. The platform stores fuel consumption data and geographical coordinates along with emission records. Data classification was based on operational parameters such as average speed, engine status, and O_2 proportion.

The NO_x sensors were installed in fourteen HDDVs equipped with either Exhaust Gas Recirculation (EGR) or Selective Catalytic Reduction (SCR) control systems.

The vehicles were grouped according to the area of the city they were passing through and the type of cargo they were carrying (Table 3.3). These are the WM vehicles, which travel from the MRRJ to the state's mountainous regions, where they deliver large quantities of goods every day. The M vehicles, which circulate in the MRRJ, mainly in the southern zone of Rio

de Janeiro, are responsible for delivering dry cargo to supermarkets in Rio de Janeiro.

The 204 kW WM vehicles are equipped with a 6-cylinder, 6.871 cm^3 MAN D08 engine, using common rail injection. On the other hand, the 13 kW WM vehicles are equipped with the same MAN D08 engine but with 4 cylinders and 4.580 cm^3, maintaining the same injection technology. The 188 kW M vehicles are equipped with a 4-cylinder, 4.8 L OM 924 LA engine. All vehicles analyzed operate with S10 diesel, which has a maximum of 10 ppm of sulfur and meets the PROCONVE P-7 environmental standards, in addition to containing a 12 % biodiesel blend. S10 diesel has a cetane number of up to 48, which can impact combustion efficiency and NO_x emissions. Vehicle operating conditions were also considered, with trucks operating at speeds ranging from 20 km h^{-1} in urban areas to up to 70 km h^{-1} on highways.

3.8.2. Vehicle exhaust emissions

Vehicle exhaust emissions were determined using a gas analyzer (sensor) and expressed in parts *per* million (ppm). A formula was used to convert the measured gas concentration (ppm) to specific fuel consumption (g kWh^{-1}) for HDDV vehicles to facilitate comparisons with established vehicle emission standards. The formula used empirical constants from the literature and considered the exhaust gas molecular mass and engine power (HESEDING; DASKALOPOULOS, 2006; PILUSA; MOLLAGEE; MUZENDA, 2012).

$$NOx\ \left(\frac{g}{kWh}\right) = 6.636\ x10^{-3}\ x\ NOx\ (ppm) \qquad \textbf{(Equation 3.15)}$$

The ppm conversion measured in g kWh^{-1} is based on the empirical relationship presented by Pilusa *et al.* (2012). However, this factor depends on the relationship between exhaust flow and power output. This engine-specific value will provide an approximate figure for converting ppm into g

kWh^{-1}, but it certainly cannot be generalized. In addition, any exhaust after-treatment system (such as EGR or SCR systems of different efficiency) is not considered in the conversion.

3.8.3. Data preparation

3.8.3.1. Outliers

An outlier is a part of a dataset that does not conform to the available dataset. Outlier detection refers to finding patterns in data that do not conform to the expected behavior. Outliers, widely separated from the main body of data points in a sample, are a common feature of real-world datasets. Furthermore, the occurrence of outliers can have an adverse effect on any further processing or analysis of the data. It can lead to misleading results if the dataset with outliers is used (SANDBHOR; CHAPHALKAR, 2019). Therefore, preprocessing NO_x data is performed to detect and eliminate outliers from the database.

Table 3.3. Summary of vehicles tested with NO_x sensor.

Truck ID	Type	Year	The Gross Vehicle Weight (GVW) (kg)	Maximum Net Power hp(kW) @rpm (*)	Amount of data measured (each data with 1,200 valid measurements)	Aftertreatment	Area	PROCONVE phase
M118	TRUCK	2019	23,000	256(188) @ 2,200	42	EGR	South of Rio de Janeiro's city (RJ)	P7
M119	TRUCK	2019	23,000	25 (188) @ 2,200	449	EGR		P7
WM445	TOCO	2013	16,000	186(137) @ 2,400	1188	EGR		P7
WM456	TOCO	2013	16,000	186(137) @ 2,400	2545	EGR	Metropolitan Region of Rio de Janeiro ((MRRJ)	P7
WM160	TRUCK	2014	23,000	277(204) @ 2.300	1585	EGR		P7
WM457	TRUCK	2019	23,000	277(204) @ 2,300	810	EGR		P7

WM595	TRUCK	2014	23,000	277(204) @ 2,300	1737	EGR		P7
WM905	TRUCK	2013	23,000	277(204) @ 2.300	883	EGR		P7
WM931	TRUCK	2013	23,000	277(204) @ 2.300	589	EGR		P7
WM932	TRUCK	2013	23,000	277(204) @ 2.300	198	EGR	Metropolitan Region of Rio de Janeiro (MRRJ)	P7
WM951	TRUCK	2013	23,000	277(204) @ 2.300	499	EGR		P7
WM1381	TRUCK	2019	16,000	260(191) @ 2,200	1041	SCR		P7
WM453	TRUCK	2013	16,000	186(137) @ 2,400	802	EGR		P7
WM65	TRUCK	2018	16,000	277(204) @ 2,300	212	EGR		P7

The method used was the Z score, which uses the mean and standard deviation of the data. However, outlier detection was performed for each vehicle separately since they have different emission patterns.

3.8.3.2. Global Positioning System (GPS) data

The smart meter used is equipped with GPS, so while the NO_x measurements are taken, it is possible to know the vehicle's geographic location. However, it is possible that there may be an error or loss of georeferencing signal. Therefore, an algorithm was developed to keep only latitude and longitude values belonging to Brazil in the database. The Haversine formula is used to calculate geographic distance on earth between two coordinates. If there are two different latitude and longitude values, then with the help of Haversine formula, it can be easily computed the distance. Haversine maintains an equilibrium between accuracy and computational efficiency (MONAWAR; BIN MAHMUD; HIRA, 2017). With the distance traveled between two points and the time elapsed, the instantaneous speed can be easily calculated. Even when processing GPS data, it is considered here that the speed is an estimate.

3.8.4. Statistical analysis

Statistical analysis and graphs were conducted using PyCharm 2023.2.5 for Windows. The one-way ANOVA test assessed the variance in NO_x emission factors per vehicle and in groups.

3.9. Research Article 6 –Application of WRF-Chem for Predicting Air Quality Resulting from the Formation of Photochemical Compounds in a subtropical urban environment

The following description of methods refers to chapter 9, page 167.

3.9.1. Air Quality Monitoring Network in Rio de Janeiro

We use observed concentrations of the main regulated pollutants: nitrogen monoxide (NO), nitrogen dioxide (NO_2), nitrogen oxides (NO_x), ozone (O_3), sulfur dioxide (SO_2), and meteorological data. The period

analyzed was from February 1st to April 23rd, 2023. The concentrations are measured by automatic stations in the air quality monitoring network operated by the State Environmental Institute (INEA) in the state of Rio de Janeiro (Figure 3.4) (Supplementary material 3, Table S1). The pollutants and meteorological data were employed to assess the model's performance.

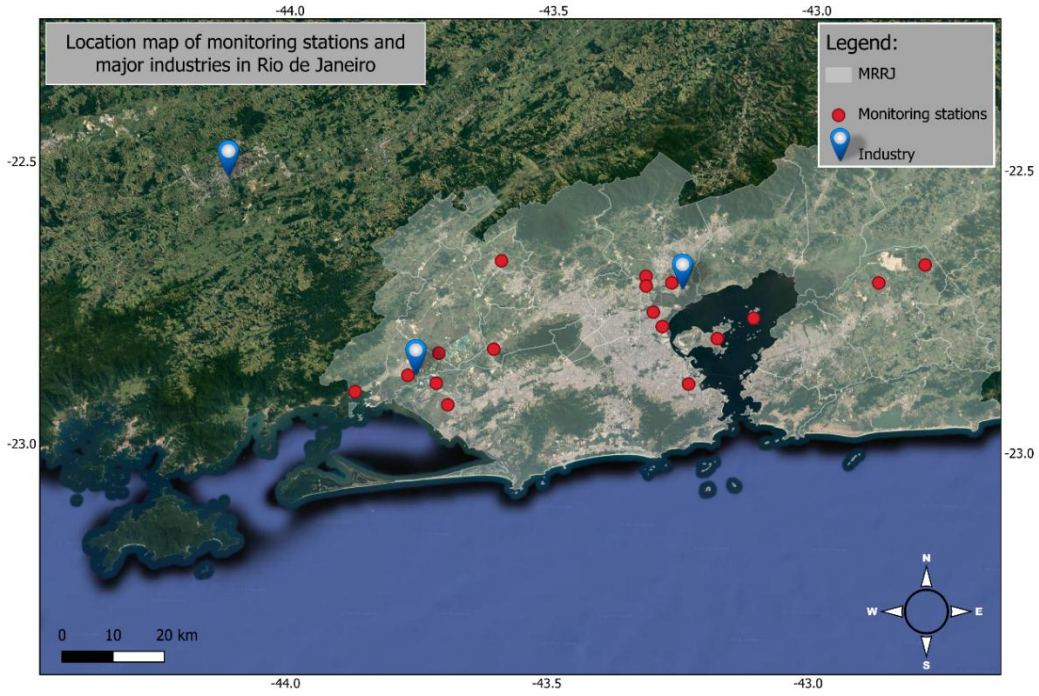

Figure 3.4. Automatic stations by the State Environmental Institute (INEA) and major industries in metropolitan region of Rio de Janeiro (MRRJ). QGIS 3.26.3.

3.9.2. Selection of Three Time Periods

We use observed concentrations of the main regulated pollutants Three 8-day periods are retained during the year 2023 which are associated with a strong deterioration of the air quality. We aim to focus on contrasting periods containing high and low O_3 and NO_x events. The three selected 8-day periods are:

1. From 6 to 14 February,
2. From 12 to 20 March,
3. From 4 to 12 April.

Thus, for the analysis of the measurement network of MRRJ, we have selected three periods and city averages to compare the observed

pollutant concentrations in MRRJ with the regional model. The average of all the stations can be used as a representation of the hourly variations in pollutant concentrations because it shows a level of agreement between the stations in the monitoring network (DEROUBAIX et al., 2024).

3.9.3. WRF-chem model

The Weather Research and Forecasting (WRF) model coupled to the chemical model (WRFchem) version 4.3.3, provided by the Max Planck Institute for Meteorology (MPI), was used for the simulations. This WRF-chem model integrates a non-hydrostatic mesoscale meteorological model (WRF) coupled online to an atmospheric and chemical transport model, allowing simultaneous forecasting of meteorology and atmospheric composition.(DEROUBAIX et al., 2024; NATIONAL CENTER FOR ATMOSPHERIC RESEARCH, 2024) Our simulation was carried out in forecast mode. The model configuration is shown in Table 3.4.

Table 3.4. Configuration of the air quality model analyzed in forecast mode with the WRFchem model carried out in the MPI.

Forecast	F-REF
Institution	MPI
Model	WRFchem (version 4.3.3)
Domain	
Horizontal resolution	10 km
Domain extension	80 x 80
Vertical levels	37
Output frequency	1h
Emission	
Anthropogenic	CAMS-GLOB-ANTv1.2 (GRANIER et al., 2019)

Anthr. temporal profiles	(CRIPPA et al., 2020)
Anthr. vertical profiles	(MAILLER; KHVOROSTYANOV; MENUT, 2013)
Biogenic	MEGANv2.1 (GUENTHER et al., 2006)
Fires	FINNv1 (WIEDINMYER et al., 2011)
Gas and aerosol	
Chemical mechanism	MOZART4 (EMMONS et al., 2010)
Aerosol scheme	GOCART (CHIN et al., 2002)
Boundary conditions	WACCM
Meteorology	
Surface scheme	Noah (EK et al., 2003)
PBL scheme	Yonsei University (YSU) (HONG; NOH; DUDHIA, 2006)
Radiation scheme	RRTMG (MLAWER et al., 1997)
Micro-Physics scheme	Thompson (THOMPSON; EIDHAMMER, 2014)
Convection scheme	Grell-3 (GRELL; DÉVÉNYI, 2002)

Met. boundary cond.	NCEP-FNL and ECMWF-ERA5

4. Research Article 1 – Spatial Variability and Source Apportionment of Particulate Matter ($PM_{2.5}$) in Rio de Janeiro: Insights from Urban, Preserved, and Biomass Burning Areas

Luis Fhernando Mendonça da Silva [1], Hellen Gonçalves Vieira [2], Ivan Víctor Silva Guillen [1], Rodrigo Stellet Ferreira [2], Vanessa A. dos Anjos [3], Ricardo Henrique M. Godoi 3, Maria Cristina Canela [2], Cibele Maria Stivanin de Almeida [2], Tatiana Dillenburg Saint'Pierre [1], Adriana Gioda [1,*]

[1]Pontifical Catholic University of Rio de Janeiro, 22451-900, Rio de Janeiro, RJ, Brazil.
[2]Universidade Estadual do Norte Fluminense Darcy Ribeiro, Laboratório de Ciências Químicas, Brazil.
[3]Departamento de Engenharia Ambiental, Universidade Federal do Paraná, 81531-980 Curitiba-PR, Brazil.

Working paper

Abstract

Air pollution is a critical environmental issue influenced by both natural and anthropogenic sources. This study analyzed particulate matter ($PM_{2.5}$) concentrations and chemical composition (black carbon (BC), elements, and ions) in three locations in Rio de Janeiro state: Gávea (urban area), PARNASO (environmental preservation area), and Campos dos Goytacazes (urban with burning biomass). The results show that $PM_{2.5}$ concentrations varied significantly among the sampled sites, with the average highest values recorded in PARNASO (20 ± 13 µg m^{-3}), followed by Gávea (12 ± 7 µg m^{-3}), and Campos (8 ± 4 µg m^{-3}). Although no daily samples exceeded Brazilian air quality standards, 23 % surpassed WHO guidelines. In all sites, Fe and Al were the most abundant elements, indicating strong soil resuspension influence, with higher concentrations in Campos. BC was higher in PARNASO (2.2 ± 0.9 µg m^{-3}) but contributed

more to $PM_{2.5}$ in Campos (22-24 %), highlighting the biomass burning influence. Water-soluble ions, particularly Cl^-, Na^+, SO_4^{2-}, and NO_3^-, were predominant across all sites, with K^+ showing statistical differences between seasonality in Campos. A Principal Component Analysis identified soil resuspension, vehicular emissions, and biomass burning as major contributors to $PM_{2.5}$ pollution. These findings underscore the need for targeted air quality policies and continuous monitoring to assess long-term trends and mitigation efforts.

Keywords: Particulate matter, ions, trace elements, black carbon, Rio de Janeiro, Principal component analysis.

4.1. Introduction

Particulate matter (PM), with an aerodynamic diameter of up to 2.5 μm ($PM_{2.5}$) is composed of various pollutants, including dust, dirt, soot, and liquid droplets. It can remain suspended in the air for long periods, posing a significant health risk as it can penetrate the lungs and even enter the bloodstream. In addition to directly affecting the respiratory system, studies indicate that toxic substances present in PM also harm the heart, leading to heart failure, cardiac arrhythmia/ischemia, and myocardial infarction (BAI et al., 2019; GORR; FALVO; WOLD, 2017; SANTA-HELENA et al., 2021). Additionally, $PM_{2.5}$ can negatively impact the environment by reducing visibility and contributing to air pollution. Due to its complexity and heterogeneity, the effects attributed to these pollutants can vary depending on the particle size, solubility, and chemical composition (CORREA et al., 2023; MAKKONEN et al., 2010; MENG et al., 2019).

$PM_{2.5}$ consists of inorganic ions (30 % to 50 %), metals (between 1 % and 5 %), black carbon (approximately 5 % to 25 %), and organic compounds in varying concentrations (SEARES et al., 2021; SEINFELD; PANDIS, 2016; SILVA et al., 2024a). Among these contaminants, metals are widely known for their toxicological potential. However, black carbon (BC) has received considerable attention due to its ability to absorb solar radiation, leading to atmospheric warming (GIDHAGEN et al., 2021; SEINFELD; PANDIS, 2016; YAMASOE et al., 2000). Furthermore, there is

evidence of adverse health effects associated with BC, such as hypertension (especially in pregnant women) and potential carcinogenicity due to its penetration into the bloodstream and organs (ZHU et al., 2024).

Legislation on $PM_{2.5}$ varies by country and organization, with regulatory setting limits to protect public health and the environment. In Brazil, it is one of the nine air pollutants monitored by the State Institute for the Environment (INEA), and it is used as an indicator of air quality, with limits established by Brazilian legislation (CONAMA, 2024). In Brazil, $PM_{2.5}$ is associated mainly with vehicular emissions, with BC being a pollutant used as a marker for heavy vehicles. The state of Rio de Janeiro has the second-largest metropolis in the country and ranks second among the states with the largest economies in Brazil (ANDRADE et al., 2012; DE MIRANDA et al., 2012). Several studies have already been conducted in this state to understand the chemical composition of PM present in the atmosphere of various cities (BERINGUI et al., 2021; FERREIRA et al., 2021; MATEUS et al., 2020; SEARES et al., 2021). However, as far as this work could assess, this is the first study to compare regions with different contamination profiles. For this purpose, the study locations selected were the Serra dos Órgãos National Park (PARNASO), based in the city of Guapimirim; Gávea, a neighborhood in the southern part of the city of Rio de Janeiro and sited at the Pontifical Catholic University of Rio de Janeiro (PUC-Rio), and the State University of Northern Rio de Janeiro (UENF) in the city of Campos dos Goytacazes (Campos). PARNASO is an environmental preservation area of the Atlantic Forest; however, anthropogenic pollution sources, such as agricultural activities and vehicular emissions, have already been reported in this region. On the other hand, PUC-Rio is located in a highly urbanized area near the coast. Finally, UENF is located in the north of the state and characterized by agricultural activities, mainly sugarcane cultivation. It has been recently influenced by truck traffic accessing the Açu Port Complex in São João da Barra-RJ (MATEUS et al., 2020; SILVA et al., 2024a; VIEIRA et al., 2023).

In this context, this article aims to analyze the composition of $PM_{2.5}$ in different regions of Rio de Janeiro with distinct levels of human activities, focusing on organic and inorganic ions, elements, and black carbon. The

findings will improve our understanding of the dynamics of these particulate compounds, quantifying their concentrations and detailing seasonal variations, as well as providing a more comprehensive view of the reactions and dynamics of these compounds present in the atmosphere of the state of Rio de Janeiro and the interactions between them. This study is part of a larger project that aims to chemically characterize samples of particulate matter and precipitation in three regions of the state of Rio de Janeiro.

4.2. Materials and Methods

Description in topic 3.4, page 39.

4.3. Results and Discussion

4.3.1. Quality assurance and quality control (QA/QC)

4.3.1.1. Analysis of ultrapure water and nitric acid

Ion chromatography analysis of the ultrapure water used in the extraction, with and without filtration, indicated that the Li^{+}, Mg^{2+}, Ca^{2+}, F^{-}, NO_2^{-}, Br^{-}, $CH_2(COO)_2^{2-}$, $C_2O_4^{2-}$ ions had concentrations below the instrumental detection limit (LOD). The remaining ions were present in low concentrations, with most values below the instrumental quantification limit (LOQ).

The double-distilled nitric acid used in the study was also analyzed to assess its quality. Most of the elements analyzed were below the LOD. The metals with the highest measured concentrations were Al and Fe, with average values of 0.25 ± 0.02 mg kg^{-1} and 0.06 ± 0.01 mg kg^{-1} respectively.

4.3.1.2. Blank Filters

As part of the quality control, BFs were extracted with both water and double-distilled nitric acid. Analysis of the extracts showed that some ions and metals were present in significant concentrations in the composition of the filters. In the aqueous extraction, the ions Na^{+}, K^{+}, CH_3COO^{-}, $CHOO^{-}$, Cl^{-}, NO_3^{2-} and SO_4^{2-} were detected in concentrations above the instrumental LOD, while the ions Mg^{2+}, Ca^{2+}, Br^{-} and $C_2O_4^{2-}$ were below the LOD.

On the other hand, in the acid extracts, the metals with concentrations higher than the LOQ were Al, Ca, Co, Cu, Fe, Mn, Ti, and Zn. The presence of these metals is related to the manufacturing processes. According to the manufacturer, the filters contain high concentrations of Fe (200 mg kg^{-1}), Mn (10 mg kg^{-1}), Zn (20,000 mg kg^{-1}), and Cu (4.5 mg kg^{-1}). It is also important to note that incorrect handling, inadequate transportation or storage conditions can influence the quality of the filters. The elements Cd, Ce, Cr, La, Ni, Pb, Sb, Se and V were not detected in the composition of the filter strips analyzed. After analyzing the BF extracts, those anomalous values were eliminated using the Grubbs test.

Finally, the discounted value of the samples was the average of the values that were not considered anomalous.

4.3.1.3. Washed and unwashed blank filters

Due to the lack of options for Hi-vol filters, the fact that their composition is not homogeneous throughout and the need to find ways of reducing the interference of contaminants in the filters, some tests were carried out to find ways of reducing some of the problems related to them. Pre-treating the filters aimed to minimize background contamination prior to analysis, assessing the ion and element concentrations between washed and unwashed filters (Figure 4.1). The results showed that washing effectively removes some ions, while others remained unchanged or, in some cases, increased after treatment. There was a significant reduction in the concentrations of Mg^{2+} ($p = 2.58 \times 10^{-5}$), Ca^{2+} ($p = 0.004$), Cl^- ($p = 0.020$), Br^- ($p = 0.012$), NO_3^- ($p = 0.006$) and SO_4^{2-} ($p = 0.006$) in the washed filters, indicating that these ions were mainly present as surface contaminants and were effectively removed by washing with ultrapure water. On the other hand, the CH_3COO^- ($p = 0.004$) and $HCOO^-$ ($p = 0.0003$) ions showed a significant increase after washing, which may indicate contamination during the cleaning process, possibly from the handling of the filters. In addition, other ions such as F^-, NO_3^-, $(C_2O_4)^{2-}$, and PO_4^{3-} did not show statistically significant differences between the washed and unwashed filters, suggesting that the washing procedure did not effectively alter their concentrations.

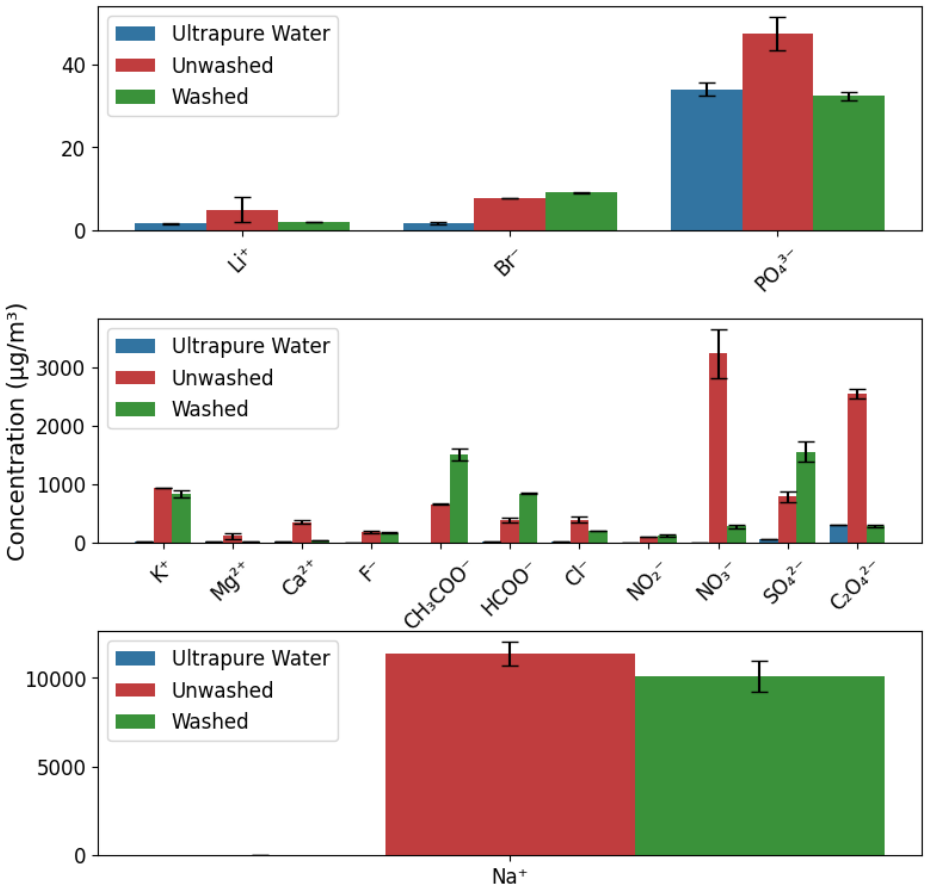

Figure 4.1. Concentrations of the ions present in the blank filter extracts (error bar ± SD).

Similarly, the acid wash procedure was applied to evaluate its effectiveness in removing contaminants from filter (Figure 4.2). The results demonstrated that the treatment significantly reduced the concentrations of Cu ($p = 0.026$), Br ($p = 0.012$), Y ($p = 0.044$), Zr ($p = 0.048$), Ag ($p = 0.021$), Cs ($p = 0.033$), Er ($p = 0.025$), Pb ($p = 0.016$) and Bi ($p = 0.039$), suggesting that these metals were mainly present as surface contaminants and were effectively removed by the acid wash. These results highlight the efficiency of the acid treatment in eliminating certain trace metals that could interfere in the subsequent analyses and indicate possible alternatives that can help eliminate some contaminants from BF. On the other hand, the concentrations of other elements did not show significant differences ($p > 0.5$), and they may indicate that these elements are more strongly retained by the filter matrix, making their removal less effective, or that their initial concentrations were too low to detect a significant change.

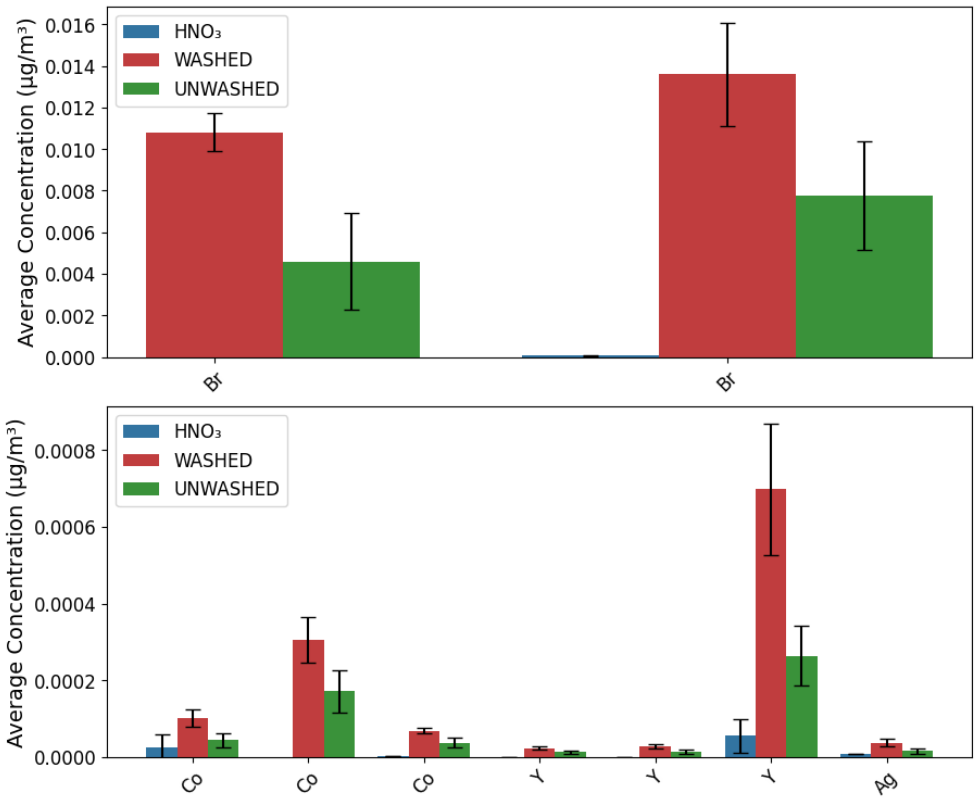

Figure 4.2. Concentrations of the elements present in the blank filter extracts (error bar ± SD).

4.3.1.4. Analysis of BF extracts with and without filtration

The aqueous extracts of the blanks go through a filtration process to remove particles that could damage the columns or other parts of the Ion Chromatograph. The membranes used for filtration are 0.22 µm cellulose acetate. This pore size removes particles and microorganisms. These membranes were also assessed for their quality. In the tests carried out on the aqueous extract, with and without filtration, it was observed that the F^-, SO_4^{2-}, K^+, Ca^{2+}, NO_3^- and PO_4^{3-} ions showed higher concentrations in the extracts without filtration, with the most significant differences being observed for NO_3^- and K^+. The $CHOO^-$, Cl^-, Na^+, CH_3COO^- and $C_2O_4^{2-}$ ions showed higher concentrations in the filtered extracts. The NO_2^-, Li^+ and Mg^{2+} ions showed similar values in the two methodologies. Figure 4.3 shows the values found in the two methodologies. Although some ions showed higher values depending on the extraction, this difference was not statistically significant ($p > 0.5$).

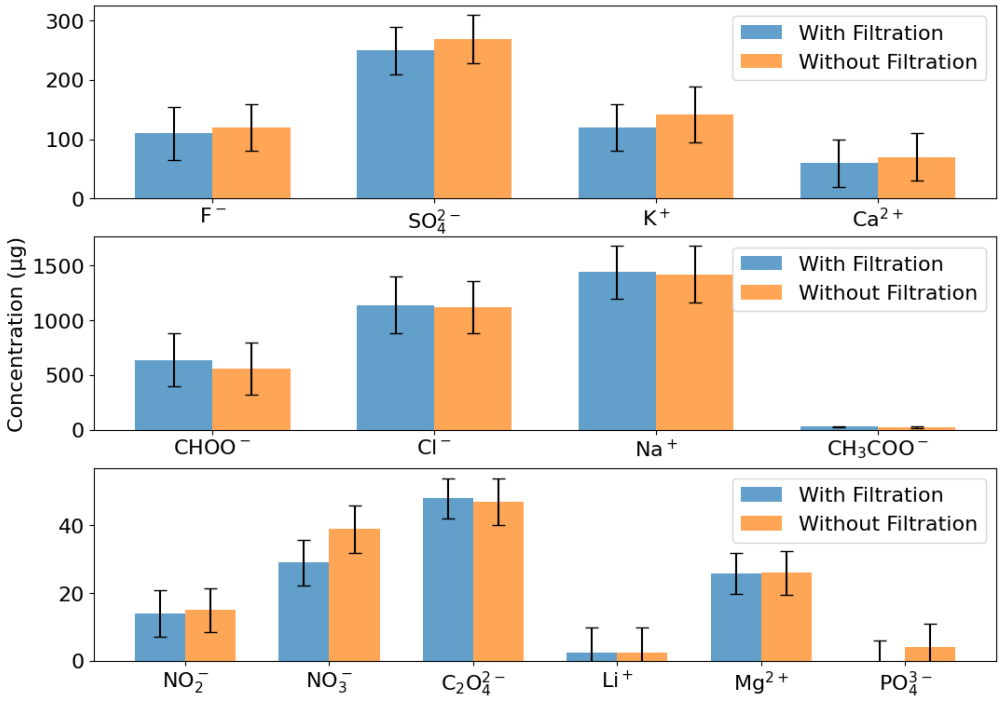

Figure 4.3. Ion concentrations in blanck filters with and without filtration through a 0.22 µm cellulose-acetate membrane (erro bar ± SD).

As the results showed no significant differences, we opted to use filtration with a cellulose acetate membrane. The advantage of this method is that it minimizes the entry of particles into the system, and even microorganisms, which could affect the analysis.

4.3.1.5. Evaluation of Acid Extraction Efficiency (SRM 1648a)

The efficiency of the acid extraction method for PM was evaluated by extraction of the standard reference material (SRM 1648a - Urban dust). This reference sample contains among its components all the elements that are naturally present in PM collected in urban areas, thus enabling the effectiveness of the extraction process to be assessed. The analysis of the SRM 1648a was carried out by ICP-MS only because there is no certified standard for the ions present in the PM (Table S2). The extraction efficiencies ranged from 12 % (Ti) to 97 % (Cu). The elements with the lowest extraction efficiencies were Cr (25 %), Sb (22 %), Ti (12 %). The low recoveries of the other metals may indicate the need for more vigorous extractions since some of these metals, such as Cr, tend to appear in the

form of refractory oxides.

Metals such as Al, Cu, Fe, Mn, Pb, V, and Zn showed recovery percentages of over 70 %. Although the extractions were not complete for all the elements, nitric acid was efficient, as the extraction percentage was high for most of the elements (Table 4.1). Similar values were reported by Mateus *et al.*, 2013, except for Al and V, which were below 70 %.

Table 4.1. Measured concentration (average ± standard deviation) and extraction efficiencies for the analysis by ICP-MS of the certified reference material NIST-SRM 1648a.

Element	Reference (mg kg^{-1})	Measurement (mg kg^{-1})	Efficient of extraction (%)
Al	34300 ± 1300	25646 ±1472	75
Ca	58400 ± 1900	39846 ± 6342	68
Cd	74 ± 2	71 ± 4	96
Ce	55 ± 2	26 ± 3	47
Co	18 ± 1	13 ± 2	72
Cr	402 ± 17	104 ± 16	26
Cu	610 ± 86	591 ± 2	97
Fe	39200 ± 2100	33849 ± 1991	86
La	39 ± 3	23 ± 1	59
Mn	790 ± 44	751 ± 70	95
Ni	81 ± 7	69 ± 4	85
Pb	6550 ± 330	6242 ± 581	95
Sb	45 ± 1	10 ± 1	22
Ti	4021 ± 86	480 ± 14	12
V	127 ± 11	98 ± 16	77
Zn	4800 ± 270	4560 ± 294	95

4.3.2. $PM_{2.5}$ concentration in Rio de Janeiro

In Brazil, air quality standards (annual arithmetic mean concentration and 24-hour average) are established by the National Environmental Council (CONAMA) through Resolution (RE) 506/2024. The RE defines the new interim quality standards (IS), established as temporary values to be met in stages, and the final air quality standard (FS), based on guide values defined by the World Health Organization (WHO) in 2021 (15 µg m^{-3}) (WHO, 2021). At the time the samples were taken, interim standard 1 (IS-1) was in force, where the annual arithmetic average of $PM_{2.5}$ must not exceed 20 µg m^{-3}, and the 24-h average concentration must not exceed 60 µg m^{-3} more than once a year (CONAMA, 2024). In this study, none of the sampled days exceeded the threshold Brazilian regulations (60 µg m^{-3}) recommended. However, 23 % of the samples exhibited daily concentrations surpassing the guidelines set by the WHO (15 µg m^{-3}). The average concentration of $PM_{2.5}$, standard deviation (SD), minimum, maximum and number of daily PM exceedances according to the WHO standard are displayed in Table 4.2.

Table 4.2. Descriptive statistics concentration (µg m^{-3}) of $PM_{2.5}$ by location from February 2022 to July 2023, and the number of violations of the daily WHO guideline (15 µg m^{-3}) and CONAMA legislation (60 µg m^{-3}).

	Gávea	PARNASO	Campos
Average concentration ± SD (µg m^{-3})	12 ± 7	20 ± 13	8 ± 4
Minimum (µg m^{-3})	5	9	4
Maximum (µg m^{-3})	32	45	17
CONAMA violation (IS-1)	0	0	0
WHO violation	4	6	1

n	17	14	16

The Gávea region, located in a dense urban area, showed $PM_{2.5}$ average concentrations of 12 ± 7 μg m^{-3}. This value is consistent with that found in the same region in other studies carried out (DE LA CRUZ et al., 2024) and similar values found in other regions of Rio de Janeiro, such as Urca, Recreio dos Bandeirantes, Lagoa and Copacabana (DE LA CRUZ et al., 2024; GODOY et al., 2009; VENTURA et al., 2019). These neighborhoods and also Gávea and the city of Campos dos Goytacazes are located near the ocean, where the sea breeze favors the dispersion of atmospheric pollutants (VENTURA et al., 2018).

The Serra dos Órgãos National Park (PARNASO) had the highest average of $PM_{2.5}$. This can be explained by factors such as the location where the sample was taken being close to the park entrance, as well as the influence of regional transport of pollutants, especially from adjacent urban areas, and the possible contribution of seasonal fires, which are common in forested areas. This finding also suggests that nearby human activities and fires can seriously affect air quality even in protected areas.

It was observed that $PM_{2.5}$ concentrations were notably higher during the dry season (May to November) compared to the rainy season (December to April) across all regions, with significant statistical differences between the two periods (p-value = 0.001 in Gávea; 0.02 in Campos; and 0.04 in PARNASO). Furthermore, a strong negative correlation between PM levels and precipitation (r = -0.8) was found, indicating that during the rainy season, when rainfall peaks, PM concentrations in the atmosphere tend to decrease in the studied regions. This trend has been documented in several previous studies (DE LA CRUZ et al., 2024; GIODA et al., 2016; MATEUS et al., 2013; SILVA et al., 2024a), with the "cleansing effect" of rain being commonly cited as the main reason for this phenomenon, where precipitation captures and removes airborne particles (LATIF; OTHMAN; HASSAN, 2021; SILVA et al., 2024a; THOMPSON; EIDHAMMER, 2014; WANG et al., 2023a).

4.3.3. Soluble ions in $PM_{2.5}$

Figure 3 shows the distribution of the sum of ions concentrations (µg m^{-3}) for each location (Gávea, PARNASO, and Campos) and ions levels between the dry season (May–November) and the rainy season (December–April) for each site during the sampling period from February 2022 to June 2023. The major ions (Cl^-, Na^+, SO_4^{2-} and NO_3^-) were detected at all sites (Supplementary material 1, Table S2).. Ions are derived from anthropogenic and biogenic sources, such as biomass burning, fossil fuels, natural plant emissions, and marine aerosol particles (BERINGUI et al., 2021). The sampling locations suggest a significant marine influence, with sea spray being a possible natural source of Cl^-, SO_4^{2-}, Na^+, K^+, Ca^{2+} and Mg^{2+} ions.

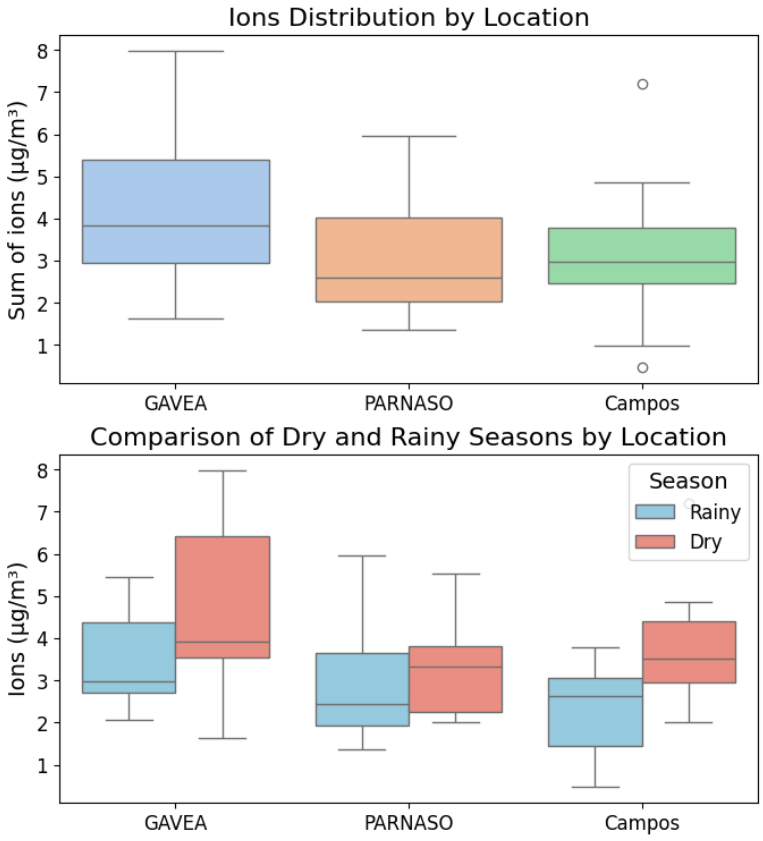

Figure 4.4. Distribution of the sum of ions concentrations (µg m^{-3}) for each location (Gávea, PARNASO, and Campos) and ions levels between the dry season (May–November) and the rainy season (December–April) for each site, during the sampling period from February 2022 to June 2023.

There was no significant statistical difference between the ions and seasonality ($p > 0.05$) in all sites, except for K^+ in Campos, which showed a marked variation between the dry (0.1 ± 0.1 µg m^{-3}) and rainy periods (0.05 ± 0.03 µg m^{-3}) ($p = 0.02$) (Figure 4.5). Various emission sources contribute to K^+ emissions, including sea salt, dust, coal combustion, and waste incineration (KONG et al., 2014; XIAO et al., 2017). In Campos dos Goytacazes, biomass burning occurs during the sugarcane harvest season (dry period). In receptor models, K^+ is commonly used as a tracer for biomass burning due to its presence in plants in the forms of KCl, K_2SO_4, and KNO_3 (LI et al., 2003).

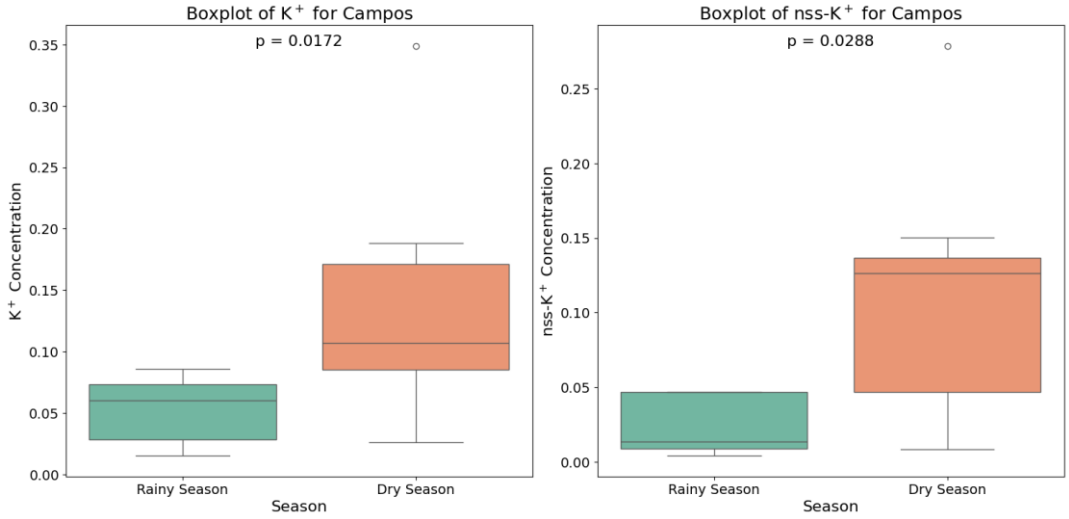

Figure 4.5. The concentration of K^+ and nss-K^+ (µg m^{-3}) exhibited seasonal variation during the sampling period in Campos dos Goytacazes from February 2022 to June 2023.

Our previous study on mercury in particulate matter (SILVA et al., 2024a) analyzed air mass trajectories and pollutant transport, revealing distinct seasonal patterns across the three sites. During the dry season, Gávea was influenced by air masses from the Andes and central/southern Brazil, whereas in the rainy season, the predominant origin shifted to the Atlantic Ocean. PARNASO, in contrast, exhibited the opposite pattern. In Campos, air masses primarily arrived from the Atlantic year-round, leading to lower pollutant concentrations. Unlike Gávea and PARNASO, Campos dos Goytacazes was mainly affected by local emissions, with minimal external contributions.

In addition, during winter, Gávea and PARNASO experienced predominantly west-southwest (WSW) winds with speeds between 0 and 6 m s^{-1}, reflecting limited oceanic influence (INMET, 2024). After the dry season, marine contributions to K^+ increased, reaching approximately 60% in Gávea and PARNASO.

The findings show no significant differences between nss-SO_4^{2-}/SO_4^{2-}, nss-K^+/K^+, and nss-Ca^{2+}/Ca^{2+} across the studied sites (Table S3). In general, the sources of emissions for other ions remained consistent. According to the data, 12 - 25 % of the sulfate detected is of marine origin, with the dominant source being anthropogenic (75 – 91 %). Furthermore, nss-K^+ was correlated with NO_3^- (r = 0.9), SO_4^{2-} (r = 0.9), and Cl^- (r = 0.7), corroborating the hypothesis that biomass burning is a major contributor of K^+ in Campos.

4.3.4. Elements in $PM_{2.5}$

This study only considered the 7 main ones (Al, Cu, Fe, Mn, Pb, Ti, V and Zn), whose concentrations in $PM_{2.5}$ were above the LOQ at the 3 studied sites. The average concentrations and standard deviations of these elements in $PM_{2.5}$ samples from the studied sites (Gávea, PARNASO and Campos) are shown in Table S4.

None of the elements showed any statistical difference between the dry and rainy periods (Figure 5). Among the elements detected, Fe and Al were the most abundant in all $PM_{2.5}$ samples. Gávea presented the lowest concentrations of Fe and Cu, while Campos presented the significant concentrations (p = 0.002 and 0.001).

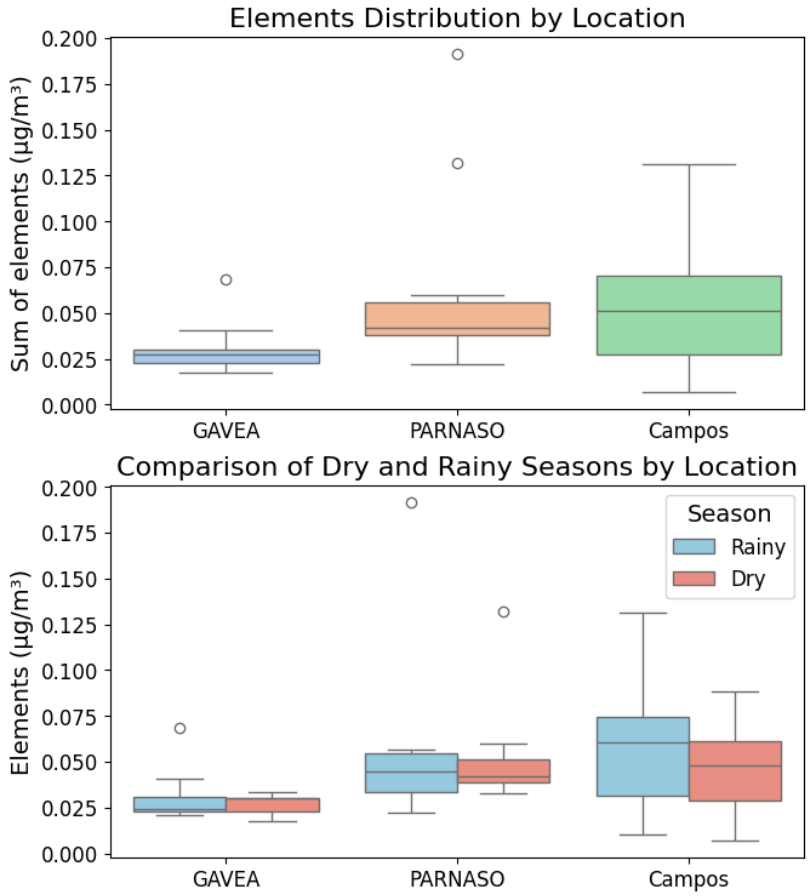

Figure 4.6. Distribution of the sum of elements concentrations (µg m^{-3}) for each location (Gávea, PARNASO, and Campos) and levels between the dry season (May–November) and the rainy season (December–April) for each site during the sampling period from February 2022 to June 2023.

Campos showed the highest concentration of Al with a significative difference between the locations ($p = 0.01$). This trend occurs mainly due to the higher concentrations of Al in these samples, which may be derived from the soil in this region. This city has soil originating from granites and gneisses, the latter being characterized by the presence of silicon and aluminum (ABBASI et al., 2020; NOGUEIRA COSTA et al., 2008).

Among the minor elements, Mn, Pb, and V showed variations in concentrations among the sites. Gávea presented the lowest average concentrations of Mn (0.17 ± 0.11 ng m^{-3}). PARNASO had average concentrations of Mn of 0.56 ± 0.36 ng m^{-3}. In Campos, the values for Mn were much higher, with averages of 3.8 ± 4.0 ng m^{-3}. Campos presented a statistical difference for Mn, but no significant difference for Pb and V, when

compared to the other sites.

In general, the distribution of concentrations of these elements in $PM_{2.5}$ samples reflects the influence of atmospheric sources, such as fossil fuel emissions and interaction with the soil. Elements such as Fe, Mn, Cu, Zn, Pb originate mainly from anthropogenic sources, such as vehicle emissions and brake wear. However, natural sources can also influence them, such as soil dust resuspension. The higher concentration of some elements, such as Fe and Cu, in Campos may indicate a greater intensity of mobile sources or industrial activities influenced by the Port of Açu. Otherwise, Gávea, located near the coast, has lower concentrations of these elements. This can be explained by the dilution caused by the sea wind, only elements coming from the prevailing sea air and little influence from the urban area (SILVA et al., 2024a). Furthermore, there is no industrial zone in the Gávea neighborhood, and the collection was carried out at PUC-Rio, where the presence of vehicular sources is more significant, as it is close to urban tunnels, bus terminals and metro lines. In general, PARNASO presented higher concentrations than Gávea and lower than Campos, showing natural sources from soil and vegetation, but also from anthropogenic sources, mainly vehicular.

4.3.5. Black carbon in $PM_{2.5}$

Black carbon (BC) is a significant component of $PM_{2.5}$, emitted mainly by combustion sources such as vehicle traffic and biomass burning (LI et al., 2019b). The values found in this study can be seen in Table 4.3. Campos dos Goytacazes, an urban area affected by sugarcane burning, presented an average BC concentration of 1.19 ± 0.63 μg m^{-3}, with values ranging from 0.33 to 2.19 μg m^{-3}. Despite being a region where sugar cane is burned, Campos has lower concentrations of BC due to its location in a flat area with a strong wind influence. This environmental factor favors the dispersion of pollutants, leading to a reduction in local concentrations of particulate matter, as well as being close to the sea, helping to dilute pollutants (VIEIRA et al., 2023). Gávea, an urban coastal location affected by vehicle traffic, exhibited an average concentration of 1.73 ± 0.49 μg m^{-3}, with a range from 0.68 to 2.54 μg m^{-3}. PARNASO presented the highest

mean concentration of BC of 2.25 ± 0.89 μg m^{-3} (0.51 to 3.85 μg m^{-3}). This finding is likely due to the location of the sampling site, which was positioned in the park parking lot, less than 100 meters from a major highway that connects Rio de Janeiro to other cities and states and the potential impact of seasonal fires.

The relative contribution of BC to $PM_{2.5}$ also varied among sites. Campos dos Goytacazes had the highest proportion, with BC accounting for 22 % ± 24 % of the $PM_{2.5}$ mass. In Gávea, BC contributed 17 % ± 7%, while in PARNASO, the proportion was the lowest, at 15 % ± 9 %. These values are consistent with previous studies that reported BC contributions ranging from 11 % to 24 % in urban environments (DE LA CRUZ et al., 2024; DE MIRANDA et al., 2012; GODOY et al., 2009; SOLURI et al., 2007).

Table 4.3. Comparison of black carbon (BC) mass concentration measured in $PM_{2.5}$ at various locations of Brazil and other countries.

	Period	Concentration of BC (μg m^{-3})		Reference
		Average ± SD	Range	
Gávea	2022 - 2023	1.7 ± 0.5	0.68 - 2.54	This study
PARNASO		2.2 ± 0.9	0.51 - 3.85	
Campos		1.2 ± 0.6	0.33 - 2.19	
Rio de Janeiro (Brazil)	2008 - 2009	3.4 ± 2.5		(DE MIRANDA et al., 2012)
Rio de Janeiro (Brazil)	2018 - 2019	1.9 ± 0.7		(DE LA CRUZ et al., 2024)
Londrina (Brazil)	2017 - 2018	1.7 ± 0.60		(JUNIOR et al., 2019)
Paranaguá (Brazil)	2017	2.3 ± 0.7	0.3 - 4.81	(GURGATZ et al., 2024)
Stockholm (Sweden)	2013 - 2018	1.3		(KRECL et al., 2024)

Chungcheong (Korea)	2015 2016	-	1.7 ± 0.5	(CHA; LEE; LEE, 2019)
Beijing (China)	2012 2019	-	5.4 ± 3.2	(ZHANG et al., 2023)
Caracas, (Venezuela)	2018 2019	-	1.8 ± 0.9	(ENGELHARDT et al., 2022)

Compared to previous studies conducted in the Metropolitan Region of Rio de Janeiro (MRRJ) during 2018-2019, our findings indicate generally lower BC concentrations, except in PARNASO. However, all sites exhibited lower values than those reported in Rio de Janeiro in 2008. This decreasing trend in BC concentrations may be linked to stricter emission control policies and fuel regulations. Several programs implemented at both national and state levels have likely contributed to this reduction, including the National Alcohol Program (PROÁLCOOL), which supplies ethanol as fuel and additive for gasoline for light vehicles, the Air Pollution Control Program for Motorcycles and Similar Vehicles (PROMOT), introduced in 2002 to regulate emissions from these vehicles, and the National Biodiesel Production Program (PNPB), which promotes biodiesel production and reduces emissions, by adding it to diesel oil. Additionally, the Vehicle Emissions Control Program (PROCONVE), established by the Brazilian National Council (CONAMA), sets emission limits for motor vehicles and regulates air pollution control measures, alongside adopting technologies to reduce pollutant emissions. Furthermore, our results remain comparable to those reported in other Brazilian cities, such as Londrina and Paranaguá (GURGATZ et al., 2024).

At the international level, the BC measured in this study were close to those observed in Caracas, Venezuela (1.8 ± 0.9 μg m^{-3}) (ENGELHARDT et al., 2022), Chungcheong, South Korea (1.7 ± 0.5 μg m^{-3}) (CHA; LEE; LEE, 2019) and Stockholm, Sweden (1.3 μg m^{-3}) (KRECL et al., 2024), but significantly lower than those recorded in Beijing, China (5.4 ± 3.2 μg m^{-3}) (ZHANG et al., 2023). Beijing has a larger population, territorial extension, vehicle fleet and industries than Rio de Janeiro, which may have contributed to the higher BC issuance.

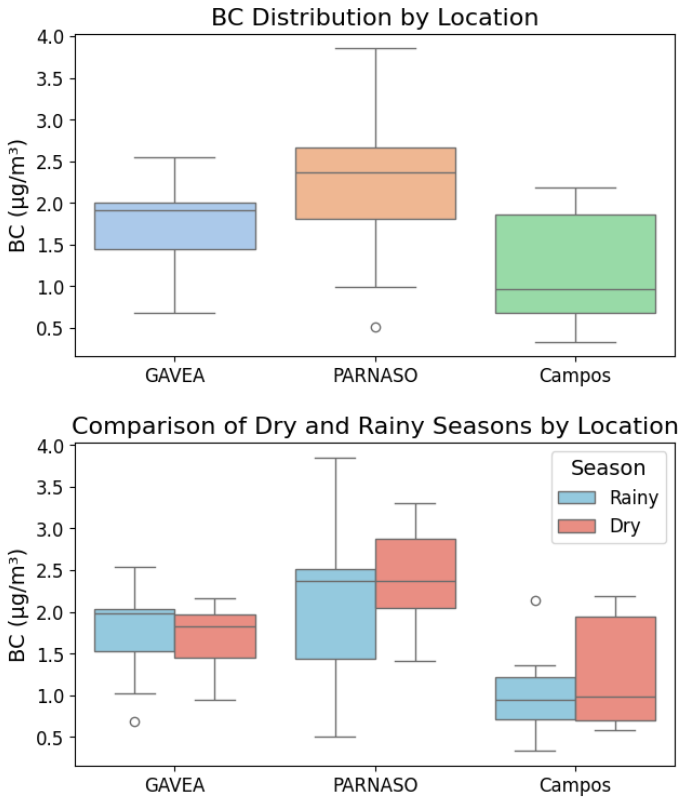

Figure 4.7. Distribution of Black Carbon (BC) concentrations (µg m^{-3}) for each location (Gávea, PARNASO, and Campos) and BC levels between the dry season (May–November) and the rainy season (December–April) for each site, during the sampling period from February 2022 to June 2023.

Despite observing higher BC concentrations during the dry season, our study found no statistically significant difference between the dry and rainy seasons (Figure 4.7). However, a significant statistical difference was identified between locations ($p = 0.01$), particularly between PARNASO and Campos dos Goytacazes. The elevated BC levels in PARNASO suggest that vehicular emissions from the nearby highway may have influenced the collected samples. In Campos dos Goytacazes, the contribution of biomass burning from sugarcane fields likely played a dominant role in the observed BC levels, and suggesting that region-specific factors, such as differences in population density and local emission sources, influence BC concentrations (ZHANG et al., 2024).

The contribution of BC to $PM_{2.5}$ in this study (15 - 22 %) is in line with findings from previous research, where BC was responsible for 17-31 % of $PM_{2.5}$ in different Brazilian cities (DE MIRANDA et al., 2012; GODOY et al.,

2009; SOLURI et al., 2007). The results reinforce the importance of traffic and biomass burning as primary sources of BC emissions in urban and semi-urban environments.

4.3.6. Principal Component Analysis

Due to the large number of samples used in this study, Principal Component Analysis (PCA) was employed to assist in data interpretation and understand each region's characteristics. The model was built using the first six principal components, retaining 65.6 % of the explained variance. The biplot presented in Figure 5 (scores and loadings plot) represents the projection of the samples onto the newly formed axes, considering PC1 versus PC2, which together explain 35.3 % of the variance (Figure 4.8). It is worth noting that no sample was identified as an outlier in the data set used in Hotelling's t^2 test.

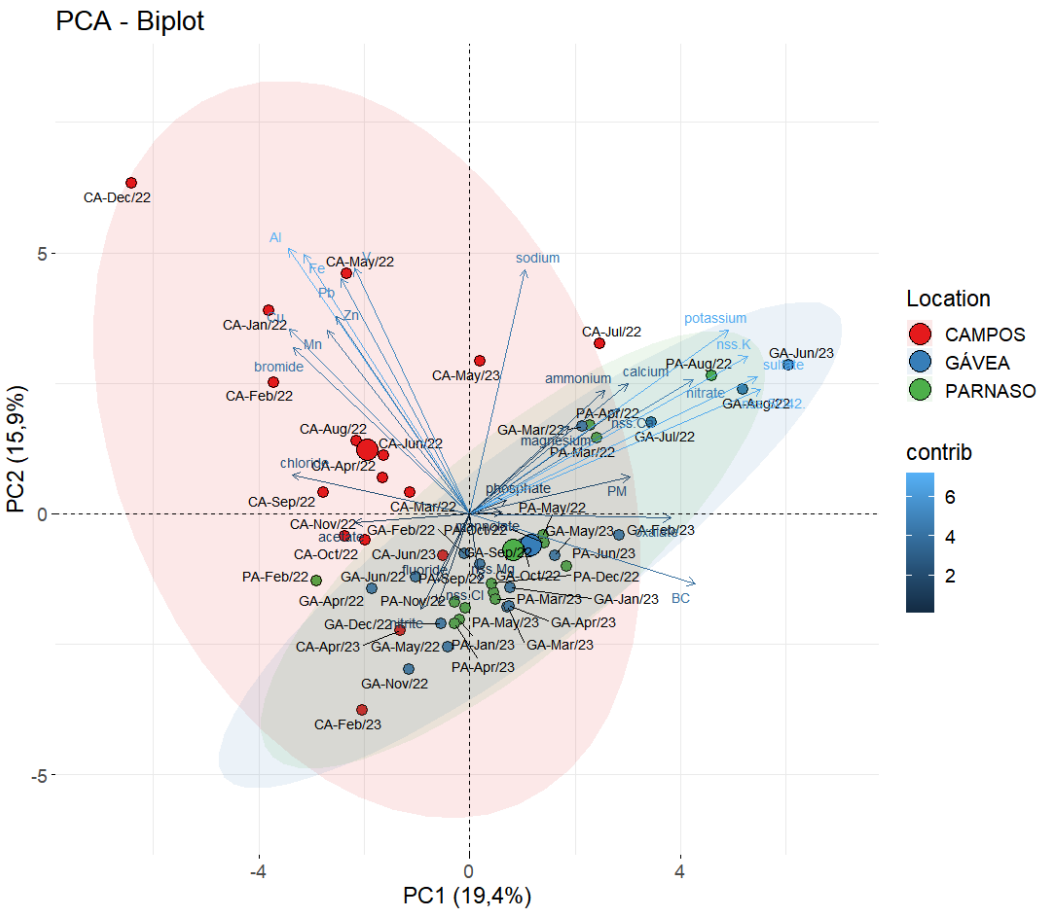

Figure 4.8. Biplot graphical with samples projected onto the new space (PC1 × PC2).

The distribution of samples along the PC1 axis indicates a tendency for separating Campos dos Goytacazes samples from the other two sites. This behavior is mainly associated with the contribution of Al, Cu, and Fe, which showed higher concentrations in these samples. Fe, and Al are elements characteristic of soil resuspension or anthropogenic sources (SEARES et al., 2021). As previously reported, the soil of Campos dos Goytacazes is rich in aluminum. Thus, soil resuspension and its specific characteristics may be associated with separating samples from this region (ABBASI et al., 2020; COSTA; POLIVANOV; ALVES, 2008). Notably, the December sample showed the highest concentrations of Fe, Ti, and Cu. Additionally, this month recorded the highest wind speed during the sampling period (average speed = 4.1 m s^{-1}), which supports the observed data.

On the other hand, the PC1 versus PC2 plot is not sufficient to fully distinguish the differences between the studied regions. The separation of PARNASO and GÁVEA samples occurs along the PC1 and PC4 axes (Figure 4.9), which explain 26.8 % of the variance.

The PARNASO and Gávea samples are separated along the PC4 axis, where the main variables are acetate, calcium, nss-Ca, bromide, BC, V, nitrate, Cu, Pb, chloride, PM, and Zn. The separation of PARNASO samples is mainly related to the higher concentrations of PM, BC, and PO_4^{3-}. Phosphate anion in atmospheric particulate matter is strongly linked to biological processes and may indicate the influence of natural sources. Phosphate is an essential nutrient for metabolic processes, and its main source in the atmosphere is biological aerosol (spores, pollen, plant matter fragments, and microorganisms). These particles can be suspended in the atmosphere by wind and other natural mechanisms (BIGIO; ANGERT, 2018).

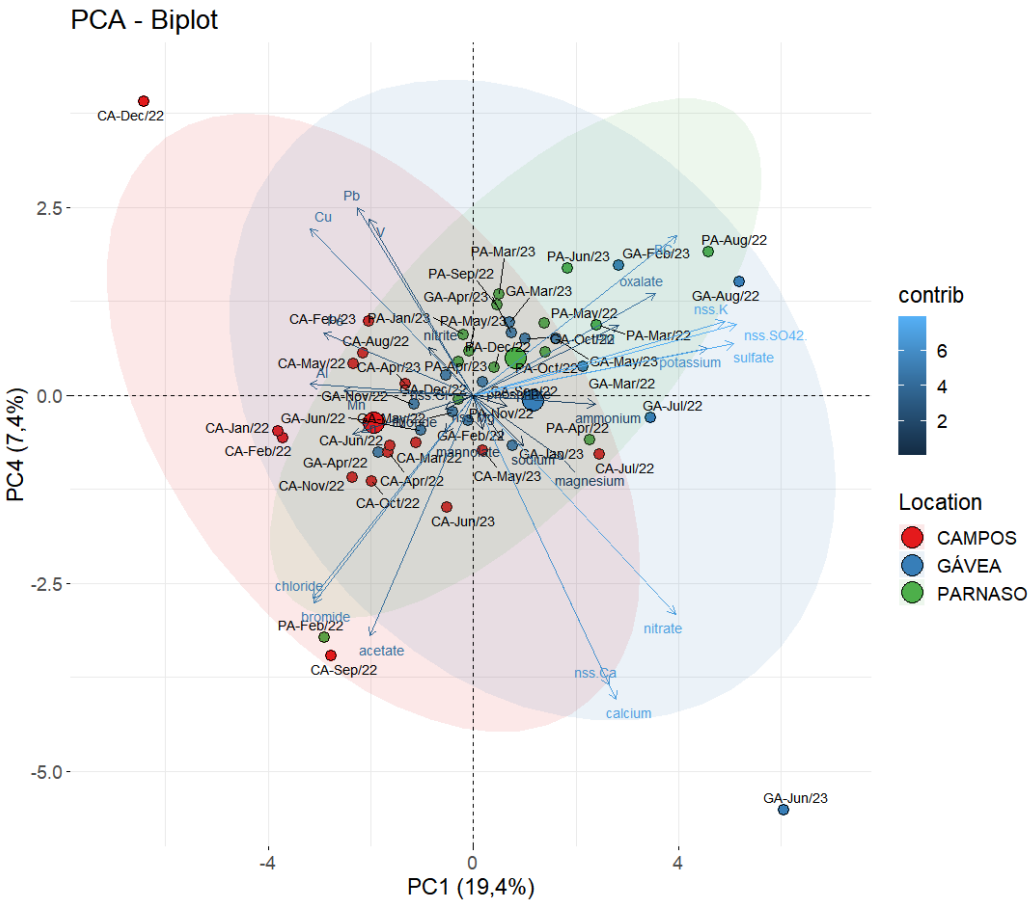

Figure 4.9. Biplot graphical with samples projected onto the new space (PC1 × PC4).

The presence of phosphate in the PARNASO samples reflects the influence of the region's local characteristics, which are marked by extensive vegetation cover (BIGIO; ANGERT, 2018). However, these samples also had the highest average concentrations of BC (2.25 µg m^{-3}) and $PM_{2.5}$ (20 µg m^{-3}). In a regional context, $PM_{2.5}$ concentrations in Brazil are associated mainly with vehicular emissions and biomass burning. Additionally, BC is often used as a marker for heavy vehicle emissions. Therefore, the levels observed in PARNASO suggest the influence of various sources, including the transport of pollutants from nearby urban areas, forest fires, and vehicle passage along the nearby highway. This can be attributed to factors such as the sampling site's proximity to the park entrance, the regional transport of pollutants from nearby urban areas, and the potential impact of seasonal fires, which are common in forested regions. These findings highlight how human activities and wildfires can significantly impact air quality, even within protected areas.

On the other hand, the Gávea samples are differentiated due to the contribution of the variables acetate, calcium, nss-Ca, nitrate, and ammonium. This region is highly urbanized, and therefore, the higher concentrations of nitrate ions (< LOD – 1.09 μg m^{-3}, mean = 0.69 μg m^{-3}) reflect the influence of anthropogenic sources, particularly vehicular emissions (CERQUEIRA et al., 2014). Calcium cation, on the other hand, can have both natural origins, such as marine aerosols and soil resuspension, and anthropogenic sources, such as burning fossil fuels and biomass. The correlation between nitrate ions, characteristic of vehicular emissions, and calcium suggests that the burning of fossil fuels is a common source of these ions in the region.

The NO_3^-/NH_4^+ ratio in PM is a useful tool for inferring the origin and chemical processes involving these ions in the atmosphere. This ratio can indicate whether the primary emission source is associated with the burning of fossil fuels and biomass or agricultural and livestock activities. When the $[NO_3^-]/[NH_4^+]$ ratio is greater than 1, there is a higher influence of ammonium nitrate (NH_4NO_3) and other forms of NO_3^-. In contrast, lower values indicate an excess of ammonium, typically associated with the use of nitrogenous fertilizers. The calculated values for the samples in this region suggest that vehicular emissions are the main sources of these ions.

The difficulty in separating PARNASO and CAMPOS may be due to the location of the collections in both regions. The collection in Gávea took place at PUC-Rio, a private university located in the Gávea, a neighborhood with a high level of vehicular influence. In PARNASO, the collection took place at the entrance to the park, near the avenue and inside the parking lot. Both have vehicle contributions, but in PARNASO the occurrence of biomass burning contributes to a higher concentration of BC.

These findings underscore the complex interplay of natural and anthropogenic sources in influencing air quality in the studied regions. While PARNASO reflects the impact of local vegetation and natural processes, it also shows the presence of pollutants commonly associated with human activities, such as traffic and forest fires. Similarly, the Gávea region, although highly urbanized, with influence from vehicular emissions, also exhibits a strong influence from the sea wind. The results highlight the

importance of monitoring both natural and anthropogenic sources to fully understand the dynamic air pollution in urban and semi-urban environments. These insights can inform policies and strategies for air quality management and pollution mitigation.

A monthly sampling frequency reduces the ability to capture specific short-term events, affecting the seasonal representativeness of the results. The PCA analysis explained only ~66 % of the total variance, suggesting that other important unidentified factors may be significantly influencing the obtained data.

4.4. Conclusion

The study revealed significant variations in $PM_{2.5}$ concentrations across the sampled sites, with the highest levels in PARNASO and the lowest in Campos dos Goytacazes. Gávea and Campos dos Goytacazes are located near the ocean, where the sea breeze favors the dispersion of atmospheric pollutants. While no samples exceeded Brazilian regulatory limits, 23 % surpassed the WHO-recommended values. Fe and Al were the most abundant elements in all sites. BC was highest in PARNASO but had a greater relative contribution to $PM_{2.5}$ in Campos, associated with biomass burning. Surprisingly, BC concentrations were higher in PARNASO than in Campos. In PARNASO, the likely source is fossil fuel combustion, given the collector's proximity to the park's parking lot and the road. In contrast, in Campos, BC was primarily associated with biomass burning. Soluble ion analyses indicated the predominance of Cl^-, Na^+, SO_4^{2-}, and NO_3^-, with 75–91 % of sulfate originating from anthropogenic sources, mainly fossil fuel combustion. PCA identified three primary sources: soil resuspension, biomass burning in Campos, pollution transport and wildfires in PARNASO, and vehicle emissions in Gávea.

The results obtained reinforce the importance of specific public policies for air pollution control, considering the particularities of the regions. In addition, continuous monitoring of $PM_{2.5}$, BC, trace elements, and soluble ions is essential to assess long-term trends and the effectiveness of mitigation measures.

4.5. Supplementary Material 1

Table S1. Particulate matter sampling period performed using fiberglass filter

Date	Gávea	PARNASO	Campos dos Goytacazes
09/02/2022	X	X	X
11/03/2022	X	X	X
04/04/2022		X	X
06/04/2022	X		
04/05/2022	X	X	X
02/06/2022	X		
07/06/2022			X
03/07/2022	X		X
02/08/2022	X		X
08/08/2022		X	
01/09/2022	X	X	X
01/10/2022			X
04/10/2022	X	X	
06/11/2022	X	X	X
06/12/2022	X	X	X
26/01/2023	X		
30/01/2023		X	X
06/02/2023	X		X
08/03/2023	X	X	
05/04/2023	X	X	X
23/05/2023	X	X	X
06/06/2023	X	X	X
Total of samples (n)	17	14	16

Table S2. Concentrations (average ± standard deviations) of water-soluble ions (μg m^{-3}) and ratio of ion in $PM_{2.5}$ in the sites.

[μg m^{-3}]	Gávea	PARNASO	Campos
Na^+	0.82 ± 0.54	0.62 ± 0.47	1.0 ± 0.54
K^+	0.14 ± 0.13	0.14 ± 0.11	0.10 ± 0.09
Mg^{2+}	0.01 ± 0.01	0.02 ± 0.04	0.01 ± 0.01
Ca^{2+}	0.14 ± 0.28	0.05 ± 0.05	0.11 ± 0.06
Cl^-	0.51 ± 0.24	0.45 ± 0.31	0.63 ± 0.34
NO_3^-	0.69 ± 0.69	0.48 ± 0.28	0.46 ± 0.25
SO_4^{2-}	1.7 ± 0.94	1.2 ± 0.72	0.96 ± 0.68
NH_4^+	0.03 ± 0.05	0.01 ± 0.02	0.06 ± 0.09
Org. Acids	0.38 ± 0.23	0.29 ± 0.17	0.16 ± 0.13
Min. An.	0.03 ± 0.04	0.05 ± 0.03	0.05 ± 0.12
nss-K^+	0.10 ± 0.11	0.12 ± 0.10	0.07 ± 0.08
nss-Mg^{2+}	0.004 ± 0.001		
nss-Ca^{2+}	0.12 ± 0.30	0.03 ± 0.04	0.08 ± 0.05
nss-Cl^-	0.28 ± 0.26		
nss-SO_4^{2-}	1.5 ± 0.89	1.1 ± 0.68	0.72 ± 0.65
nss-K^+/K^+	0.71	0.86	0.70
nss-Ca^{2+}/Ca^{2+}	0.86	0.60	0.80
nss-SO_4^{2-} /SO_4^{2-}	0.88	0.91	0.75
[NO_3^-] /[SO_4^{2-}]	0.43 ± 0.27	0.45 ± 0.32	0.51 ± 0.18

ND: not detected; Org. Acids: sum of organic acids (CH_3COO^-, $HCOO^-$, $CH_2(COO)_2^{2-}$, $(C_2O_4)^{2-}$); Min. An.: sum of trace anions (F^-, NO_2^-, Br^-, and PO_4^{3-}).

Table S3. Average concentrations and standard deviation of carboxylic acid anions (µg m^{-3}) in $PM_{2.5}$ in the sites.

Ions [µg m^{-3}]	Gávea	PARNASO	Campos
Oxalate	0.41 ± 0.20	0.30 ± 0.15	0.14 ± 0.11
Malonate	0.03 ± 0.01	0.05 ± 0.08	0.02 ± 0.02
Acetate	N.D.	0.06 ± 0.08	0.03 ± 0.02

ND: not detected.

Table S4. Average concentrations and standard devation of elements (ng m^{-3}) in $PM_{2.5}$ in the sites.

Elements (ng m^{-3})	Gávea	PARNASO	Campos
Al	14 ± 4.2	23 ± 15	30± 125
Cu	2.7 ± 1.5	0.43 ± 0.17	3.5 ± 51
Fe	6.8 ± 6.9	29 ± 22	34 ± 67
Mn	0.17 ± 0.11	0.56 ± 0.36	1.8 ± 4.0
Pb	1.7 ± 1.1	1.3 ± 1.0	1.5 ± 1.0
Ti	0.15 ± 0.14	0.50 ± 0.65	1.6 ± 7.0
V	1.0 ± 1.1	1.3 ± 0.94	1.3 ± 0.90
Zn	3.3 ± 0.78	2.9 ± 0.80	2.7 ± 2.1

5. Research Article 2 – Characterization of mercury in atmospheric particulate matter in the State of Rio de Janeiro, Brazil

Luis Fhernando Mendonça da Silva,[1] Caio Silva Assis Felix,[2,3] Madson Moreira Nascimento,[2,3,4] Jaílson Bittencourt de Andrade, [2,3,4] Maria Cristina Canela,[5] Cibele Maria Stivanin de Almeida,[5] Carla Semiramis Silveira,[6] Renato da Silva Carreira,[1] and Adriana Gioda.[1*]

[1]Pontifical Catholic University of Rio de Janeiro, 22451-900, Rio de Janeiro, RJ, Brazil.

[2]Centro Interdisciplinar em Energia e Ambiente - CIEnAm, Universidade Federal da Bahia, Salvador, BA, Brazil.

[3]Instituto Nacional de Ciência e Tecnologia em Energia e Ambiente - INCT, Universidade Federal da Bahia, Salvador, BA, Brazil.

[4]Centro Universitário SENAI-CIMATEC, Salvador, BA, Brazil.

[5]Universidade Estadual do Norte Fluminense Darcy Ribeiro, Laboratório de Ciências Químicas.

[6]Universidade Federal Fluminense - UFF, Niterói, RJ, Brazil.

Corresponding author: Adriana Gioda - agioda@puc-rio.br

Published: Environmental Science: Atmospheres (2024) available online since 25/06/2024.

Abstract

Despite its low atmospheric concentration, mercury in particulate matter (PHg) significantly impacts its biogeochemical cycle. This research focused on the airborne mercury concentrations in fine particulate matter ($PM_{2.5}$) collected from three distinct sites: an urban area, an urban area affected by sugarcane burning, and protection reserve area within the State

of Rio de Janeiro, Brazil, across various seasons during 2022-2023. The findings revealed average concentration of $PM_{2.5}$ in Gávea was 19 ± 8 µg m^{-3} (with values ranging from 8 to 37 µg m^{-3}), in PARNASO, it was 24 ± 11 µg m^{-3} (with values ranging from 0.25 to 46 µg m^{-3}), and in Campos, it was 10 ± 6 µg m^{-3} (with values ranging from 1 to 19 µg m^{-3}). Given these values, none day surpassed the threshold outlined by Brazilian regulations. However, 63 % of the samples showed daily concentrations exceeding the standards established by the World Health Organization. The average mercury concentrations in $PM_{2.5}$ were 81 ± 116 (3–366) pg m^{-3}, 169 ± 139 (2–392) pg m^{-3}, and 110 ± 71 (8–272) pg m^{-3} for the urban region of the capital, interior with sugarcane burning and forest locations, respectively, throughout the study period. The study also found that PHg concentrations were about twice as high during the dry period compared to the summer season, suggesting contributions from both local sources and transboundary pollution. Furthermore, significant seasonal variation in PHg concentrations was observed, with notably higher levels detected in the interior urban area impacted by burns than in the capital and preserved sites.

Environmental significance

This research paper makes a significant contribution to atmospheric science and the understanding of air quality in South America. It addresses the emerging issue of mercury found in $PM_{2.5}$ concentrations in three regions of Rio de Janeiro, Brazil: urban areas, areas affected by sugarcane burn, and forested areas. The study reveals that 63% of the samples showed daily concentrations exceeding the standards established by the World Health Organization (WHO) for $PM_{2.5}$ concentrations. Additionally, it was found that regions affected by sugarcane burning and environmental preservation areas exhibited the highest concentrations of mercury in particulate matter. The study also highlights seasonal variability and the contribution of both local and transboundary pollution.

5.1. Introduction

Mercury (Hg) represents a ubiquitous environmental pollutant with profound implications for human health and ecosystems worldwide, owing

to its persistence, bioaccumulative nature, and capacity for long-range atmospheric transport. Existing in diverse forms, including elemental mercury (Hg0), reactive mercury gas (RGM), and particle-bound mercury (PHg), the latter poses a significant concern as it can deposit into ecosystems and water bodies, where it transforms into methylmercury — a potent neurotoxin readily assimilated within aquatic food webs (GALAPPATHTHI; SURAWEERA, 2020; HENRIQUES et al., 2019; PARDO et al., 2011; SUN et al., 2021).

The global distribution of mercury emissions exhibits marked heterogeneity, shaped by regional disparities in industrial practices, energy generation methods, and natural emissions. The origins of mercury are attributed to natural phenomena such as forest fires and volcanic activity (PAVITHRA et al., 2023). While anthropogenic activities such as coal combustion, non-ferrous metal production, and cement manufacturing stand as primary contributors to atmospheric mercury releases, the interplay of natural sources and re-emissions from previously deposited mercury further complicates the global mercury cycle (SONKE et al., 2023; SUN et al., 2021; TCHOUNWOU et al., 2012). The intricate transport dynamics of mercury, encompassing atmospheric processes, precipitation regimes, and interactions with terrestrial and aquatic surfaces, further underscore its complex behavior on a global scale (BROCZA et al., 2024; ROULET et al., 2001; SONKE et al., 2023). Researchers have been widely concerned about mercury in recent decades, and the World Health Organization (WHO) has listed it as one of the ten most important chemicals for public health (WHO, 2017, 2020).

In Brazil, mercury contamination has garnered significant attention, mainly stemming from the nation's extensive historical and ongoing gold mining endeavors, particularly prevalent in the Amazon region, where mercury amalgamation is utilized in gold extraction from sediments, resulting in widespread environmental degradation and health ramifications. In addition to mining activities, Brazil's industrial operations, energy production, and urban pollutants collectively contribute to its mercury emission landscape (FELIX et al., 2022; SOLA et al., 2022b; TCHOUNWOU et al., 2012). Notably, the State of Rio de Janeiro serves as a pertinent case

study, representing a pivotal nexus of industrialization and urbanization, emblematic of the challenges associated with managing mercury emissions in rapidly developing urban locales. Detecting particulate mercury (PM) within urban environments underscores broader concerns regarding air quality and public health.

A comprehensive understanding of the dynamics surrounding particle-bound mercury, encompassing its sources, transport mechanisms, and deposition patterns, is imperative for formulating effective mitigation strategies to curb its deleterious effects (BROCZA et al., 2024). This study endeavors to augment our comprehension of particulate mercury dynamics, specifically focusing on quantifying concentrations, delineating seasonal variations, and discerning potential emission sources within the global and Brazilian contexts.

5.2. Material and Methods

Description in topic 3.5, page 45

5.3. Results and Discussion

5.3.1. $PM_{2.5}$ concentrations

The average concentration (during the period 2022 and 2023) of $PM_{2.5}$ in Gávea (n = 18) was 19 ± 8 μg m^{-3} (with values ranging from 8 to 37 μg m^{-3}), in PARNASO (n = 14) it was 24 ± 11 μg m^{-3} (with values ranging from 0.25 to 46 μg m^{-3}), and in Campos (n = 16) it was 10 ± 6 μg m^{-3} (with values ranging from 1 to 19 μg m^{-3}). Given these values, none of the days sampled exceeded the threshold recommended by Brazilian regulations (60 μg m^{-3}). However, 63 % of the samples exhibited daily concentrations surpassing the guidelines set by the World Health Organization (15 μg m^{-3}).

$PM_{2.5}$ concentrations were observed to be relatively elevated during the dry season (May to November) in contrast to the wet season (December to April). This pattern has been documented in numerous prior studies (DE LA CRUZ et al., 2024; GIODA et al., 2016; JUSTO et al., 2020; MATEUS et al., 2013). Many researchers attribute this phenomenon to the cleansing

impact of rainfall, which captures and deposits suspended particles in the atmosphere.

5.3.2. Mercury in PM (PHg) concentration

The concentrations of PHg in $PM_{2.5}$ at urban and preserved sites from 2022 to 2023 are summarized in Table 5.1. The average PHg concentrations (range) were 81 ± 116 (3 – 366) pg m^{-3}, 169 ± 139 (2 – 392) pg m^{-3} and 110 ± 71 (8 – 272) pg m^{-3} at the urban region of the capital, interior with sugarcane burning and forest sites during the sampling period, respectively. The average concentration of PHg in the urban with sugarcane burning (CAMPOS) and forest (PARNASO) sites was approximately two times higher than in the urban site (GAVEA).

The results showed that PHg concentrations at urban sites in coastal cities, such as Gávea, a city on the coast of China, and regions in Bahia (Brazil), are considerably lower than those in other cities, The surface winds in coastal areas influence the concentrations of PM in these regions (WANG et al., 2023a). PHg concentrations in urban areas were 6-11 times higher than the nearby values found in Asian countries, and North America (Detroit, USA), indicating that a large amount of anthropogenic mercury has been released into the atmosphere in Brazil.

5.3.3. Seasonal distribution of Hg in $PM_{2.5}$ at sites

The concentrations of PHg in PM In this study, particulate mercury concentrations (PHg) were analyzed across three sampling locations to assess seasonal variations. The highest percentages of PHg were found in the autumn, at 37 %, followed by 28 % in the spring, 24 % in the winter and 11 % in the summer, respectively (Figure 5.1). The difference between the mercury in fine particles was found to be much more significant in spring, autumn and winter than in summer, which corroborates other work carried out in China and the USA (LIU et al., 2007; XU et al., 2019). The observed patterns can be explained by the fact that PHg from combustion primarily

Table 5.1. Comparison of atmospheric PHg concentrations ($PM_{2.5}$) among different cities.

Location	Classification	Time	PHg concentration (pg m^{-3})		
			Mean (range)	S.D.	REF.
Gávea	Urban	Feb./2022 – Jun./2023	81 (3-366)	116	This study
Campos	Urban with sugarcane burning		169 (2-392)	139	
PARNASO	Preserved		110 (8-272)	71	
Navy base of Aratu – (Bahia)	Urban area near industrial complex	2010	118.0	45.5	(DE JESUS et al., 2020)
Maré Island (Bahia)			81.6	27.0	
Itaparicá (Bahia)			20.5	5.29	
Southeast coastal cities of China	Urban	Nov./2010, Jan., Apr., and Aug./ 2011	141.2 (7.6-956.5)	128.1	(SUN et al., 2021)
	Rural		37.0 (5.6-89.4)	19.2	
	Remote		24.0 (3.2-59.9)	14.6	
Beijing	Urban	Jan./2014	240 (20-820)	180	(XU et al., 2019)
Changchun	Industrial		240 (60-730)	150	
Chengdu	Urban		1300 (240-5020)	1090	
Hong Kong	Urban		60 (20-140)	40	
Detroit (USA)	Urban	2003	20.8 (1.8-611)	30	(LIU et al., 2007)

exists in fine particles, significantly reduced in summer (MACIEJCZYK; CHEN; THURSTON, 2021; PIRRONE; GLINSORN; KEELER, 1995). Additionally, atmospheric PHg can form through two mechanisms: adsorption of gaseous mercury on particles and gas-particle chemical transformation (BO et al., 2016; XIU et al., 2005). Mercury in coarse particles typically results from the adsorption of gaseous mercury, while mercury in fine particles is formed through both mechanisms. The high temperatures and intense solar radiation in summer can facilitate gas-particle transformation (MACIEJCZYK; CHEN; THURSTON, 2021; XIU et al., 2005; ZHANG et al., 2010). Therefore, the size distribution of mercury in different seasons may be influenced by both primary mercury emissions and secondary mercury formation processes (DRISCOLL et al., 2013).

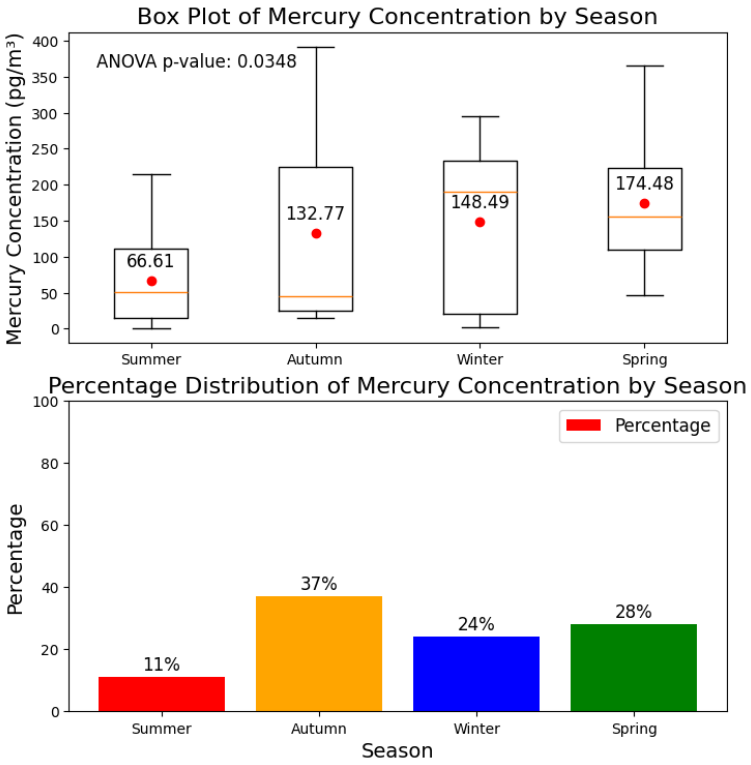

Figure 5.1. Distribution of the average concentrations and percentages of mercury in $PM_{2.5}$ t three sites (Gavea, PARNASO, and Campos).

The seasonal concentrations of PHg at individual sampling sites are shown in Figure 5.2. There was a statistically significant difference in PHg

concentration between the seasons (ANOVA test; $p<0.05$). The highest levels of PHg were found in Campos and PARNASO, while the lowest concentrations of PHg were present in Gavea (Figure 5.2). The high concentration of PHg at the sites may be associated with anthropogenic emissions. In Campos, the most significant contributions may come from vehicular traffic, the port area and, above all, the burning of sugar cane. PARNASO, despite being an environmental conservation area, usually receives many visitors to the park, with vehicles being the primary commuter. In addition, it is less than 200 m away from BR-116, one of the main avenues linking the metropolitan region of Rio de Janeiro to the Serra and other states in the country, with heavy vehicle traffic (BERINGUI et al., 2024).

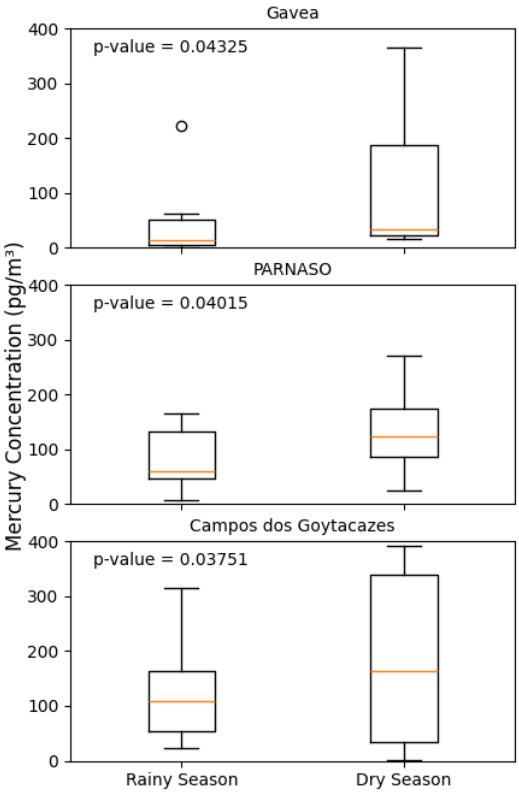

Figure 5.2. Seasonal variation of PHg concentration during the sampling period.

PHg concentrations were lowest in rainy at all sampling sites. Precipitation is a pivotal element in atmospheric dynamics, influencing the

dispersion of airborne pollutants. It is well-established that rainwater has the capacity to capture atmospheric particles, thereby aiding in their removal from the air (WANG et al., 2023a). However, despite the recognized role of precipitation in mitigating pollutant concentrations, our study did not reveal any significant correlation between precipitation and the levels of mercury and particulate matter.

The atmospheric concentration of PHg in the rainy season may be influenced by air masses coming from the ocean. Most of the mercury was emitted in Hg0 species from the ocean and contributed less to PHg (Figure 5.2). On the other hand, clean air masses could dilute the PHg concentration to a large extent. In addition, wet precipitation was more frequent and intense in the summer, eliminating a large amount of PHg in the ambient air (XIU et al., 2005; XU et al., 2013). In Campos, in the summer, the sugar cane crop is growing and there is no burning during this period, which also explains the low concentration of Hg in the area.

It is widely recognized that air masses originating from different regions carry various chemical components within aerosols, thus providing information on their possible sources (KONG et al., 2010; WANG et al., 2006).

It was found that PHg concentrations in the dry season were evidently higher compared to the rainy season at all the sampling sites. There are several reasons for this. Firstly, the autumn and winter sampling period in this study took place during the beginning (mid-September) and end (mid-March) of the heating season; therefore, the northwest monsoon can transport a large amount of particles with condensed mercury to southeastern coastal cities in spring and autumn, as well as in winter, which can be confirmed by reverse trajectory analysis.

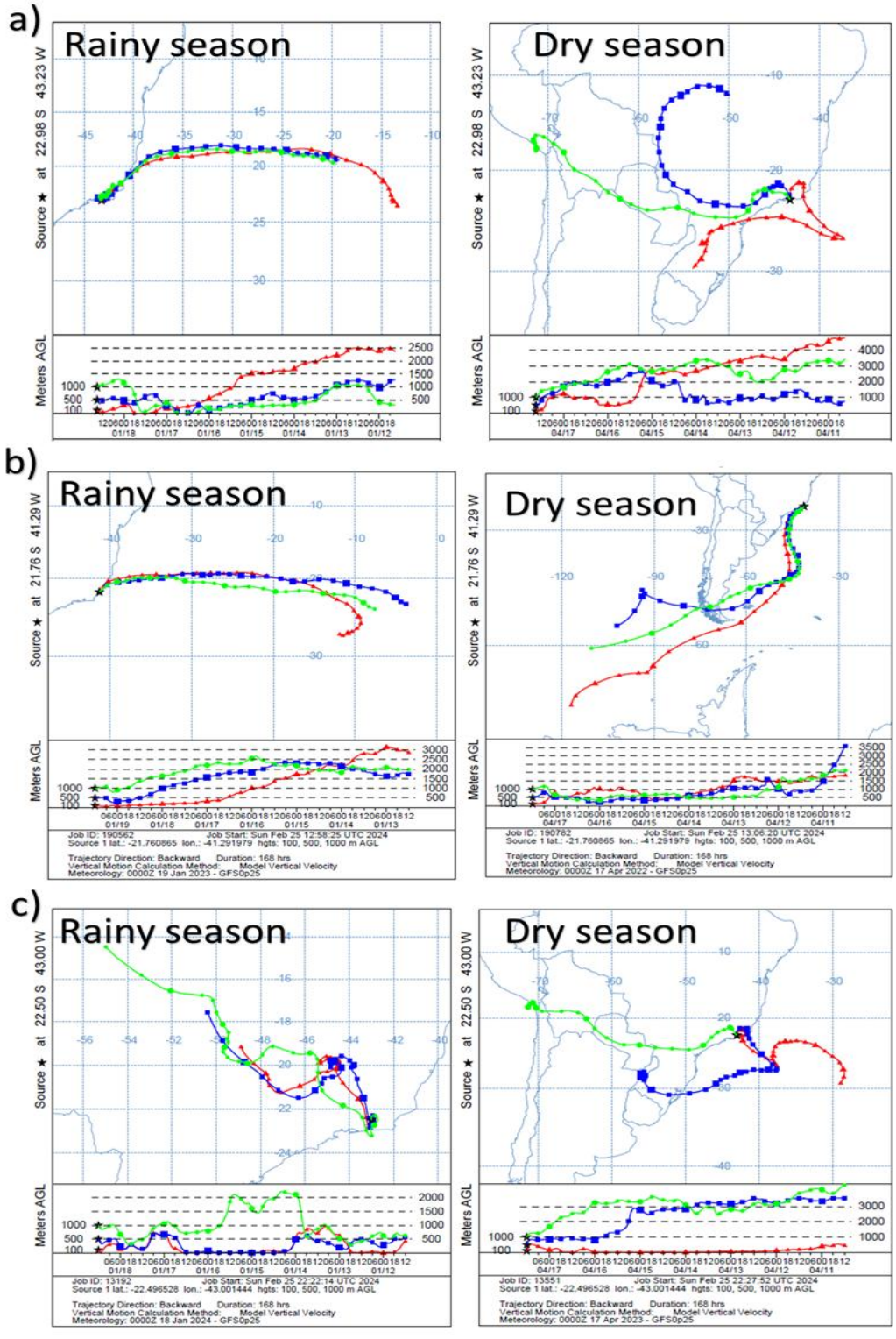

Figure 5.3. A–week air parcel backward trajectories for different seasons. The end point is at 100, 500, and 1 000 m AGL at A) Gávea, B) Campos, and C) PARNASO stations.

The results of the analysis of the reverse trajectory of the air are

shown in Figure 5.3. Very different origins were observed for the air masses that arrived at Gávea and PARNASO at different levels and in different seasons. In spring, the air masses at heights of 500 and 1,000 m originated from the continental areas of the Andes with volcanoes, Central Brazil, while the trajectory at a height of less than 100 m came from the south of the country. At a height of 1,000 m, they passed through other areas of South America, such as Bolivia, Paraguay and the interior of Brazil. The rainy season usually began at the end of November and lasted until mid-March, so the air masses brought a large amount of mercury emitted and ultimately increased the concentrations of PHg in the areas investigated during the dry season. Completely different trajectories were found during the summer. In this season, the trajectories originated from the Atlantic Ocean until they reached the study sites, Gavea and Campos. In contrast to the continental air masses, the oceanic air masses led, to a certain extent, to a decrease in PHg concentrations. Campos during the rainy season and in the dry season does not receive any influence from other countries, being mostly from the ocean in both seasons.

5.4. Conclusion

During the sampling period, it was found that the concentration of $PM_{2.5}$ varied across the studied locations. In Gávea, PARNASO, and Campos, the average concentrations were within acceptable limits according to Brazilian regulations, with none exceeding the specified threshold. However, a significant portion of the samples from all locations surpassed the daily concentration standards recommended by the WHO, indicating potential health concerns. Regarding Hg concentrations, variations were observed across different environments, with higher levels detected in areas associated with sugarcane burning compared to urban and preserved sites.

Mercury levels were found to be highest at urban fire sites, surpassing those in both urban and preserved areas. The summer season

recorded the lowest PHg concentrations in comparison to other seasons, with a consistent pattern of significantly elevated PHg levels during the dry season across all examined periods.

Analysis of backward air trajectories revealed that air masses reaching the study area predominantly originated from oceanic sources, leading to a dilution of PHg concentrations in the atmosphere during the summer at Gávea and Campos dos Goytacazes. In contrast, during other seasons, PHg levels were primarily affected by air masses coming from other South American countries and the continental areas of the Andes with volcanoes at PARNASO and Gávea. This explains why PHg concentrations were similar during the dry season but significantly higher than those recorded in the rainy season. Furthermore, Campos during the rainy season and in the dry season does not receive any influence from other countries, being mostly from the ocean in both seasons.

The main limitation of this study is that the sampling in the preservation area (PARNASO) is close to the highway. Ideally, it would have been conducted in a more central part of the park to get natural samples, but this was not possible due to the lack of electricity. In addition, for future studies we intend to do more research on Hg in the regions in particulate and gaseous form, in order to understand the cycle of this pollutant in the Rio de Janeiro region.

6. Research Article 3 – Tracing Organic Pollutants in Particulate Matter: Source Identification and Implications for Air Quality and Public Health

Luis Fhernando Mendonça da Silva [1], Adriana Gioda [1], Carlos German Massone [1], Madson Moreira Nascimento [2,3], Lilian Lefol Nani Guarieiro [2,3], Jailson Bittencourt de Andrade [2,3], Gisele Olimpio da Rocha [3,4], Marllon Wellington Faria Campos [1], Rodrigo Stellet Ferreira [5], Maria Cristina Canela [5], Renato da Silva Carreira [1,*]

[1]Pontifical Catholic University of Rio de Janeiro, 22451-900, Rio de Janeiro, RJ, Brazil.

[2]Universidade SENAI-CIMATEC, Salvador 41650-110, BA, Brazil.

[3]Instituto Nacional de Ciência e Tecnologia INCT, Universidade Federal da Bahia, Campus de Ondina, Salvador 40170-115, BA, Brazil.

[4]Instituto de Química, Universidade Federal da Bahia, Campus de Ondina, Salvador 40170-115, BA, Brazil.

[5]Universidade Estadual do Norte Fluminense Darcy Ribeiro, Laboratório de Ciências Químicas, Brazil.

Paper submitted: Environment International

Abstract

Air pollution significantly impacts public health and environmental quality, making it essential to identify its sources and chemical composition. This study examines organic compounds, including polycyclic aromatic hydrocarbons (PAHs), nitro-PAHs, oxy-PAHs, aliphatic hydrocarbons, and anhydrosugars, in atmospheric particulate matter from Rio de Janeiro, Brazil, focusing on three locations: Gávea (urban), PARNASO

(environmental protection area), and Campos dos Goytacazes (metropolitan area linked to sugarcane burning). While $PM_{2.5}$ concentrations were within Brazilian air quality standards, 63 % of samples exceeded World Health Organization guidelines. PAH concentrations were highest in PARNASO (385 ± 639 pg m^{-3}), followed by Campos dos Goytacazes (236 ± 320 pg m^{-3}) and Gávea (184 ± 291 pg m^{-3}). High molecular weight PAHs, linked to gasoline combustion, were prevalent, with retene indicating sugarcane burning and levoglucosan serving as a reliable combustion marker. Nitro-PAHs and oxy-PAHs, present in lower concentrations, provided further insights into combustion sources. The findings highlight the impact of human activities on air quality and emphasize the need for continuous monitoring of PAHs and their derivatives, particularly in vulnerable areas like PARNASO.

Keywords: polycyclic aromatic hydrocarbons, anhydro sugars, *n*-alkanes, biomass burning, Rio de Janeiro, particulate matter.

6.1. Introduction

Air quality has emerged as a significant global environmental and health concern in recent decades (FULLER et al., 2022). Particulate matter (PM), particularly $PM_{2.5}$ and PM_{10} (particles with an aerodynamic diameter of less than or equal to 2.5 and 10 µm, respectively), has been the subject of considerable scientific and public interest due to its significant role in atmospheric processes, adverse health impacts, and global climate change (SEINFELD; PANDIS, 2016). $PM_{2.5}$ has been demonstrated to significantly impact human health and atmospheric processes, including cloud nucleation and radiative forcing (FUZZI et al., 2015; KIM; KABIR; KABIR, 2015; WANG et al., 2015, 2023b). Due to its smaller size, $PM_{2.5}$ tends to contain higher fractions of organic compounds, emphasizing its characterization's importance for epidemiological studies and

environmental regulations (LENZI; FAVERO, 2019; SEINFELD; PANDIS, 2016).

Particulate matter can have a wide range of chemical compositions. These may include trace metals, ions, black carbon, and organic compounds. The organic fraction of particulate matter is constituted by a complex mixture of compounds, including polycyclic aromatic hydrocarbons (PAHs), aliphatic hydrocarbons, and monosaccharides, among other categories. The origin of these compounds can be natural (including terrestrial dust, volcanic action, sea spray, and reactions between natural gaseous emissions) or anthropogenic, including industrial emissions, vehicle exhaust, and biomass burning (LENZI; FAVERO, 2019; SEINFELD; PANDIS, 2016).

PAH are organic compounds consisting of two or more fused aromatic rings. They are produced by incomplete combustion or pyrolysis of organic materials, such as biomass burning, coal, crude oil, and industrial processes. PAHs are mainly found in the fine particulate matter fraction (RAVINDRA; SOKHI; VAN GRIEKEN, 2008). Polycyclic aromatic hydrocarbons and their derivates (nitrated and oxygenated), for instance, are known for their mutagenic and carcinogenic effects, and the relative molecular and homolog distribution of these compounds are effective proxies of source apportionments (ARLT et al., 2007; RAMOS DE RAINHO et al., 2013; SANTOS; DA ROCHA; DE ANDRADE, 2019).

Aliphatic hydrocarbons represent a considerable part of the total organic fraction in atmospheric particulate matter and, although they do not exhibit relevant toxicities, contain valuable markers that can provide information on the sources of pollution in each area (OMAR et al., 2007; SIMONEIT et al., 2004). The homologous distribution of these compounds can help identify different origins of contamination. Natural *n*-alkanes, for instance, can originate from biological sources such as plant wax, soil, phytoplankton, marine bacteria, and biomass burning and usually show a distribution with a predominance of odd over even carbon chains

(SIMONEIT et al., 2004). *n*-alkanes derived from anthropogenic sources do not display a distinctive spatial distribution in urban areas. Consequently, the observed *n*-alkane profiles may prove helpful in identifying emission sources (CAUMO; BRUNS; VASCONCELLOS, 2020; READMAN et al., 2002).

Anhydrous sugars in particulate matter are decomposition products of cellulose and hemicellulose pyrolysis, particularly present as levoglucosan, mannosan, and galactosan and their isomers. Therefore, these anhydrous sugars are considered specific tracers of biomass-burning emissions. The ratios among these compounds vary according to the type of biomass and factors like burning temperature and anhydrous sugar degradation by free radicals (MARYNOWSKI; SIMONEIT, 2022).

The state of Rio de Janeiro (22.84 S, 43.15 W), one of Brazil's most populous states, faces significant challenges with air pollution. These issues are primarily caused by the state's high population density, severe traffic congestion, and industrial activities. The state is located near industrial zones and vegetated areas, making it vulnerable to various pollution sources, including biomass burning and vehicle emissions (GIODA et al., 2018; MARTINS et al., 2017; MENDES et al., 2020; PREFEITURA DO RIO DE JANEIRO, 2013). Therefore, thoroughly examining the particulate matter and its organic fraction is essential for understanding the local pollution dynamics. Additionally, the city's mountainous topography and proximity to the sea greatly influence the dispersion and concentration of pollutants, resulting in unique air quality patterns (IBGE, 2021a; PREFEITURA DO RIO DE JANEIRO, 2013).

Most studies have focused on inorganic composition, including elements, ions, and gases (BERINGUI et al., 2021; DA SILVEIRA et al., 2021; GODOY et al., 2009; MARTINS et al., 2017; SILVA et al., 2024a; SOLURI et al., 2007). Studies focusing on the organic components of aerosol particles are even more limited, especially regarding biomarkers.

In this context, this article aims to analyze the composition of

particulate matter ($PM_{2.5}$) in different regions of the state of Rio de Janeiro with distinct levels of human activities, with a focus on organic compounds such as PAHs, nitro-PAHs, quinones (oxy-PAHs), *n*-alkanes, and monosaccharides. This is the first research to detect and quantify nitro-PAHs and quinones in $PM_{2.5}$ in Rio de Janeiro. The findings will enhance our understanding of the dynamics of these particulate organic compounds by quantifying their concentrations and detailing seasonal variations. This study is part of a larger project that aims to chemically characterize samples of particulate matter and precipitation in three regions of the state of Rio de Janeiro.

6.2. Material and Methods

Description in topic 3.6, page 46.

6.3. Results

6.3.1. $PM_{2.5}$ concentrations

The average mass concentration of $PM_{2.5}$ during the period from February 2022 to June 2023 in Gávea (n = 18) was 19 ± 8.0 μg m^{-3}, with values ranging from 8.0 to 37 μg m^{-3}. In PARNASO (n = 14), the average mass concentration was 24 ± 11 μg m^{-3}, with values ranging from 0.25 to 46 μg m^{-3}, and in Campos (n = 16) was 10 ± 6.0 μg m^{-3}, with values ranging from 1.0 to 19 μg m^{-3}. PARNASO had a higher concentration than Gávea and Campos, even though it is an area with a preserved environment. Campos had lower concentrations, although it is a region with sugar cane burning.

The mass concentration of $PM_{2.5}$ was observed to be relatively elevated during the dry season (May to November) compared to the rainy season (December to April) (Figure 6.1). The black line within each box plot indicates the median concentration, and the circles are outliers. The left and right sides of the box represent the lower and upper quartiles, covering the

interquartile range where 50 % of the data is found, while the whiskers are the two lines outside the box, extending from the minimum to the lower quartile (the start of the box) and from the upper quartile (the end of the box) to the maximum.

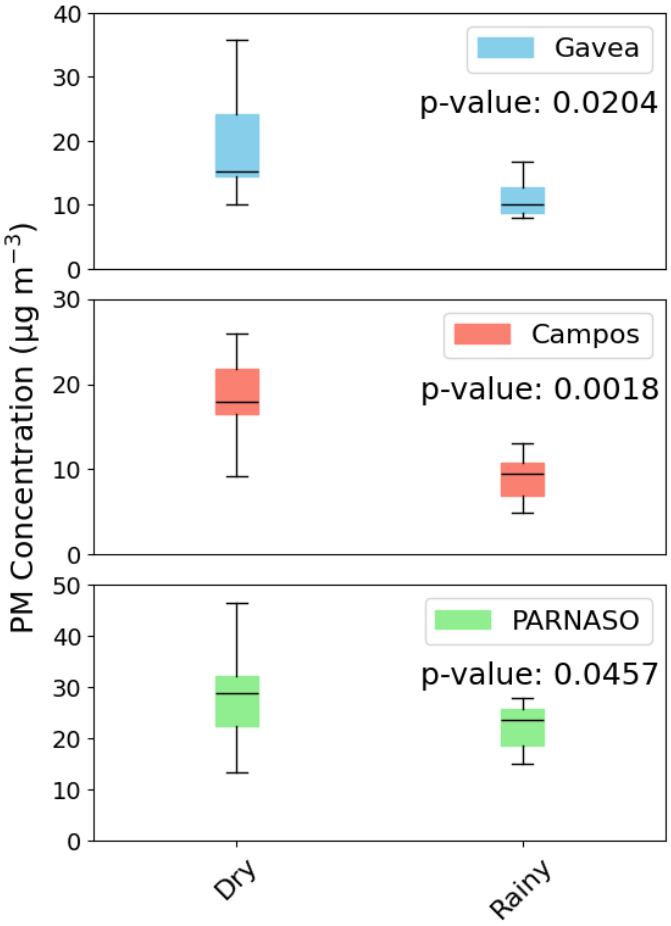

Figure 6.1. Seasonal variation of $PM_{2.5}$ concentration during the sampling period from February 2022 to June 2023 by location.

6.3.2. PAH concentrations

From the total of 37 individual PAHs included in the analytical protocol, only 14 of them were present in the $PM_{2.5}$ (Supplementary material 2, Table S4). The total concentrations of PAHs ($\sum_{37}$PAHs) over the entire study period showed an average concentration of 208 ± 315 pg m^{-3}, ranging from 6.0 to 1167 pg m^{-3} in urban area (Gávea). The average concentration

in the preserved site (PARNASO) was 287 ± 384 pg m^{-3}, ranging from 27 to 1373 pg m^{-3}. For the interior with sugarcane burning (Campos dos Goytacazes), the average concentration was 238 ± 320 pg m^{-3}, ranging from 13 to 1038 pg m^{-3}. The concentration levels of individual PAHs in $PM_{2.5}$ are illustrated in Figure 6.2. Some analytes showed coelution, so the sum of the compounds will be presented as Bbft + Bkft = benzo[b]fluoranthene + benzo[k]fluoranthene, and BaA + Cri = benzo[a]anthracene + chrysene.

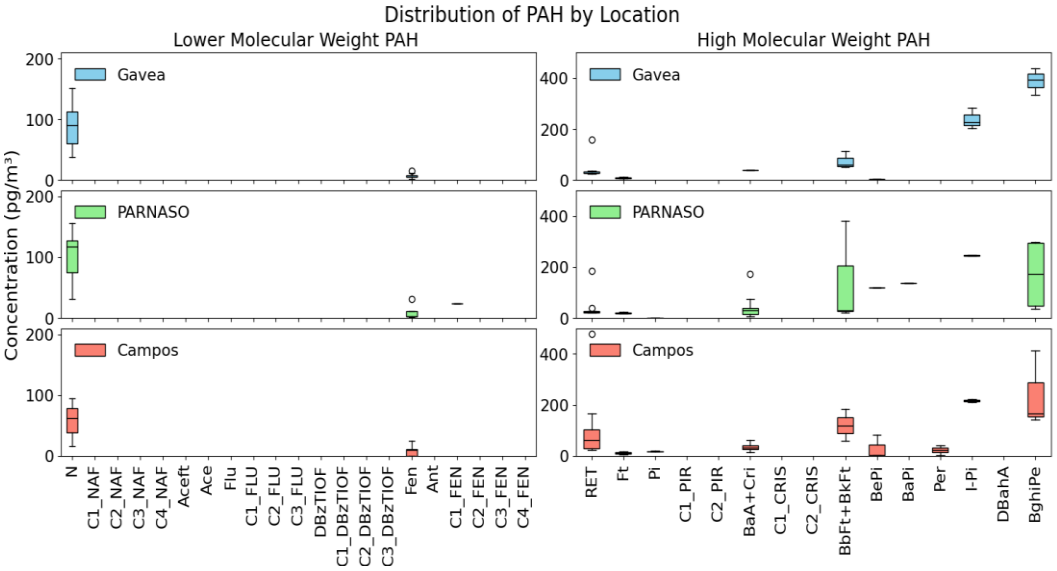

N = naphthalene, C1-C4_NAF = C1–C4-naphtalenes, Aceft = acenaphthene, Ace = acenaphthylene, Flu = fluorene, C1-C3_FLU = C1–C3-fluorenes, DBzTIOF = dibenzothiophene, C1-C3_DBzTIOF = C1–C3-dibenzothiophenes, Fen = phenanthrene, Ant = anthracene, C1-C4_FEN = C1–C4-phenanthrenes, RET = retene, Ft = fluoranthene, Pi = pyrene, C1-C2_PIR = C1 and C2-pyrenes, BaA + Cri = benzo[a]anthracene + chrysene, C1-C2_CRIS = C1-C2-chrysenes, Bbft + Bkft = benzo[b]fluoranthene + benzo[k]fluoranthene, BePi = benzo[e]pyrene, BaPi = benzo[a]pyrene, Per = perylene, I-Pi = indeno[1,2,3-c,d]pyrene, DBahA = dibenzo[a,h]anthracene, and BghiPe = benzo[g,h,i]perylene.

Figure 6.2. Boxplots of 37 polycyclic aromatic hydrocarbons (PAHs) in $PM_{2.5}$ during the sampling period from February 2022 to June 2023 by location.

Benzo[g,h,i]perylene (BghiPe) was the most abundant PAH across all locations, constituting 25 % of the ΣPAHs in $PM_{2.5}$. Among the other identified PAHs, indeno[1,2,3-c,d]pyrene (I-Pi), benzo[b]fluoranthene + benzo[k]fluoranthene (BbF + BkF), and naphthalene (N) were the next most abundant. This study found that the atmospheric mass distribution of particle-bound PAHs was primarily influenced by the six-ring compounds,

which represented 42 % of the total PAHs, followed by four-ring (29 %), five-ring (16 %), and two- and three-ring (13 %) compounds

Some ratios were calculated (Table 6.1). Retene to ΣPAHs (RET/ΣPAHs) ratio, PARNASO exhibited the lowest ratio, while Campos displayed the highest ratio value. Indeno[1,2,3-c,d]pyrene to benzo[g,h,i]perylene (I-Pi/B[ghi]Pe) ratio, Campos exhibited the lowest ratio and Gávea, the highest ratio value.

Most of the PAHs in the analytical protocol were undetected. Consequently, other ratios could not be calculated.

Table 6.1. Ratio values of polycyclic aromatic hydrocarbons (PAHs) in $PM_{2.5}$ by location.

Ratio	Gávea		PARNASO		Campos	
	Average ± SD	Range	Average ± SD	Range	Average ± SD	Range
RET/ΣPAHs	0.51 ± 0.37	0.040-1.0	0.33 ± 0.19	0.20-0.80	0.67 ± 0.37	0.030-0.95
I-Pi/B[ghi]Pe	0.47 ± 0.089	0.47-0.65	0.43 ± 0.057	0.40–0.53	0.49 ± 0.063	0.45-0.54

SD = standard deviation

6.3.3. Nitro-PAH and quinones (Oxy-PAH)

The total concentrations of Nitro-PAHs ($\sum_{19}$NitroPAHs) over the entire study period were 5.9 ± 5.5 ng m^{-3}, ranging from 0.18 to 21 ng m^{-3} in Gávea. In PARNASO, the average concentration was 6.6 ± 5.1 ng m^{-3}, with a range from 0.030 to 17 ng m^{-3}, and in Campos, it was 4.8 ± 3.6 ng m^{-3}, with a range between 0.54 and 13 ng m^{-3}. Although PARNASO presented the highest value of the sum of nitro-PAHs, the Gávea region showed the highest contribution (18 out of 19 in the analytical protocol) of nitro compounds. The concentration levels of individual PAH in $PM_{2.5}$ are illustrated in Figure 4.

The nitro-PAHs with the highest concentrations across all locations were 1-nitronaphthalene (1-NNAP), 4-nitrobiphenyl (4-NBP), and 9-nitrophenantrene (9-NPHE). In addition, 2-nitronaphtalene (2-NNAP) showed high concentrations only in Gávea, where it was the second highest contributor to the overall nitro-PAH levels. In Gávea, the average concentration of 1-NNAP was 4.3 ± 3.0 ng m^{-3}, ranging from 0.69 to 7.5 ng m^{-3}. The average concentration of 2-NNAP in Gávea was 2.6 ± 0.76 ng m^{-3}, ranging from 2.1 to 3.5 ng m^{-3}. For 4-NBP, the average concentration was 2.4 ± 1.0 ng m^{-3}, with values ranging from 0.84 to 3.7 ng m^{-3}. The concentration of 9-NPHE in Gávea averaged 2.0 ± 1.7 ng m^{-3}, ranging from 0.80 to 5.7 ng m^{-3}.

In PARNASO, 1-NNAP had an average concentration of 6.6 ± 0.66 ng m^{-3}, with values ranging from 6.1 to 7.0 ng m^{-3}, with this compound being responsible for the most significant contribution to the high value of the sum of nitro-PAH in the region. The average concentration of 4-NBP in PARNASO was 2.1 ± 0.69 ng m^{-3}, ranging from 0.60 to 3.0 ng m^{-3}. For 9-NPHE, the average concentration was 2.7 ± 1.9 ng m^{-3}, ranging from 0.69 to 6.9 ng m^{-3}.

In contrast to the other regions, Campos had the lowest contribution of 1-NNAP (2.6 ± 1.2 ng m^{-3}, from 0.60 to 4.6 ng m^{-3}) and the most significant contribution of 4-NBP (2.7 ± 2.6 ng m^{-3}, from 0.015 to 5.8 ng m^{-3}), whereas the concentration of 9-NPHE (1.6 ± 0.94 ng m^{-3}; 0.012 to 2.3 ng m^{-3}) was similar to the other regions.

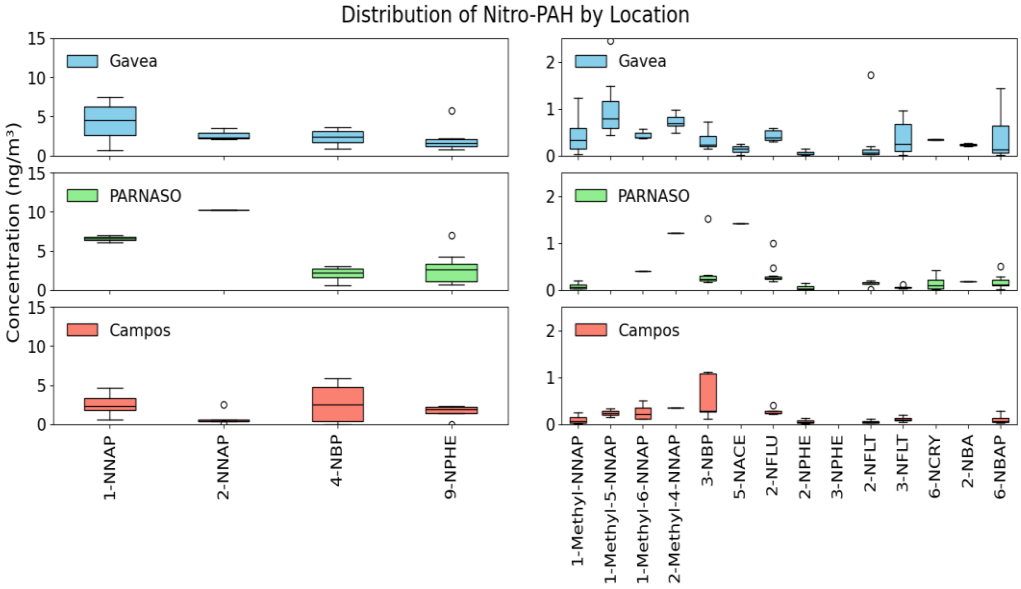

1-NNAP = 1-Nitronaphthalene, 1-Methyl-NNAP = 1-Methyl-3-nitronaphtalene, 2-NNAP = 2-Nitronaphthalene, 2-NBP = 2-Nitrobiphenyl, 1-Methyl-5-NNAP = 1-Methyl-5-nitronaphtalene, 1-Methyl-6-NNAP = 1-Methyl-6-nitronaphtalene, 2-Methyl-4-NNAP = 2-Methyl-4-nitronaphtalene, 3-NBP = 2-Nitrobiphenyl, 4-NBP = 4-Nitrobiphenyl, 5-NACE = 5-Nitroacenaphthene, 2-NFLU = 2-Nitrofluorene, 2-NPHE = 2-Nitrophenanthrene, 3-NPHE = 3-Nitrophenathrene, 9-NPHE = 9-Nitrophenanthrene, 2-NFLT = 2-Nitrofluoranthene, 3-NFLT = 3-Nitrofluoranthene, 6-NCRY = 6-Nitrochrysene, 2-NBA = 2-Nitrobenzanthrone, and 6-NBAP = 6-Nitrobenzo[a]pyrene.

Figure 6.3. Box plots of 19 nitro-PAH in $PM_{2.5}$ during the sampling period from February 2022 to June 2023 by location.

The total concentrations of Oxy-PAHs ($\sum_3$OxyPAHs) over the entire study period were 160 ± 160 pg m^{-3}, ranging from 0.41 to 577 pg m^{-3} in Gávea. In PARNASO, the average concentration was 105 ± 236 pg m^{-3}, with a range from 0.14 to 843 pg m^{-3}, in Campos was 14 ± 25 pg m^{-3}, with a range between 0.10 and 71 pg m^{-3}.

The compound 1,4-Naphtoquinone (1,4-NQ) was not detected in all locations. Two quinones (oxy-PAH) are present in the samples in Gávea, but only one showed concentrations in PARNASO and Campos. Among the three oxy-PAHs detected, benzanthrone (BA) presented the highest concentration. Figure 6.4 illustrates the concentration levels of individual quinones in $PM_{2.5}$.

In Gávea, 9,10-Anthraquinone (9,10-AQ) concentration was 114 ±

71 pg m^{-3}, with values ranging from 19 to 267 pg m^{-3}, and BA was 105 ± 112 pg m^{-3}, with values ranging from 0.41 to 392 pg m^{-3}.

The average concentration of BA in PARNASO was 113 ± 223 pg m^{-3}, ranging from 0.5 to 843 ng m^{-3}. In Campos, the average concentration was 33 ± 29 pg m^{-3}, ranging from 0.20 to 71 pg m^{-3}.

BA is present in all three regions, but 2-nitrobezantrone (2-NBA), one of its isomers, was only detected in PARNASO and Campos.

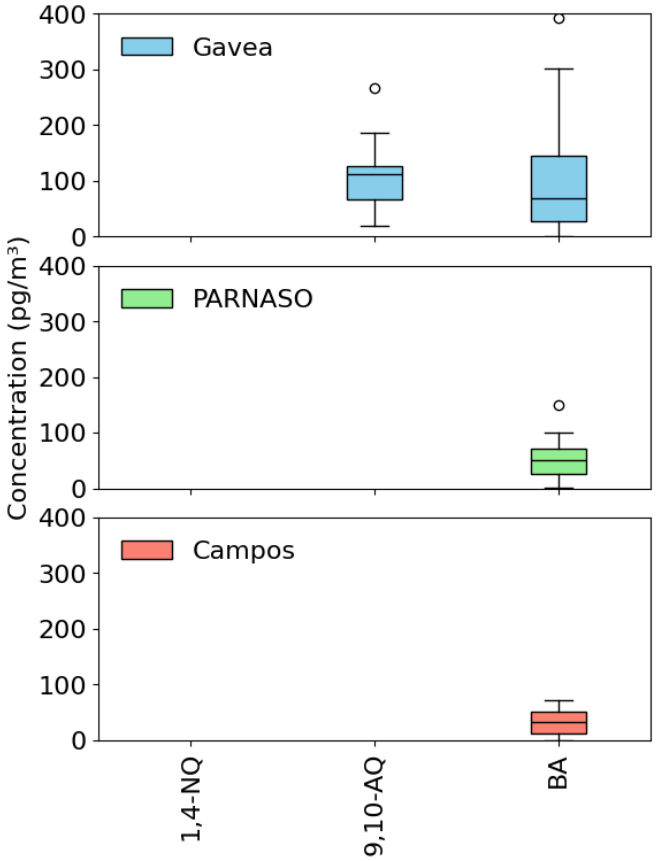

1,4-NQ = 1,4-Naphtoquinone, 9,10-AQ = 9,10-Anthraquinone, and BA = Benzanthrone.

Figure 6.4. Box plots of three quinones in $PM_{2.5}$ during the sampling period from February 2022 to June 2023 by location.

6.3.4. Aliphatic hydrocarbons (AH) concentrations.

Thirty-one *n*-alkane compounds (*n*-C_{13} to *n*-C_{40}) and branched isoprenoids (pristane and phytane) bound to $PM_{2.5}$ were quantified in this study. The average total target *n*-alkanes and branched isoprenoid concentrations were 586 ± 229 ng m^{-3}, ranging from 110 to 1131 ng m^{-3} in

Gávea. In PARNASO, the average concentration was 823 ± 180 ng m^{-3}, with a range from 538 to 1134 ng m^{-3}, and in Campos, it was 1075 ± 278 ng m^{-3}, with a range between 699 and 1626 ng m^{-3}. Figure 6 shows the average concentration of individual *n*-alkane and branched isoprenoids.

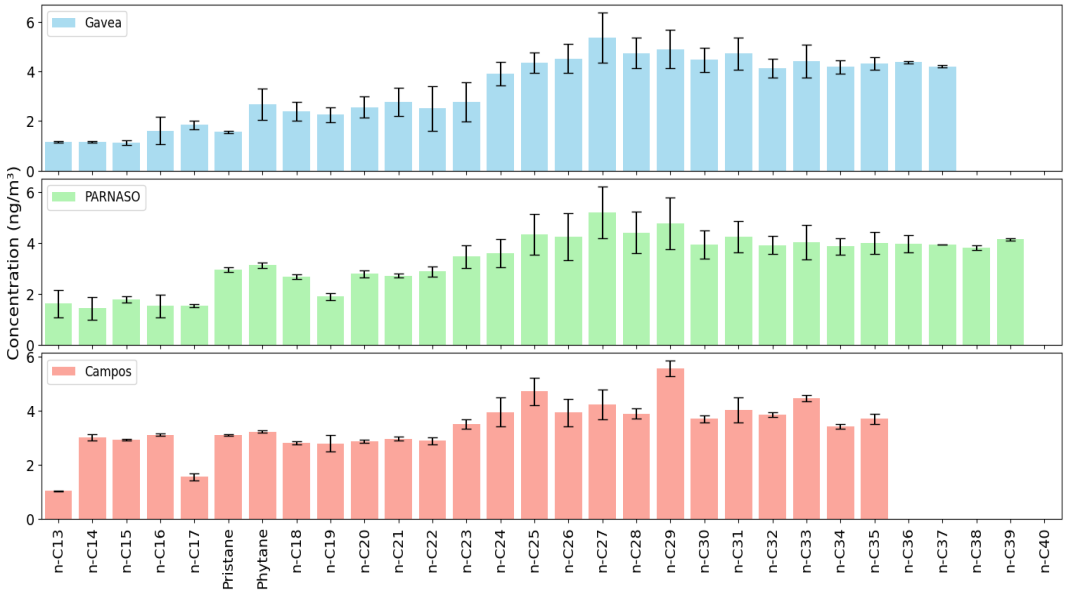

Figure 6.5. Boxplots of 28 *n*-alkanes and branched isoprenoids (Pristane and Phytane) in $PM_{2.5}$ by location during the sampling period from February 2022 to June 2023. Bar graph of the averages of *n*-alkanes with their respective standard deviations.

The concentrations of long-chain *n*-alkanes (>C_{23}) were 60 % higher than for the short-chain ones for all locations (Figure 6.5). It was not marked by the prevalence of odd over even carbon-chain compounds in the *n*-C_{23} to *n*-C_{33} range. The most abundant compound (*n*-Cmax) in Gávea and PARNASO was *n*-C_{27}, while Campos had a predominance of *n*-C29. Although odd compounds are prominent in the range of *n*-C_{23} to *n*-C_{33}, no clear pattern emerges in the range below *n*-C_{23}, and pristane and phytane exist in all three regions.

The CPI values were relatively similar in Gávea (1.4 ± 0.85; in PARNASO, it was 1.1 ± 0.48; and in Campos, it was 1.5 ± 0.98). The percentual concentration of wax *n*-alkanes (% WNA) in Gávea was 2.1 %,

in PARNASO 1.2 %, and in Campos 3.0 %.

6.3.5. Anhydro saccharides

During the study period, the average concentrations of monosaccharide anhydrides were observed in different locations and varied according to the type of area (Figure 6.6). The lower concentrations were measured at Gavea, with 14 ± 3.8 ng m^{-3} (5.3 – 30 ng m^{-3}) for LEV, 6.2 ± 4.4 ng m^{-3} (1.1 – 17 ng m^{-3}) for MAN and 13 ± 12 ng m^{-3} (0.37 – 42 ng m^{-3}) for GAL.

PARNASO exhibited values up to one order of magnitude higher than at GAVEA, with average concentrations of 85 ± 123 ng m^{-3} for LEV, 97 ± 295 ng m^{-3} for MAN and 24 ± 24 ng m^{-3} for GAL. In addition, in PARNASO, the seasonal variation in concentration was considerable, ranging from 0.090 to 396 ng m^{-3} for LEV, from 0.10 to 1119 ng m^{-3} for MAN, and from 0.20 to 77 ng m^{-3} for GAL.

In Campos, where sugar cane burning is still an agricultural practice, only the concentration of levoglucosan (LEV) was much higher in comparison to the other monitored sites, with a mean concentration of 251 ± 294 ng m^{-3} and range of 0.20 to 835 ng m^{-3} (Figure 6.6). The other two saccharides, MAN with 23 ± 30 ng m^{-3} (0.10 to 98 ng m^{-3}) and GAL with 29 ± 36 ng m^{-3} (0.20 to 94 ng m^{-3}), with mean and range of concentrations similar to the Gavea station. In fact, the concentrations of mannosan and galactosan are considerably lower than those of levoglucosan (*p*-value = 0.014) in Campos dos Goytacazes, where levoglucosan concentrations are approximately eight hundred times higher than in Gávea and three times higher than in PARNASO.

The ratio between the sugars can provide information on the type of biomass that has been burnt (which will be presented in the discussion topic). In Campos, the LEV/MAN was 11 and LEV/GAL = 8.0.

The monosaccharides exhibited significant statistical differences (p-value = 0.025 for LEV, 0.045 for MAN, and 0.039 for GAL) and seasonal

variability across the study regions, with higher concentrations observed during the dry season.

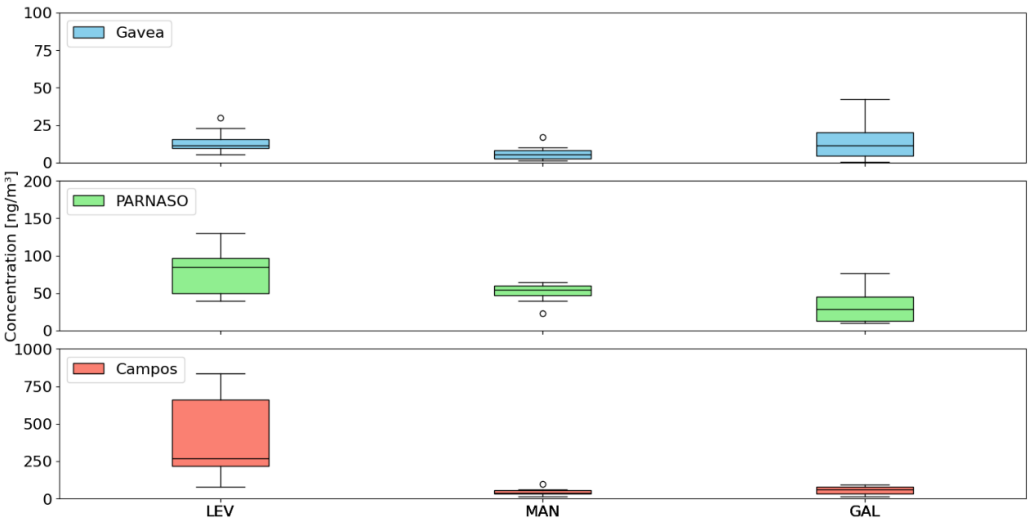

LEV is levoglucosan, MAN is mannosan, and GAL is galactosan.

Figure 6.6. Boxplots of monosaccharide concentrations in $PM_{2.5}$ by location during the sampling period from February 2022 to June 2023 by location.

6.4. Discussion

6.4.1. Level of PM contamination in the studied areas

Given the importance of PM and its effects on human health and the environment, several international organizations have established limits for the daily and annual average concentrations of $PM_{2.5}$. Based on epidemiological studies, the World Health Organization (WHO) provides guidelines for air quality standards concerning pollutants that endanger public health, aiming to reduce their impact. For $PM_{2.5}$, the WHO suggests air quality standards of 15 µg m^{-3} for daily concentrations and 5 µg m^{-3} for annual averages, respectively (WHO, 2021b).

The results of $PM_{2.5}$ indicate that none of the sampled days exceeded the threshold recommended by Brazilian regulations (60 µg m^{-3}). However, 63 % of the samples exhibited daily concentrations that surpassed the guidelines set by the World Health Organization (WHO) (15 µg m^{-3}) (Figure 6.7).

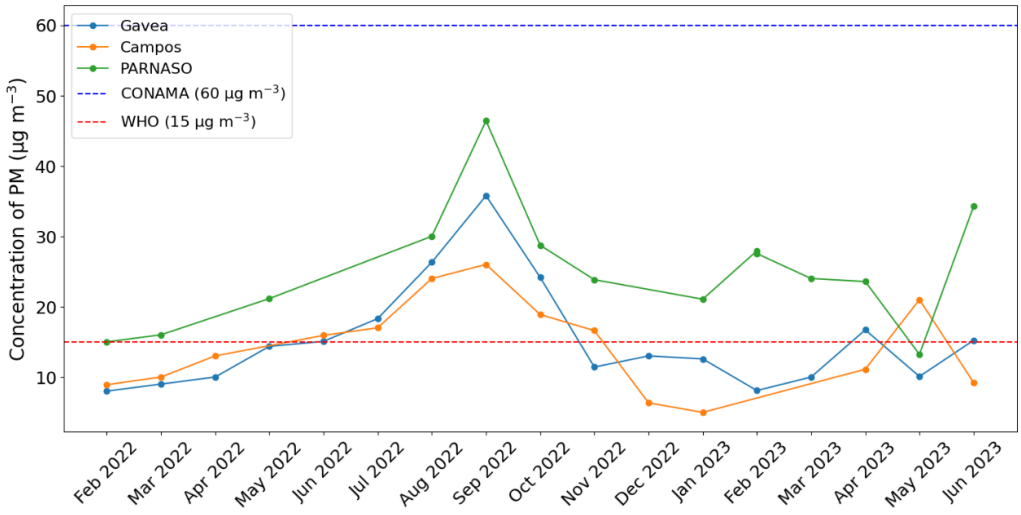

Figure 6.7.Timeseries of particulate matter concentration ($PM_{2.5}$) of samples collected in three regions of Rio de Janeiro from February 2022 to June 2023. The red dashed line indicates the daily limit value suggested by the World Health Organization (WHO) and the the blue dashed line indicates the value legislated in the Brazilian CONAMA Resolution no. 506/2024.

Historically, Brazil has been slow to adopt WHO-recommended air quality standards, as evidenced by the country's delay in implementing the 2005 WHO guidelines until 2018. Several factors contributed to this lag, including outdated legislation, inadequate monitoring infrastructure, and resistance from certain sectors. However, with the establishment of the National Air Quality Policy (PNQAr) and the revision of CONAMA Resolution 506/2024 by the National Environmental Council (CONAMA) regarding air quality standards, Brazil is beginning to adopt stricter regulations aligned with the United Nations (UN) 2030 Agenda goals. Despite this progress, the established deadlines, particularly the final target for 2044, may not be met, as the WHO could update its guidelines by that time, suggesting that shorter timelines would be preferable to align with global air quality standards (BERINGUI et al., 2021; CONAMA, 2024; TAVELLA et al., 2024).

It was observed that the concentration of $PM_{2.5}$ was relatively high during the dry season compared to the rainy season in all regions, with a statistical difference between the seasons (p-value = 0.023 in Gávea; in

Campos, it was 0.018; and in PARNASO, it was 0.046) (Figure 2). In addition, a negative correlation was observed between PM and precipitation ($r = -0.84$), which suggests that in the period with the highest rainfall (rainy season), the concentration of PM in the atmosphere tends to decrease in the regions studied. This pattern has been documented in numerous prior studies (DE LA CRUZ et al., 2024; GIODA et al., 2016; MATEUS et al., 2013; SILVA et al., 2024a). The cleansing effect of rainfall is often cited as the cause of this phenomenon, whereby precipitation captures and removes suspended particles from the atmosphere (LATIF; OTHMAN; HASSAN, 2021; SILVA et al., 2024a; THOMPSON; EIDHAMMER, 2014; WANG et al., 2023a).

In addition to the seasonal variations observed in $PM_{2.5}$ concentrations, it is important to consider the impact of factors such as urbanization and agricultural activities on air quality (KIM; KABIR; KABIR, 2015; MANISALIDIS et al., 2020). Urbanization, with its increase in vehicle fleets and infrastructure construction, can be a significant source of particulate matter emissions, particularly in densed populated areas. Agricultural activities, such as the burn-and-slash practice of land management, the burning of sugar cane, or the use of pesticides, can also contribute to increased $PM_{2.5}$ levels (BERINGUI et al., 2021; DE ALMEIDA AZEVEDO; DOS SANTOS; DE AQUINO NETO, 2002; LIMA et al., 2020).

In the case of PARNASO, a protected area, one would expect particle pollution to be lower. However, even in theoretically preserved regions, there can be an influence from nearby human activities or sporadic pollutant emission events. Examining these variations and assessing whether the area's protection significantly reduces PM levels or whether the proximity of areas of human activity still influences air quality is crucial. On the other hand, although it is a region that burns sugarcane, Campos exhibits lower $PM_{2.5}$ concentrations due to its location on a flat area significantly influenced by winds. This environmental factor promotes the dispersion of pollutants, reducing local particulate matter concentrations

(VIEIRA et al., 2023). These issues will be explored in detail in the following topics as we attempt to identify potential sources of air pollution in the regions studied.

6.4.2. Distribution and contamination by PAHs

Polycyclic aromatic hydrocarbons (PAHs), particularly the high molecular weight (HMW) compounds, are well-known by-products of the incomplete combustion of fossil fuels and biomass. They are widely recognized for their toxicity and carcinogenic potential (KEYTE; HARRISON; LAMMEL, 2013; LAWAL, 2017), HMW are primarily adsorbed on the surface of airborne particles and have lower vapor pressure, which means they take longer to detach from particles and migrate to the gas phase. Conversely, lower molecular weight (LMW) PAHs have a higher volatility and are predominantly in the gas phase, with minimal detection in particle mass (OLIVEIRA et al., 2018; SCARAMBONI et al., 2024; ZHANG et al., 2020, 2016). Therefore, the prevalence of HMW compounds, which comprised up to 87 % of total PAHs in the samples analyzed, is consistent with their physicochemical properties.

Total PAH concentrations in the present study varied widely among the monitored regions. In Rio de Janeiro (Gávea station), the relatively high concentration of 208 ± 315 pg m^{-3} (6.0 – 1167 pg m^{-3}) may be ascribed to the influence of urban sources. However, these values were lower than those already recorded in other city regions, such as the entrance of the Rebouças Tunnel (high flux of light vehicles), and the Jardim Botânico neighborhood, with heavy traffic (DE MELO LIMA; PEREIRA NETTO, 2009; OLIVEIRA et al., 2014; PEREIRA NETTO et al., 2005; RAMOS DE RAINHO et al., 2013). These values were also lower than the concentrations reported for urbanized regions in European countries (CALLÉN; ITURMENDI; LÓPEZ, 2014; SLEZAKOVA et al., 2011), USA (MARTELLINI et al., 2012), and China (CHEN et al., 2017), indicating that the places studied are in a better situation regarding air pollution by PAHs than these urbanized

countries.

In PARNASO, the concentrations of PAHs in $PM_{2.5}$ ($\sum_{37}$PAHs = 287 ± 324 pg m^{-3}) were considerably higher than those found in Gávea (208 ± 315 pg m^{-3}) and Campos (238 ± 320 pg m^{-3}). One possible reason for this could be the collector's proximity to the BR-116 highway. This important longitudinal road crosses ten states, including Rio de Janeiro, and connects the state to various other regions of Brazil. The heavy traffic on this highway contributes to pollutant emissions in the area. In addition, the park, which attracts many visitors daily, has a parking lot for visitors and employees. The collector was installed at this location due to the availability of an electricity supply, being one of the few points in the park with this infrastructure. This increases the area's exposure to road traffic emissions and worsens the region.

Specific compounds such as indeno[1,2,3-c,d]pyrene (I-Pi), benzo[g,h,i]perylene (BghiPe), benzo[b]fluoranthene (Bbft) and benzo(k)fluoranthene (Bkft), typically associated with gasoline combustion (BERGVALL; WESTERHOLM, 2009; CARICCHIA; CHIAVARINI; PEZZA, 1999; HO et al., 2009; RIDDLE et al., 2007; ROGGE et al., 1993a), were identified at all sites. These compounds are considered to be HMW. The four PAHs mentioned above were correlated with each other, with correlation coefficients ranging from r = 0.60 to 0.82. This suggests that they may have a common origin, which is corroborated by the I-Pi/B[ghi]Pe ratio (~0.4), which indicates the predominance of gasoline as the main source of emissions of these compounds. The I-Pi/B[ghi]Pe ratio is commonly associated with the combustion of fossil fuels, especially gasoline (CARICCHIA; CHIAVARINI; PEZZA, 1999; RAVINDRA; SOKHI; VAN GRIEKEN, 2008), and its value in the observed range reinforces the hypothesis that vehicle emissions are the main source of PAHs in the area studied. The values of the I-Pi/B[ghi]Pe ratios recorded in other regions of the city, such as the Jardim Botanico neighborhood (OLIVEIRA et al., 2014), an area of Rio de Janeiro impacted by emissions from light vehicles running

on petrol mixed with ethanol, were similar to those found in our studies.

The state of Rio de Janeiro has more than 7 million vehicles, of which 38 % are light gasoline vehicles (GVs), 29 % are flexible-fuel vehicles (FFV), and 5 % are heavy-duty diesel vehicles (HDDVs) (DETRAN-RJ, 2023).

The relationship between gasoline, vehicle fleet, and PAH concentrations in the air is significant when analyzing the context of densely populated urban areas with high vehicle traffic, such as Rio de Janeiro's state. The vehicle fleet in Rio de Janeiro, composed of a significant number of light vehicles powered by gasoline, exerts considerable pressure on air quality. Gasoline, as the primary fuel for light vehicles, is responsible for the emission of several pollutant compounds, including high molecular weight PAHs, formed during the incomplete combustion of gasoline (BERGVALL; WESTERHOLM, 2009; OLIVEIRA et al., 2014; RIDDLE et al., 2007). The high number of vehicles in circulation, especially in regions with heavy traffic, such as Gávea and other urban areas, results in high concentrations of these compounds in the air.

Pollution sources significantly affect the distribution of PAHs in urban areas, with the composition of the vehicle fleet in Rio de Janeiro being one of the main contributors. While gasoline-powered vehicles account for the majority of the fleet, flex-fuel vehicles and heavy trucks also add to pollutant emissions. The substantial presence of gasoline and flex-fuel vehicles (which often operate using gasoline) indicates that gasoline is the primary source of PAH emissions in high-traffic areas. Additionally, the growth of the vehicle fleet over the years is likely to intensify the emission of these compounds, particularly in regions where public transport infrastructure fails to alleviate dependence on cars, as seen in the city of Rio de Janeiro.

In addition to the emission of HMW PAHs derived from fuel combustion, another relevant PAH detected and quantified in all locations, with high concentrations in the Campos station, is retene (RET) (Figure 6.2). Its presence in the particulate matter is derived from the thermal degradation of resin compounds in wood and plants.(SIMONEIT et al.,

2004) The ratio of Ret/ΣPAHs in all locations (Gávea was 0.51 ± 0.37, PARNASO was 0.33 ± 0.19, and Campos was 0.67 ± 0.37) suggests the presence of wood/biomass combustion emissions, with values greater than 0.1 (EL-MUBARAK et al., 2014), with higher concentrations of retene being found in Campos (p-value = 0.044). In this region, sugar cane burning takes place (EL-MUBARAK et al., 2014; SIMONEIT et al., 2004).

Retene is often regarded as a molecular tracer for conifer wood combustion in source apportionment studies, based on the assumption that it is primarily emitted from softwood burning (RAMDAHL, 1983; SHEN et al., 2012). However, measurements of retene emissions from non-softwood combustion have raised questions about its exclusivity as a marker specifically for conifer wood combustion (BARI et al., 2009; HEDBERG et al., 2002; SHEN et al., 2012). Some studies have detected retene from lignite and sub-bituminous coal combustion with levels exceeding those of softwood combustion. It has also been reported in the open burning of rice and wheat straw, as well as from emissions of hardwoods (oak, aspen, eucalyptus) (MCDONALD et al., 2000; ROGGE et al., 1993b; SCHAUER et al., 2001), vehicle exhaust, and road dust (BARI et al., 2009).

Rio de Janeiro lacks conifers, so retene can be sourced from other materials within the state. PARNASO exhibited lower retene concentrations; however, despite being an environmentally protected area, nearby highways, and heavy vehicle traffic may have affected the levels of PAHs, including retene. Retene has also been detected in $PM_{2.5}$ samples collected from a road tunnel partially affected by diesel-powered vehicles in Portugal (ALVES et al., 2016), and tunnels in Brazil (PEREIRA et al., 2023), and Sweden (KRISTENSSON et al., 2004; WINGFORS et al., 2001). This compound can also form during the incomplete combustion of fuels. Medium correlations were found between retene and nitro-PAH (r = 0.56), a compound often used as an indicator of vehicle emission sources (see next discussion). Therefore, vehicle emissions, rather than biomass or wood burning, may represent a significant source of retene in PARNASO.

In contrast, Campos exhibited the highest retene values, with a Ret/ΣPAHs ratio exceeding 0.1. This indicates that sugarcane burning, a prevalent practice in the area, is a significant source of this compound. Sugarcane burning in Brazil releases retene, which explains the higher concentrations observed in Campos. This underscores the importance of biomass burning in PAH emissions in this region. Retene concentrations were higher in the dry season (Gávea: 45 pg m^{-3}, PARNASO: 67 pg m^{-3}, and Campos: 109 pg m^{-3}) compared to the rainy season (Gávea: 32 pg m^{-3}, PARNASO: 23 pg m^{-3}, and Campos: 83 pg m^{-3}) across all sites. However, there was no statistically significant difference between the seasons.

6.4.3. Nitro-PAH and quinones (Oxy-PAH): Evidence of Primary and Secondary Sources

Nitro-PAHs and quinones (oxy-PAHs) are significant air pollutants because of their known mutagenic and carcinogenic properties. The primary sources of nitro-PAHs are vehicle exhaust emissions and in situ formation. Nitro-PAHs are mainly formed through the photochemical reaction of PAHs in the atmosphere (PAIM et al., 2023; REISEN; AREY, 2004). Although they are usually found in lower concentrations than their parent PAHs, they still pose environmental and health risks due to their carcinogenic effects, and their presence is predominantly in urban and industrialized areas (DE CASTRO VASCONCELLOS et al., 2008; PAIM et al., 2023).

This study found that 1-nitronaphthalene (1-NNAP) and 2-nitronaphthalene (2-NNAP) were present in 35% of samples. These compounds are not typically found in particulate matter due to their relatively high volatilities, which promote their accumulation in the gas phase and lead to further losses through volatilization during aerosol collection (ATKINSON et al., 1989; DE CASTRO VASCONCELLOS et al., 2008; STRANDBERG et al., 2023).

1-NNAP exhibited the highest concentrations across all sampled sites (Figure 6.8). These values are greater than those recorded in other

urban areas worldwide, such as Chinese cities (LIU et al., 2017), where 1-NNAP concentrations in $PM_{2.5}$ ranged from 0.030 to 0.40 ng m^{-3}. In these same Chinese cities, these compounds (1-NNAP and 2-NNAP) were also regarded as the main contributors, with contributions one or two orders of magnitude higher than those of other nitro-PAHs. Similarly, in Córdoba (Argentina) (CARRERAS et al., 2013) concentration was 0.020 ng m^{-3}. Previous studies in São Paulo and Porto Alegre also detected 1-NNAP (DE CASTRO VASCONCELLOS et al., 2008; GARCIA et al., 2014; SOUZA et al., 2014; TEIXEIRA et al., 2011), but at lower concentration levels, underscoring the elevated levels found in Rio de Janeiro.

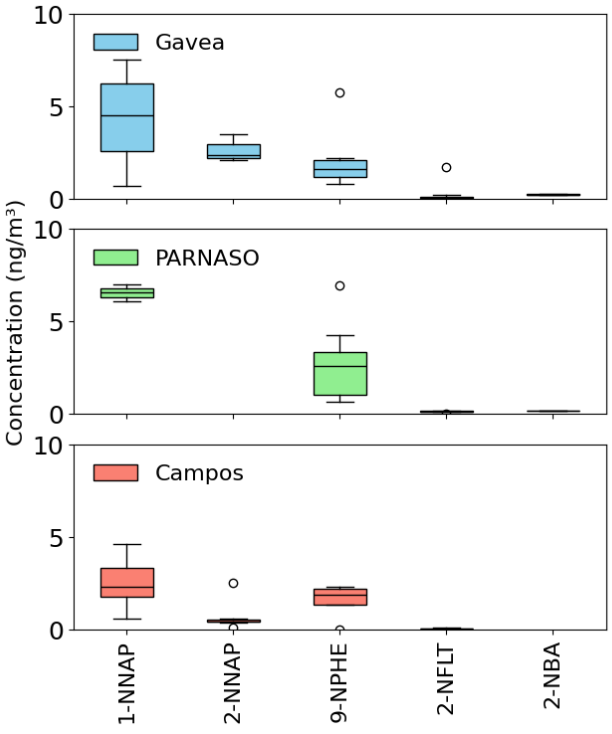

1-NNAP = 1-Nitronaphthalene, 2-NNAP = 2-Nitronaphthalene, 2-NFLT = 2-Nitrofluoranthene, 9-NPHE = 9-Nitrophenanthrene, 2-NBA = 2-Nitrobenzanthrone.

Figure 6.8. Box plots of the 5 nitro-PAHs with the highest concentrations during the sampling period from February 2022 to June 2023 by location.

Concentrations of 2-NNAP were higher only in Gávea (2.6 ± 0.76 ng m^{-3}), at levels that were also significantly higher than those observed in

other urban regions. For example, in Chinese cities (LIU et al., 2017), the 2-NNAP concentrations ranged from 0.070 to 0.10 ng m^{-3}, and in a sugar cane burning region, Brazil, it was 1.80 ng m^{-3} (DE CASTRO VASCONCELLOS et al., 2008). This trend suggests a substantial contribution of diesel combustion in the metropolitan region of Rio de Janeiro, which can be derived from the high number of buses whose engines use this type of fuel.

Additionally, the study observed elevated levels of 9-nitrophenanthrene (9-NPHE), which had an average concentration of 2.1 ± 1.7 ng m^{-3} in Gávea, 1.6 ± 0.94 ng m^{-3} in Campos, and 2.7 ± 1.9 ng m^{-3} in PARNASO. These values are higher than those recorded in several cities around the world, such as Córdoba and São Paulo, where concentrations were much lower. Diesel engines are known to emit 1-NNAP, 2-NNAP and 9-NPHE in particulate emissions, which are reliable indicators of diesel combustion (ATKINSON et al., 1989; IARC, 2014; MINERO et al., 2010; RINGUET et al., 2012; ZIELINSKA et al., 2004). In this context, the presence of heavy-duty diesel vehicles (HDDVs) in Rio de Janeiro, accounting for approximately 5 % of the vehicle fleet, significantly contributes to these emissions, further linking the elevated levels of these nitro-PAHs to diesel combustion in the region.

In general, main compounds of NPAH in this study were approximately 10 times higher concentrations compared to those reported in the previous studies cited above. This could be attributed to the sampling method used in the current study, which likely promoted the formation of secondary compounds and the degradation of certain compounds through reactions with atmospheric oxidants (GORIAUX et al., 2006). Additionally, the deposition of PAHs on the filters may have been converted into NPAHs due to the influx of NO_2 (GORIAUX et al., 2006), further contributing to higher NPAH concentrations. Furthermore, road dust is resuspended by wind, along with the mass transfer of NPAHs from fine to larger particles (ALBINET et al., 2008).

Despite these factors, a potential underestimation of NPAH

concentrations cannot be ruled out in the present study due to the volatilization of organic compounds (including PAHs) from the filter particles (GORIAUX et al., 2006; MCMURRY, 2000). Moreover, environmental factors such as climate, topography, and winds from other regions of Brazil and neighboring countries may also play a role in the formation and/or persistence of these compounds in the atmosphere of Rio de Janeiro. Although the country has a tropical climate, which typically results in lower contributions from volatile PAHs, the three main nitro-PAHs (1-nitronaphthalene, 2-nitronaphthalene, and 9-nitrophenanthrene) recorded in Rio de Janeiro were higher than those found in countries with temperate climates. Further research is needed to better understand these compound's presence and behavior in Rio de Janeiro's atmosphere.

The formation of other NPAHs, such as 2-nitrofluoranthene (2-NFlt), was observed with a moderate correlation with the parent compound fluoranthene (Ft) ($r = 0.57$). This formation occurs through atmospheric reactions involving NO_2. During the day, fluoranthene reacts with hydroxyl radicals ($OH\cdot$) in the presence of NO_2, while at night, it reacts with nitrate radicals ($NO_3\cdot$). The high availability of NO_x in the atmosphere of Rio de Janeiro, originating from vehicle emissions, contributes to the in-situ formation of these nitro-PAHs. The high concentration of NO_x and the intense solar radiation in the tropical climate of Rio de Janeiro favor these photochemical reactions, which are essential for forming secondary pollutants such as nitro-PAHs (MACHADO; CARDOSO; ALLEN, 2007; RINGUET et al., 2012; SOUZA et al., 2014; WANG et al., 2011).

Among the three regions, Campos presented the lowest nitro- and oxy-PAH concentrations. These results are also related to the region's topographic conditions. As a plain, it has greater dispersion of pollutants, reducing the residence time of primary pollutants in the atmosphere and, therefore, the formation of secondary pollutants originating from photochemical transformations (VIEIRA et al., 2023).

In addition to nitro-PAHs, quinones, a group of oxygenated

compounds, were also detected. Quinones can be emitted directly as primary pollutants during the incomplete combustion of fossil fuels (ZIELINSKA et al., 2004), but they can also form through secondary processes in the atmosphere (WALGRAEVE et al., 2010). They are produced from PAHs by photochemical processes or reactions with reactive oxygen species, such as hydroxyl radicals, nitrate, and ozone (VIONE et al., 2006; WANG; ATKINSON; AREY, 2007). However, understanding the mechanisms behind their formation and presence in ambient air remains limited. Compared to other regions, the levels of oxy-PAHs (Σ_3Oxy-PAHs) in Rio de Janeiro were relatively lower than those found in cities in Central Europe (DEGRENDELE et al., 2021), cities in China (LI et al., 2015), São Paulo (Brazil) (PEREIRA et al., 2017; SERAFEIM et al., 2023), and São Carlos (Brazil) (DO NASCIMENTO et al., 2023). Oxy-PAHs contributed the least (10 %) of this class in the samples from the regions studied. Only 2 of the 3 oxy-PAHs were quantified in the samples (9,10-AQ and BA).

Among the oxy-PAHs detected, benzanthrone (BA) was the most prevalent across the three studied regions, highlighting its significance as a primary pollutant emitted by human activities, including vehicle exhaust, industrial operations, and sugar cane burning (KOJIMA et al., 2010; SOUZA et al., 2014). Benzanthrone (BA) displayed medium to strong correlations with high molecular weight PAHs, ranging from 0.51 to 0.83. These findings suggest that the most significance source contributing to benzanthrone concentrations in Rio de Janeiro originates from vehicle emissions, particularly those powered by diesel. While BA and 9,10-anthraquinone (9,10-AQ) can also be released from biomass burning, such as forest fires, the data revealed no correlation with biomarkers of biomass burning, such as saccharides, further supporting the conclusion that vehicle emissions are the primary source of these compounds in the region.

2-nitrobenzantrone (2-NBA), a secondary reaction product, was detected in Gávea and PARNASO. The formation of 2-NBA occurs through a reaction between BA and NO_x or other oxidants under typical atmospheric

conditions (ARLT et al., 2007; ARLT; PHILLIPS; REYNISSON, 2011; KOJIMA et al., 2010; PHOUSONGPHOUANG; AREY, 2003). The intense solar radiation and high temperatures are characteristic of tropical regions like Rio de Janeiro favor this process, resulting in higher concentrations of 2-NBA. 2-NBA was observed in studies conducted in Brazilian cities such as São Paulo (DO NASCIMENTO et al., 2023; PEREIRA et al., 2017; SERAFEIM et al., 2023) and Salvador (SANTOS; DA ROCHA; DE ANDRADE, 2019), with concentrations similar to this study (around 0.21 ng m^{-3}), where photochemical conditions facilitated the production of 2-NBA.

9,10-anthraquinone (9,10-AQ) was detected only in Gávea. The source of this compound cannot be determined, as it may be emitted directly or formed through secondary reactions. A recent study suggested that 9,10-AQ could be produced via the heterogeneous reaction between NO_2 and anthracene (Ant) adsorbed on sea salt (NaCl) particles (WANG; ATKINSON; AREY, 2007). However, since anthracene was not detected in this study, whether the exact mechanism occurs in Rio de Janeiro cannot be confirmed. Given Gávea's proximity to the sea, one hypothesis is that sea salt particles might contribute to the potential formation of 9,10-AQ. This suggests that atmospheric conditions in Gávea, influenced by its coastal location, may play a role in the presence of this compound. However, further research would be necessary to validate this hypothesis.

6.4.4. Sources and contributions of *n*-alkanes

n-Alkanes are important organic components found in particulate matter, which can originate from anthropogenic sources such as vehicle exhaust, fossil fuel, and biomass combustion (LIU et al., 2013; XU et al., 2017; YANG et al., 2023), as well as from biogenic emissions of terrestrial microorganisms and plants (ROGGE et al., 1993c; SIMONEIT, 1989). These non-polar saturated hydrocarbons are stable, highly concentrated in the atmosphere, and tend to adsorb quickly onto particles (CHEN et al., 2019).

The concentrations of *n*-alkanes and branched isoprenoids observed in the three regions of Rio de Janeiro monitored here reflect a trend of increasing concentrations as one moves from urban areas (Gávea: 586 ± 229 ng m^{-3} of total concentration), preserved areas (PARNASO: 823 ± 180 ng m^{-3}), and urban areas with burning (Campos: 1075 ± 278 ng m^{-3}). This pattern can be attributed to the impact of the pollution sources discussed below.

A comparison of the data obtained in the Gávea, PARNASO, and Campos regions with data from other locations around the world, such as São Paulo (VASCONCELLOS et al., 2011) and New Delhi (LI et al., 2014), shows that the concentrations observed in Campos are within a range of values typical for areas with biomass burning. In New Delhi, for example, *n*-alkane concentrations can reach high levels due to the combination of urban (traffic emissions) with waste incineration and biomass burning. However, the values observed in Campos are also significantly lower than those found in areas with high industrial or metropolitan pollution, such as São Paulo (VASCONCELLOS et al., 2011).

n-Alkanes can participate in chemical reactions in the atmosphere, with their volatility and reactivity decreasing as the carbon chain length increases (AUMONT et al., 2013). Short-chain *n*-alkanes (C ≤16) play a significant role in the formation of secondary organic aerosols (MICHOUD et al., 2012), while long-chain *n*-alkanes (C >16) are more stable in the environment and tend to accumulate on particles (CHRYSIKOU; SAMARA, 2009). The carbon number distribution, molecular composition, and mixtures of *n*-alkanes on particles can help assess aerosol migration and identify particle sources.

The evaluation of the most abundant compound (C_{max}) and the distribution range are indicators used to infer sources.(MAZUREK; CASS; SIMONEIT, 1989; YADAV; TANDON; ATTRI, 2013b) The most abundant compound (*n*-Cmax) in Gávea and PARNASO was *n*-C_{27}, while Campos showed a predominance of *n*-C_{29}, characteristic of biogenic contributions.

In this study, there is no evident prominence of odd-numbered compounds in the range of *n*-C_{23} to *n*-C_{33}, and below *n*-C_{23}, no distinct pattern is observed (Figure 10). Pristane (Pr) and phytane (Ph) were found in all three studied regions and are typically indicative of petroleum residue contamination. The ratio of these compounds (pristane/phytane, or Pr/Ph) is a significant indicator for distinguishing between fossil fuel sources and biological material. In this study, all sites showed a Pr/Ph ratio close to 1: in Gávea, it was 0.70; in PARNASO, 0.95; and in Campos, 0.96. This value is comparable to those reported for typical urban samples. In Athens (Greece), a ratio greater than 1.1 was reported for $PM_{2.5}$ (ANDREOU; RAPSOMANIKIS, 2009), and 1.0 in São Paulo (Brazil) (VASCONCELLOS et al., 2010). The presence of pristane and phytane aligns with fossil fuel sources (ABAS; SIMONEIT, 1996; TEN HAVEN et al., 1988). This can be attributed to the lack of preference for chains with different carbon numbers that characterize the incomplete combustion of fuels and emissions from lubricating oils (ABAS; SIMONEIT, 1996; SIMONEIT, 1984); Phytane is rarely found in biological material, and most biological hydrocarbons have a pristane/phytane ratio much greater than 1 (ALVES, 2008).

Figure 6.9 shows the *n*-alkane profiles for each region studied in the dry and rainy seasons. The profiles do not present significant variations between the seasons, even in the dry season. When biomass burning occurs, it does not affect the profile or concentrations significantly in Campos and in the other regions studied (ANOVA, $p>0.05$).

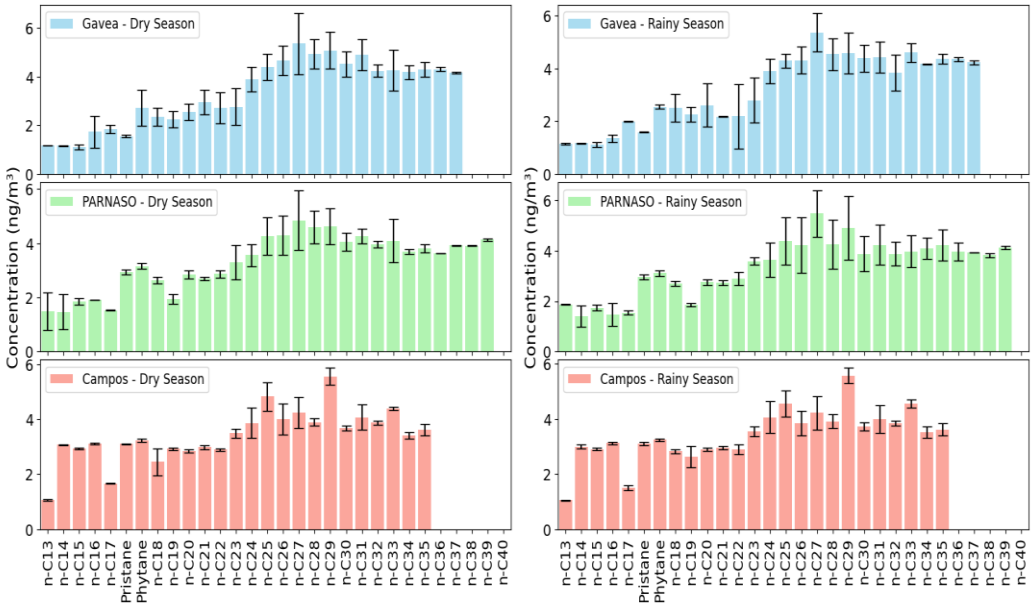

Figure 6.9. Boxplots of 28 *n*-alkanes and branched isoprenoids (Pristane and Phytane) in $PM_{2.5}$ by location and season during the sampling period from February 2022 to June 2023. Bar graph of the averages of *n*-alkanes with their respective standard deviations.

The Carbon Preference Index (CPI) in all locations is near unity, indicating the presence of *n*-alkanes derived from petroleum derivatives or incomplete combustion. From the calculation of the concentration of wax *n*-alkanes (% WNA), it is verified that only 8.0 % of the *n*-alkanes found in the samples from Gávea, 3.0 % in Campos and 5.0 % in PARNASO correspond to the biogenic contribution, revealing a variation from 92 to 95 % of the contributions are from anthropogenic sources.

The *n*-alkanes further confirmed that anthropogenic emissions were the primary contributors in samples from all studied regions of Rio de Janeiro. The patterns of *n*-alkanes can identify different emission sources. There are distinct differences between the *n*-alkane patterns emitted from gasoline and diesel vehicle exhaust particles. The *n*-C_{max} for *n*-alkanes is lower, and the proportion of short-chain *n*-alkanes is higher in particles from diesel vehicle exhaust compared to gasoline vehicles (AMADOR-MUÑOZ et al., 2011; FUJITANI et al., 2012; YANG et al., 2023). This characteristic can help differentiate between *n*-alkanes emitted by diesel and gasoline

vehicles in fine particulate matter. The patterns observed in the three regions indicated emissions from gasoline vehicles, with *n*-alkanes bound to particles (YANG et al., 2023). Overall, vehicle exhaust, primarily from gasoline vehicles, is the main source of *n*-alkanes, which aligns with the current energy consumption structure in Rio de Janeiro and contributes to the levels of PAHs and nitro- and oxy-PAHs.

6.4.5. Anhydro saccharides (AM) as indicators of biomass-burning sources of PM

Anhydro saccharides, including levoglucosan (LEV), mannosan (MAN), and galactosan (GAL), are some of the most common polar (water-soluble) compounds found in aerosol particulate matter (MARYNOWSKI; SIMONEIT, 2022; NOLTE et al., 2001). LEV is a significant component present in atmospheric aerosols, often accompanied by minor stereoisomeric monosaccharide anhydrides such as mannosan and galactosan (LARSEN; SCHANTZ; WISE, 2007; NOLTE et al., 2001; SIMONEIT et al., 1999). These two compounds mainly result from the pyrolysis of hemicelluloses, although they are emitted in much smaller quantities than levoglucosan due to the lower content of hemicelluloses (approximately 30% of dry wood weight) compared to cellulose (about 50%), as well as the lesser amounts of mannose and galactose in hemicelluloses relative to glucose (MARYNOWSKI; SIMONEIT, 2022; SIMONEIT et al., 1999). LEV is emitted in substantial quantities, is a stable molecule, and is specific to the combustion of cellulose-containing materials, making it an ideal molecular marker for biomass burning, distinct from the pyrolysis of fossil fuels. Biomass combustion typically produces a characteristic range of compounds, including LEV, which are absent in fossil fuel combustion. While fossil fuel combustion emits various organic compounds, the specific chemical signature and concentration of LEV are generally much higher in biomass combustion due to the unique nature of cellulose combustion. Therefore, by analyzing the presence and abundance

of LEV, it is possible to distinguish between biomass combustion and fossil fuel combustion, as these sources possess distinct molecular profiles (LARSEN; SCHANTZ; WISE, 2007; SIMONEIT et al., 1999).

In Gávea, the average concentrations of LEV, MAN, and GAL observed in this study are relatively low and consistent with urban areas where biomass-burning activity is limited (Table 6.2), as seen in Frase Valley (Canada) and Elche (Spain).

Table 6.2. Concentrations of monosaccharide anhydrides (ng m^{-3}) reported for different backgrounds.

Local	**Background**	**Concentration of saccharides (ng m^{-3})**		
		LEV	**MAN**	**GAL**
Gávea	Urban	14 ± 4.0	6 ± 4.0	13 ± 11
PARNASO	Preserved area	85 ± 123	57 ± 295	24 ± 24
Campos	Urban with sugarcane burning	251 ± 294	23 ± 30	30 ± 35
Frase Valley (Canada) (LEITHEAD et al., 2006)	Urban	14		
Barcelona (Spain) (RECHE et al., 2012)	Urban	60	6.0	5.0
Balbina (Brazil) (GRAHAM et al., 2003)	Remote	2.0	0.10	0.10
Piracicabá (Brazil)	Urban with burning	66	2.0	3.6

(SOUZA et al., 2014a)				
Elche (Spain) (CLEMENTE et al., 2024)	Urban	34	4.0	2.0
Rondonia (Brazil) (GRAHAM et al., 2002)	Pasture activity	2460	126	55
Rondonia (Brazil) (Graham et al., 2002)	Forest	1180	50	23
Campos dos Goytacazes (Brazil) (DOS SANTOS; AZEVEDO; DE AQUINO NETO, 2002)	Urban with burning	0.15 – 29	0.020 – 0.080	0.050 – 1.2

In 2023, the state of Rio de Janeiro recorded approximately 11,037 vegetation fires, marking a 5.7% increase compared to the previous year. Out of these fires, around 20% occurred in the mountainous region of the state, where PARNASO is situated (CBMERJ – CORPO DE BOMBEIROS DO RIO DE JANEIRO, 2023). In the preserved area of PARNASO, concentrations of these compounds increased compared to Gávea. A possible relationship exists between these fires and the concentration of saccharides found in the region.

In the Campos region, the observed concentrations were significantly

higher. The levels of LEV, MAN, and GAL reflect the direct impact of agricultural activities and the use of fire in the cultivation process, particularly the burning of sugarcane fields, which is a common practice in the area. These levels exceed those noted in Gávea and PARNASO, reinforcing the connection between biomass burning and increased concentrations of atmospheric anhydrosaccharides (DE ALMEIDA AZEVEDO; DOS SANTOS; DE AQUINO NETO, 2002).

When comparing the values from Campos with studies conducted in other regions of Brazil, such as the state of Rondônia, where burning for agriculture and pasture is common, a significant difference in concentrations is evident. During the burning season, LEV concentrations in Rondônia reached 2460 ng m^{-3} in pastures and 1180 ng m^{-3} in forest areas - extremely high values (CLAEYS et al., 2010; DE OLIVEIRA ALVES et al., 2015; GRAHAM et al., 2002), far exceeding any data observed in Campos or the other study areas. These elevated concentrations are directly linked to the intense burning of biomass, especially during the dry season, when the practice of burning pastures to renew the grass is heightened. Furthermore, other areas of the Amazon, such as Balbina (GRAHAM et al., 2003), where burning is less frequent, displayed much lower concentrations.

The concentrations of MAN and GAL are considerably lower than those of LEV (p-value = 0.015) in Campos dos Goytacazes. MAN and GAL result from the pyrolysis of hemicelluloses, which are of a smaller mass than the cellulose present in sugarcane residue (CAUMO et al., 2016; GRAHAM et al., 2002; VASCONCELLOS et al., 2010).

The relative amounts of anhydrosaccharides in PM samples released during biomass combustion can provide valuable insights into the type of biomass burned (SIMONEIT et al., 1999). The LEV/MAN (L/M) ratio has been widely employed to distinguish between the dominant biomass types and combustion methods, as this ratio varies depending on the biomass type and the combustion method used (CHAN et al., 2011; CHENG

et al., 2013). For instance, during controlled burning of sugarcane, the L/M ratio was found to be 10 (HALL et al., 2012), a value similar to values observed in atmospheric PM samples from sugarcane regions in São Paulo state (CAUMO et al., 2016; VASCONCELLOS et al., 2010). In contrast, burning biomass in the Amazon region yielded a significantly higher L/M ratio of approximately 20 (FERNANDES et al., 2022; RIBEIRO et al., 2020). In contrast, the combustion of various wood species in Europe and the United States produced L/M ratios ranging from 1 to 6 (MEDEIROS; SIMONEIT, 2008). This variation in L/M ratios reflects the diverse combustion characteristics and predominant biomass types associated with different regions and burning practices.

The ratio obtained in Campos (L/M = 11) was similar to those obtained in a study of a chamber with sugarcane burning (L/M = 10) and studies carried out during the period of sugarcane burning in São Paulo (CAUMO et al., 2016; PEREIRA et al., 2017; VASCONCELLOS et al., 2010) and in the region itself in 2002 (DE ALMEIDA AZEVEDO; DOS SANTOS; DE AQUINO NETO, 2002). The LEV/GAL (L/G =8.0) ratio suggests that it comes from regional sugarcane burning and not from air coming from places impacted by forest fires source.

The anhydro saccharides showed notable variations, with the Campos dos Goytacazes region exhibiting distinctive patterns (Figure 9). The highest concentrations of LEV (p-value = 0.025), MAN (p-value = 0.045), and GAL (p-value = 0.039) were recorded during the dry season, reaching 800 ng m^{-3} (Figure 6.10). This increase can be attributed to the intensification of burning, particularly the burning of sugarcane fields, a common practice in the Campos dos Goytacazes region. The dry season, marked by low rainfall and high temperatures, promotes biomass burning, resulting in peaks in emissions of these compounds. Furthermore, low humidity contributes to the accumulation of PM in the atmosphere. However, during the rainy season, concentrations tend to decrease due to a reduction in burning facilitated by rainfall, which not only limits burning but

also aids in dispersing and removing pollutants.

Other studies have frequently documented high levels of anhydro saccharides during dry periods, supporting our results (DE ALMEIDA AZEVEDO; DOS SANTOS; DE AQUINO NETO, 2002; MARQUES et al., 2009; VASCONCELLOS et al., 2010, 2011). The dry season in southern Brazil coincides with the peak of the burning season, which is characterized by minimal precipitation (DE ALMEIDA AZEVEDO; DOS SANTOS; DE AQUINO NETO, 2002; FERREIRA et al., 2021; INMET, 2024; LIMA et al., 2020; SILVA et al., 2024a). This seasonal pattern reflects the interaction between agricultural practices and climatic conditions, with the dry season having a greater impact on pollutants, emissions, and air quality.

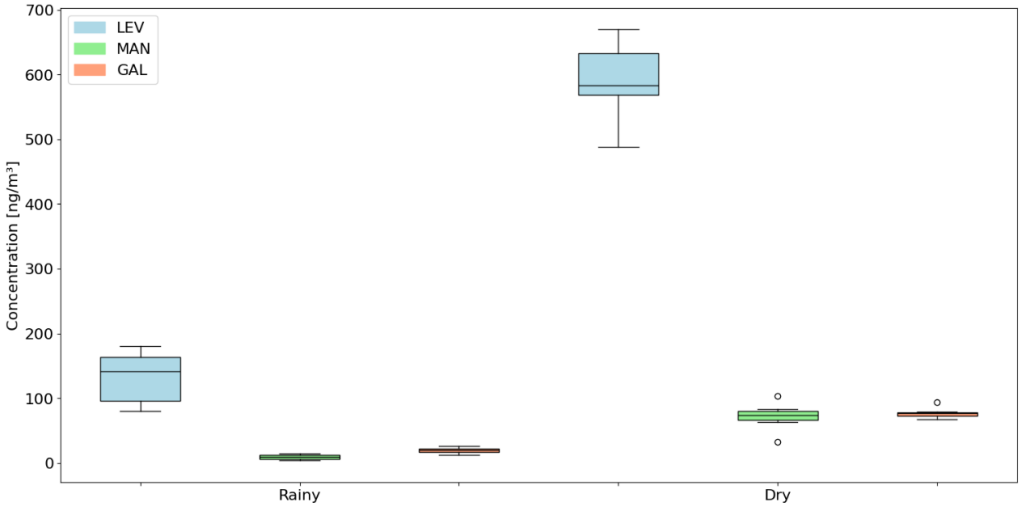

Figure 6.10. The concentration of anhydro saccharides exhibited seasonal variation during the sampling period in Campos dos Goytacazes from February 2022 to June 2023.

In our previous study on mercury in particulate matter across the three regions monitored here during the dry and rainy seasons (SILVA et al., 2024a), we discussed the trajectory of air masses and the contribution and dilution of pollutants from air masses in other regions of Brazil and abroad.

The air masses arriving at Gávea and PARNASO showed very different origins at various levels and during different seasons. At Gávea, in the dry season, the air masses came from the continental regions of the

Andes, including the volcanoes, as well as Central and South Brazil. In the rainy season, their trajectories shifted to originate from the Atlantic Ocean. At PARNASO, the situation contrasts with that of Gávea.

The results of the analysis of the reverse trajectory of Campos air are illustrated in Figure 6.11. In Campos, during both the dry and rainy seasons, the air trajectories predominantly originated from the Atlantic Ocean, moving toward the study site. Compared to continental air masses, the oceanic air masses resulted in a noticeable reduction in pollutant concentrations. Throughout the dry and rainy seasons, Campos was not significantly influenced by air from other countries, being primarily affected by air masses from the ocean. This pattern indicates that the pollutants detected in the region's samples were mainly released by local activities, without contributions from external sources.

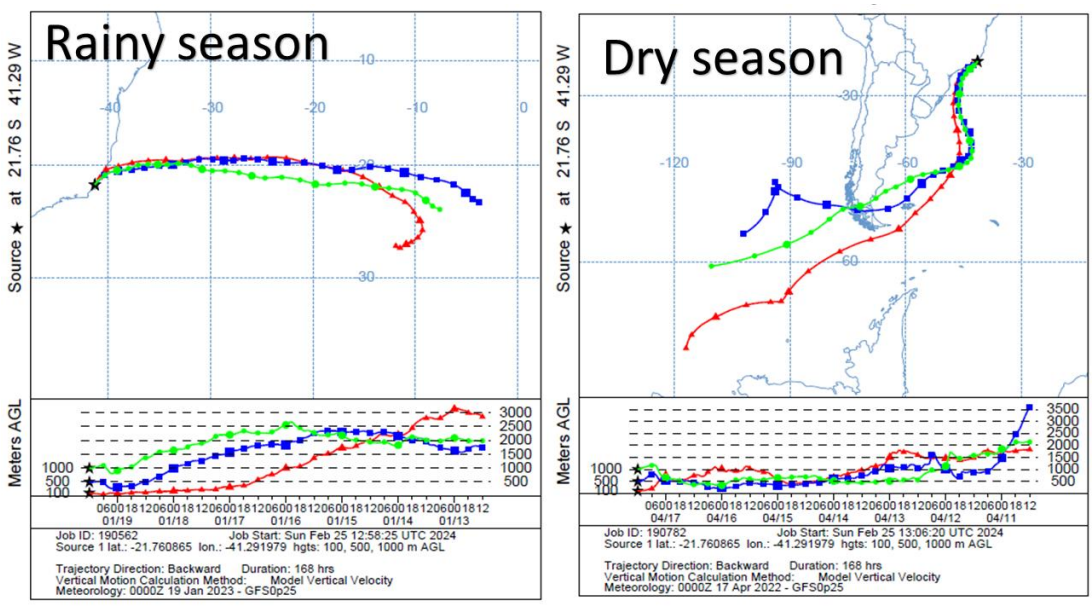

Figure 6.11. A-week air parcel backward trajectories for different seasons. The end point is at 100, 500, and 1000 m AGL at Campos dos Goytacazes station.

6.5. Conclusion

This study provided a detailed analysis of the concentrations and sources of various atmospheric organic compounds, including particulate matter (PM), polycyclic aromatic hydrocarbons (PAHs), nitro-PAHs, quinones (oxy-PAHs), aliphatic hydrocarbons (*n*-alkanes), and anhydrous saccharides, in regions with distinct environmental influences: a densely populated urban area, a less densely populated urban area influenced by sugarcane burning, and a protected forest region. Despite the observed $PM_{2.5}$ concentrations not exceeding the Brazilian regulatory limit, around 63% of the samples surpassed the World Health Organization guidelines, particularly during the dry season when decreased rainfall promotes the persistence of particles in the air.

PAH concentrations, primarily HMW, indicated sources linked to incomplete combustion of fossil fuels and biomass, highlighting urban and protected areas close to heavy traffic and biomass burning, as observed in Campos dos Goytacazes. PAH profiles suggest that gasoline is the main source of pollutants in these areas, while nitro-PAHs and quinones reflect the influence of secondary and photosynthetic sources. Seasonal variations were noted in compounds such as anhydro saccharides, which achieved significantly higher concentrations during the dry season and were associated with burning sugarcane.

Regarding sources, PAHs indicated gasoline as a source, while *n*-alkanes reflected a predominance of petrogenic sources, corroborating the fact that fossil fuel emissions are involved. Nitro-PAHs and oxy-PAHs revealed some contributions from diesel in the region, and saccharides indicated biomass burning, particularly in Campos, an area where sugarcane is burned.

6.6. Supplementary Material 2

Table S1. Particulate matter sampling period performed using fiberquartz filter.

Date	Gávea	PARNASO	Campos dos Goytacazes
21/02/2024	X	X	X
17/03/2022	X	X	X
19/04/2024	X		X
16/05/2022	X	X	
14/06/2022	X		X
15/07/2022	X		X
18/08/2022	X	X	X
13/09/2022	X	X	X
13/10/2022	X	X	X
17/11/2022	X	X	X
19/12/2022	X		X
18/01/2023	X		
26/01/2023	X	X	X
06/02/2023		X	
15/02/2023	X	X	
20/03/2023	X	X	X
17/04/2023	X	X	X
24/04/2023			X
17/05/2023	X	X	X
14/06/2023	X	X	

19/06/2023			X
Total of samples (*n*)	18	14	16

Table S2. the mass-to-charge ratio (*m/z*) and retention time employed in the determination of 37 PAH.

Conf 1	Conf 2	Quan	Analyte	RT
		136	NAF-d8	12,09
127	129	**128**	NAF	12,16
		142	2ME-NAF	14,50
		142	1ME-NAF	14,83
		156	C2NAF	17,20
		170	C3NAF	19,74
		184	C4NAF	22,27
		184	RETENE	22,29
151	153	**152**	ACENAFT	17,75
		164	ACE-d10	18,3
152	153	**154**	ACE	18,39
165	167	**166**	FLUOR	20,41
		180	C1FLUOR	22,66
		194	C2FLUOR	24,76
		208	C3FLUOR	27,21
	185	**184**	DBZ	23,56
		198	C1DBZ	25,63
		212	C2DBZ	27,41
		226	C3DBZ	28,72
		240	C4DBZ	-
		188	FEN-d10	23,98
176	179	**178**	FEN	24,06
176	179	**178**	ANT	24,27
		192	C1FEN	26,26
		206	C2FEN	28,32
		220	C3FEN	30,02
		234	C4FEN	31,96
101	203	**202**	FLUOR	28,69
200	203	**202**	PIR	29,5
		216	C1PIR	31,21
		230	C2PIR	32,96
		244	C3PIR	34,63
		244	p-TERPH	30,46
229	226	**228**	BzA(ANT)	34,27
		240	CRIS-d12	34,29

226	229	**228**	CRIS	34,34
		242	C1CRIS	35,96
		256	C2CRIS	37,72
125	253	**252**	BzB	38,1
125	253	**252**	BzK	38,21
	253	**252**	BzE	39,02
125	253	**252**	BzAPIR	39,2
	253	**252**	PER	39,43
		264	PER-d12	39,48
		276	IND	43,74
139	279	**278**	DBZ(ah)	43,91
138	277	**276**	BZ(ghi)	44,57

Table S3. Analytical parameters of the method employed in the determination of nitro-PAH and oxy-PAH.

Nitro-PAH	**Linear range (ng mL^{-1})**	**R^2**	**Regression equation**	**LOD (pg)**	**LOQ (pg)**
1-Nitronaphthalene	9.9 - 100	0.9979	y = 237.18x + 45.076	3.0	9.9
2-Nitronapthalene	6.2 - 100	0.9992	y = 189.58x + 66.463	1.9	6.2
1-Methyl-4-nitronaphthalene	11.2 - 100	0.9973	y = 333.37x + 944.46	3.4	11.2
1-Methyl-5-nitronaphthalene	9.7 - 100	0.9985	y = 203.77x + 633.87	2.9	9.7
1-Methyl-6-nitronaphthalene	7.0 - 100	0.9992	y = 179.69x - 237.13	2.1	7.0
2-Methyl-4-	10.1 -	0.9984	y = 239.49x +	3.0	10.1

nitronaphthalene	100		227.24		
2-Nitrobiphenyl	7.7 - 100	0.9990	y = 29.235x + 255.7	2.3	7.7
3-Nitrobiphenyl	7.5 - 100	0.9991	y = 255.49x - 48.391	2.2	7.5
4-Nitrobiphenyl	8.8 - 100	0.9988	y = 171.97x + 222.7	2.6	8.8
5-Nitroacetaphthene	6.6 - 100	0.9993	y = 219.16x + 87.582	2.0	6.6
2-Nitrofluorene	7.1 - 100	0.9992	y = 289.44x + 748.67	2.1	7.1
2-Nitrophenanthrene	7.9 - 100	0.9979	y = 669.17x - 699.98	2.4	7.9
3-Nitrophenanthrene	19.6 - 100	0.9951	y = 7756.8x - 35725	5.9	19.6
9-Nitrophenanthrene	9.8 - 100	0.9978	y = 546.69x - 816.7	2.9	9.8
2-Nitrofluoranthene	11.7 - 100	0.9961	y = 508.22x - 1070.9	3.5	11.7
3-Nitrofluoranthene	16.6 - 100	0.9922	y = 2102.6x - 5993.7	5.0	16.6
2-Nitropyrene	6.4 - 100	0.9988	y = 112.83x + 55.135	1.9	6.4

6-Nitrochrysene	8.2 - 100	0.9981	y = 2442.2x - 5358.2	2.4	8.2
2-Nitrobenzanthrone	8.2 - 100	0.9985	y = 112.56x - 173.58	2.5	8.2
6-Nitrobenzo[*a*]pyrene	7.0 - 100	0.9989	y = 1323.5x - 1951.1	2.1	7.0

Oxy-PAH	**Linear range**	**Linearity**	**Regression equation**	**LOD (pg)**	**LOQ (pg)**
1,4-Naphtoquinone	2.69 - 100	0.9994	y = 6059x – 3028.9	0.81	2.69
9,10-Anthraquinone	7.20 - 100	0.9969	y = 5714x – 2768.8	2.16	7.20
Benzanthrone	5.50 - 100	0.9981	y = 13549x – 8480.9	1.70	5.50

Table S4. Concentrations (pg m^{-3}) of individual PAH, aliphatic hydrocarbons (alkans and isoprenoids), nitro-PAHs, oxy-PAHs and anydrosaccharides. See text for codes of compound names. (nd = not detected)

Comp.	GÁVEA		PARNASO		CAMPOS	
	Average ± SD	Range	Average ± SD	Range	Average ± SD	Range
N	90 ± 38	38 - 152	102 ± 49	31 – 157	57 ± 39	15 – 94
C1_NAF	nd	nd	nd	nd	nd	nd
C2_NAF	nd	nd	nd	nd	nd	nd
C3_NAF	nd	nd	nd	nd	nd	nd
C4_NAF	nd	nd	nd	nd	nd	nd
Aceft	nd	nd	nd	nd	nd	nd
Ace	nd	nd	nd	nd	nd	nd
Flu	nd	nd	nd	nd	nd	nd
C1_FLU	nd	nd	nd	nd	nd	nd
C2_FLU	nd	nd	nd	nd	nd	nd
C3_FLU	nd	nd	nd	nd	nd	nd
DBzTIOF	nd	nd	nd	nd	nd	nd
C1_DBzTIOF	nd	nd	nd	nd	nd	nd
C2_DBzTIOF	nd	nd	nd	nd	nd	nd
C3_DBzTIOF	nd	nd	nd	nd	nd	nd
Fen	7.1 ± 4.3	2.0 –	8.9 ± 11	1.2 –	9.14 ± 10	0.25 - 25

		15		32		
Ant	nd	nd	nd	nd	nd	nd
C1_FEN	nd	nd	23 ± 0.47	23. – 25	nd	nd
C2_FEN	nd	nd	nd	nd	nd	nd
C3_FEN	nd	nd	nd	nd	nd	nd
C4_FEN	nd	nd	nd	nd	nd	nd
RET	39 ± 36	25 - 159	43 ± 54	20 - 186	97 ± 122	22 - 478
Ft	7.7 ± 4.86	0.90 – 12	20 ± 3.0	17 – 23	11.48 ± 8.53	5.44 - 17.51
Pi	nd	nd	0.35 ± 0.31	0.13 - 0.57	18 ± 1.3	17 - 19
C1_PIR	nd	nd	nd	nd	nd	nd
C2_PIR	nd	nd	nd	nd	nd	nd
BaA+Cri	39 ± 0.65	38 - 39	40 ± 44	5.8 - 172	35 ± 19	13 – 60
C1_CRIS	nd	nd	nd	nd	nd	nd
C2_CRIS	nd	nd	nd	nd	nd	nd
BbFt+BkFt	75 ± 33	52- 113	144 ± 205	23 – 380	120 ± 61	60 - 183
BePi	4.5 ± 1.2	3.1 - 5.2	119 ± 1.7	118 - 121	30 ± 45	3.8 – 82

BaPi	nd	nd	137 ± 0.26	137 – 137	nd	nd
Per	nd	nd	nd	Nd	22 ± 26	4.0 - 41
I-Pi	239 ± 41	204 – 284	240 ± 2.7	244 - 247	216 ± 8.9	210 – 222
DBahA	nd	nd	nd	nd	nd	nd
BghiPe	389 ± 53	334 - 438	280 ± 84	35- 298	255 ± 149	142 – 412
Σ_{37}PAH	184 ± 291	6.2 – 1167	385 ± 639	27 – 2237	236 ± 320	13 - 1037
Σ*n*-alkanes	59 ± 18	24 - 93	74 ± 13	55 – 110	62 ± 13	44 - 81
Pristane	1.6 ± 0.040	1.5 - 1.6	2.9 ± 0.090	2.8 - 3.0	3.1 ± 0.030	3.0 - 3.1
Phytane	2.7 ± 0.63	1.6 - 3.7	3.1 ± 0.11	2.9 - 3.2	3.2 ± 0.040	3.1 - 3.3
1,4-NQ	nd	nd	nd	nd	nd	nd
9,10-AQ	114 ± 71	19 – 267	nd	nd	nd	nd
BA	105 ± 111	0.41 – 392	112 ± 223	0.55 - 842	33 ± 28	0.20 – 71
1-NNAP	4.3 ± 3.0	0.69 - 7.53	6.5 ± 0.66	6.1 - 7.0	2.5 ± 1.2	0.60 - 4.6

1-Methyl-NNAP	0.45 ± 0.39	0.030 - 1.2	0.08 ± 0.08	0.030 - 0.19	0.11 ± 0.13	0.010 - 0.25
2-NNAP	2.6 ± 0.8	2.1 - 3.5	10 ± 0.011	9 - 11	0.74 ± 0.88	0.10 - 2.5
2-NBP	nd	nd	nd	nd	0.18 ± 0.010	0.18 - 0.20
1-Methyl-5-NNAP	1.0 ± 0.68	0.43 - 2.46	nd	nd	0.24 ± 0.13	0.15 - 0.33
1-Methyl-6-NNAP	0.45 ± 0.11	0.37 - 0.58	0.40 ± 0.03	0.39 - 0.41	0.26 ± 0.18	0.11 - 0.50
2-Methyl-4-NNAP	0.72 ± 0.17	0.49 - 0.98	1.2 ± 0.0010	1.2 - 1.3	0.36 ± 0.20	0.36 - 0.38
3-NBP	0.31 ± 0.19	0.15 - 0.72	0.34 ± 0.37	0.16 - 1.5	0.57 ± 0.48	0.12 - 1.1
4-NBP	2.4 ± 0.96	0.84 - 3.6	2.1 ± 0.70	0.61 - 3.0	2.6 ± 2.6	0.01 - 5.8
5-NACE	0.13 ± 0.12	0.010 - 0.25	1.4 ± 0.012	1.4 - 1.5	nd	nd
2-NFLU	0.42 ± 0.11	0.30 - 0.58	0.34 ± 0.24	0.18 - 0.99	0.28 ± 0.090	0.22 - 0.41
2-NPHE	0.060 ± 0.050	0.010 - 0.15	0.050 ± 0.050	0.010 - 0.14	0.060 ± 0.050	0.02 - 0.13
3-NPHE	nd	nd	nd	nd	nd	nd

9-NPHE	2.08 ± 1.68	0.80 - 5.7	2.7 ± 1.9	0.69 - 6.9	1.5 ± 0.94	0.010 - 2.31
2-NFLT	0.30 ± 0.63	0.020 - 1.7	0.13 ± 0.070	0.010 - 0.20	0.060 ± 0.040	0.020 - 0.12
3-NFLT	0.39 ± 0.40	0.010 - 0.96	0.060 ± 0.030	0.030 - 0.11	0.11 ± 0.060	0.050 - 0.20
6-NCRY	0.34 ± 0.0012	0.34 - 0.36	0.16 ± 0.18	0.020 - 0.41	nd	nd
2-NBA	0.23 ± 0.040	0.20 - 0.26	0.19 ± 0.012	0.19 - 0.20	nd	nd
6-NBAP	0.60 ± 1.1	0.010 - 3.9	0.16 ± 0.14	0.020 - 0.51	0.10 ± 0.090	0.020 - 0.28
ΣNPAH	6.0 ± 5.5	0.18 - 21	6.6 ± 5.1	0.030 - 16.7	4.8 ± 3.6	0.53 – 12
LEV	13 ± 6.8	5.3 – 30	78 ± 33	39 – 129	406 ± 303	79 – 834
GAL	13 ± 12	0.37 – 42	33 ± 22	10 - 76	56 ± 31	12 – 94
MAN	6.2 ± 4.4	1.1 – 17	201 ± 404	23 - 1118	47 ± 28	15 - 97

7. Research Article 4 – Real-time monitoring of nitrogen oxides emission factors using sensors in the exhaust pipes of heavy vehicles in the Metropolitan Region of Rio de Janeiro

Luis F. M. Silva [1], Alex R. H. De La Cruz [1], André H. M. Nunes [2] and Adriana Gioda [1],*

[1]Pontifical Catholic University of Rio de Janeiro, 22451-900, Rio de Janeiro, RJ, Brazil.

[2]ZANE-Tecnologia da Informação LTDA, 22451-900 Rio de Janeiro-RJ, Brazil

Corresponding author: Adriana Gioda - agioda@puc-rio.br

Published: Journal of the Brazilian Chemical Society (2024) available online since 24/10/2023.

Abstract

The Metropolitan Region of Rio de Janeiro is one of the most populous in Brazil, besides being one of the most important routes for marketing goods through heavy vehicles. This type of vehicle is the main source of nitrogen oxides (NO_x) emission into the atmosphere. To assess NO_x emission factors, this pilot study used sensors to monitor in real-time the exhaust of 9 trucks from July to September 2022. To the best of our knowledge, this is the first study carried out in the city using low-cost sensors. Although there is legislation to reduce the emission of pollutants from the vehicle fleet, the results showed that 7 out of 9 trucks, exceeded the stipulated limits, reaching 6 g kWh^{-1}. Furthermore, carrying out the maintenance of the engine of one of the vehicles decreased 60 % of the NO_x emission, even being an old vehicle. Thus, with this data, it was verified that the sensor performed excellently in monitoring NO_x, demonstrating

robust performance. This pilot study is part of a project that aims to make a long-term study of NO_x emissions factors from heavy-duty diesel vehicles using sensors and other parameters.

Keywords: NO_x, emission factor, remote sensing, Rio de Janeiro.

7.1. Introduction

Air pollution is at the top of the list of environmental issues facing humanity today as a result of the world's booming population and industrial activities. Air quality is the reason behind several types of fatal diseases, including respiratory, lung, heart, cerebrovascular, and lung cancer (AJMAL et al., 2022; GULL et al., 2013; KAMAREHIE et al., 2017). The World Health Organization (WHO) recently reported that about 7 million people die every year from air smoke. In the same WHO report, it is estimated that 9 out of 10 people breathe with a quality that exceeds WHO recommendations. The main contaminants that increase air pollution are nitrogen oxides (NO_x), sulfur oxides (SOx), ozone (O_3) and particulate matter (PM) (AJMAL et al., 2022; HAN; PARK; JEONG, 2019; WHO, 2022b). During the COVID-19 pandemic, a concerning association has been observed between exposure to atmospheric pollutants, such as NO_x, and the increase in morbidity and mortality related to the disease (BARNETT-ITZHAKI; LEVI, 2021).

Emissions of NO_x are a major issue when it comes to air quality and the environment as a whole. These chemicals, which include nitric oxide (NO) and nitrogen dioxide (NO_2), are produced mainly during combustion processes, especially in internal combustion engines present in the vehicle fleet (DA SILVA JUNIOR; ANDRADE, 2013; PILUSA; MOLLAGEE; MUZENDA, 2012; RAVINA et al., 2022). In the diesel engine, NO_x is formed from two mechanism, i.e., from N content of the fuel and combustion conditions and from chemical formation of NO using N_2 and O_2 from the air and high temperatures (exceeding 1400 °C) (GUARDIOLA et al., 2017).

Furthermore, NO_x is one of the main precursors of tropospheric O_3 (a component of photochemical smog), which is highly harmful to human health and can cause respiratory problems, especially in children and the elderly. In addition, NO_x also contributes to the formation of fine particles in the air, which are able to penetrate deep into the lungs and cause even more serious respiratory problems (MENDOZA-VILLAFUERTE et al., 2017; NING; WUBULIHAIREN; YANG, 2012; PARDO et al., 2011; SLEZAKOVA et al., 2011).

To assess the amount of NO_x released into the atmosphere by the vehicle fleet, emission factors are used. Factors are influenced mainly by age and maintenance status of vehicles, type of fuel used, traffic conditions and driving style of drivers (AGUIAR et al., 2015; CETESB, 2023). Older, poorly maintained cars tend to emit greater amounts of NO_x than newer, and well-maintained vehicles. In addition, fuel type plays a key role, with fossil fuels such as gasoline and diesel generally resulting in higher NO_x emissions compared to cleaner fuels such as Natural Gas Vehicle (NGV) or electric vehicle technologies (BURUIANA et al., 2021; MCCAFFERY et al., 2021; MENDOZA-VILLAFUERTE et al., 2017; PILUSA; MOLLAGEE; MUZENDA, 2012).

In Brazil, the transport of passengers and cargo is carried out mostly by road, having significant dependence on fossil fuels. Thus, this sector has contributed decisively to the increase of emissions of air pollutants (LOPES et al., 2018) According to the National Energy Balance for 2021 (MINISTÉRIO DE MINAS E ENERGIA, 2022), the transport sector consumed 73 % of petroleum products in relation to the commercial, agricultural, public, residential, and industrial sectors. Of this percentage, about 94 % were used in road transport, with more than 30 % of the national greenhouse gas emissions (GEEs) coming from the transport sector.

Although vehicle emission standards have become increasingly stringent over time around the world, most current road fleets continue to meet the oldest emission standards and ageing engines, as well as

emission control devices, contributes significantly to the exacerbation of air quality on the road (NING; WUBULIHAIREN; YANG, 2012). For the control of vehicular pollution in Brazil, the National Environmental Council (CONAMA) created the Air Pollution Control Program for Automotive Vehicles (PROCONVE) in 1986 (Resolution 18/1986) (CONAMA, 1986). In 2022, the last phases of L-7 for light vehicles and P-8 for heavy vehicles took place (CONAMA, 1986, 2018a). The P-8 standard specifies maximum emission limits for exhaust, particulate and noise, as well as durability requirements, more stringent on-board diagnostic systems (OBD) and on-road testing, among other requirements. It is equivalent to the Euro VI standard and will align the regulations for heavy vehicles from Brazil to the European Union (CONAMA, 2018a). The introduction of the P-8 standard in Brazil will bring extensive benefits for the control of harmful emissions by heavy vehicles and the reduction of the associated impacts on air quality and public health. Compared to the P-7 standard, introducing the P-8 standard would bring about $11 in health benefits for every $1 invested in more advanced vehicle emission control technologies (MILLER et al., 2016).

Measurements of NO_x emission in vehicles in real conditions of use are very important, since the P-8 phase of PROCONVE, measurements of emissions in real traffic are mandatory. Recently, research projects have been conducted to investigate low-cost sensors that can be deployed in vehicles and effectively monitor pollutant emissions (CASTELL et al., 2017; GONZALEZ et al., 2022; KAIVONEN; NGAI, 2020; KARAGULIAN et al., 2019; LIU; ZIMMERMAN, 2021). Many companies have used sensors to carry out real-time monitoring of pollutants, based on the Internet-of-Things (IoT). IoT is a network of devices that can collect and exchange data, allowing devices (sensors and electronic components) to connect and collaborate with other IoT devices (KOPETZ, 2011).

The Metropolitan Region of Rio de Janeiro (MRRJ) has a population of more than 13 million and 5 million vehicles, which 38 % are light gasoline

vehicles (GVs), and 4 % are HDDVs (DETRAN-RJ, 2022). The humid and hot climate and the high solar radiation also affect the air quality due to the possibility of chemical/photochemical reactions. Therefore, this scenario is conducive to carrying out studies that include emissions from the transport sector. There is a need for emission factors for HDDVs in the estimation of emission inventories in the city of Rio de Janeiro derived from real-time measurement sensors. This pilot study aimed to measure the NO_x emission factors from exhaust pipe of heavy vehicles in the city of Rio de Janeiro using a low-cost sensor. This study is unprecedented in Rio de Janeiro and the university-startup partnership benefits society as a whole.

7.2. Material and Methods

Description in topic 3.7, page 53.

7.3. Results and Discussion

7.3.1. Sensing performance

Table 7.1 shows the number and percentage of the zero and non-zero measurements. Around 173,000 records were used, including the records retrieved from the backup database when measuring the sensor probe performance.

Table 7.1. Success rate for the NO_x air quality sensors.

	NOx
Non-zero measurements	172,942
Percentage	96.3 %
Zero measurements	5,250
Percentage	3.7 %

NO_x sensor probe achieved a robust performance, since the percentage of zero measurements was low (3.7 %).

7.3.2. NO_x emission factor

NO_x measurement occurs when the vehicle is both stationary and in motion; however, the NO_x emission limit calculation is based only on vehicles in motion. When the vehicle is idle, the standard is low and consistent for all vehicles. The distribution of average NO_x emission factors for individual trucks on a g kWh^{-1} basis along the test route is provided in Figure 7.1. The emission factors were evaluated both with the truck in motion (A) and stationary (P).

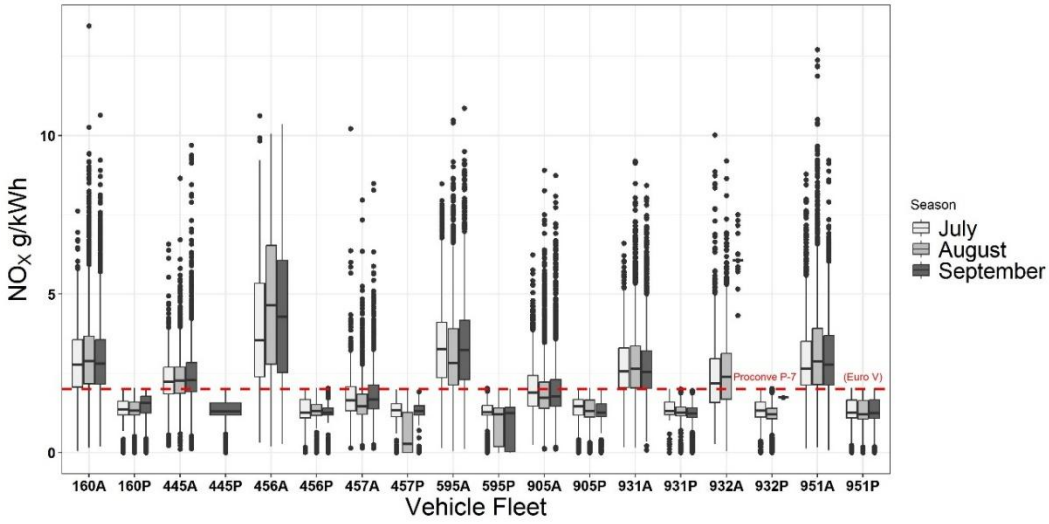

Figure 7.1. Monthly NO_x emission factors in nine heavy vehicles monitored with sensor during 2022. Vehicles are identified using a letter to designate the vehicle (P = stationary, A = in motion), a number to identify the engine model.

Vehicles in motion had a mean and standard deviation of emission factors of 2.9 ± 1.0 g kWh^{-1} during the campaign, with the average emission factors ranged from 1.6 to 6.1 g kWh^{-1}, while at a standstill had a mean and standard deviation of 1.2 ± 0.2 g kWh^{-1} with the average ranged 0.064 to 1.7 g kWh^{-1}. There was statistical difference in the emissions in motion and stationary, however no differences were observed among the monthly emissions, suggesting an emission pattern.

Although the current Brazilian standard, PROCONVE P-8, has been in operation since 2022, the vehicles in this study are in the PROCONVE P-

7 phase since 2012. The NO_x standard in PROCONVE P-7 legislation is 2 g kWh^{-1}, while in the P-8 is 0.4 g kWh^{-1}. exceeded the maximum permissible emissions in the P7 and P8 phases. The NO_x emission factors from seven out of the nine HDDVs exceeded the maximum permissible emissions in the P-7 and P-8 phases, and emitted very high levels of NO_x during operation, even with the EGR system.

Despite the best technologies and cleaner fuels, high emissions of pollutants are still observed, indicating that lack of maintenance may be the reason (BAPTISTA VENTURA et al., 2020). Figure 7.2 shows a 60 % reduction in NO_x emissions after changing the pressure control valve in the 456A vehicle. The average emission factors decreased from 3.76 g kWh^{-1} to 1.48 g kWh^{-1} after maintenance.

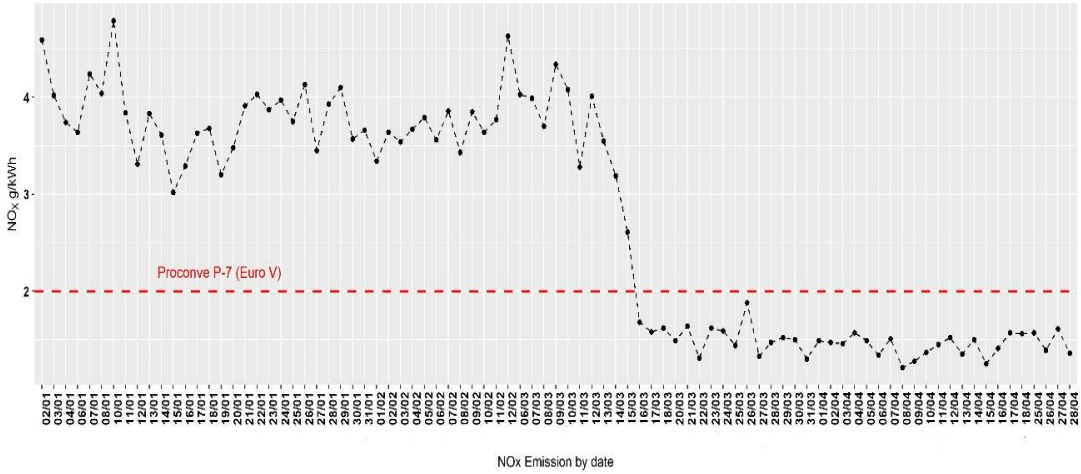

Figure 7.2. NO_x emission factor before and after maintenance of the 456A vehicle engine.

Emission measurement techniques for Heavy-Duty Diesel Vehicles (HDDVs) usually encompass tests conducted on engine and chassis dynamometers, tunnel investigations (BURGARD et al., 2006; FREY; ROUPHAIL; ZHAI, 2008; GAJENDRAN; CLARK, 2003; YANOWITZ et al., 1999). However, numerous engine dynamometer test cycles rely on steady-state modal profiles that might not accurately mirror actual vehicle activity patterns. Chassis dynamometer tests come at a significant cost, and the

availability of such dynamometers is limited. Tunnel studies have limitations in their capacity to distinguish between distinct vehicle types (FREY; ROUPHAIL; ZHAI, 2008; KIRCHSTETTER et al., 1999; LI et al., 2023; MILLER et al., 2003). Thus, real-time measure NO_x emission factors using low-cost sensor is an alternative. The use of sensors can help reduce vehicle issues related to NO_x emissions and ensure compliance with PROCONVE legislation.

Pollutant and air quality monitoring is conducted at monitoring stations, which have high installation and monitoring costs. Conventional air monitoring stations are large, expensive, and non-scalable, which limits data access. Researchers are exploring other solutions for air pollution monitoring, dubbed the future air pollution monitoring system (IDREES; ZHENG, 2020; KAIVONEN; NGAI, 2020). The sensor, together with the IoT module, is only $350, making it a cost-effective alternative.

In recent years, significant efforts have been devoted to monitoring air pollution. However, existing and proposed systems lack the capability to provide sufficient spatial and temporal resolutions of pollution information accurately and economically (CHIANG; ZHANG, 2016; HAN; PARK; JEONG, 2019). Therefore, it is necessary to explore more cost-effective ways of conducting such monitoring. This pilot study represents the initial step in this direction.

7.4. Conclusion

The first results aim to evaluate the behavior of the sensor and present the first data. The sensor achieved its goal, with 96.3 % of the non-zero measurements, demonstrating robust performance. Regarding the values for NO_x emission factor, seven out of nine monitored vehicles (80 %) presented averages above the stipulated by the Brazilian legislation (2 g kWh^{-1} PROCONVE, P-7), reaching up to 6 g kWh^{-1}. If the MRRJ vehicle fleet follows this behavior, with emissions up to three times higher than the P-7 standard, the levels of NO_x in the atmosphere can be considered high

and cause an increase in O_3 levels. Fleet monitoring is essential to know which vehicles meet the legislation and which ones must be replaced or repaired. In general, better emission control or the adoption of zero and almost zero emission technologies for professional vehicles is required to achieve significant NO_x reductions in urban areas, considering their high NO_x emissions in use observed in this study. In addition, the performance of engine maintenance promoted a decrease in the NO_x emission rate, lower than that stipulated in phase P-7. This pilot study is part of a project that aims to make a long-term study of NO_x emissions from heavy-duty diesel vehicles using sensors and other parameters.

8. Research Article 5 – Real-Time Analysis of NO_x Emissions in Heavy-Duty Diesel Vehicles: Impact of Speed and Variations Across Vehicle Groups

Luis Fhernando Mendonça da Silva [1], Mariana Ribeiro Barros de Alencar[2], André Heriberto Moraes Nunes [2] and Adriana Gioda [1],*

[1]Pontifical Catholic University of Rio de Janeiro, 22451-900, Rio de Janeiro, RJ, Brazil.

[2]ZANE-Tecnologia da Informação LTDA, 22451-900 Rio de Janeiro-RJ, Brazil

Paper submitted with major review: Atmospheric Pollution Research

Abstract

This study analyzes the NO_x emission factors of heavy-duty diesel vehicles monitored in the Metropolitan Region of Rio de Janeiro (MRRJ) between February 2022 and April 2024, with the aim of assessing compliance with the PROCONVE (Air Pollution Control Program for Vehicles) program. To the best of our knowledge, this study is unprecedented in the country and one of the few studies conducted in Latin America. The results showed great variability in NO_x emissions, reflecting differences in emission control technologies, vehicle age, maintenance conditions, and operational characteristics. The average NO_x emissions for the 14 vehicles were 3322 ± 106 ppm, ranging from 1.51 to 1257 ppm. The analysis indicated that vehicle weight influenced emissions, with greater variability in the lightest vehicles (16,000 kg). Although the average emissions across weight groups (16,000 kg and 23,000 kg) were similar, the variability was greater in the lightest group. Engine power was another relevant factor, with intermediate-power vehicles (188 kW and 191 kW) presenting the lowest emissions, challenging the assumption that more

powerful engines always generate more emissions. Regarding the age of the vehicles, the newer ones emitted less NO_x than the older ones. When converting the emission factors to g kWh^{-1}, more than 50% of the vehicles exceeded the 2 g kWh^{-1} limit established by the PROCONVE P-7 standard. Most of the monitored vehicles operated at low speeds (up to 40 km/h), typical of urban environments, highlighting the influence of traffic conditions on emissions. The analysis revealed different behaviors among the vehicle groups, with emissions increasing for the WM group and decreasing for the M group as speed increased. The results reinforce the need for environmental policies aimed at fleet renewal, adoption of advanced emission control technologies, and promotion of more efficient driving practices. Future studies should investigate the relationship between operating conditions, speed variability and NO_x emissions in different contexts.

Keywords: NO_x, emission factor, HDDV, PROCONVE, air pollution.

8.1. Introduction

Air pollution represents a significant and growing concern in urban areas, particularly in developing countries such as Brazil. Of the various air pollutants, nitrogen dioxide (NO_2) which originates from NO_x emissions is particularly harmful. They contribute to the formation of acid rain and photochemical smog, and they have significant negative impacts on human health (AJMAL et al., 2022; GULL et al., 2013; KAMAREHIE et al., 2017; RAVINA et al., 2022). As reported by the World Health Organization (WHO), millions of individuals perish annually as a consequence of exposure to elevated levels of pollutants, with 90 % of the global population breathing air with a quality below the recommended (WHO, 2022b).

The transport sector plays a significant role in air pollutant emissions. According to the International Energy Agency (IEA), the global transport

sector is responsible for around 25 % of total emissions from fuel combustion, with road transport accounting for most of these emissions (IEA, 2015a). In Brazil, the transport sector accounts for about 20 % of global greenhouse gas (GHG) emissions. In 2020, fossil fuel combustion activities accounted for 95 % of energy sector emissions, with 80 % of these emissions coming from transportation (MCT, 2022). NO_x emissions are 70 % concentrated in the Energy sector, with almost 40 % coming from the transport sub-sector specifically from road transport (SEROA DA MOTTA et al., 2011).

To mitigate these impacts and limit the increase in global average temperature to 2 °C, the IEA estimates that emissions from the transport sector must be reduced by more than 34 % by 2050 compared to current levels and emphasizes that most energy efficiency investments should be directed to the transport sector (IEA, 2015b, 2015c). Achieving these targets can be facilitated by a better understanding of the evolution of vehicle fleets (fleet dynamics), considering the impacts of changes in the material composition, weight, and propulsion systems of new vehicles, as well as on energy systems and consumer behavior (SERRENHO; NORMAN; ALLWOOD, 2017).

Given that NO_x emissions are predominantly associated with anthropogenic sources, especially the burning of fossil fuels, road transportation stands out as one of the main contributors to air pollution in urban areas around the world (ASGHAR et al., 2021; MENDOZA-VILLAFUERTE et al., 2017). In Brazil, this impact is even more evident due to the large circulation of heavy-duty diesel vehicles (HDDV) in urban centers, making the transport sector a significant source of NO_x emissions (CLARK; GAJENDRAN; KERN, 2003; SILVA et al., 2024b). HDDV are particularly relevant in this scenario, as they are responsible for a significant proportion of NO_x emissions in urban environments due to their high fuel consumption and long operating hours (HALLMARK; WANG; SPERRY, 2013; JOHNSON, 2011). Recent studies have highlighted that despite

advances in emission control technologies, real-world NO_x emissions from HDDVs often exceed regulatory limits, highlighting the need for continuous monitoring and mitigation efforts (BURGARD et al., 2006; HALLMARK; WANG; SPERRY, 2013; SHAH et al., 2006; WU et al., 2012; ZHANG et al., 2014).

In-vehicle measurements of NO_x emissions from HDDVs have advanced in recent years, particularly with the use of portable emission measurement systems (PEMS), which allow for real-world data collection under different driving conditions. Studies have shown that real-world NO_x emissions can be significantly higher than those recorded in laboratory tests, highlighting the importance of in-use monitoring to ensure regulatory compliance (HE et al., 2017; JIANG et al., 2022; ZHANG et al., 2014).

As urbanization and the vehicle fleet continue to expand, it is more necessary than ever to obtain comprehensive data on NO_x emissions to implement effective mitigation strategies. Furthermore, the implementation of more efficacious emission control technologies is essential to enhance air quality and safeguard public health. The Program for the Control of Air Pollution from Motor Vehicles (PROCONVE) is responsible for regulating emission standards in Brazil. Since 2022, the PROCONVE P-8 phase has been implemented, imposing significantly stricter limits for NO_x emissions in comparison to the previous phase, PROCONVE P-7 of 2012 (BRASIL, 2023). Brazilian legislation has always followed European standards, and phase P-8 is based on Euro VI, which was adopted in Europe in 2013 and has been equivalent to US requirements since 2010.

In addition to stricter limits, emissions testing has been improved. The World Harmonized Transient Cycle (WHTC), and the World Harmonized Stationary Cycle (WHSC) have been introduced to better simulate real-world driving conditions (BRASIL, 2023). The WHTC includes a cold start phase when emissions are highest. Another innovation was the Off Cycle Emission (OCE) concept, which requires compliance with limits in a variety of conditions rather than in standardized tests, making the tests

more realistic (CONAMA, 2018b). These modifications align Brazilian regulations with global efforts to reduce vehicular emissions and improve air quality. However, a large part of the fleet is still operating under old standards, reinforcing the need for renewal and the introduction of new technologies (LI et al., 2023; REŞITOĞLU; ALTINIŞIK; KESKIN, 2015).

Previous research on NO_x emissions has shown that speed is the most significant contributor to the emissions that vehicles release into the atmosphere (HU et al., 2022; TANG et al., 2019). In urban areas, vehicles typically travel slowly, resulting in higher NO_x emissions due to inherent inefficiencies and frequent stop-and-go cycles. However, at higher speeds, better engine performance can improve fuel efficiency, resulting in lower emissions. However, engine performance with respect to NO_x emissions as a function of speed can be largely determined by vehicle characteristics such as engine technology, emission control systems, and maintenance procedures (AGUIAR et al., 2015; CETESB, 2023; SILVA et al., 2024b). Real-world emissions are also affected by driving behavior, road gradient, and ambient conditions, factors that are often overlooked in regulatory testing but have a significant impact on NO_x formation (BRODRICK et al., 2004; CLARK et al., 2002).

The aim of this study is to fill the current knowledge gap on NO_x emissions from heavy-duty diesel vehicles in a Brazilian urban environment, as it is one of the first studies in Rio de Janeiro. This study will comprehensively investigate heavy-duty vehicle NO_x emission factors and their correlation with average speed, providing valuable information that can help to understand how the Brazilian fleet has qualified against NO_x emission limits. In Brazil, with its vast continental dimensions, most of the cargo and passenger transportation relies on diesel-powered trucks and buses, and the fleet averages 10 to 12 years in age. These two factors result in significant emissions from these vehicles, which critically impact air quality (SEROA DA MOTTA et al., 2011). Despite the existence of studies on NO_x emissions from HDDVs in various regions worldwide, there remains

a lack of real-world measurements specifically for Brazil. The present study aims to address this knowledge gap by providing experimental data on NO_x emissions from in-use heavy-duty diesel vehicles operating in Rio de Janeiro, with the objective of offering insights that can inform regulatory policies and emission control strategies. Moreover, this study can serve as a reference for other countries facing similar challenges. A previous pilot study of this project was published in 2024 with a smaller number of vehicles and a shorter period (SILVA et al., 2024b).

8.2. Material and Methods

Description in topic 3.8, page 56.

8.3. Results and Discussion

8.3.1. Sensing performance

Table 8.1 shows the records utilized, including data extracted from a backup database during assessing the sensor's probe performance. The table data indicates that the NO_x sensor achieved a remarkable success rate: 99.88 % of the measurements were different from zero, and only 0.12 % were null. After processing the data and excluding negative data during the heating and calibration process.

Table 8.1. NO_x emissions data from heavy-duty diesel vehicles recorded by the UniNOx sensor from February 2022 to April 2024 at both locations—the Metropolitan Region of Rio de Janeiro (MRRJ) and South region of the city of Rio de Janeiro, Brazil.

	NO_x
Non-zero measurements	12,491
Percentage	99.85 %
Zero measurements	19
Percentage	0.15 %

8.3.2. NO_x emission

The distribution of NO_x emission in ppm for the fourteen monitored HDDVs is shown in Figure 8.1. The mean and standard deviation of the emissions were 3322 ± 106 ppm, and the emission factors ranged from 1.51 to 1257 ppm. These values reflect the high variability of vehicle emissions, which demonstrates the use of different emission reduction technologies, vehicle age, and maintenance conditions.

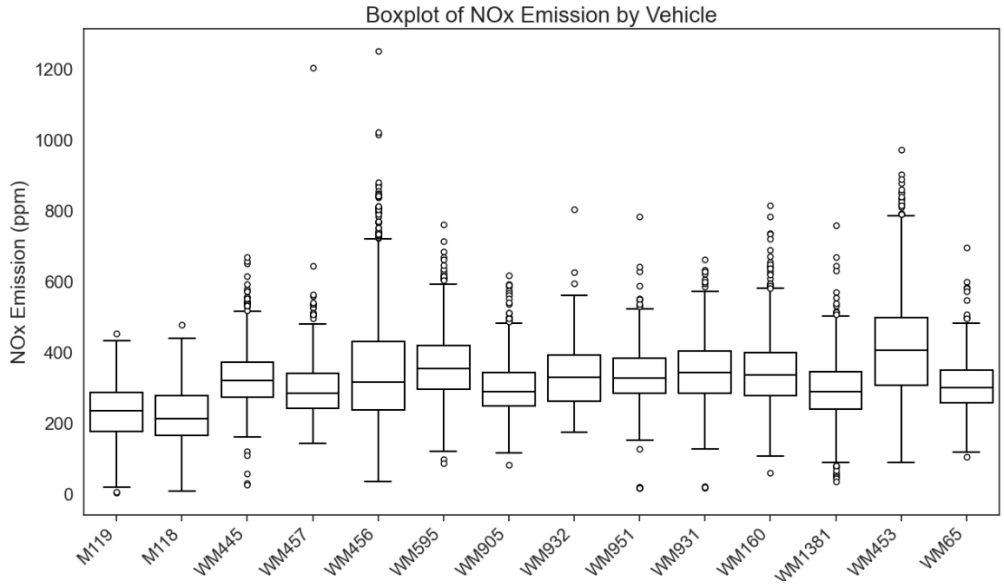

Figure 8.1. NO_x emission (in ppm) in fourteen heavy vehicles monitored with the sensor in MRRJ from February 2022 to April 2024. Vehicles are identified by a letter designating the brand (WM for vehicles operating in MRRJ and M for vehicles operating in the south region of Rio de Janeiro's city) and a number corresponding to the engine model.

M vehicles recorded the lowest NO_x emissions compared to W vehicles, regardless of technology, year, weight, or power. The reasons for this may be multifactorial, but without considering specific variations in weight, power, year, or after-treatment technology, M vehicles consistently have lower emissions. On the other hand, despite the varying conditions, W vehicles showed relatively similar emissions values, regardless of the variations (year, weight, power). Further analysis that considers individual factors such as weight, power, year, and after-treatment technology will

provide a clearer understanding of these trends.

8.3.2.1 Vehicle weight

The analysis of NO_x emissions by vehicle weight revealed differences between the two groups of heavy vehicles, divided between those weighing 16,000 kg and those weighing 23,000 kg (Figure 8.2). The group of vehicles weighing 16,000 kg had an average of 344 ± 129 ppm, with a range from 24.0 to 1252 ppm, while the 23,000 kg vehicles had an average of 327 ± 95 ppm, with a range from 2.00 to 1204 ppm.

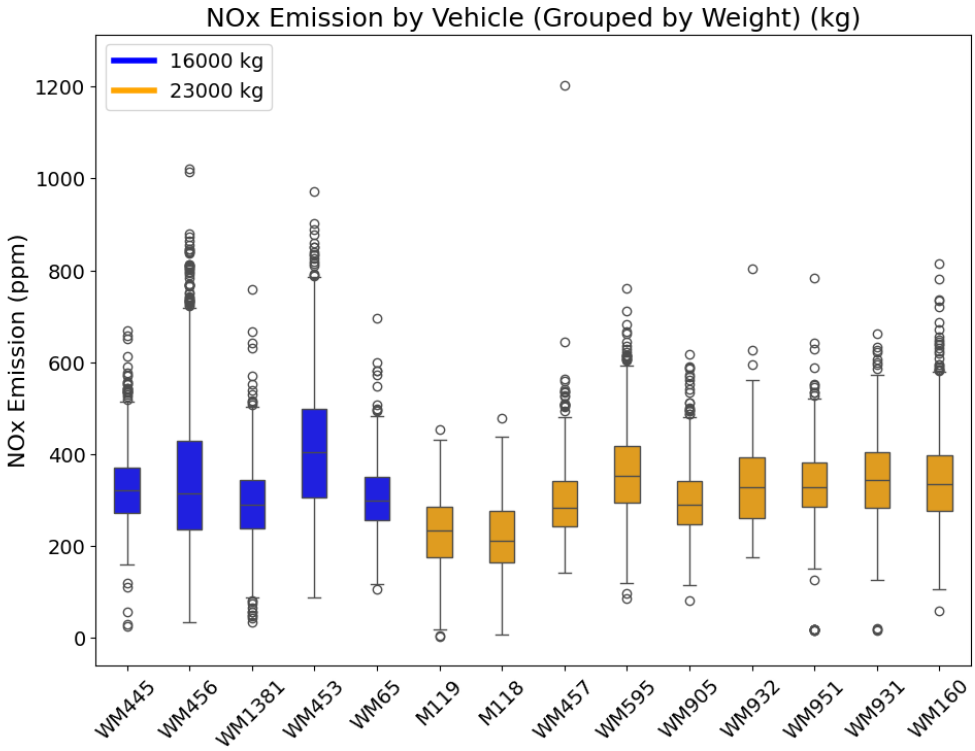

Figure 8.2. NO_x emissions (in ppm) from 14 heavy vehicles monitored in MRRJ from February 2022 to April 2024. The vehicles are grouped by weight (kg). Vehicles are identified by a letter designating the brand (WM for vehicles operating in MRRJ and M for vehicles operating in the south region of Rio de Janeiro's city) and a number corresponding to the engine model.

Although the average NO_x emissions for both groups are quite close, the emission variability was higher among the 16,000 kg vehicles.

Furthermore, the minimum and maximum emission values showed that 16,000 kg vehicles had a wider range of variation, with emissions ranging from 24.0 ppm to 1252 ppm, while 23,000 kg vehicles had a narrower range, ranging from 2.00 ppm to 1204 ppm. These data indicate that although the averages are similar, some vehicles, especially 16,000 kg vehicles, generated considerably higher emissions.

Furthermore, the weight groups showed a statistically significant difference ($p = 0.024$). The significant difference can be interpreted as an indication that, despite similar means, the distribution of emissions is affected by variables other than weight, such as engine technology and emission control systems, which may have differential impacts depending on vehicle weight.

The results suggest that reducing vehicle weight can influence NO_x emissions, but this relationship is not simple or linear. Although weight reduction often leads to lower energy requirements and emissions during operation (CLARK et al., 2002; JOOST, 2012; KO et al., 2020; KOFFLER; ROHDE-BRANDENBURGER, 2010), the data from this study indicate that weight is not the only determining factor for NO_x emissions. The greater variability observed in emissions between vehicles suggests that other operational and technological factors also affect the amount of NO_x emitted.

8.3.2.2 Vehicle power

The data obtained on NO_x emissions for vehicles, divided by power categories, demonstrated the following characteristics (Figure 8.3): for the 137 kW category, the mean was 356 ± 135 ppm, ranging from 24.0 to 1252 ppm; for the 188 kW category, the mean was 230 ± 79.0 ppm, ranging from 2.00 to 478 ppm. The mean value for the 191 kW category was 294 ± 85.3 ppm, with a minimum emission of 34.0 ppm and a maximum of 759 ppm. In the 204 kW, the mean value was 335 ± 92.0 ppm, with a minimum value of 16.0 ppm and a maximum of 1204 ppm. Furthermore, a statistically

significant difference was observed among the different power categories (p-value = 0.0012), indicating that NO_x emissions vary according to engine power. This result confirms that power is a relevant factor in determining emissions, although it is not the only one.

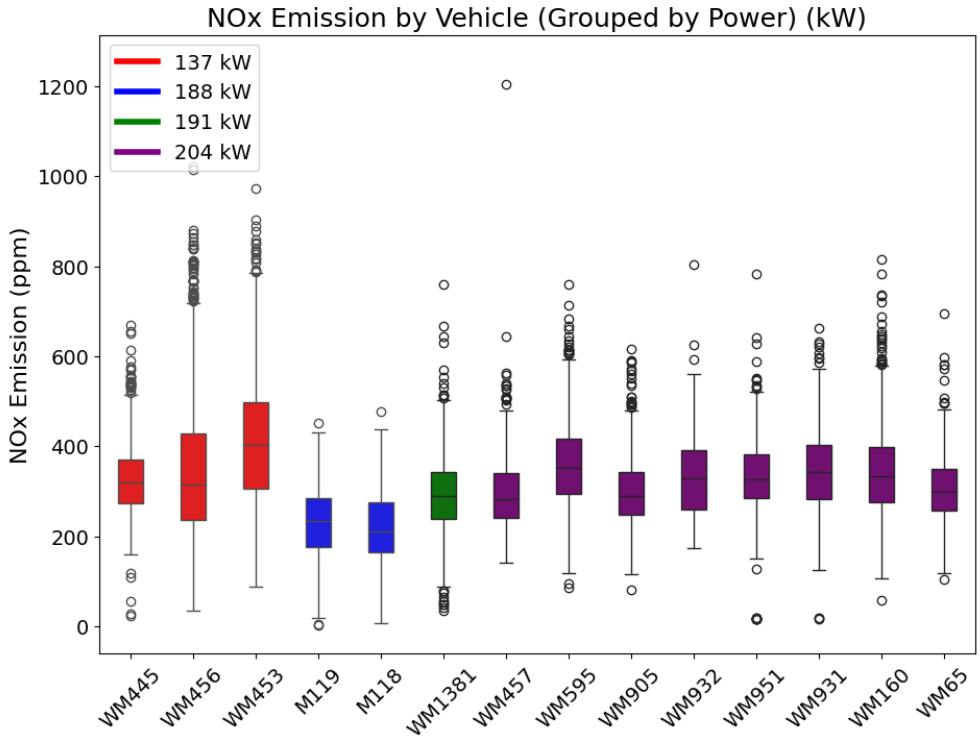

Figure 8.3. NO_x emissions (in ppm) from 14 heavy vehicles monitored in MRRJ from February 2022 to April 2024. The vehicles are grouped by power (kW). Vehicles are identified by a letter designating the brand (WM for vehicles operating in MRRJ and M for vehicles operating in the south region of Rio de Janeiro's city) and a number corresponding to the engine model.

A thorough examination of the available data reveals that engine power has a substantial impact on NO_x emissions. However, the relationship between these variables is not as direct as one might initially presume. Vehicles with intermediate power outputs, such as 188 kW and 191 kW, exhibited the lowest average emissions, at 230 ppm and 294 ppm, respectively. In contrast, vehicles with lower power outputs, such as 137 kW, exhibited the highest average emissions, reaching 356 ppm. This result

contradicts the assumption that higher power engines always emit more NO_x due to higher fuel demand and operating load (CLARK et al., 2002). However, the 204 kW category, which exhibited the highest power output, demonstrated an average emission level of 335 ppm, lower than that of the 137 kW category but higher than that of the 188 kW and 191 kW categories. This observation suggests that the relationship between power and NO_x emissions may not follow a linear trend. It should also be noted that the 137 kW vehicles, except for WM1381 and WM65, are the same as those with the lowest weight (16,000 kg). These vehicles, with lower weight and power, had the highest emissions, suggesting that there is another factor influencing the increase in emissions in addition to weight and power.

Although engine power is an important factor in the variation of NO_x emissions, it does not explain all the observed variability. The statistical test reinforces the idea that power has a significant influence, but other aspects also play important roles. Compared to the influence of vehicle weight, engine power appears to have a more direct and relevant relationship with NO_x emissions. Weight reduction can help improve energy efficiency and reduce emissions in some circumstances, but in the context of this study, engine power emerges as a key factor to consider.

8.3.2.3 Vehicle age

The analysis of NO_x emissions between vehicles of different ages showed a statistically significant difference (p-value = 0.00015), suggesting that vehicle age influences NO_x emissions. When the vehicles were divided into age groups (2013, 2014, 2018, 2019), there was a significant difference in the average emissions between the groups (Figure 8.4). For the 2013 vehicles, the average emissions were 345 ± 123 ppm, with values ranging from 16.0 to 1252 ppm. For the 2014 category, the average was 352 ± 93.4 ppm, with emissions ranging from 59.0 to 815 ppm. For 2018 vehicles, the average emissions were 313 ± 88.0 ppm, with values ranging from 105 to 695 ppm. Finally, for the 2019 category, the average was 282 ± 87.0 ppm,

with emissions ranging from 2.00 to 1204 ppm.

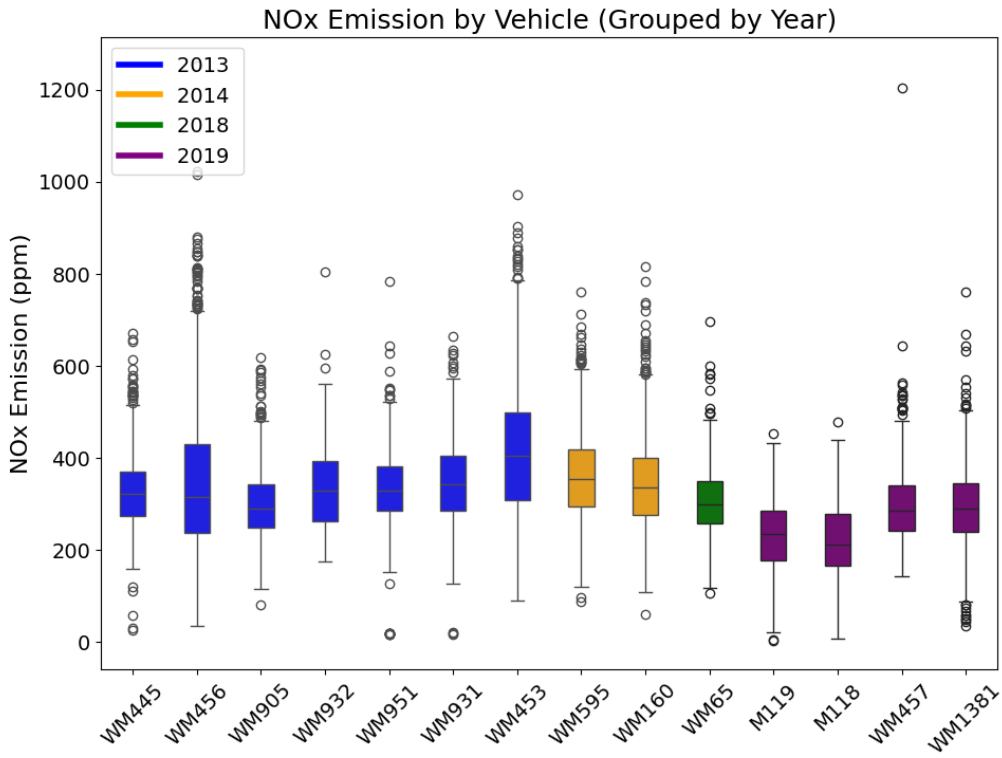

Figure 8.4. NO_x emissions (in ppm) from 14 heavy vehicles monitored in MRRJ from February 2022 to April 2024. The vehicles are grouped by age. Vehicles are identified by a letter designating the brand (WM for vehicles operating in MRRJ and M for vehicles operating in the south region of Rio de Janeiro's city) and a number corresponding to the engine model.

In general, average emissions decrease with increasing vehicle age, with 2019 vehicles having the lowest average emissions (282 ppm). However, the relationship between age and emissions is not simple and the variability within each age category is quite significant, with extreme emissions exceeding 1200 ppm even in newer categories such as 2019. This suggests that factors such as maintenance, emission control technology, and operating conditions play an important role in NO_x emissions in addition to the simple age of the vehicle.

There are two main factors that influence NO_x emissions in vehicles of different ages. The first is related to the natural engine degradation that

occurs over time and can lead to elevated emissions levels as the vehicle ages and accrues mileage (CLARK et al., 2002; SILVA et al., 2024b; ZHANG et al., 2018) The second factor is technological development, which means that newer engines meet stricter emission standards and are more efficient at reducing emissions than older models. The combination of these factors can have a significant impact on emissions, with newer cars tending to have lower NO_x levels due to improvements in emission control technology (CLARK et al., 2002; FU et al., 2013; HOUNTALAS; MAVROPOULOS; BINDER, 2008; JAIN; SINGH; AGARWAL, 2017; KO et al., 2020). Additionally, vehicle maintenance over time can also affect emissions, as emission control systems that are not properly maintained can lose efficiency, which can result in higher NO_x levels (SILVA et al., 2024b).

Although the reduction in emissions with increasing vehicle age is expected, it is important to note that the variability within each age group suggests that factors other than age and emission control technology may influence these results, since all vehicles have EGR as a system, except for vehicle WM1381, which uses an SCR system. Operating conditions and vehicle use characteristics, such as the type of route (urban or highway), the load transported, and the maintenance performed, can significantly affect NO_x emissions.

8.3.3. NO_x emission factors

The distribution of NO_x emission factors for the fourteen monitored HDDVs is shown in Figure 8.5. The mean and standard deviation of the emission factors were 2.2 ± 0.7 g kWh^{-1}, and the average emission factors ranged from 0.01 to 8.3 g kWh^{-1}. These values reflect the high variability of vehicle emissions, which reflects the use of different emission reduction technologies, vehicle age, and maintenance conditions.

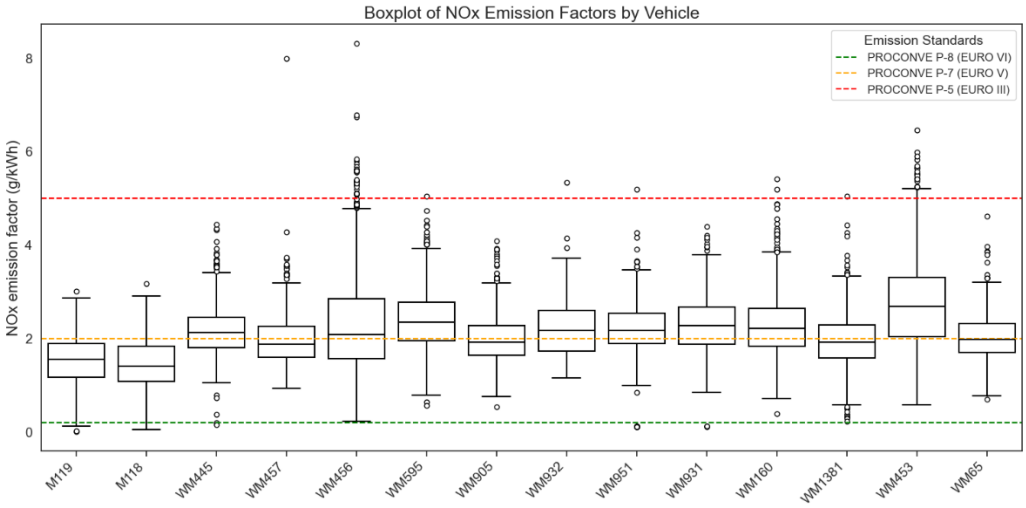

Figure 8.5. NO_x emission factors (use of constant conversion factor, g kW^{-1}) in fourteen heavy vehicles monitored with sensor in MRRJ from February 2022 to April 2024. Vehicles are identified using a letter to designate the vehicle brand, a number to identify the engine model. WM vehicles that run in MRRJ and M vehicles that run in the south region of Rio de Janeiro's city. The P7 and P8 are tested over a load cycles (ESC/ETC, and WHTC) and they were added for illustration only.

Moreover, the conversion of the NO_x emission unit from ppm to g kWh^{-1} may not precisely represent the actual emission factor of the vehicle, given that the vehicle's fuel consumption during the measurement would likely differ. Therefore, the regulatory limits utilized in this study serve as a reference point for comparing the results of NO_x emissions obtained using a sensor. It is important to note that exceeding these limits does not necessarily indicate non-compliance with the standards, given the inherent differences between test cycles, regulatory conditions, and on-road measurements.

A statistically significant difference in emissions was found (p-value = 0.0004) between vehicles. This variability can be explained by several factors, including engine type, vehicle age, and maintenance conditions (BAPTISTA VENTURA et al., 2020; SILVA et al., 2024b; WANG et al., 2022a), as was seen in the previous section.

The results show that eight of the fourteen vehicles (57 %) would

exceed the PROCONVE P-7 limit of 2 g kWh^{-1} under normal operating conditions. However, it is important to note that the P-7 limit is tested according to specific load cycles (such as ESC/ETC and WHTC) and the test procedure. P-7 and P-8 regulatory limits are tested under specific load cycles, such as the ESC/ETC (European Stationary Cycle/European Transient Cycle) and WHTC (World Harmonized Transient Cycle) (CONAMA, 2018b). These cycles simulate real-world driving conditions, providing a more comprehensive assessment of vehicle emissions during typical usage. This study did not carry out a study under the same conditions as PROCONVE. In the context of these tests, the vehicles did not exceed the P-7 limit. Furthermore, all monitored HDDVs exceeded the emission limits set by the PROCONVE P-8 regulations (0.4 g kWh^{-1}), which have been in force since 2022. These HDDVs were not designed to meet P-8 standards, particularly given the absence of after-treatment systems. It is also noteworthy that the P-7 limits are typically 5-10 times higher than the P-8 limits when both are operating within their certification standards.

The vehicles that are emitting NO_x above the legislated value are predominantly older models, which suggests that as vehicles age and accumulate mileage, that real-world operational characteristics, such as idling time and duty cycles, as well as the deterioration of emissions control systems resulting from natural degradation or inadequate maintenance, contribute to elevated real-world ICE vehicle emissions relative to the certification standard, it already reported in previous studies (SOFWAN; LATIF, 2021; ZHANG et al., 2018).

By analyzing the relationship between the age of vehicles, their weight and NO_x emissions, some important insights emerge about how these factors can interact and affect pollution levels. It is observed that older vehicles, especially those from 2013 and 2014, tend to have higher NO_x emissions, which can be expected due to the wear and tear of components and the reduced efficiency of emission control systems over time. However, weight analysis reveals that these older vehicles, especially the 16,000 kg

ones, are not necessarily heavier, but rather more susceptible to increased emissions due to aging systems. On the other hand, the newer vehicles, manufactured in 2018 and 2019, have significantly lower average emissions, which is in line with the evolution of technology and environmental regulations.

An important observation is that among the newest vehicles (2018 and 2019), 16,000 kg vehicles tend to have lower emissions compared to 23,000 kg vehicles. This suggests that, over the years, weight reduction can play a relevant role in fuel efficiency and NO_x emissions. For heavier vehicles (23,000 kg), the combination of more advanced technologies and weight reduction can help improve fuel efficiency and reduce emissions, reflecting advances in engine design and after-treatment systems.

When the interaction between age and weight is considered, a new insight emerges. Although heavier vehicles, such as those weighing 23,000 kg, are associated with greater power, and theoretically greater fuel consumption, the presence of more modern and efficient technology, such as in the 2018 and 2019 models, seems to counterbalance this impact. This suggests that as engines become more efficient and emissions control systems improve, the greater load on vehicles can be offset by better technology, resulting in lower emissions, even for heavier vehicles. In contrast, older and lighter vehicles, such as those from 2013, may show greater variability in emissions, especially due to the wear and tear of emissions control systems, despite their lower weight.

The discussion concerning the vehicle fleet and emission standards serves to illustrate a significant aspect of the transition to cleaner technologies. At present, a considerable proportion of the engines in use are certified to the P7 (EURO V) standard, indicating that a significant number of vehicles remain above the threshold for the most rigorous emission standards. The turnover of the fleet is an important factor in this context, as the replacement of old vehicles with newer, more efficient models can considerably reduce pollutant emissions. However, if emerging

technologies are excessively expensive, this transition can be considerably hindered, resulting in the persistence of an obsolete fleet that contributes to air pollution. It is therefore essential to consider not only the effectiveness of new technologies but also their affordability, to promote a significant and sustainable change in the transportation sector (MARINO et al., 2020).

8.3.4. Influence of speed on NO_x emission factors

Figure 7 shows the NO_x emission factors for each vehicle type as a function of average speed. It can be seen that NO_x emissions are highest at low speeds (below 40 km h^{-1}), accounting for 90 % of emissions, followed by 9 % at medium speeds (41 to 70 km h^{-1}) and only 1 % at high speeds (above 70 km h^{-1}) (BRODRICK et al., 2004). It is worth noting that these vehicles rarely traveled at speeds above 70 km h^{-1}.

The emission profiles of the monitored vehicles in group M do not match the trends reported in previous studies, which indicated that emissions generally decrease with speed and increase after a certain value is reached (GAJANAND; NARENDRAN, 2013; JIANG et al., 2021; PARK; SEO; PARK, 2023; YAO; SONG, 2013). However, our results show that NO_x emissions tend to increase with increasing speed. This may be influenced by the conditions under which the vehicles are used, which mainly come from the vehicle fleet in urban areas.

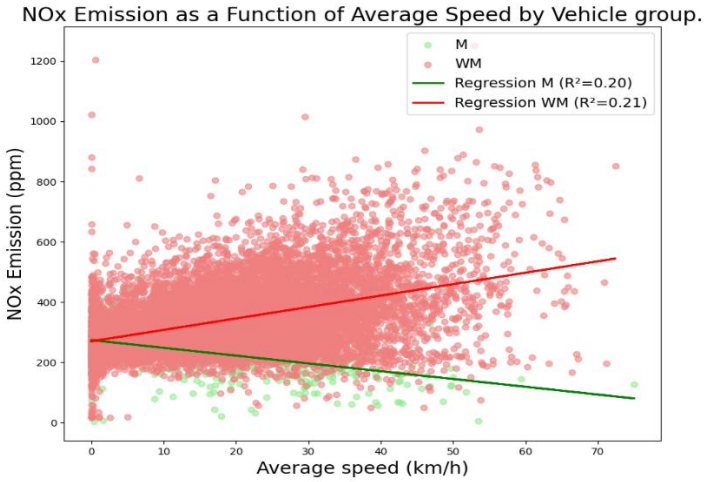

Figure 8.6. Vehicle emission regression of different vehicle groups.

A comparative analysis of the different vehicle groups (M and WM) shows that NO_x emissions vary with speed. In the WM group (red line), NO_x emissions increased as speed increased, while in the M group (green line), emissions decreased as speed increased. Similar situations were found in studies carried out in China (YAO et al., 2015). Vehicles in different groups drive under different load conditions and on different routes, which affects emissions. For example, vehicles in the WM group may drive more frequently in urban traffic with many stops, while vehicles in the M group may drive on medium-length routes. Different operating conditions lead to different emission patterns (KIRCHSTETTER et al., 1999; MENDOZA-VILLAFUERTE et al., 2017). Furthermore, newer vehicles have lower concentration values, as well as lower NO_x concentrations when speed increases. No statistically significant difference in emissions was found between regressions.

The presence of emissions at lower speeds is related to the typical usage profile of vehicles in the fleet, which is mainly used in urban environments where average speeds are relatively low. This situation is at odds with the controlled conditions of laboratory or single vehicle testing often mentioned in the literature. Understanding these operational realities is essential for developing and implementing effective regulatory policies and technical solutions to reduce NO_x emissions from the vehicle fleet (JIANG et al., 2021; SHAH et al., 2006).

Although the vehicles analyzed belong to the same phase of the PROCONVE program, they have different characteristics that influence NO_x emissions, such as engine technology, after-treatment systems, fuel quality, vehicle operating and maintenance conditions, as well as the year of manufacture and the specific characteristics of each model. Factors such as the injection systems (common rail), EGR, and SCR, the quality of the S10 diesel with biodiesel, and the operating conditions (such as driving speeds and the type of road) all play a crucial role in shaping emissions. In addition, ongoing vehicle maintenance and driving style can alter the

efficiency of emission control systems and affect NO_x emissions (CLARK et al., 2002; GAJENDRAN; CLARK, 2003). The inclusion of additional variables, such as a more detailed analysis of maintenance, operating conditions, and driving style, could provide a more accurate and robust assessment of NO_x emissions, modifying the results and offering a more comprehensive view of the impact of these variables in the Brazilian urban scenario.

8.4. Conclusion

The analysis of NO_x emissions from heavy-duty vehicles monitored at MRRJ between February 2022 and April 2024 showed significant variability in emission factors, reflecting differences in emission reduction technologies, vehicle age, maintenance conditions, and operating characteristics. The average NO_x emissions for the 14 vehicles were 3322 ± 106 ppm, ranging from 1.51 to 1257 ppm, which indicates a high level of diversity in emissions across vehicles.

Vehicle weight played a notable role in emissions, with significant differences observed between the 16,000 kg and 23,000 kg groups. While average emissions were similar, variability was greater in the lighter vehicles, suggesting that while weight reduction can impact emissions, other factors like engine technology and emission control systems are also critical. Engine power was another influential factor, with intermediate-power vehicles (188 kW and 191 kW) exhibiting the lowest NO_x emissions, challenging the assumption that higher-power engines always generate more emissions. This highlights the need for a detailed analysis of the interaction between various operational and technological factors. Vehicle age also influenced emissions, with newer vehicles showing a tendency for lower average emissions. However, variability within age groups suggests that maintenance conditions and emission control technology adoption also play important roles.

When NO_x emission factors were converted to g kWh^{-1}, significant dispersion was observed, with more than half of the vehicles exceeding the 2 g kWh^{-1} limit set by the PROCONVE P-7 standard. However, comparisons to regulatory limits should be cautious, as the PROCONVE compliance tests follow specific load cycles that were not replicated in this study.

The vehicles in this study predominantly operated at low speeds (up to 40 km h^{-1}), typical of stop-and-go urban driving, which highlights the challenges of urban traffic conditions on emissions profiles. Moreover, the analysis revealed contrasting emission trends between vehicle groups: an increase in emissions with speed for the WM category, and a decrease for the M category. These differences reflect the varying composition of older and newer fleets, underscoring the importance of understanding group-specific patterns when developing targeted regulatory strategies.

The findings underscore the need for environmental policies tailored to urban transport fleets, focusing on fleet renewal, adoption of advanced emission control technologies, regular vehicle maintenance, and promotion of fuel-efficient driving practices. Future studies should further investigate the relationship between vehicle operating conditions, speed variability, and NO_x emissions in diverse driving environments.

9. Research Article 6 – Application of WRF-Chem for Predicting Air Quality Resulting from the Formation of Photochemical Compounds in a subtropical urban environment

Luis Fhernando Mendonça da Silva [1], Adrien Deroubaix [2,3], Guy P. Brasseur [2,4] and Adriana Gioda [1,*]

[1] Pontifical Catholic University of Rio de Janeiro, 22451-900, Rio de Janeiro, RJ, Brazil.

[2] Max Planck Institute for Meteorology, 20146, Hamburg, Germany.

[3] Institute of Environmental Physics, University of Bremen, 28359, Bremen, Germany.

[4] National Center for Atmospheric Research Atmospheric Chemistry Observations and Modeling Laboratory, 80307, Colorado, USA.

Paper submitted: Urban Climate

Abstract

Modelling ozone (O_3) concentrations in urban environments presents substantial challenges due to the complex interactions between anthropogenic emissions, meteorological conditions and atmospheric chemistry. This study evaluates the performance of the forecasted concentrations with the Weather Research and Forecasting (WRF) model coupled to the chemical model (WRFchem) in simulating O_3, NO_x, SO_2 and O_x (= NO_2 + O_3) concentrations in the Metropolitan Region of Rio de Janeiro, Brazil. During three contrasting periods characterized by different types of pollution events, the hourly concentrations of nitrogen oxides (NO_x), sulfur

dioxide (SO_2) and O_3 modeled by the ensemble are in moderate agreement with observations (R ≈ 0.6 for NO_x, 0.5 for SO_2, 0.7 for O_3).The modeled hourly concentration of O_3 is overestimated during the day (≈20 ppb) and underestimated at night (≈10 ppb), while nitrogen dioxide (NO_2) is overestimated at night (≈20 ppb). Persistent biases in the model results reveal a consistent overestimation of daytime O_3 and Ox levels, alongside an underestimation at night. These discrepancies result mainly from the model's treatment of anthropogenic emissions, particularly volatile organic compounds (VOCs) and NO_x, which are important for the formation of O_3 through photochemical reactions. The conclusions highlight the need to refine the anthropogenic emissions profiles. In addition, specific industrial areas, such as Santa Cruz, are identified as O_3 concentration hotspots due to intensive VOCs emissions from the metallurgical and steel industries. This study, which combines observational data with air quality forecasts, provides important information for policy makers in Rio de Janeiro State, and underlines the need for a specific anthropogenic emission inventory for Rio.

Keywords: Ozone; NO_x; WRFChem; VOCs; photochemistry; Rio de Janeiro.

9.1. Introduction

Photochemistry is a branch of chemistry that studies the chemical reactions triggered by light and is fundamental to understanding atmospheric processes that affect climate, air quality and public health. These reactions play a fundamental role in the formation of various atmospheric pollutants, such as ozone (O_3) (GEORGE et al., 2015; RAVINA et al., 2022). In urban environments, photochemistry makes a considerable contribution to the formation of photochemical smog, a persistent problem in many large cities around the world, such as Rio de Janeiro (GEORGE et

al., 2015; RAVINA et al., 2022).

The Metropolitan Region of Rio de Janeiro (MRRJ), with its combination of high industrialization, dense population, coastline, complex topography and tropical climate, presents a unique case for the study of photochemistry. These factors contribute to the creation of favorable conditions for photochemical reactions, contributing to the production of pollutants that degrade air quality and pose substantial health risks (DANTAS et al., 2020; MANISALIDIS et al., 2020).

Analyzing the interactions between industrial and vehicular emissions and natural biogenic sources is complex, especially in the context of Rio de Janeiro, where the main anthropogenic sources of photochemical pollutants are emissions from vehicles and industries. These sources release nitrogen oxides (NO_x) and volatile organic compounds (VOCs), which are essential precursors for the formation of tropospheric O_3 and secondary organic aerosols. The abundance of sunlight in the region favors the photolysis of NO_2, resulting in the release of atomic oxygen which, when reacting with O_2, forms O_3. This pollutant is known for its adverse effects on respiratory and cardiovascular health (DA SILVA et al., 2016; GERALDINO et al., 2017).

Highly urbanized areas tend to have O_3 production controlled mainly by VOCs and is therefore saturated with NO_x (DANTAS et al., 2020; MONKS et al., 2015; PARRISH et al., 2016). Moreover, the study of the oxidant level (i.e. $Ox = NO_2 + O_3$) is useful and interesting for monitoring O_3 production because NO_2 can act as an O_3 reservoir (DEROUBAIX et al., 2024; WOOD et al., 2009). The interaction between O_3 production and loss mechanisms during the day is crucial, as the titration of O_3 by nitrogen monoxide (NO) is neutralized by the photolysis of NO_2 (RAVINA et al., 2022). The result is a partition between nitrogen dioxide (NO_2) and O_3 governed by the diurnal photostationary state, in which O_x levels increase during the day, predominantly indicating the formation of O_3 (LIU et al., 2021; WOOD et al., 2010). However, O_x levels remain relatively stable at

night and are not affected by O_3 titration, which makes it a valuable parameter for analysis due to its lower diurnal variability compared to O_3.

In addition to its impact on human health, photochemistry significantly influences the environment. The formation of O_3 can result in damage to vegetation, a reduction in agricultural productivity, and the disruption of natural ecosystems. Moreover, this pollutant contributes to global warming and alters precipitation patterns, underscoring the necessity for a comprehensive understanding of photochemical processes to develop effective mitigation strategies (DEITRICK; GOLDBLATT, 2023; MANISALIDIS et al., 2020; MONOD; CARLIER, 1999).

Recent research highlights that O_3 continues to be an urgent air quality problem in MRRJ, with concentrations often exceeding national (140 mg m^{-3}) and international (100 mg m^{-3}) air quality standards (CONAMA, 2018b; DA SILVEIRA et al., 2021; DANTAS et al., 2019; GERALDINO et al., 2017; GIODA et al., 2018; MENDES et al., 2020; WHO, 2022b). Studies in the MRRJ suggest that many sites have high O_3 concentrations in limited VOCs scenario. However, other regions, as Ilha de Paquetá and Ilha do Governador, happen reactions with total hydrocarbons (THC) and NO_x under sunlight (GIODA et al., 2018). The formation of O_3 in urban troposphere typically follows a complex and nonlinear process. In the presence of THC, an imbalance between O_3 formation and consumption processes occurs, which is heavily influenced by the NO to NO_2 ratio. Radicals generated from the oxidation of THC by hydroxyl radicals (OH•) consume NO, as illustrated in reactions 1 to 5 (BRASSEUR, 1992; SEINFELD; PANDIS, 2016).

$$RH + OH^{\bullet} \rightarrow R^{\bullet} + H_2O \ (\mathbf{1})$$

$$R^{\bullet} + O_2 \rightarrow RO_2 \ (\mathbf{2})$$

$$RO_2^{\bullet} + NO \rightarrow RO^{\bullet} + NO_2 \ (\mathbf{3})$$

$$RO^{\bullet} + O_2 \rightarrow RCHO + HO_2^{\bullet} \ (\mathbf{4})$$

$$HO_2^{\bullet} + NO \rightarrow OH^{\bullet} + NO_2 \ (\mathbf{5})$$

In these reactions, RH represents THC, $OH^{\bullet}$ denotes the hydroxyl

radical, $R^{\bullet}$ signifies a THC without hydrogen, $RO_2^{\bullet}$ denotes the peroxide radical, RCHO represents carbonyls, and $HO_2^{\bullet}$ denotes the hydroperoxide radical. The hydroxyl ($HO_2^{\bullet}$) and peroxy ($RO_2^{\bullet}$) radicals consume NO, facilitating the conversion of NO to NO_2 without O_3 consumption. The ratio of THC to NO_x also plays a pivotal role in tropospheric O_3 formation. Lower proportions of THC and NO_x favor the reaction between OH and NO_2, thereby delaying O_3 formation. Conversely, higher proportions of THC and NO_x enhance ozone formation by promoting reactions with the OH radical (BATISTA et al., 2020; BRASSEUR, 1992; DANTAS et al., 2019; GIODA et al., 2018).

The interaction between anthropogenic and biogenic emissions requires modeling approaches for a comprehensive understanding, and atmospheric modeling is fundamental in this context. It offers tools to simulate and predict the dispersion of pollutants, chemical reactions and their impacts. However, the implementation of atmospheric models in tropical urban environments, such as Rio de Janeiro, faces significant challenges, including complex chemical reactions, accurate representation of emission sources and consideration of local meteorological conditions. Despite these difficulties, advances in modeling techniques can provide crucial information on the dynamics of pollutants and support evidence-based policy decisions to improve air quality and public health (BAKLANOV; ZHANG, 2020; DA SILVA et al., 2016; FREITAS et al., 2017; IM et al., 2011; MENDES et al., 2020).

The objective of this study is to assess, by comparison with observation data, the regional air quality model's ability to accurately simulate atmospheric pollutant dynamics in the MRRJ, with a focusing on areas that are most affected by high O_3 concentrations. The investigation, which follows the structure of the study AQ modeling made by Deroubaix et al. (2024) (DEROUBAIX et al., 2024), will examine the intricate interrelationships between pollution sources, meteorological variability, and photochemical processes. The research aims to gain detailed insights into

the variability of O_3 and oxidant formation.

9.2. Material and Methods

Description in topic 3.9, page 63.

9.3. Results and Discussion

9.3.1. Evolution of the model

9.3.1.1 Simulated Meteorological Parameters

To characterize the meteorological conditions across the three selected periods, we analyzed relative humidity, wind speed, and wind direction using city-wide averages from all monitoring stations. Throughout these periods, consistently high relative humidity levels (greater than 80 %) and low wind speeds (greater than 3 m s^{-1}) were observed over several days, indicative of typical weather patterns without storm activity (DEROUBAIX et al., 2024) (Figure 9.1).

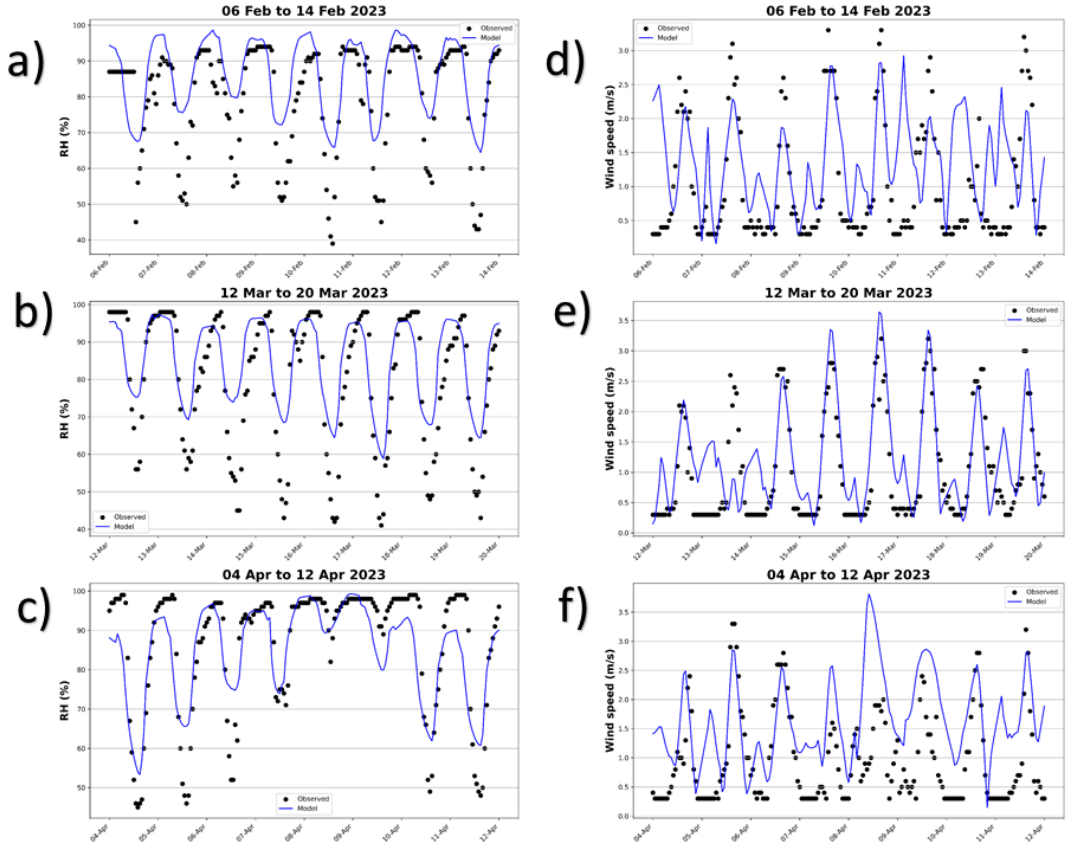

Figure 9.1. Time series of hourly concentrations of Relativity Humidity (a, b and c) and Wind speed (d, e and f) observed and modeled.

Overall, the regional model accurately captured the daily variability observed in relative humidity and generally aligned well with wind speed and direction observations across the MRRJ. Strong agreement was found for relative humidity ($r > 0.8$), indicating robust model performance in simulating this meteorological parameter. However, while wind speed showed good agreement (r approximately 0.7), slight discrepancies were noted, suggesting room for model refinement in capturing wind dynamics.

The regional model ensemble demonstrates good agreement to meteorological observations in the MRRJ. Based on these findings, discrepancies in modeled pollutant concentrations cannot be attributed to significant deviations in modeled meteorology, underscoring the importance of other factors, such as emission inputs and chemical processes, in influencing modeled air quality outcomes.

9.3.1.2. Simulated Pollutants

Regarding local pollution sources, two primary anthropogenic pollutants, NO_x and SO_2, are pivotal. In Rio de Janeiro, NO_x emissions predominantly originate from vehicular traffic, whereas industrial activities contribute significantly to SO_2 emissions (SOKHI et al., 2021). Hourly observations of NO_x and SO_2 concentrations across multiple monitoring stations during the study periods reveal significant variability. NO_x concentrations fluctuate widely, ranging from below 10 ppb to peaks exceeding 40 ppb during traffic-related pollution events (Figure 9.2).

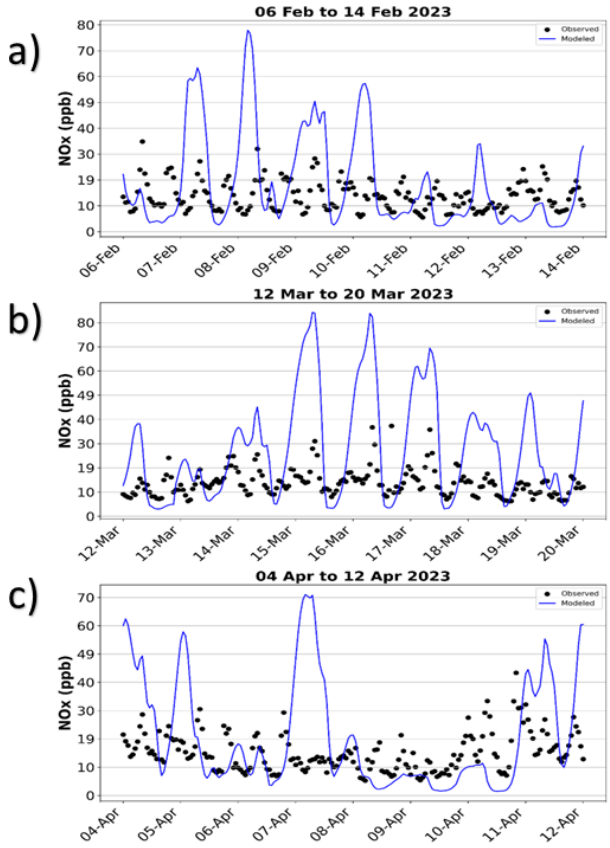

Figure 9.2. Time series of hourly concentrations of NO_x (a, b and c) observed and modeled in MRRJ.

However, the regional model ensemble exhibits notable discrepancies in simulating the observed range of NO_x variation (with r values ranging from 0.06 to 0.51) throughout the study periods.

In contrast, observed SO_2 concentrations consistently remain low (less than 60 ppb), reflecting the regulatory controls enforced on industrial emissions in Rio de Janeiro (Figure 9.3). Despite these controls, the model significantly overestimates SO_2 concentrations, suggesting potential issues with emission factor accuracy and spatial representation of emission sources specific to Rio de Janeiro. This discrepancy underscores the need for improved sector-specific emission data to enhance the model's predictive capability for SO_2 concentrations in urban environments (DEROUBAIX et al., 2024).

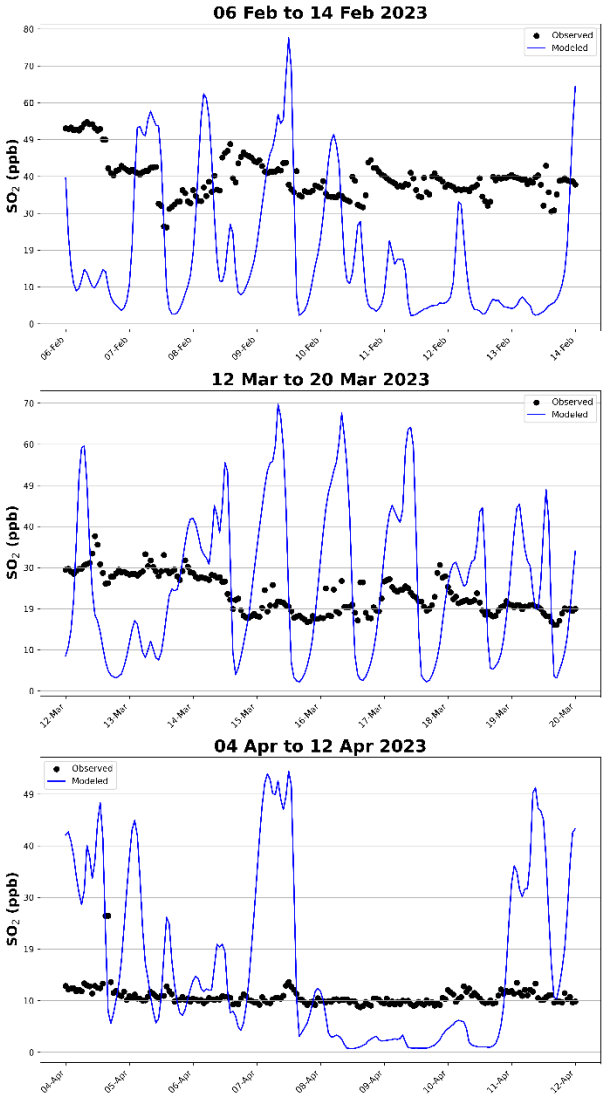

Figure 9.3. Time series of hourly concentrations of SO_2 (a, b, and c) observed and modeled in MRRJ.

9.3.2. Photochemistry

9.3.2.1. Ozone and Oxidant Level

We investigate the temporal variability of O_3 concentration and oxidant levels (O_x = NO_2 + O_3) observed and modeled in the subtropical urban environment of Rio de Janeiro (Figure 9.4).

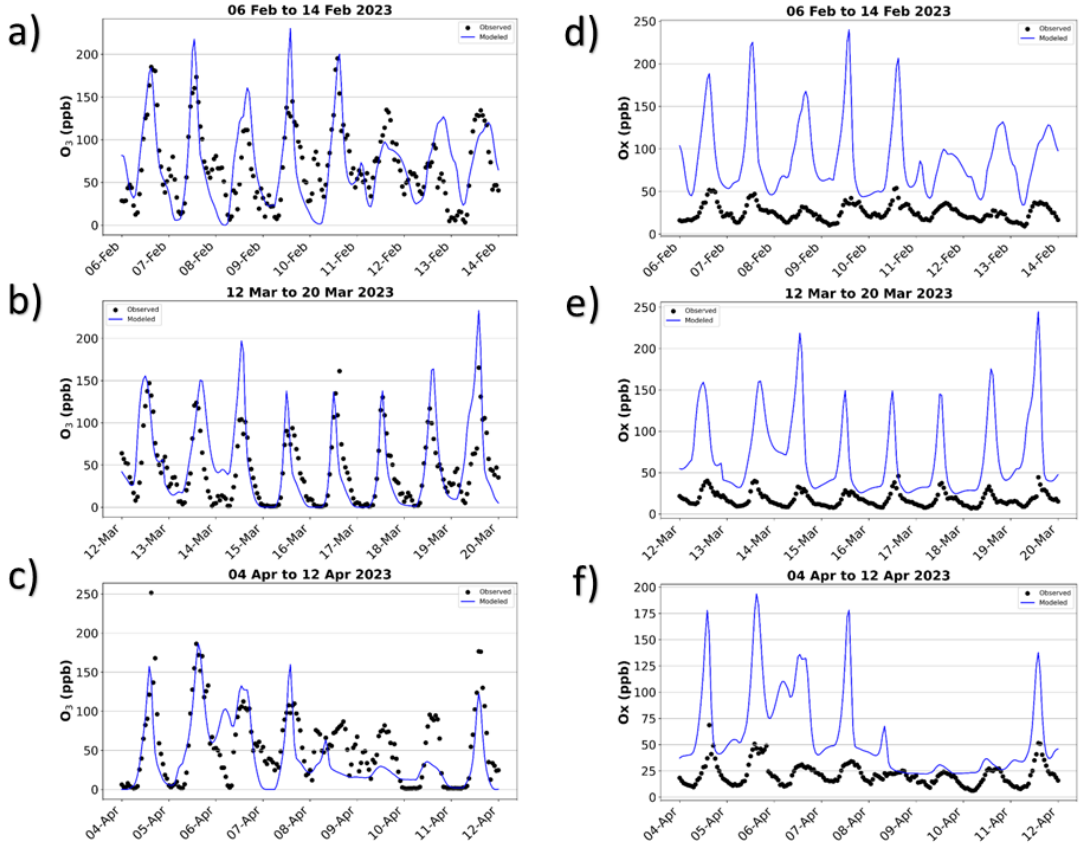

Figure 9.4. Time series of hourly concentrations of O_3 (a, b and c) and Ox (d, e and f) observed and modeled in MRRJ.

Observed O_3 concentrations in Rio de Janeiro exhibit a distinct diurnal cycle, typically reaching a minimum below 1 ppb at night and peaking above 100 ppb during the day on most days. Concurrently, O_x levels show daytime increases corresponding to elevated O_3 formation. However, O_x levels are consistently overestimated by the regional model ensemble. Despite this, the regional model ensemble closely approximates

the observed temporal variations in O_3 (with an r value of approximately 0.8).

9.3.2.2. Ozone and NO_x diurnal cycles

Ozone and NO_x exhibit notable diurnal variability across the three periods under study. We conducted an analysis of hourly average diurnal cycles for O_3 and NO_x concentrations.

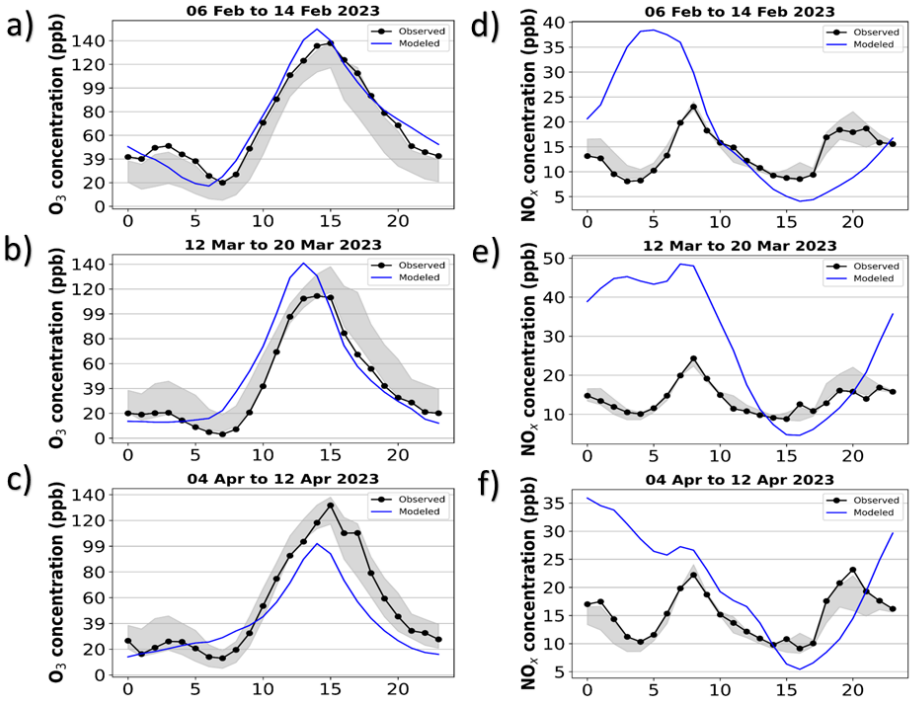

Figure 9.5. Hourly average diurnal cycles of concentrations of O_3 (a, b, and c) and NO_x (d, e, and f) observed and modeled in MRRJ.

In MRRJ, O_3 concentrations typically follow a distinct pattern: concentrations below 50 ppb from midnight to 08:00; increasing until 15:00, and gradually decreasing thereafter until midnight. The regional model set represents well the temporal phases observed in the O_3 diurnal cycle (Figure 9.5). Conversely, for NO_x, the model accurately simulates the morning peak occurring at 8:00. However, it tends to underestimate concentrations during the day (from 10:00 to 16:00) and erroneously

predicts periods of high NO_x concentrations from 20:00 to 03:00 too early. This discrepancy is attributed to the model's handling of the NO_x-to-VOCs ratio, which influences the production of O_3. The model consistently overestimates O_3 concentrations, particularly during daylight hours, reflecting an imbalance in the NO_x and VOCs emissions ratios simulated.

9.3.2.3. NO_2/NO_x and NO_2/O_x ratios

The analysis of observed NO_2 to NO_x and NO_2 to O_x ratios reveals less variability compared to the regional model ensemble, offering valuable insights into the interpretation of modeled O_3 biases. Across the city, average ratios consistently range from 60 % at night to 20 % during the day, reflecting typical diurnal variations influenced by traffic patterns. Specifically, a morning peak at 07:00 correlates with a 20 % decrease in the NO_2 to NO_x ratio and a corresponding 20 % increase in the NO_2 to O_x ratio.

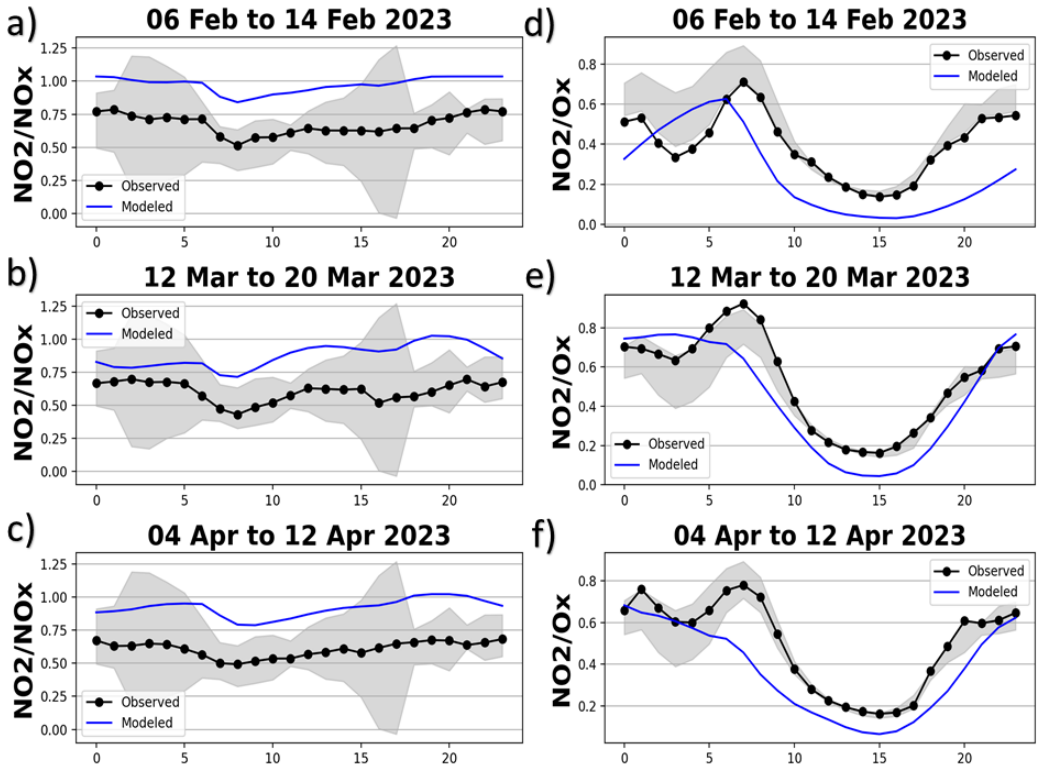

Figure 9.6. Hourly average diurnal cycles of ratios of NO_2 in NO_x (a, b and c) and in O_x (d, e, and f) observed and modeled in MRRJ.

The discrepancies in modeled NO_2/O_x ratios directly correlate with biases in modeled O_3 concentrations, particularly during daylight hours. When NO_2/O_x ratios are underestimated by the model, O_3 tends to be overestimated, and vice versa (Figure 9.6). Moreover, the model's overestimation of NO_2/ NO_x ratios at night is linked to underestimations of O_3 and overestimations of NO_x, highlighting potential issues with vertical anthropogenic profiles as an important parameter. While the regional model ensemble replicates meteorological conditions and generally agrees well with observed O_3 concentrations, it demonstrates moderate agreement with observed NO_x concentrations.

9.3.3. Oxidant Level Overestimation

The analysis continues by examining the temporal biases observed for NO_2, O_3, and O_x, alongside their hourly average diurnal cycles, with the objective of elucidating distinct diurnal phases and identifying primary contributors to model biases (Figure 9.7). Throughout the three periods studied, biases in Ox consistently show positive values. Conversely, biases in NO_2 and O_3 exhibit distinct diurnal patterns that often oppose each other (Figures 9.7a, 9.7b, and 9.7c), patterns that are well-reflected in the average diurnal cycles observed across all periods (Figures 9.7d, 9.7e, and 9.7f). These differing diurnal phases of bias for NO_2 and O_3 underscore the involvement of unique driving factors influencing these discrepancies.

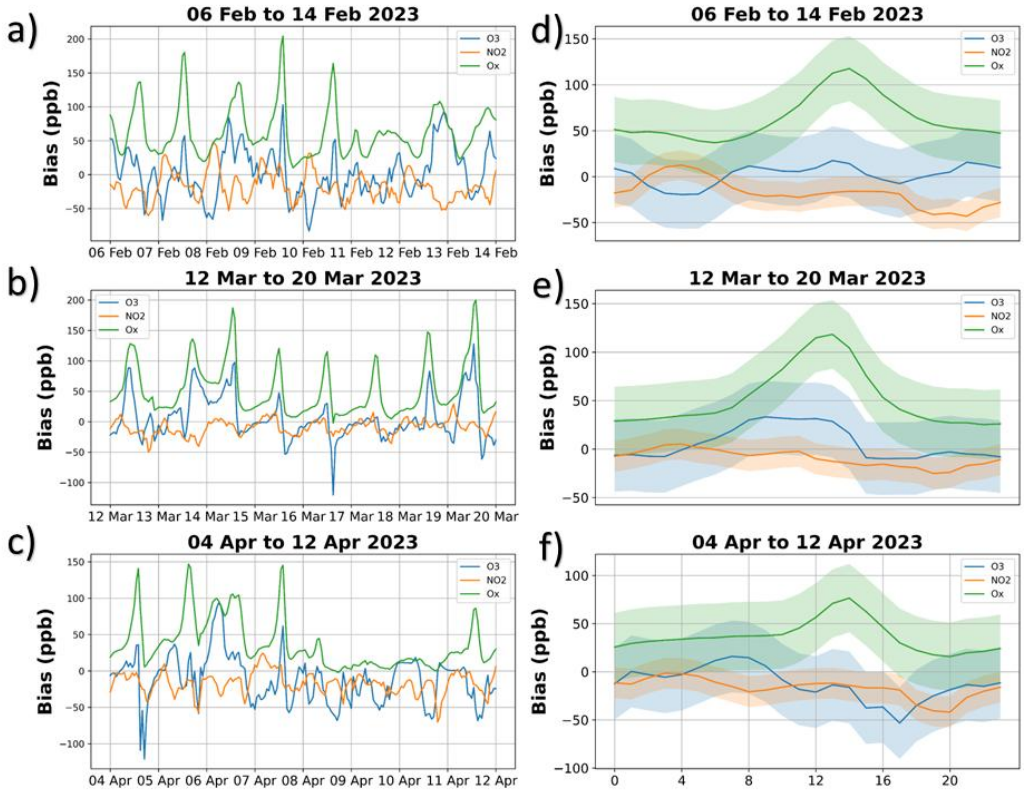

Figure 9.7. Time series of the hourly bias (modeled minus observed concentration) of the model for O_3, NO_2 and Ox (a, b, and c) and their associated average diurnal cycles (d, e, and f) in MRRJ.

During nighttime hours (from 20:00 to 06:00), there is a consistent overestimation of NO_2, while O_3 is consistently underestimated, except for the first period. The accurate portrayal of vertical profiles in anthropogenic emissions emerges as an important parameter for mitigating the NO_2 bias and consequently reducing the bias in O_3 levels.

In the morning period (from 06:00 to 10:00), biases in both NO_2 and O_3 peak during the rush hour at 07:00, with subsequent reductions. The pronounced overestimation of NO_2 concentrations and concurrent underestimation of O_3 concentrations at this peak traffic hour highlight significant impacts stemming from anthropogenic emissions.

During daytime hours (from 10:00 to 16:00), while the NO_2 bias diminishes, O_3 continues to be consistently overestimated. Individual model simulations show varied daily O_3 maxima, indicating substantial variability

around observed peaks. Similar planetary boundary layer (PBL) heights and low NO_x concentrations suggest that discrepancies in O_3 levels may relate to NO_x to VOCs ratios between models, particularly influenced by anthropogenic and biogenic emissions (ZHANG et al., 2009).

In the evening period (from 16:00 to 19:00), substantial overestimations for NO_2 and underestimations for O_3 concentrations persist. Differences in how anthropogenic emissions are treated likely contribute significantly to these biases.

The model consistently displays a pattern of underestimating O_3 during nighttime and overestimating it during the day, alongside a persistent overestimation of O_x by approximately 100 ppb. This analysis underscores the substantial influence of anthropogenic emissions treatment during each diurnal phase and underscores their important role in improving model accuracy.

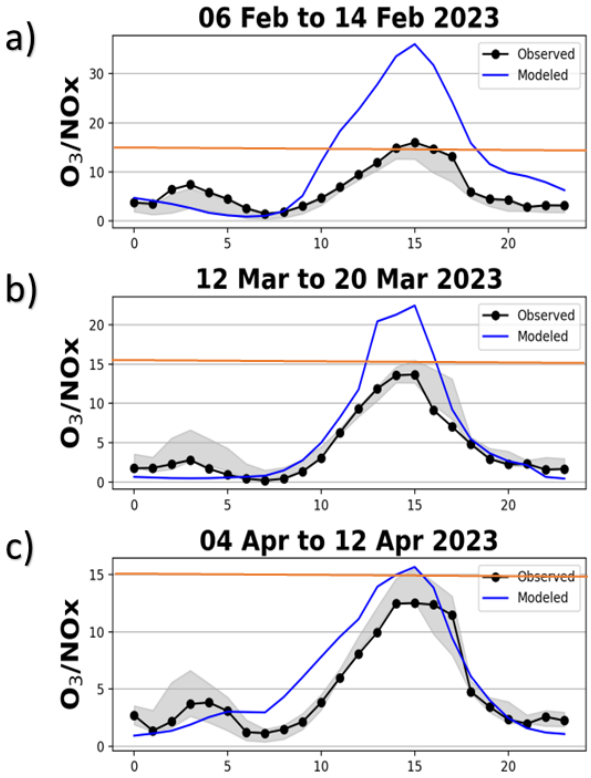

Figure 9.8. Average diurnal cycles of the model for O_3 in NO_x ratio (a, b, c) in MRRJ. The orange line indicates the value of the O_3/NO_x ratio (=15), which serves as a photochemical indicator.

Moreover, the study of the WRFchem model's performance in simulating O_3 concentrations in Rio de Janeiro reveals significant overestimations compared to observed values. The calculated O_3/ NO_x ratio serves as a photochemical indicator utilized to enhance comprehension of O_3 chemistry. A ratio equal to or greater than 15 signifies O_3 chemistry limited by NO_x, whereas ratios below 15 indicate limitation by VOCs (DANTAS et al., 2020; LI et al., 2022b; ZHANG et al., 2009). In Figure 9.8, these ratios were computed, and it was observed that the model exhibits NO_x limitation during the daytime, whereas station data reflect VOC limitation. This highlights the pivotal role of anthropogenic emissions, particularly volatile organic compounds, in driving these discrepancies. VOCs act as precursors in O_3 formation through intricate photochemical reactions, and their overestimated representation in the model exacerbates the discrepancies between simulated and observed O_3 levels.

Furthermore, our findings highlight the intricate relationship between anthropogenic emissions and the overestimation of O_3 in urban environments like Rio de Janeiro. The study suggests that while anthropogenic emissions, including VOCs, are essential for accurately modeling O_3 concentrations, their current representation in WRFchem leads to significant overestimates. Addressing these disparities is pivotal for refining atmospheric models and enhancing their predictive accuracy, thereby supporting informed policy decisions aimed at mitigating the adverse health and environmental impacts associated with elevated O_3 levels in urban areas.

9.3.4. Analysis of Pollution Distribution

9.3.4.1 Areas of the metropolitan region of Rio de Janeiro most affected by high O_3 concentration

During the study periods, a heterogeneous distribution of O_3 was modeled in MRRJ. Areas most affected by O_3 do not necessarily correspond

to those with high concentrations of NO_x, often associated with centralized urban pollution. Instead, districts such as Irajá district and Bangu have emerged as O_3 hotspots (Figure 9.9). In general, urban areas with high NO_x values have lower O_3 concentrations due to being in a VOC-controlled regime. An examination of the distribution reveals that O_3 concentrations are notably elevated in urban areas situated beyond the confines of Rio's metropolitan region, with Volta Redonda serving as a case in point.

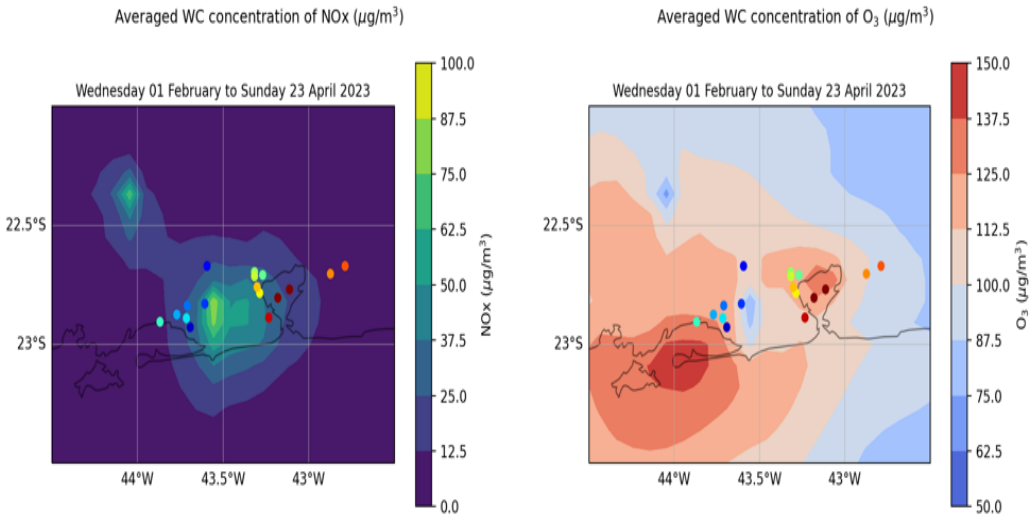

Figure 9.9. NO_x and O_3 simulation of MRRJ during from 01 February to 23 April 2023.

The results indicate that the elevated concentrations of O_3 observed in these regions are the result of a complex interplay of factors. Primarily, the presence of large industrial areas, such as Volta Redonda, Duque de Caxias and Santa Cruz, plays a pivotal role due to emissions of VOCs associated with intensive industrial processes, including metallurgy and steelmaking. These VOCs act as precursors to ozone in the atmosphere, contributing to its high formation. As can be seen in the map below, obtained by calculating the O_3/ NO_x ratio seen previously, where the regions with the presence of industries have limited VOCs (Figure 9.10).

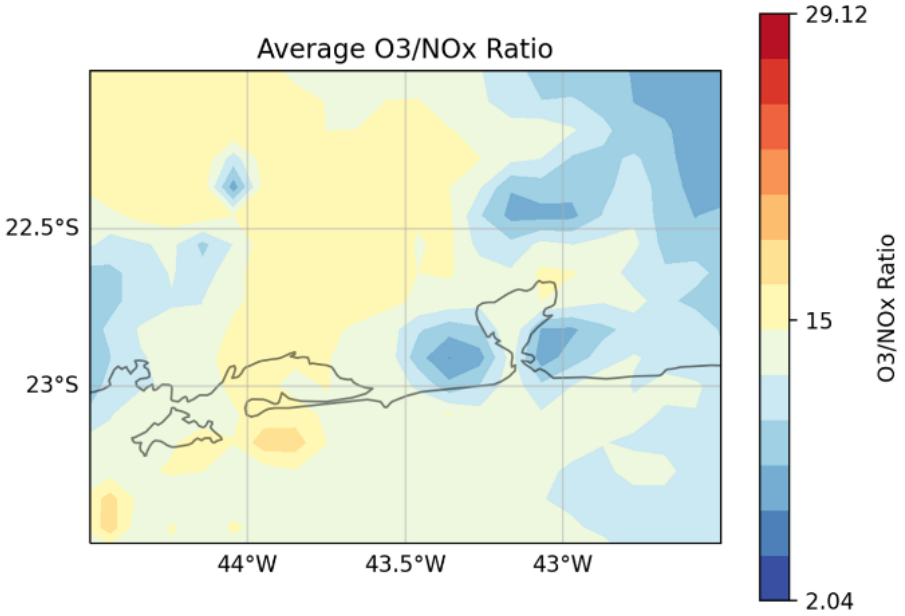

Figure 9.10. O_3/NO_x simulation of MRRJ during from 01 February to 23 April 2023. The value of ration equals to or greater than 15 signifies O_3 chemistry limited by NO_x, whereas ratios below 15 indicate limitation by VOCs.

Furthermore, these industrial areas host over 800 industries across various sectors, including chemistry, petrochemistry, oil refining, fuel storage, power generation, gas production, plastics, metallurgy, and steelmaking (DANTAS et al., 2020; IBGE, 2021a). In addition, high levels of VOCs compared to NO_x in the studied areas suggest a favorable environment for O_3 formation, as previously studied (DANTAS et al., 2019, 2020; MENDES et al., 2020). The low presence of NO_x may limit the destruction capacity of O_3, allowing this pollutant to accumulate more easily.

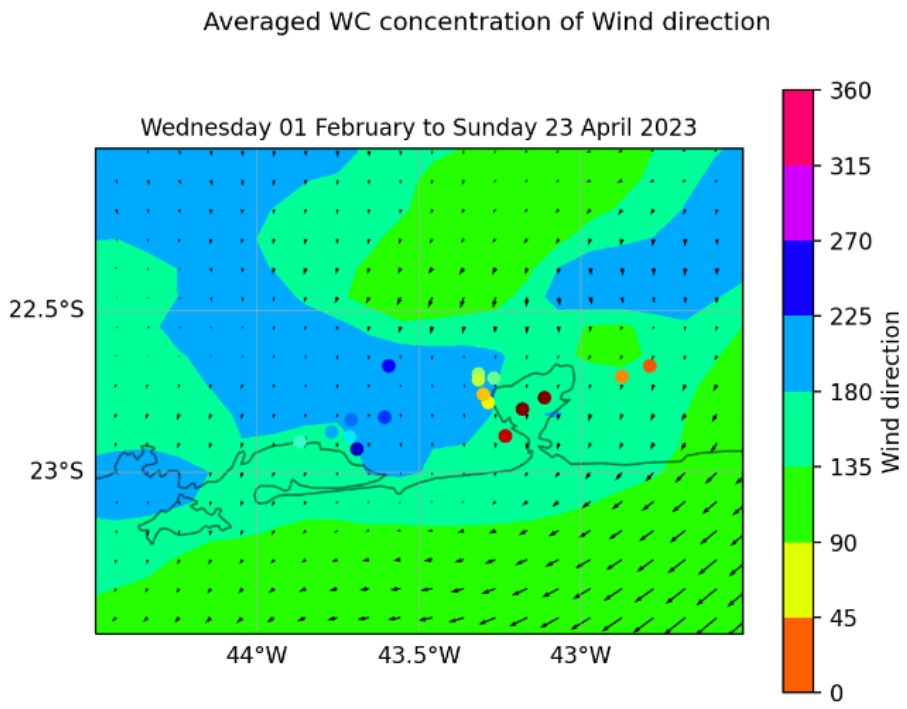

Figure 9.11. Wind direction simulation of MRRJ during from 01 February to 23 April 2023.

The dispersion and concentration of O_3 in the studied areas is significantly influenced by atmospheric transport (figure 9.11). Air masses moving northward from industrial areas can transport a range of pollutants, including VOCs, which contribute to elevated O_3 concentrations in regions such as Irajá and Bangu (BRAGA et al., 2019; DANTAS et al., 2020; GERALDINO et al., 2017; GIODA et al., 2018; MENDES et al., 2020). This atmospheric transport pattern is a crucial element in understanding the geographical distribution of O_3 concentrations in RMRJ.

In other locations, such as Ilha do Governador and Ilha de Paquetá, elevated O_3 levels were observed despite low levels of NO_x. Nevertheless, atmospheric transport alone may not be a sufficient explanation. Previous studies in the region indicate that a potential explanation is the characteristic photochemical processes involved in the formation of THC and NO_x under sunlight (GIODA et al., 2018).

9.4. Conclusion

Based on the comprehensive data analysis of the forecasted O_3 concentrations in MRRJ, significant challenges are highligted by this study. The discrepancies observed between simulated and observed NO_2, O_3, and Ox concentrations consistently show O_3 overestimation during the day, underestimation at night, and a persistent overestimation of Ox levels. These biases largely due to anthropogenic emissions, particularly VOCs, used by the WRFchem regional model.

The findings underscore the important role of anthropogenic emissions, especially VOCs, in O_3 formation. The exaggerated representation of these compounds in the model directly contributes to discrepancies in simulated O_3 concentrations. Moreover, the varying diurnal bias patterns for NO_2 and O_3 emphasize the necessity for refining emission temporal profiles used for atmospheric modeling. Furthermore, the study highlights the significant role of industrial emissions, particularly VOCs, in driving ozone formation, with areas such as Volta Redonda and Santa Cruz emerging as focal points of O_3 concentration in the MRRJ.

This study underscores the importance of an integrated approach that combines precise observational data with advanced modeling techniques to tackle the multifaceted challenges related to air quality in major cities like Rio de Janeiro.

9.5. Supplementary Material 3

Table S1. Names of air quality monitoring stations correspond to the Rio de Janeiro metropolitan region with their coordinates.

Station	Latitude (˚)	Longitude (˚)
Largo do Bodegão – SC	-22.926667	-43.694167
Engenheiro Pedreira –JP	-22.670833	-43.594167
Jardim Guandu - NI	-22.827500	-43.607500
Piranema - SP	-22.835278	-43.711944
Monte Serrat – ITG	-22.875000	-43.770556
Adalgisa Nery - SC	-22.888611	-43.716389
Coroa Grande – ITG	-22.904722	-43.871111
Campos Elíseos - DC	-22.706667	-43.269722
Jardim Primavera – DC	-22.695556	-43.318889
São Bento – DC	-22.712778	-43.318333
Vila São Luiz - DC	-22.784167	-43.286667
Pilar – DC	-22.758889	-43.304167
Porto das Caixas – ITB	-22.701944	-42.875556
Sambaetiba – ITB	-22.669167	-42.787778
Engenhão – RJ	-22.885556	-43.235278
Manguinhos – RJ	-22.885556	-43.235278
Ilha de Paquetá- RJ	-22.767778	-43.113056
Ilha do Governador -RJ	-22.804444	-43.181667

10. General Conclusion

The integrated analysis of air quality studies in Rio de Janeiro revealed a series of environmental and public health challenges related to air pollutant emissions. $PM_{2.5}$ concentrations varied significantly between the sites sampled, with the highest levels observed in the Serra dos Órgãos National Park (PARNASO) and the lowest in Campos dos Goytacazes. Although no sample exceeded the Brazilian regulatory limits, a significant proportion exceeded the values recommended by the WHO, showing potential health risks.

The chemical composition of the particulate matter indicated the predominance of elements such as Fe and Al for all sites, but black carbon (BC) was more abundant in PARNASO, but had a greater contribution relative to $PM_{2.5}$ in Campos, mainly associated with biomass burning. Analysis of soluble ions revealed the predominant presence of Cl^-, Na^+, SO_4^{2-} and NO_3^-, with 75 to 91 % of the sulphate being of anthropogenic origin. The sources identified included soil resuspension, vehicle emissions, pollution transportation and burning.

The presence of organic compounds was also analyzed, indicating sources predominantly related to the incomplete combustion of fossil fuels and biomass. During the dry season, concentrations of these compounds were higher due to reduced rainfall, favoring the permanence of particles in the atmosphere. In addition, atmospheric mercury (PHg) showed seasonal patterns, with the highest concentrations in the dry season and the influence of atmospheric transport from volcanic regions of the Andes and fires.

NO_x emissions from heavy vehicles showed high variability. Engine maintenance was identified as an important factor in reducing these emissions. The variability of emissions was influenced by vehicle weight, engine power and age, suggesting the need for public policies aimed at monitoring and renewing the fleet.

The modeling of O_3 concentrations in the Metropolitan Region of Rio

de Janeiro (MRRJ) highlighted the overestimation of daytime concentrations and underestimation at night, attributed to the excessive representation of VOCs in the WRF-Chem model. Industrial emissions, especially in Volta Redonda and Santa Cruz, were identified as the main contributors to O_3 formation, reinforcing the need to refine temporal emission profiles and monitor sources.

The studies reinforce the importance of adopting pollution control measures, including continuous air quality monitoring, improved atmospheric models and stricter regulations for vehicle and industrial emissions. The implementation of effective public policies can contribute to reducing the impacts of air pollution and improving the quality of life of the population in the region.

11. References

ABAS, M. R. BIN; SIMONEIT, B. R. T. Composition of extractable organic matter of air particles from malaysia: Initial study. **Atmospheric Environment**, v. 30, n. 15, p. 2779–2793, 1 ago. 1996.

ABBASI, S. A. et al. Quantification of elemental composition of Granite Gneiss collected from Neelum Valley using calibration free laser-induced breakdown and energy-dispersive X-ray spectroscopy. **Journal of Radiation Research and Applied Sciences**, v. 13, n. 1, p. 362–372, 1 jan. 2020.

ABREU-MOTA, M. A. DE et al. Sedimentary biomarkers along a contamination gradient in a human-impacted sub-estuary in Southern Brazil: A multi-parameter approach based on spatial and seasonal variability. **Chemosphere**, v. 103, p. 156–163, 1 maio 2014.

AGUIAR, S. DE O. et al. Avaliação das emissões de escapamento veicular em condições específicas do motor: partida e marcha-lenta. **TRANSPORTES**, v. 23, n. 3, p. 35–43, 23 dez. 2015.

AHMED, T. et al. Measurement of black carbon (BC) by an optical method and a thermal-optical method: Intercomparison for four sites. **Atmospheric Environment**, v. 43, n. 40, p. 6305–6311, 1 dez. 2009.

AJMAL, Z. et al. Recent advancement in conjugated polymers based photocatalytic technology for air pollutants abatement: Cases of CO2, NOx, and VOCs. **Chemosphere**, v. 308, p. 136358, 1 dez. 2022.

ALBINET, A. et al. Nitrated and oxygenated derivatives of polycyclic aromatic hydrocarbons in the ambient air of two French alpine valleys: Part 1: Concentrations, sources and gas/particle partitioning. **Atmospheric Environment**, v. 42, n. 1, p. 43–54, 1 jan. 2008.

ALVES, C. Aerossóis atmosféricos: perspectiva histórica, fontes, processos químicos de formação e composição orgânica. **Química Nova**, v. 28, n. 5, p. 859–870, 2005.

ALVES, C. A. Characterisation of solvent extractable organic constituents in atmospheric particulate matter: an overview. v. 80, n. 1, p. 21–82, 2008.

ALVES, C. A. et al. Indoor/Outdoor Relationships between PM10 and Associated Organic Compounds in a Primary School. **Aerosol and Air Quality Research**, v. 14, n. 1, p. 86–98, fev. 2014.

ALVES, C. A. et al. Polycyclic aromatic hydrocarbons (PAHs) and their derivatives (oxygenated-PAHs, nitrated-PAHs and azaarenes) in size-

fractionated particles emitted in an urban road tunnel. **Atmospheric Research**, v. 180, p. 128–137, 1 nov. 2016.

AMADOR-MUÑOZ, O. et al. Organic compounds of PM2.5 in Mexico Valley: Spatial and temporal patterns, behavior and sources. **Science of The Total Environment**, v. 409, n. 8, p. 1453–1465, 15 mar. 2011.

ANDRADE, M. DE F. et al. Vehicle emissions and PM 2.5 mass concentrations in six Brazilian cities. **Air Quality, Atmosphere and Health**, v. 5, n. 1, p. 79–88, 20 mar. 2012.

ANDREOU, G.; RAPSOMANIKIS, S. Origins of n-alkanes, carbonyl compounds and molecular biomarkers in atmospheric fine and coarse particles of Athens, Greece. **Science of The Total Environment**, v. 407, n. 21, p. 5750–5760, 15 out. 2009.

ARLT, V. M. et al. Mutagenicity and DNA adduct formation by the urban air pollutant 2-nitrobenzanthrone. **Toxicological sciences : an official journal of the Society of Toxicology**, v. 98, n. 2, p. 445–457, ago. 2007.

ARLT, V. M.; PHILLIPS, D. H.; REYNISSON, J. Theoretical investigations on the formation of nitrobenzanthrone-DNA Adducts. **Organic & Biomolecular Chemistry**, v. 9, n. 17, p. 6100–6110, 11 ago.

2011.

ASGHAR, U. et al. Review on the progress in emission control technologies for the abatement of CO2, SOx and NOx from fuel combustion. **Journal of Environmental Chemical Engineering**, v. 9, n. 5, p. 106064, 1 out. 2021.

ATKINSON, R. et al. Gas-phase atmospheric chemistry of 1- and 2-nitronaphthalene and 1,4-naphthoquinone. **Atmospheric Environment (1967)**, v. 23, n. 12, p. 2679–2690, 1 jan. 1989.

ATKINSON, R. W. et al. Urban ambient particle metrics and health: a time-series analysis. **Epidemiology (Cambridge, Mass.)**, v. 21, n. 4, p. 501–511, jul. 2010.

AUMONT, B. et al. Modeling the influence of alkane molecular structure on secondary organic aerosol formation. **Faraday Discussions**, v. 165, n. 0, p. 105–122, 17 dez. 2013.

BAEK, S. O. et al. A review of atmospheric polycyclic aromatic hydrocarbons: Sources, fate and behavior. **Water, Air, and Soil Pollution**, v. 60, n. 3–4, p. 279–300, dez. 1991.

BAI, L. et al. Exposure to ambient air pollution and the incidence of

congestive heart failure and acute myocardial infarction: A population-based study of 5.1 million Canadian adults living in Ontario. **Environment International**, v. 132, p. 105004, 1 nov. 2019.

BAKLANOV, A.; ZHANG, Y. Advances in air quality modeling and forecasting. **Global Transitions**, v. 2, p. 261–270, 1 jan. 2020.

BAPTISTA VENTURA, L. M. et al. Inspection and maintenance programs for in-service vehicles: An important air pollution control tool. **Sustainable Cities and Society**, v. 53, p. 101956, 1 fev. 2020.

BARI, M. A. et al. Wood smoke as a source of particle-phase organic compounds in residential areas. **Atmospheric Environment**, v. 43, n. 31, p. 4722–4732, 1 out. 2009.

BARNETT-ITZHAKI, Z.; LEVI, A. Effects of chronic exposure to ambient air pollutants on COVID-19 morbidity and mortality - A lesson from OECD countries. **Environmental Research**, v. 195, p. 110723, 1 abr. 2021.

BATISTA, J. et al. IMPACTOS DOS BTEX EM ÁREAS URBANAS DA CIDADE DO RIO DE JANEIRO. **Quim. Nova**, v. 43, n. 7, p. 870–877, 2020.

BERGVALL, C.; WESTERHOLM, R. Determination of highly

carcinogenic dibenzopyrene isomers in particulate emissions from two diesel- and two gasoline-fuelled light-duty vehicles. **Atmospheric Environment**, v. 43, n. 25, p. 3883–3890, 1 ago. 2009.

BERINGUI, K. et al. **Assessment of the concentration and inorganic composition of particulate matter collected in the State of Rio De Janeiro**. **Quimica Nova**Sociedade Brasileira de Quimica, , 2021.

BERINGUI, K. et al. Tracing the Origins of Air Contaminants Near Environmental Protection Areas. **Environmental Forensics**, 2024.

BIGIO, L.; ANGERT, A. Isotopic signature of atmospheric phosphate in airborne tree pollen. **Atmospheric Environment**, v. 194, p. 1–6, 1 dez. 2018.

BO, D. et al. Mercury concentration in fine atmospheric particles during haze and non-haze days in Shanghai, China. **Atmospheric Pollution Research**, v. 7, n. 2, p. 348–354, 1 mar. 2016.

BOND, T. C. et al. Bounding the role of black carbon in the climate system: A scientific assessment. **Journal of Geophysical Research: Atmospheres**, v. 118, n. 11, p. 5380–5552, 16 jun. 2013.

BRAGA, A. L. et al. Levels of volatile carbonyl compounds in the

Atlantic rainforest, in the city of Rio de Janeiro. **Bull Environ Contam Toxicol**, v. 102, n. 6, p. 757–762, 15 jun. 2019.

BRASIL. **RESOLUÇÃO CONAMA nº 5, de 15 de junho de 1989**. Disponível em: <https://urbanismoemeioambiente.fortaleza.ce.gov.br/images/urbanismo-e-meio-ambiente/resolucao/resolucao_conama_005_de_1989.pdf>. Acesso em: 24 mar. 2023.

BRASIL. **Resolução CONAMA n. 491, de 19 de novembro de 2018, 19 novembro 2018.** Disponível em: <https://www.in.gov.br/web/guest/materia/-/asset_publisher/Kujrw0TZC2Mb/content/id/51058895/do1-2018-11-21-resolucao-n-491-de-19-de-novembro-de-2018-51058603>. Acesso em: 8 jan. 2023.

BRASIL. Programa de controle de emissões veiculares (Proconve). 2023.

BRASSEUR, G. P. Natural and anthropogenic perturbations of the stratospheric ozone layer. **Planetary and Space Science**, v. 40, n. 2–3, p. 403–412, 1 fev. 1992.

BRAY, E. E.; EVANS, E. D. Distribution of n-paraffins as a clue to

recognition of source beds. **Geochimica et Cosmochimica Acta**, v. 22, n. 1, p. 2–15, 1 fev. 1961.

BRITO, G. F. S.; SODRE, F. F.; ALMEIDA, F. V. O impacto do material particulado na qualidade do a. **Rev. Virtual Quim**, v. 10, n. 5, p. 1335–1354, 2018.

BROCZA, F. M. et al. Global scenarios of anthropogenic mercury emissions. **EGUsphere [preprint]**, n. 41, 2024.

BRODRICK, C. J. et al. Effect of Vehicle Operation, Weight, and Accessory Use on Emissions from a Modern Heavy-Duty Diesel Truck. **https://doi.org/10.3141/1880-14**, v. 1880, n. 1880, p. 119–125, 1 jan. 2004.

BURGARD, D. A. et al. Remote sensing of in-use heavy-duty diesel trucks. **Environmental Science and Technology**, v. 40, n. 22, p. 6938–6942, 15 nov. 2006.

BURUIANA, D. L. et al. Important Contributions to Reducing Nitrogen Oxide Emissions from Internal Combustion Engines. **International Journal of Environmental Research and Public Health**, v. 18, n. 17, 1 set. 2021.

BUSECK, P. R. et al. Are black carbon and soot the same? **Atmospheric Chemistry and Physics Discussions**, v. 12, n. 9, p. 24821–

24846, 21 set. 2012.

CALLÉN, M. S.; ITURMENDI, A.; LÓPEZ, J. M. Source apportionment of atmospheric PM2.5-bound polycyclic aromatic hydrocarbons by a PMF receptor model. Assessment of potential risk for human health. **Environmental Pollution**, v. 195, p. 167–177, 1 dez. 2014.

CARICCHIA, A. M.; CHIAVARINI, S.; PEZZA, M. Polycyclic aromatic hydrocarbons in the urban atmospheric particulate matter in the city of Naples (Italy). **Atmospheric Environment**, v. 33, n. 23, p. 3731–3738, 1 out. 1999.

CARRERAS, H. A. et al. Composition and mutagenicity of PAHs associated with urban airborne particles in Córdoba, Argentina. **Environmental Pollution**, v. 178, p. 403–410, 1 jul. 2013.

CASTELL, N. et al. Can commercial low-cost sensor platforms contribute to air quality monitoring and exposure estimates? **Environment International**, v. 99, p. 293–302, 2017.

CAUMO, S.; BRUNS, R. E.; VASCONCELLOS, P. C. Variation of the Distribution of Atmospheric n-Alkanes Emitted by Different Fuels' Combustion. **Atmosphere 2020, Vol. 11, Page 643**, v. 11, n. 6, p. 643, 16 jun. 2020.

CAUMO, S. E. S. et al. Physicochemical characterization of winter PM10 aerosol impacted by sugarcane burning from São Paulo city, Brazil. **Atmospheric Environment**, v. 145, p. 272–279, 1 nov. 2016.

CBMERJ – CORPO DE BOMBEIROS DO RIO DE JANEIRO. **Anuario 2023**. Disponível em: <https://www.cbmerj.rj.gov.br/>. Acesso em: 26 nov. 2024.

CERQUEIRA, M. R. F. et al. Chemical characteristics of rainwater at a southeastern site of Brazil. **Atmospheric Pollution Research**, v. 5, n. 2, p. 253–261, 1 abr. 2014.

CETESB. Emissão Veicular. 2023.

CHA, Y.; LEE, S.; LEE, J. Measurement of Black Carbon Concentration and Comparison with PM10 and PM2.5 Concentrations Monitored in Chungcheong Province, Korea. **Aerosol and Air Quality Research**, v. 19, n. 3, p. 541–547, 1 mar. 2019.

CHAN, C.-Y. et al. Biofuel Combustion Emissions - Chemical and Physical Smoke Properties. **Environmental Impact of Biofuels**, 6 set. 2011.

CHEN, C. et al. Concentrations, Source Identification, and Lung Cancer Risk Associated with Springtime PM2.5-Bound Polycyclic Aromatic Hydrocarbons (PAHs) in Nanjing, China. **Archives of Environmental Contamination and Toxicology**, v. 73, n. 3, p. 391–400, 1 out. 2017.

CHEN, Q. et al. Seasonal characteristics and health risks of PM2.5-bound organic pollutants in industrial and urban areas of a China megacity. **Journal of Environmental Management**, v. 245, p. 273–281, 1 set. 2019.

CHENG, Y. et al. Biomass burning contribution to Beijing aerosol. **Atmospheric Chemistry and Physics**, v. 13, n. 15, p. 7765–7781, 2013.

CHIANG, M.; ZHANG, T. Fog and IoT: An Overview of Research Opportunities. **IEEE Internet of Things Journal**, v. 3, n. 6, p. 854–864, 1 dez. 2016.

CHIN, M. et al. Tropospheric Aerosol Optical Thickness from the GOCART Model and Comparisons with Satellite and Sun Photometer Measurements. **Journal of the Atmospheric Sciences**, v. 59, n. 3, p. 461–483, 1 fev. 2002.

CHRYSIKOU, L. P.; SAMARA, C. A. Seasonal variation of the size distribution of urban particulate matter and associated organic pollutants in the ambient air. **Atmospheric Environment**, v. 43, n. 30, p. 4557–4569, 1

set. 2009.

CLAEYS, M. et al. Polar organic marker compounds in atmospheric aerosols during the LBA-SMOCC 2002 biomass burning experiment in Rondônia, Brazil: Sources and source processes, time series, diel variations and size distributions. **Atmospheric Chemistry and Physics**, v. 10, n. 19, p. 9319–9331, 2010.

CLARK, N. N. et al. Factors Affecting Heavy-Duty Diesel Vehicle Emissions. **Journal of the Air & Waste Management Association**, v. 52, n. 1, p. 84–94, 2002.

CLARK, N. N.; GAJENDRAN, P.; KERN, J. M. A predictive tool for emissions from heavy-duty diesel vehicles. **Environmental Science and Technology**, v. 37, n. 1, p. 7–15, 1 jan. 2003.

CLEMENTE, Á. et al. Organic tracers in fine and coarse aerosols at an urban Mediterranean site: contribution of biomass burning and biogenic emissions. v. 31, p. 25216–25226, 2024.

CONAMA. **RESOLUÇÃO CONAMA nº 18, de 6 de maio de 1986;Diário Oficial da União (DOU)**. Brasília: [s.n.]. Disponível em: <http://conama.mma.gov.br/?option=com_sisconama&task=arquivo.download&id=41>. Acesso em: 25 mar. 2023.

CONAMA. **RESOLUÇÃO N. 492, DE 20 DE DEZEMBRO DE 2018Diário Oficial da União (DOU)**. Brasília: [s.n.]. Disponível em: <https://conama.mma.gov.br/?option=com_sisconama&task=arquivo.download&id=765>. Acesso em: 25 mar. 2023a.

CONAMA. **RESOLUÇÃO Nº 490, DE 16 DE NOVEMBRO DE 2018**. Disponível em: <https://conama.mma.gov.br/?option=com_sisconama&task=arquivo.download&id=767>. Acesso em: 31 jan. 2025b.

CONAMA. **CONAMA - Resolution No 506, of July 5, 2024. Establishes national air quality standards and provides guidelines for their application**.

CORREA, M. A. et al. Characterization Methods of Ions and Metals in Particulate Matter Pollutants on PM2.5 and PM10 Samples from Several Emission Sources. **Sustainability 2023, Vol. 15, Page 4402**, v. 15, n. 5, p. 4402, 1 mar. 2023.

COSTA, A. N.; POLIVANOV, H.; ALVES, M. D. G. Mapeamento geológico-geotécnico preliminar, utilizando geoprocessamento, no município de Campos dos Goytacazes, Estado do Rio de Janeiro. 2008.

CRIPPA, M. et al. High resolution temporal profiles in the Emissions Database for Global Atmospheric Research. **Scientific Data 2020 7:1**, v. 7, n. 1, p. 1–17, 17 abr. 2020.

CRONEMBERGER, C.; VIVEIROS DE CASTRO, E. B. **Ciência e Conservação na Serra dos Órgãos.** . Disponível em: <https://www.ibama.gov.br/sophia/cnia/livros/cienciaeconservacaonaserradosogaosdigital.pdf>. Acesso em: 9 dez. 2024.

DA SILVA, C. M. et al. Kinetic and mechanistic reactivity. Isoprene impact on ozone levels in an urban area near Tijuca Forest, Rio de Janeiro. **Bull Environ Contam Toxicol**, v. 97, n. 6, p. 781–785, 1 dez. 2016.

DA SILVA JUNIOR, R. S.; ANDRADE, M. D. F. Validação de poluentes fotoquímicos e inclusão do inventário de emissões no modelo de qualidade do ar WRF/CHEM, para a região metropolitana de São Paulo. **Revista Brasileira de Meteorologia**, v. 28, n. 1, p. 105–121, mar. 2013.

DA SILVEIRA, V. R. et al. Analysis of urban - industrial expansion and increasing level of ozone concentration as subsiding an environmental management plan for the east of Rio de Janeiro metropolitan area – Brazil. **Land Use Policy**, v. 101, p. 105148, 1 fev. 2021.

DANTAS, G. et al. Why did ozone levels remain high in Rio de

Janeiro during the Brazilian truck driver strike? **Atmospheric Pollution Research**, v. 10, n. 6, p. 2018–2029, 1 nov. 2019.

DANTAS, G. et al. A reactivity analysis of volatile organic compounds in a Rio de Janeiro urban area impacted by vehicular and industrial emissions. **Atmospheric Pollution Research**, v. 11, n. 5, p. 1018–1027, 1 maio 2020.

DAVIS, E. et al. Source apportionment of polycyclic aromatic hydrocarbons (PAHs) in small craft harbor (SCH) surficial sediments in Nova Scotia, Canada. **The Science of the total environment**, v. 691, p. 528, 11 nov. 2019.

DE ALMEIDA AZEVEDO, D.; DOS SANTOS, C. Y. M.; DE AQUINO NETO, F. R. Identification and seasonal variation of atmospheric organic pollutants in Campos dos Goytacazes, Brazil. **Atmospheric Environment**, v. 36, n. 14, p. 2383–2395, 1 maio 2002.

DE CASTRO VASCONCELLOS, P. et al. Occurrence and concentration levels of nitro-PAH in the air of three Brazilian cities experiencing different emission impacts. **Water, Air, and Soil Pollution**, v. 190, n. 1–4, p. 87–94, 15 maio 2008.

DE JESUS, R. M. et al. Fine and Coarse Particle-Bound Mercury in

(Bio)fuels and Biodiesel/ Diesel Exhaust under Real World Circumstances. **Energy and Fuels**, v. 34, n. 12, p. 16173–16180, 17 dez. 2020.

DE LA CRUZ, A. H. et al. Black Carbon and Particulate Matter Concentrations: Air Pollution Levels in Rio de Janeiro, Brazil. **Article J. Braz. Chem. Soc.**, v. 35, p. 1–12, 2024.

DE MELO LIMA, F.; PEREIRA NETTO, A. D. Annual variation of total suspended particulate and associated polycyclic aromatic hydrocarbons in the tropical city of Niterói, RJ, Brazil. **Journal of the Brazilian Chemical Society**, v. 20, n. 3, p. 488–495, 2009.

DE MIRANDA, R. M. et al. Urban air pollution: A representative survey of PM 2.5 mass concentrations in six Brazilian cities. **Air Quality, Atmosphere and Health**, v. 5, n. 1, p. 63–77, 4 mar. 2012.

DE OLIVEIRA ALVES, N. et al. Biomass burning in the Amazon region: Aerosol source apportionment and associated health risk assessment. **Atmospheric Environment**, v. 120, p. 277–285, 1 nov. 2015.

DEGRENDELE, C. et al. NPAHs and OPAHs in the atmosphere of two central European cities: Seasonality, urban-to-background gradients, cancer risks and gas-to-particle partitioning. **Science of The Total Environment**, v. 793, p. 148528, 1 nov. 2021.

DEITRICK, R.; GOLDBLATT, C. Effects of ozone levels on climate through Earth history. **Climate of the Past**, v. 19, n. 6, p. 1201–1218, 20 jun. 2023.

DEROUBAIX, A. et al. Intercomparison of Air Quality Models in a Megacity: Toward an Operational Ensemble Forecasting System for São Paulo. **Journal of Geophysical Research: Atmospheres**, v. 129, n. 1, p. e2022JD038179, 16 jan. 2024.

DETRAN-RJ. **Anuário Estatístico 2022**. Rio de Janeiro: [s.n.].

DETRAN-RJ. **Anuário Estatístico 2023**. Rio de Janeiro: [s.n.]. Disponível em: <https://www.detran.rj.gov.br/>. Acesso em: 25 nov. 2024.

DO NASCIMENTO, R. DE K. S. et al. In vitro toxicity and lung cancer risk: Atmospheric particulate matter from a city in southeastern Brazil impacted by biomass burning. **Chemosphere**, v. 338, p. 139484, 1 out. 2023.

DOS SANTOS, C. Y. M.; AZEVEDO, D. DE A.; DE AQUINO NETO, F. R. Selected organic compounds from biomass burning found in the atmospheric particulate matter over sugarcane plantation areas. **Atmospheric Environment**, v. 36, n. 18, p. 3009–3019, 1 jun. 2002.

DRISCOLL, C. T. et al. Mercury as a Global Pollutant: Sources, Pathways, and Effects. **Environmental Science & Technology**, v. 47, n. 10, p. 4967, 5 maio 2013.

EK, M. B. et al. Implementation of Noah land surface model advances in the National Centers for Environmental Prediction operational mesoscale Eta model. **Journal of Geophysical Research: Atmospheres**, v. 108, n. D22, p. 8851, 27 nov. 2003.

EL-MUBARAK, A. H. et al. Identification and source apportionment of polycyclic aromatic hydrocarbons in ambient air particulate matter of Riyadh, Saudi Arabia. **Environmental Science and Pollution Research**, v. 21, n. 1, p. 558–567, 30 jan. 2014.

EMMONS, L. K. et al. Description and evaluation of the Model for Ozone and Related chemical Tracers, version 4 (MOZART-4). **Geoscientific Model Development**, v. 3, n. 1, p. 43–67, 2010.

ENGELHARDT, V. et al. Black carbon and particulate matter mass concentrations in the Metropolitan District of Caracas, Venezuela: An assessment of temporal variation and contributing sources. **Elementa**, v. 10, n. 1, 4 jan. 2022.

FELIX, C. S. A. et al. Determination and human health risk assessment of mercury in fish samples. **Talanta**, v. 247, p. 123557, 1 set. 2022.

FERNANDES, K. S. et al. Characterization, Source Apportionment and Health Risk Assessment of PM 2.5 for a Rural Classroom in the Amazon: A Case Study. **Article J. Braz. Chem. Soc**, v. 32, n. 2, p. 363–375, 2021.

FERNANDES, K. S. et al. WSOC and Its Relationship with BC, Levoglucosan and Transition Metals in the $PM_{2.5}$ of an Urban Area in the Amazon. **Journal of the Brazilian Chemical Society**, v. 33, n. 6, p. 570–581, 30 maio 2022.

FERREIRA, M. M. C. Quimiometria III - Revisitando a análise exploratória dos dados multivariados. **Química Nova**, v. 45, n. 10, p. 1251–1264, 23 jan. 2023.

FERREIRA, R. S. et al. Multivariate Optimization of Extraction Variables of PAH in Particulate Matter (PM 10) in Indoor/Outdoor Air at Campos dos Goytacazes, Brazil. **Article J. Braz. Chem. Soc**, v. 32, n. 3, p. 618–625, 2021.

FRASER, M. P.; LAKSHMANAN, K. Using Levoglucosan as a

Molecular Marker for the Long-Range Transport of Biomass Combustion Aerosols. **Environmental Science and Technology**, v. 34, n. 21, p. 4560–4564, 1 nov. 2000.

FREITAS, A. DE M.; SOLCI, M. C. CARACTERIZAÇÃO DO MP 10 E MP 2,5 E DISTRIBUIÇÃO POR TAMANHO DE CLORETO, NITRATO E SULFATO EM ATMOSFERA URBANA E RURAL DE LONDRINA. **Quim. Nova**, v. 32, n. 7, p. 1750–1754, 2009.

FREITAS, S. R. et al. The Brazilian developments on the Regional Atmospheric Modeling System (BRAMS 5.2): An integrated environmental model tuned for tropical areas. **Geoscientific Model Development**, v. 10, n. 1, p. 189–222, 13 jan. 2017.

FREY, H. C.; ROUPHAIL, N. M.; ZHAI, H. Link-Based Emission Factors for Heavy-Duty Diesel Trucks Based on Real-World Data. **https://doi.org/10.3141/2058-04**, n. 2058, p. 23–32, 1 jan. 2008.

FU, M. et al. NOx emissions from Euro IV busses with SCR systems associated with urban, suburban and freeway driving patterns. **Science of The Total Environment**, v. 452–453, p. 222–226, 1 maio 2013.

FUJITANI, Y. et al. Effect of isothermal dilution on emission factors of organic carbon and n-alkanes in the particle and gas phases of diesel

exhaust. **Atmospheric Environment**, v. 59, p. 389–397, 1 nov. 2012.

FULLER, R. et al. Pollution and health: a progress update. **The Lancet. Planetary health**, v. 6, n. 6, p. e535–e547, 1 jun. 2022.

FUZZI, S. et al. Particulate matter, air quality and climate: Lessons learned and future needs. **Atmospheric Chemistry and Physics**, v. 15, n. 14, p. 8217–8299, 24 jul. 2015.

GAJANAND, M. S.; NARENDRAN, T. T. Green route planning to reduce the environmental impact of distribution. **International Journal of Logistics Research and Applications**, v. 16, n. 5, p. 410–432, 2013.

GAJENDRAN, P.; CLARK, N. N. Effect of truck operating weight on heavy-duty diesel emissions. **Environmental Science and Technology**, v. 37, n. 18, p. 4309–4317, 15 set. 2003.

GALAPPATHTHI, H. K. A.; SURAWEERA, I. Risk of Mercury exposure during childhood: A review of Sri Lankan situation. **Reviews on Environmental Health**, v. 35, n. 3, p. 229–232, 1 set. 2020.

GARCIA, K. O. et al. Assessment of nitro-polycyclic aromatic hydrocarbons in PM1 near an area of heavy-duty traffic. **Science of The Total Environment**, v. 479–480, n. 1, p. 57–65, 1 maio 2014.

GEORGE, C. et al. Heterogeneous Photochemistry in the Atmosphere. **Chemical Reviews**, v. 115, n. 10, p. 4218–4258, 27 maio 2015.

GERALDINO, C. G. P. et al. An analytical investigation of ozone episodes in Bangu, Rio de Janeiro. **Bull Environ Contam Toxicol**, v. 98, n. 5, p. 632–637, 1 maio 2017.

GIDHAGEN, L. et al. An integrated assessment of the impacts of PM2.5 and black carbon particles on the air quality of a large Brazilian city. **Air Quality, Atmosphere and Health**, v. 14, n. 9, p. 1455–1473, 1 set. 2021.

GIODA, A. et al. Half Century Monitoring Air Pollution in a Megacity: A Case Study of Rio de Janeiro. **Water, Air, and Soil Pollution**, v. 227, n. 3, p. 1–17, 1 mar. 2016.

GIODA, A. et al. Understanding ozone formation at two islands of Rio de Janeiro, Brazil. **Atmospheric Pollution Research**, v. 9, n. 2, p. 278–288, 1 mar. 2018.

GODOY, M. L. D. P. et al. Coarse and fine aerosol source apportionment in Rio de Janeiro, Brazil. **Atmospheric Environment**, v. 43,

n. 14, p. 2366–2374, 1 maio 2009.

GOGOU, A. et al. Organic aerosols in Eastern Mediterranean: components source reconciliation by using molecular markers and atmospheric back trajectories. **Organic Geochemistry**, v. 25, n. 1–2, p. 79–96, 1 dez. 1996.

GONZALEZ, A. et al. Measuring the Air Quality Using Low-Cost Air Sensors in a Parking Garage at University of Minnesota, USA. **International Journal of Environmental Research and Public Health**, v. 19, n. 22, p. 15223, 1 nov. 2022.

GORIAUX, M. et al. Field comparison of particulate PAH measurements using a low-flow denuder device and conventional sampling systems. **Environmental Science and Technology**, v. 40, n. 20, p. 6398–6404, 15 out. 2006.

GORR, M. W.; FALVO, M. J.; WOLD, L. E. Air Pollution and Other Environmental Modulators of Cardiac Function. **Comprehensive Physiology**, v. 7, n. 4, p. 1479–1495, 1 out. 2017.

GRAHAM, B. et al. Water-soluble organic compounds in biomass burning aerosols over Amazonia 1. Characterization by NMR and GC-MS. **Journal of Geophysical Research: Atmospheres**, v. 107, n. D20, p. LBA

14-1, 27 out. 2002.

GRAHAM, B. et al. Composition and diurnal variability of the natural Amazonian aerosol. **Journal of Geophysical Research: Atmospheres**, v. 108, n. D24, 27 dez. 2003.

GRANIER, C. et al. The Copernicus Atmospere Monitoring Service global and regional emissions (April 2019 version). **The Copernicus Atmosphere Monitoring Service (CAMS) report**, 2019.

GREENBERG, N. et al. Modeling long-term effects attributed to nitrogen dioxide (NO2) and sulfur dioxide (SO2) exposure on asthma morbidity in a nationwide cohort in Israel. **Journal of toxicology and environmental health. Part A**, v. 80, n. 6, p. 326–337, 19 mar. 2017.

GRELL, G. A.; DÉVÉNYI, D. A generalized approach to parameterizing convection combining ensemble and data assimilation techniques. **Geophysical Research Letters**, v. 29, n. 14, p. 38–1, 1 jul. 2002.

GUARDIOLA, C. et al. Cycle by cycle NOx model for diesel engine control. **Applied Thermal Engineering**, v. 110, p. 1011–1020, 5 jan. 2017.

GUENTHER, A. et al. Estimates of global terrestrial isoprene

emissions using MEGAN (Model of Emissions of Gases and Aerosols from Nature). **Atmos. Chem. Phys. Discuss**, v. 6, p. 109, 2006.

GULL, N. et al. Industrial Air Pollution and Its Effects on Human's Respiratory System (A Sociological Study of Bhoun shugar Mill District Jhang, Pakistan). **Academic Journal of Interdisciplinary Studies**, 1 nov. 2013.

GURGATZ, B. M. et al. Assessment and source apportionment of PM2.5 in a major Latin American port: elevated concentrations from traffic in the Great Atlantic Forest Reserve. **Air Quality, Atmosphere & Health 2024**, p. 1–17, 2 dez. 2024.

HALL, D. et al. PAHs, carbonyls, VOCs and PM2.5 emission factors for pre-harvest burning of Florida sugarcane. **Atmospheric Environment**, v. 55, p. 164–172, 1 ago. 2012.

HALLMARK, S. L.; WANG, B.; SPERRY, R. Comparison of on-road emissions for hybrid and regular transit buses. **Journal of the Air and Waste Management Association**, v. 63, n. 10, p. 1212–1220, 2013.

HAN, Y.; PARK, B.; JEONG, J. A Novel Architecture of Air Pollution Measurement Platform Using 5G and Blockchain for Industrial IoT Applications. **Procedia Computer Science**, v. 155, p. 728–733, 1 jan.

2019.

HE, L. et al. Investigating Real-World Emissions of China's Heavy-Duty Diesel Trucks: Can SCR Effectively Mitigate NOx Emissions for Highway Trucks? **Aerosol and Air Quality Research**, v. 17, n. 10, p. 2585–2594, 1 out. 2017.

HEDBERG, E. et al. Chemical and physical characterization of emissions from birch wood combustion in a wood stove. **Atmospheric Environment**, v. 36, n. 30, p. 4823–4837, 1 out. 2002.

HENRIQUES, M. C. et al. Exposure to mercury and human reproductive health: A systematic review. **Reproductive Toxicology**, v. 85, p. 93–103, 1 abr. 2019.

HESEDING, M.; DASKALOPOULOS, P. **Exhaust Emission Legislation-Diesel-And Gas Engines**. Frankfurt Am Main: VDMA, 2006.

HO, K. F. et al. Emissions of gas- and particle-phase polycyclic aromatic hydrocarbons (PAHs) in the Shing Mun Tunnel, Hong Kong. **Atmospheric Environment**, v. 43, n. 40, p. 6343–6351, 1 dez. 2009.

HONG, S. Y.; NOH, Y.; DUDHIA, J. A New Vertical Diffusion Package with an Explicit Treatment of Entrainment Processes. **Monthly**

Weather Review, v. 134, n. 9, p. 2318–2341, 1 set. 2006.

HOUNTALAS, D. T.; MAVROPOULOS, G. C.; BINDER, K. B. Effect of exhaust gas recirculation (EGR) temperature for various EGR rates on heavy duty DI diesel engine performance and emissions. **Energy**, v. 33, n. 2, p. 272–283, 1 fev. 2008.

HU, R. et al. The NOx emission characteristics of gasoline vehicles during transient driving cycles. **Transportation Research Part D: Transport and Environment**, v. 109, p. 103386, 1 ago. 2022.

IARC. **Diesel and Gasoline Engine Exhausts and Some Nitroarenes**. Lyon (FR): [s.n.].

IBGE. **IBGE: Rio de Janeiro**. Disponível em: <https://www.ibge.gov.br/cidades-e-estados/rj/rio-de-janeiro.html>. Acesso em: 25 mar. 2023a.

IBGE. **IBGE**. Disponível em: <https://www.ibge.gov.br/cidades-e-estados/rj/rio-de-janeiro.html>. Acesso em: 26 mar. 2023b.

IBGE. **Gross Domestic Product of Municipalities**. Disponível em: <https://www.ibge.gov.br/en/statistics/economic/national-accounts/19567-gross-domestic-product-of-municipalities.html>. Acesso em: 20 ago. 2024c.

IBGE. **Campos dos Goytacazes (RJ) | Cidades e Estados**. Disponível em: <https://www.ibge.gov.br/cidades-e-estados/rj/campos-dos-goytacazes.html>. Acesso em: 20 fev. 2024.

ICMBIO. **Plano de manejo do Parque Nacional da Serra dos Órgãos**. Disponível em: <https://www.gov.br/icmbio/pt-br/assuntos/biodiversidade/unidade-de-conservacao/unidades-de-biomas/mata-atlantica/lista-de-ucs/parna-da-serra-dos-orgaos/arquivos/monitoria_avaliacao-pm-2008-2009.pdf>. Acesso em: 9 dez. 2024.

IDREES, Z.; ZHENG, L. Low cost air pollution monitoring systems: A review of protocols and enabling technologies. **Journal of Industrial Information Integration**, v. 17, p. 100123, 1 mar. 2020.

IEA. **CO2 emissions from fuel combustion**. Paris, France: [s.n.]. Disponível em: <https://www.oecd.org/content/dam/oecd/en/publications/reports/2015/11/co2-emissions-from-fuel-combustion-2015_g1g5c869/co2_fuel-2015-en.pdf>. Acesso em: 1 fev. 2025a.

IEA. **World energy outlook 2015**. Paris, France: [s.n.]. Disponível em: <https://www.iea.org/reports/world-energy-outlook-2015>. Acesso em:

1 fev. 2025b.

IEA. **Energy technology perspectives 2015: mobilising innovation to accelerate climate action.** Paris, France: [s.n.]. Disponível em: <https://www.iea.org/reports/energy-technology-perspectives-2015>. Acesso em: 1 fev. 2025c.

IM, U. et al. The impact of anthropogenic and biogenic emissions on surface ozone concentrations in Istanbul. **Science of The Total Environment**, v. 409, n. 7, p. 1255–1265, 1 mar. 2011.

INMET. **Instituto Nacional de Meteorologia**. Disponível em: <https://portal.inmet.gov.br/>. Acesso em: 6 nov. 2024.

JACKSON, R. L. et al. Dimethylsulfide (DMS), marine biogenic aerosols and the ecophysiology of coral reefs. **Biogeosciences**, v. 17, n. 8, p. 2181–2204, 21 abr. 2020.

JAIN, A.; SINGH, A. P.; AGARWAL, A. K. Effect of split fuel injection and EGR on NOx and PM emission reduction in a low temperature combustion (LTC) mode diesel engine. **Energy**, v. 122, p. 249–264, 2017.

JIANG, Y. et al. Evaluation of emissions benefits of OBD-based repairs for potential application in a heavy-duty vehicle Inspection and

Maintenance program. **Atmospheric Environment**, v. 247, p. 118186, 15 fev. 2021.

JIANG, Y. et al. Understanding elevated real-world NOx emissions: Heavy-duty diesel engine certification testing versus in-use vehicle testing. **Fuel**, v. 307, p. 121771, 1 jan. 2022.

JOHNSON, T. V. Diesel Emissions in Review. **SAE International Journal of Engines**, v. 4, n. 1, p. 143–157, abr. 2011.

JOOST, W. J. Reducing vehicle weight and improving U.S. energy efficiency using integrated computational materials engineering. **JOM**, v. 64, n. 9, p. 1032–1038, 24 set. 2012.

JUSTO, E. P. S. et al. Assessment of Atmospheric PM 10 Pollution Levels and Chemical Composition in Urban Areas near the 2016 Olympic Game Arenas. **Article J. Braz. Chem. Soc**, v. 31, n. 5, 2020.

KAIVONEN, S.; NGAI, E. C. H. Real-time air pollution monitoring with sensors on city bus. **Digital Communications and Networks**, v. 6, n. 1, p. 23–30, 1 fev. 2020.

KAMAREHIE, B. et al. Quantification of health effects related to SO2 and NO2 pollutants by using Air quality model. **Journal of Advances in**

Environmental Health Research, v. 5, n. 1, p. 44–50, 1 fev. 2017.

KARAGULIAN, F. et al. Review of the Performance of Low-Cost Sensors for Air Quality Monitoring. **Atmosphere 2019, Vol. 10, Page 506**, v. 10, n. 9, p. 506, 29 ago. 2019.

KAUSHAL, D. et al. Aerosol-associated n-alkanes over Dhauladhar region of North-Western Himalaya: seasonal variations in sources and processes. **Environmental Monitoring and Assessment**, v. 192, n. 8, p. 1–18, 1 ago. 2020.

KAVOURAS, I. G. et al. Measurement of particulate aliphatic and polynuclear aromatic hydrocarbons in Santiago de Chile: source reconciliation and evaluation of sampling artifacts. **Atmospheric Environment**, v. 33, n. 30, p. 4977–4986, 1 dez. 1999.

KEYTE, I. J.; HARRISON, R. M.; LAMMEL, G. Chemical reactivity and long-range transport potential of polycyclic aromatic hydrocarbons – a review. **Chemical Society Reviews**, v. 42, n. 24, p. 9333–9391, 18 nov. 2013.

KHEZRI, B. et al. Simultaneous online monitoring of inorganic compounds in aerosols and gases in an industrialized area. **Atmospheric Environment**, v. 80, p. 352–360, 1 dez. 2013.

KIM, K. H.; KABIR, E.; KABIR, S. A review on the human health impact of airborne particulate matter. **Environment international**, v. 74, p. 136–143, 1 jan. 2015.

KIRCHSTETTER, T. W. et al. On-road measurement of fine particle and nitrogen oxide emissions from light- and heavy-duty motor vehicles. **Atmospheric Environment**, v. 33, n. 18, p. 2955–2968, 1 ago. 1999.

KO, S. et al. NOx Emissions from Euro 5 and Euro 6 Heavy-Duty Diesel Vehicles under Real Driving Conditions. **Energies 2020, Vol. 13, Page 218**, v. 13, n. 1, p. 218, 2 jan. 2020.

KOFFLER, C.; ROHDE-BRANDENBURGER, K. On the calculation of fuel savings through lightweight design in automotive life cycle assessments. **International Journal of Life Cycle Assessment**, v. 15, n. 1, p. 128–135, 24 out. 2010.

KOJIMA, Y. et al. Influence of secondary formation on atmospheric occurrences of oxygenated polycyclic aromatic hydrocarbons in airborne particles. **Atmospheric Environment**, v. 44, n. 24, p. 2873–2880, ago. 2010.

KONG, S. et al. Receptor modeling of PM2.5, PM10 and TSP in

different seasons and long-range transport analysis at a coastal site of Tianjin, China. **The Science of the total environment**, v. 408, n. 20, p. 4681–4694, set. 2010.

KONG, S. et al. Ion chemistry for atmospheric size-segregated aerosol and depositions at an offshore site of Yangtze River Delta region, China. **Atmospheric Research**, v. 147–148, p. 205–226, 1 out. 2014.

KOPETZ, H. Internet of Things. **Real-Time Systems**, p. 307–323, 2011.

KRECL, P. et al. Long-term trends of black carbon and particle number concentrations and their vehicle emission factors in Stockholm. **Environmental Pollution**, v. 347, p. 123734, 15 abr. 2024.

KRISTENSSON, A. et al. Real-world traffic emission factors of gases and particles measured in a road tunnel in Stockholm, Sweden. **Atmospheric Environment**, v. 38, n. 5, p. 657–673, 1 fev. 2004.

LARSEN, R.; SCHANTZ, M.; WISE, S. Determination of Levoglucosan in Particulate Matter Reference Materials. **http://dx.doi.org/10.1080/02786820600596909**, v. 40, n. 10, p. 781–787, 1 out. 2007.

LATIF, M. T.; OTHMAN, M.; HASSAN, H. Composition of rainwater and influences over different regions of the world. **Precipitation: Earth Surface Responses and Processes**, p. 69–83, 1 jan. 2021.

LAWAL, A. T. Polycyclic aromatic hydrocarbons. A review. **Cogent Environmental Science**, v. 3, n. 1, 2017.

LEITHEAD, A. et al. Levoglucosan and dehydroabietic acid: Evidence of biomass burning impact on aerosols in the Lower Fraser Valley. **Atmospheric Environment**, v. 40, n. 15, p. 2721–2734, 1 maio 2006.

LENZI, E.; FAVERO, L. B. **Introdução à Química da Atmosfera: Ciência, Vida e Sobrevivência | Grupo GEN**. 2. ed. Rio de Janeiro: LTC, 2019.

LI, C. et al. Evaluation of On-Board Sensor-Based NOx Emissions from the Heavy-Duty Vehicles in an Inspection and Maintenance Program. **Emission Control Science and Technology**, v. 9, n. 1, p. 12–24, 1 mar. 2023.

LI, J. et al. Individual aerosol particles from biomass burning in southern Africa: 2. Compositions and aging of inorganic particles. **Journal of Geophysical Research: Atmospheres**, v. 108, n. 13, p. SAF 20-1-SAF 20-12, 2003.

LI, J. et al. Comparison of abundances, compositions and sources of elements, inorganic ions and organic compounds in atmospheric aerosols from Xi'an and New Delhi, two megacities in China and India. **Science of The Total Environment**, v. 476–477, p. 485–495, 1 abr. 2014.

LI, J. et al. Scattering and absorbing aerosols in the climate system. **Nature Reviews Earth & Environment 2022 3:6**, v. 3, n. 6, p. 363–379, 24 maio 2022a.

LI, Q. et al. Biomass burning source identification through molecular markers in cryoconites over the Tibetan Plateau. **Environmental Pollution**, v. 244, p. 209–217, 1 jan. 2019a.

LI, R. et al. Differences in oxidative potential of black carbon from three combustion emission sources in China. **Journal of Environmental Management**, v. 240, p. 57–65, 15 jun. 2019b.

LI, W. et al. Concentrations and origins of nitro-polycyclic aromatic hydrocarbons and oxy-polycyclic aromatic hydrocarbons in ambient air in urban and rural areas in northern China. **Environmental Pollution**, v. 197, p. 156–164, 1 fev. 2015.

LI, Y. et al. The transition from a nitrogen oxides-limited regime to a

volatile organic compounds-limited regime in the petrochemical industrialized Lanzhou City, China. **Atmospheric Research**, v. 269, p. 106035, 1 maio 2022b.

LIMA, M. A. et al. Emission of Air Pollution in the Transport Sector: Case Study of the City of Campos dos Goytacazes, Brazil. **Engineering**, v. 12, n. 12, p. 851–862, 9 dez. 2020.

LIU, B. et al. Temporal variability of mercury speciation in urban air. **Atmospheric Environment**, v. 41, p. 1911–1923, 2007.

LIU, B.; ZIMMERMAN, N. Fleet-based vehicle emission factors using low-cost sensors: Case study in parking garages. **Transportation Research Part D: Transport and Environment**, v. 91, p. 102635, 1 fev. 2021.

LIU, D. et al. Concentration, source identification, and exposure risk assessment of PM2.5-bound parent PAHs and nitro-PAHs in atmosphere from typical Chinese cities. **Scientific Reports**, v. 7, n. 1, p. 10398, 1 dez. 2017.

LIU, L. Y. et al. Anthropogenic activities have contributed moderately to increased inputs of organic materials in marginal seas off China. **Environmental Science and Technology**, v. 47, n. 20, p. 11414–11422,

15 out. 2013.

LIU, T.; CHAN, A. W. H.; ABBATT, J. P. D. Multiphase Oxidation of Sulfur Dioxide in Aerosol Particles: Implications for Sulfate Formation in Polluted Environments. **Environmental Science and Technology**, v. 55, n. 8, p. 4227–4242, 20 abr. 2021.

LIU, Y. et al. Diverse response of surface ozone to COVID-19 lockdown in China. **Science of The Total Environment**, v. 789, p. 147739, 1 out. 2021.

LÖNDAHL, J. et al. Size-resolved respiratory-tract deposition of fine and ultrafine hydrophobic and hygroscopic aerosol particles during rest and exercise. **Inhalation toxicology**, v. 19, n. 2, p. 109–116, 15 jan. 2007.

LONG, C. M.; NASCARELLA, M. A.; VALBERG, P. A. Carbon black vs. black carbon and other airborne materials containing elemental carbon: Physical and chemical distinctions. **Environmental Pollution**, v. 181, p. 271–286, 1 out. 2013.

LOPES, T. F. A. et al. Estimativa das emissões veiculares na região metropolitana de Fortaleza, CE, ano-base 2010. p. 1013–1025, 2018.

MACHADO, C. M. D.; CARDOSO, A. A.; ALLEN, A. G. Atmospheric

Emission of Reactive Nitrogen during Biofuel Ethanol Production. **Environmental Science and Technology**, v. 42, n. 2, p. 381–385, 15 jan. 2007.

MACIEJCZYK, P.; CHEN, L. C.; THURSTON, G. The Role of Fossil Fuel Combustion Metals in PM2.5 Air Pollution Health Associations. **Atmosphere 2021, Vol. 12, Page 1086**, v. 12, n. 9, p. 1086, 24 ago. 2021.

MAILLER, S.; KHVOROSTYANOV, D.; MENUT, L. Impact of the vertical emission profiles on background gas-phase pollution simulated from the EMEP emissions over Europe. **Atmospheric Chemistry and Physics**, v. 13, n. 12, p. 5987–5998, 2013.

MAKKONEN, U. et al. Size distribution and chemical composition of airborne particles in south-eastern Finland during different seasons and wildfire episodes in 2006. **Science of The Total Environment**, v. 408, n. 3, p. 644–651, 1 jan. 2010.

MANISALIDIS, I. et al. Environmental and Health Impacts of Air Pollution: A Review. **Frontiers in Public Health**, v. 8, p. 14, 20 fev. 2020.

MARINO, C. et al. Analysis of the Reduction of Pollutant Emissions by the Vehicle Fleet of the City of Reggio Calabria Due to the Introduction of Ecological Vehicles. **Sustainability 2020, Vol. 12, Page 2877**, v. 12, n.

7, p. 2877, 4 abr. 2020.

MARQUES, L. F. C. S. et al. Particle-associated polycyclic aromatic hydrocarbons in a suburban region of Rio de Janeiro, Brazil, with industrial and traffic emissions. **Journal of the Brazilian Chemical Society**, v. 20, n. 3, p. 518–529, 2009.

MARTELLINI, T. et al. One year intensive PM2.5 bound polycyclic aromatic hydrocarbons monitoring in the area of Tuscany, Italy. Concentrations, source understanding and implications. **Environmental Pollution**, v. 164, p. 252–258, 1 maio 2012.

MARTINS, E. M. et al. Concentrações de poluentes atmosféricos no Rio de Janeiro em relação a normas nacionais e internacionais. **Revista Internacional de Ciências**, v. 7, n. 1, p. 32–48, 18 jul. 2017.

MARYNOWSKI, L.; SIMONEIT, B. R. T. Saccharides in atmospheric particulate and sedimentary organic matter: Status overview and future perspectives. **Chemosphere**, v. 288, p. 132376, 1 fev. 2022.

MATEUS, V. L. et al. Study of the chemical composition of particulate matter from the Rio de Janeiro metropolitan region, Brazil, by inductively coupled plasma-mass spectrometry and optical emission spectrometry. **Spectrochimica Acta Part B: Atomic Spectroscopy**, v. 86, p. 131–136,

1 ago. 2013.

MATEUS, V. L. et al. Assessment of ambient aerosol sources in two important Atlantic Rain Forest hotspots in the surroundings of a megacity. **Urban Forestry & Urban Greening**, v. 56, p. 126858, 1 dez. 2020.

MATEUS, V. L.; GIODA, A. A candidate framework for PM2.5 source identification in highly industrialized urban-coastal areas. **Atmospheric Environment**, v. 164, p. 147–164, 1 set. 2017.

MAZUREK, M. A.; CASS, G. R.; SIMONEIT, B. R. T. Interpretation of high-resolution gas chromatography and high-resolution gas chromatography/mass spectrometry data acquired from atmospheric organic aerosol samples. **Aerosol Science and Technology**, v. 10, n. 2, p. 408–420, 1989.

MCCAFFERY, C. et al. Real-world NOx emissions from heavy-duty diesel, natural gas, and diesel hybrid electric vehicles of different vocations on California roadways. **The Science of the total environment**, v. 784, 25 ago. 2021.

MCDONALD, J. D. et al. Fine particle and gaseous emission rates from residential wood combustion. **Environmental Science and Technology**, v. 34, n. 11, p. 2080–2091, 1 jun. 2000.

MCINNES, L. M. et al. Gravimetric analysis, ionic composition, and associated water mass of the marine aerosol. **Atmospheric Environment**, v. 30, n. 6, p. 869–884, 1 mar. 1996.

MCMURRY, P. H. A review of atmospheric aerosol measurements. **Atmospheric Environment**, v. 34, n. 12–14, p. 1959–1999, 1 jan. 2000.

MCT. **Estimativas Anuais De Emissões De Gases De Efeito Estufa**. Brasil: [s.n.]. Disponível em: <https://www.gov.br/mcti/pt-br/acompanhe-o-mcti/sirene/publicacoes/estimativas-anuais-de-emissoes-gee>. Acesso em: 1 fev. 2025.

MEDEIROS, P. M.; SIMONEIT, B. R. T. Source profiles of organic compounds emitted upon combustion of green vegetation from temperate climate forests. **Environmental Science and Technology**, v. 42, n. 22, p. 8310–8316, 15 nov. 2008.

MENDES, D. et al. Impact of the Petrochemical Complex on the Air Quality of an Urban Area in the City of Rio de Janeiro, Brazil. **Bulletin of Environmental Contamination and Toxicology**, v. 104, n. 4, p. 438–443, 1 abr. 2020.

MENDOZA-VILLAFUERTE, P. et al. NOx, NH3, N2O and PN real

driving emissions from a Euro VI heavy-duty vehicle. Impact of regulatory on-road test conditions on emissions. **Science of The Total Environment**, v. 609, p. 546–555, 31 dez. 2017.

MENG, X. et al. Seasonal Characteristics and Particle-size Distributions of Particulate Air Pollutants in Urumqi. **International Journal of Environmental Research and Public Health 2019, Vol. 16, Page 396**, v. 16, n. 3, p. 396, 31 jan. 2019.

MICHOUD, V. et al. Radical budget analysis in a suburban European site during the MEGAPOLI summer field campaign. **Atmospheric Chemistry and Physics**, v. 12, n. 24, p. 11951–11974, 2012.

MILLER, J. et al. **COST-BENEFIT ANALYSIS OF BRAZIL'S HEAVY-DUTY EMISSION STANDARDS (P-8)**. Disponível em: <www.theicct.org>. Acesso em: 21 jun. 2023.

MILLER, T. L. et al. Characteristics and Emissions of Heavy-Duty Vehicles in Tennessee Under the MOBILES Model. **https://doi.org/10.3141/1842-12**, n. 1842, p. 99–108, 1 jan. 2003.

MINERO, C. et al. An overview of possible processes able to account for the occurrence of nitro-PAHs in Antarctic particulate matter. **Microchemical Journal**, v. 96, n. 2, p. 213–217, 1 nov. 2010.

MINISTÉRIO DE MINAS E ENERGIA. **Balanço Energético Nacional – Relatório Final – Ano base: 2021**. Disponível em: <https://www.epe.gov.br/pt/publicacoes-dados-abertos/publicacoes/balanco-energetico-nacional-2022>. Acesso em: 26 mar. 2023.

MLAWER, E. J. et al. Radiative transfer for inhomogeneous atmospheres: RRTM, a validated correlated-k model for the longwave. **Journal of Geophysical Research: Atmospheres**, v. 102, n. D14, p. 16663–16682, 27 jul. 1997.

MONAWAR, T.; BIN MAHMUD, S.; HIRA, A. Anti-theft vehicle tracking and regaining system with automatic police notifying using Haversine formula. **4th International Conference on Advances in Electrical Engineering, ICAEE 2017**, v. 2018- January, p. 775–779, 1 jul. 2017.

MONKS, P. S. et al. Tropospheric ozone and its precursors from the urban to the global scale from air quality to short-lived climate forcer. **Atmospheric Chemistry and Physics**, v. 15, n. 15, p. 8889–8973, 13 ago. 2015.

MONOD, A.; CARLIER, P. Impact of clouds on the tropospheric

ozone budget: Direct effect of multiphase photochemistry of soluble organic compounds. **Atmospheric Environment**, v. 33, n. 27, p. 4431–4446, 1 nov. 1999.

MOSTERT, M. M. R.; AYOKO, G. A.; KOKOT, S. Application of chemometrics to analysis of soil pollutants. **TrAC Trends in Analytical Chemistry**, v. 29, n. 5, p. 430–445, 1 maio 2010.

NATIONAL CENTER FOR ATMOSPHERIC RESEARCH. **WRF-Chem | Atmospheric Chemistry Observations & Modeling**. Disponível em: <https://www2.acom.ucar.edu/wrf-chem>. Acesso em: 22 ago. 2024.

NING, Z.; WUBULIHAIREN, M.; YANG, F. PM, NOx and butane emissions from on-road vehicle fleets in Hong Kong and their implications on emission control policy. **Atmospheric Environment**, v. 61, p. 265–274, 1 dez. 2012.

NOAA, (NATIONAL OCEANIC AND ATMOSPHERIC ADMINISTRATION). **HYSPLIT**. Disponível em: <https://www.ready.noaa.gov/HYSPLIT.php>.

NOGUEIRA COSTA, A. et al. Preliminary geological-geotechnical mapping, using geoprocessing thecniques, in the Campos dos Goytacazes county, Rio de Janeiro State. **Anuário do Instituto de Geociências**, v. 31,

n. 1, p. 50–64, 1 jan. 2008.

NOLTE, C. G. et al. Highly Polar Organic Compounds Present in Wood Smoke and in the Ambient Atmosphere. **Environmental Science and Technology**, v. 35, n. 10, p. 1912–1919, 15 maio 2001.

OLIVEIRA, R. L. et al. PM2.5-bound polycyclic aromatic hydrocarbons in an area of Rio de Janeiro, Brazil impacted by emissions of light-duty vehicles fueled by ethanol-blended gasoline. **Bulletin of Environmental Contamination and Toxicology**, v. 93, n. 6, p. 781–786, 1 dez. 2014.

OLIVEIRA, R. L. et al. Polycyclic aromatic hydrocarbon patterns in the city of Rio de Janeiro. **Air Quality, Atmosphere and Health**, v. 11, n. 5, p. 581–590, 28 mar. 2018.

OMAR, N. Y. M. J. et al. Levels and distributions of organic source tracers in air and roadside dust particles of Kuala Lumpur, Malaysia. **Environmental Geology**, v. 52, n. 8, p. 1485–1500, 20 ago. 2007.

PAIM, J. N. et al. Emissions of PAHs, Nitro-PAHs and Quinones (Oxy-PAHs) Associated to PM1.0 and PM2.5 Emitted by a Diesel Engine Fueled with Diesel-Biodiesel-Ethanol Blends. **Atmosphere 2023, Vol. 14, Page 656**, v. 14, n. 4, p. 656, 31 mar. 2023.

PARDO, L. H. et al. Effects of nitrogen deposition and empirical nitrogen critical loads for ecoregions of the United States. **Ecological Applications**, v. 21, n. 8, p. 3049–3082, 1 dez. 2011.

PARK, J.; SEO, J.; PARK, S. Development of vehicle emission rates based on vehicle-specific power and velocity. **Science of The Total Environment**, v. 857, p. 159622, 20 jan. 2023.

PARRISH, D. D. et al. Air quality improvement in Los Angeles—perspectives for developing cities. **Frontiers of Environmental Science and Engineering**, v. 10, n. 5, p. 1–13, 1 out. 2016.

PAVITHRA, K. G. et al. Mercury sources, contaminations, mercury cycle, detection and treatment techniques: A review. **Chemosphere**, v. 312, p. 137314, 1 jan. 2023.

PEREIRA, G. M. et al. Particulate pollutants in the Brazilian city of São Paulo: 1-year investigation for the chemical composition and source apportionment. **Atmos. Chem. Phys**, v. 17, p. 11943–11969, 2017.

PEREIRA, G. M. et al. Particulate matter fingerprints in biofuel impacted tunnels in South America's largest metropolitan area. **Science of The Total Environment**, v. 856, p. 159006, 15 jan. 2023.

PEREIRA NETTO, A. D. et al. PAHs in diurnal and nocturnal samples of total suspended particulate in a highly trafficked area of Rio de Janeiro City, Brazil. **Bulletin of Environmental Contamination and Toxicology**, v. 75, n. 5, p. 1004–1011, nov. 2005.

PHOUSONGPHOUANG, P. T.; AREY, J. Sources of the atmospheric contaminants, 2-nitrobenzanthrone and 3-nitrobenzanthrone. **Atmospheric Environment**, v. 37, n. 23, p. 3189–3199, 1 jul. 2003.

PILUSA, T. J.; MOLLAGEE, M. M.; MUZENDA, E. Reduction of Vehicle Exhaust Emissions from Diesel Engines Using the Whale Concept Filter. **Aerosol and Air Quality Research**, v. 12, n. 5, p. 994–1006, out. 2012.

PIRRONE, N.; GLINSORN, G.; KEELER, G. J. Ambient levels and dry deposition fluxes of mercury to Lakes Huron, Erie and St. Clair. **Water, Air, & Soil Pollution**, v. 80, n. 1–4, p. 179–188, fev. 1995.

PREFEITURA DO RIO DE JANEIRO. **MonitorAr Rio - Qualidade do Ar na Cidade do Rio de Janeiro: Relatório da Rede MonitorAr-Rio 2011-2012**. Rio de Janeiro: [s.n.]. Disponível em: <https://www.rio.rj.gov.br/documents/91265/3252594/Relatorio+Monitorar++2011-2012.pdf>. Acesso em: 20 ago. 2024.

QUIJANO, M. F. C. et al. Exploratory and comparative analysis of the morphology and chemical composition of PM 2.5 from regions with different socioeconomic characteristics. **Microchemical Journal**, v. 147, p. 507–515, 1 jun. 2019.

RAMDAHL, T. Retene—a molecular marker of wood combustion in ambient air. **Nature 1983 306:5943**, v. 306, n. 5943, p. 580–582, 1983.

RAMOS DE RAINHO, C. et al. Genotoxicity of Polycyclic Aromatic Hydrocarbons and Nitro-Derived in Respirable Airborne Particulate Matter Collected from Urban Areas of Rio de Janeiro (Brazil). **BioMed Research International**, v. 2013, n. 1, p. 765352, 1 jan. 2013.

RAVINA, M. et al. Air quality and photochemical reactions: analysis of NOx and NO2 concentrations in the urban area of Turin, Italy. **Air Quality, Atmosphere and Health**, v. 15, n. 3, p. 541–558, 1 mar. 2022.

RAVINDRA, K.; SOKHI, R.; VAN GRIEKEN, R. Atmospheric polycyclic aromatic hydrocarbons: Source attribution, emission factors and regulation. **Atmospheric Environment**, v. 42, n. 13, p. 2895–2921, 1 abr. 2008.

READMAN, J. W. et al. Petroleum and PAH contamination of the

Black Sea. **Marine pollution bulletin**, v. 44, n. 1, p. 48–62, 2002.

RECHE, C. et al. Biomass burning contributions to urban aerosols in a coastal Mediterranean City. **Science of The Total Environment**, v. 427–428, p. 175–190, 15 jun. 2012.

REISEN, F.; AREY, J. Atmospheric Reactions Influence Seasonal PAH and Nitro-PAH Concentrations in the Los Angeles Basin. **Environmental Science and Technology**, v. 39, n. 1, p. 64–73, 1 jan. 2004.

REŞITOĞLU, İ. A.; ALTINIŞIK, K.; KESKIN, A. The pollutant emissions from diesel-engine vehicles and exhaust aftertreatment systems. **Clean Technologies and Environmental Policy**, v. 17, n. 1, p. 15–27, 11 jan. 2015.

RIBEIRO, I. O. et al. Impact of biomass burning on a metropolitan area in the Amazon during the 2015 El Niño: The enhancement of carbon monoxide and levoglucosan concentrations. **Environmental Pollution**, v. 260, p. 114029, 1 maio 2020.

RIDDLE, S. G. et al. Large PAHs detected in fine particulate matter emitted from light-duty gasoline vehicles. **Atmospheric Environment**, v. 41, n. 38, p. 8658–8668, 1 dez. 2007.

RINGUET, J. et al. Particle size distribution of nitrated and oxygenated polycyclic aromatic hydrocarbons (NPAHs and OPAHs) on traffic and suburban sites of a European megacity: Paris (France). **Atmospheric Chemistry and Physics**, v. 12, n. 18, p. 8877–8887, 2012.

ROCHA MARTINS, C.; BITTENCOURT DE ANDRADE, J. QUÍMICA ATMOSFÉRICA DO ENXOFRE (IV): EMISSÕES, REAÇÕES EM FASE AQUOSA E IMPACTO AMBIENTAL. **Quim. Nova**, v. 25, n. 2, p. 259–272, 2002.

ROGGE, W. F. et al. Sources of Fine Organic Aerosol. 2. Noncatalyst and Catalyst-Equipped Automobiles and Heavy-Duty Diesel Trucks. **Environmental Science and Technology**, v. 27, n. 4, p. 636–651, 1993a.

ROGGE, W. F. et al. Sources of Fine Organic Aerosol. 3. Road Dust, Tire Debris, and Organometallic Brake Lining Dust: Roads as Sources and Sinks. **Environmental Science and Technology**, v. 27, n. 9, p. 1892–1904, 1993b.

ROGGE, W. F. et al. Sources of Fine Organic Aerosol. 4. Particulate Abrasion Products from Leaf Surfaces of Urban Plants. **Environmental Science and Technology**, v. 27, n. 13, p. 2700–2711, 1993c.

ROULET, M. et al. Spatio-temporal geochemistry of mercury in waters of the Tapajós and Amazon rivers, Brazil. **Limnology and Oceanography**, v. 46, n. 5, p. 1141–1157, 1 jul. 2001.

SANDBHOR, S.; CHAPHALKAR, N. B. Impact of Outlier Detection on Neural Networks Based Property Value Prediction. **Advances in Intelligent Systems and Computing**, v. 862, p. 481–495, 2019.

SANTA-HELENA, E. et al. From air to heart: Particle pollution (PM2.5) and induced injury on cardioblast cells. **Atmospheric Pollution Research**, v. 12, n. 4, p. 152–159, 1 abr. 2021.

SANTANA, E. et al. Padrões de qualidade do ar Experiência comparada Brasil, EUA e União Europeia. 2012.

SANTOS, A. C. A. et al. ANÁLISE DA CONCENTRAÇÃO E COMPOSIÇÃO DE AEROSSÓIS DE QUEIMADAS NO PANTANAL MATO-GROSSO. **Química Nova**, v. 39, n. 8, p. 919–924, 1 set. 2016a.

SANTOS, A. G. et al. A simple, comprehensive, and miniaturized solvent extraction method for determination of particulate-phase polycyclic aromatic compounds in air. **Journal of Chromatography A**, v. 1435, p. 6–17, 26 fev. 2016b.

SANTOS, A. G.; DA ROCHA, G. O.; DE ANDRADE, J. B. Occurrence of the potent mutagens 2- nitrobenzanthrone and 3-nitrobenzanthrone in fine airborne particles. **Scientific Reports 2019 9:1**, v. 9, n. 1, p. 1–13, 9 jan. 2019.

SCARAMBONI, C. et al. Particulate matter from a tropical city in southeast Brazil: Impact of biomass burning on polycyclic aromatic compounds levels, health risks, and in vitro toxicity. **Chemosphere**, v. 350, p. 141072, 1 fev. 2024.

SCHAUER, J. J. et al. Measurement of Emissions from Air Pollution Sources. 3. C1−C29 Organic Compounds from Fireplace Combustion of Wood. **Environmental Science and Technology**, v. 35, n. 9, p. 1716–1728, 1 maio 2001.

SEARES, A. L. F. et al. Optimization of operational ICP OES parameters and application to PM10 monitoring associated to sugarcane burning. **Microchemical Journal**, v. 163, p. 105917, 1 abr. 2021.

SEINFELD, J. H.; PANDIS, S. N. **Atmospheric Chemistry and Physics: From Air Pollution to Climate Change**. [s.l: s.n.].

SERAFEIM, E. et al. Oxidative potential of ambient PM2.5 from São Paulo, Brazil: Variations, associations with chemical components and

source apportionment. **Atmospheric Environment**, v. 298, p. 119593, 1 abr. 2023.

SEROA DA MOTTA, R. et al. **CLIMATE CHANGE IN BRAZIL**. Brasília: IPEA, 2011.

SERRENHO, A. C.; NORMAN, J. B.; ALLWOOD, J. M. The impact of reducing car weight on global emissions: the future fleet in Great Britain. **Philosophical transactions. Series A, Mathematical, physical, and engineering sciences**, v. 375, n. 2095, p. 20160364, 13 jun. 2017.

SHAH, S. D. et al. Emission rates of regulated pollutants from on-road heavy-duty diesel vehicles. **Atmospheric Environment**, v. 40, n. 1, p. 147–153, 1 jan. 2006.

SHALTOUT, A. A. et al. Method development for the determination of Cd, Cu, Ni and Pb in PM2.5 particles sampled in industrial and urban areas of Greater Cairo, Egypt, using high-resolution continuum source graphite furnace atomic absorption spectrometry. **Microchemical Journal**, v. 113, p. 4–9, 1 mar. 2014.

SHEN, G. et al. Retene emission from residential solid fuels in China and evaluation of retene as a unique marker for soft wood combustion. **Environmental Science and Technology**, v. 46, n. 8, p. 4666–4672, 17

abr. 2012.

SILVA, L. F. M. DA et al. Characterization of mercury in atmospheric particulate matter in the state of Rio de Janeiro, Brazil. **Environmental Science: Atmospheres**, v. 4, n. 8, p. 872–878, 8 ago. 2024a.

SILVA JUNIOR, C. R. et al. Black Carbon Associated to PM 1.0 and PM 2.5 : Mass Variation due to Combustion of Biodiesel/Diesel Blends (B5, B6, B7 and B8). **Article J. Braz. Chem. Soc**, v. 30, n. 4, p. 786–792, 2019.

SILVA, L. F. M. et al. Real-Time Monitoring of Nitrogen Oxides Emission Factors Using Sensors in the Exhaust Pipes of Heavy Vehicles in the Metropolitan Region of Rio de Janeiro. **Article J. Braz. Chem. Soc**, v. 35, p. 1–7, 2024b.

SIMONEIT, B. R. T. Organic matter of the troposphere—III. Characterization and sources of petroleum and pyrogenic residues in aerosols over the western united states. **Atmospheric Environment (1967)**, v. 18, n. 1, p. 51–67, 1 jan. 1984.

SIMONEIT, B. R. T. Application of Molecular Marker Analysis to Vehicular Exhaust for Source Reconciliations. **International Journal of Environmental Analytical Chemistry**, v. 22, n. 3–4, p. 203–232, 1 out. 1985.

SIMONEIT, B. R. T. Organic matter of the troposphere - V: Application of molecular marker analysis to biogenic emissions into the troposphere for source reconciliations. **Journal of Atmospheric Chemistry**, v. 8, n. 3, p. 251–275, abr. 1989.

SIMONEIT, B. R. T. et al. Levoglucosan, a tracer for cellulose in biomass burning and atmospheric particles. **Atmospheric Environment**, v. 33, n. 2, p. 173–182, 1 jan. 1999.

SIMONEIT, B. R. T. et al. Composition and major sources of organic compounds of aerosol particulate matter sampled during the ACE-Asia campaign. **Journal of Geophysical Research: Atmospheres**, v. 109, n. D19, 16 out. 2004.

SLEZAKOVA, K. et al. Air pollution from traffic emissions in Oporto, Portugal: Health and environmental implications. **Microchemical Journal**, v. 99, n. 1, p. 51–59, 1 set. 2011.

SOFWAN, N. M.; LATIF, M. T. Characteristics of the real-driving emissions from gasoline passenger vehicles in the Kuala Lumpur urban environment. **Atmospheric Pollution Research**, v. 12, n. 1, p. 306–315, 1 jan. 2021.

SOKHI, R. S. et al. A global observational analysis to understand changes in air quality during exceptionally low anthropogenic emission conditions. **Environment International**, v. 157, p. 106818, 1 dez. 2021.

SOLA, M. C. R. et al. Occurrence of mercury in polychaete species (Annelida) and their associated sediments from an important Southern Atlantic Ocean Bay. **Science of The Total Environment**, v. 851, p. 157965, 10 dez. 2022a.

SOLA, M. C. R. et al. Occurrence of mercury in polychaete species (Annelida) and their associated sediments from an important Southern Atlantic Ocean Bay. **Science of The Total Environment**, v. 851, p. 157965, 10 dez. 2022b.

SOLURI, D. S. et al. Multi-site PM2.5 and PM2.5-10 aerosol source apportionment in Rio de Janeiro, Brazil. **Journal of the Brazilian Chemical Society**, v. 18, n. 4, p. 838–845, 2007.

SONKE, J. E. et al. Global change effects on biogeochemical mercury cycling. **Ambio 2023 52:5**, v. 52, n. 5, p. 853–876, 29 mar. 2023.

SOUZA, D. Z. et al. Composition of PM2.5 and PM10 Collected at Urban Sites in Brazil. **Aerosol and Air Quality Research**, v. 14, n. 1, p. 168–176, fev. 2014a.

SOUZA, K. F. et al. Diurnal and nocturnal measurements of PAH, nitro-PAH, and oxy-PAH compounds in atmospheric particulate matter of a sugar cane burning region. **Atmospheric Environment**, v. 83, p. 193–201, 1 fev. 2014b.

STRANDBERG, B. et al. Particulate-Bound Polycyclic Aromatic Hydrocarbons (PAHs) and their Nitro- and Oxy-Derivative Compounds Collected Inside and Outside Occupied Homes in Southern Sweden. **Polycyclic Aromatic Compounds**, v. 43, n. 8, p. 7399–7415, 2023.

SUN, L. et al. Mercury concentration and isotopic composition on different atmospheric particles (PM10 and PM2.5) in the subtropical coastal suburb of Xiamen Bay, Southern China. **Atmospheric Environment**, v. 261, p. 118604, 15 set. 2021.

TANG, J. et al. Assessing the Impact of Vehicle Speed Limits and Fleet Composition on Air Quality Near a School. **International Journal of Environmental Research and Public Health 2019, Vol. 16, Page 149**, v. 16, n. 1, p. 149, 8 jan. 2019.

TAVELLA, R. A. et al. A New Dawn for Air Quality in Brazil. **The Lancet Planetary Health**, v. 8, n. 10, p. e717–e718, 1 out. 2024.

TCHOUNWOU, P. B. et al. Heavy Metals Toxicity and the Environment. **EXS**, v. 101, p. 133, 2012.

TEGEN, I. et al. Contribution of different aerosol species to the global aerosol extinction optical thickness: Estimates from model results. **Journal of Geophysical Research: Atmospheres**, v. 102, n. D20, p. 23895–23915, 27 out. 1997.

TEIXEIRA, E. C. et al. Study of nitro-polycyclic aromatic hydrocarbons in fine and coarse atmospheric particles. **Atmospheric Research**, v. 101, n. 3, p. 631–639, 1 ago. 2011.

TEN HAVEN, H. L. et al. Pristane/phytane ratio as environmental indicator. **Nature 1988 333:6174**, v. 333, n. 6174, p. 604–604, 1988.

THOMPSON, G.; EIDHAMMER, T. A Study of Aerosol Impacts on Clouds and Precipitation Development in a Large Winter Cyclone. **Journal of the Atmospheric Sciences**, v. 71, n. 10, p. 3636–3658, 1 out. 2014.

TOBISZEWSKI, M.; NAMIEŚNIK, J. PAH diagnostic ratios for the identification of pollution emission sources. **Environmental Pollution**, v. 162, p. 110–119, 1 mar. 2012.

URBAN, R. C. et al. Use of levoglucosan, potassium, and water-

soluble organic carbon to characterize the origins of biomass-burning aerosols. **Atmospheric Environment**, v. 61, p. 562–569, 1 dez. 2012.

US EPA. **Health Topics | US EPA**. Disponível em: <https://www.epa.gov/environmental-topics/health-topics>. Acesso em: 23 mar. 2023a.

US EPA. **NAAQS Table | US EPA**. Disponível em: <https://www.epa.gov/criteria-air-pollutants/naaqs-table>. Acesso em: 23 mar. 2023.

US EPA, U. S. E. P. A. **What is Particle Pollution?** Disponível em: <https://www.epa.gov/pmcourse/what-particle-pollution>. Acesso em: 8 jan. 2023b.

VASCONCELLOS, P. C. et al. Determination of anthropogenic and biogenic compounds on atmospheric aerosol collected in urban, biomass burning and forest areas in São Paulo, Brazil. **Science of The Total Environment**, v. 408, n. 23, p. 5836–5844, 1 nov. 2010.

VASCONCELLOS, P. C. et al. Seasonal variation of n-alkanes and polycyclic aromatic hydrocarbon concentrations in PM10 samples collected at urban sites of São Paulo State, Brazil. **Water, Air, and Soil Pollution**, v. 222, n. 1–4, p. 325–336, 21 nov. 2011.

VENTURA, L. M. B. et al. Evaluation of air quality in a megacity using statistics tools. **Meteorology and Atmospheric Physics**, v. 130, n. 3, p. 361–370, 1 jun. 2018.

VENTURA, L. M. B. et al. Monitoring of air quality before the Olympic Games Rio 2016. **Anais da Academia Brasileira de Ciências**, v. 91, n. 1, p. e20170984, 21 mar. 2019.

VERGEL-ORTEGA, M.; VALENCIA-OCHOA, G.; DUARTE-FORERO, J. Experimental study of emissions in single-cylinder diesel engine operating with diesel-biodiesel blends of palm oil-sunflower oil and ethanol. **Case Studies in Thermal Engineering**, v. 26, p. 101190, 1 ago. 2021.

VERONESI, A. et al. Use of carboxyhemoglobin as a biomarker of environmental CO exposure: critical evaluation of the literature. **Environmental science and pollution research international**, v. 24, n. 33, p. 25798–25809, 1 nov. 2017.

VIEIRA, H. G. et al. AVALIAÇÃO DE COMPOSTOS ORGÂNICOS VOLÁTEIS AROMÁTICOS NA ATMOSFERA EM CAMPOS DOS GOYTACAZES E ITAPERUNA APLICANDO A ANÁLISE MULTIVARIADA DE DADOS. **Quim. Nova**, v. 46, n. 1, p. 29–38, 2023.

VIONE, D. et al. Photochemical reactions in the tropospheric aqueous phase and on particulate matter. **Chemical Society Reviews**, v. 35, n. 5, p. 441–453, 24 abr. 2006.

WALGRAEVE, C. et al. Oxygenated polycyclic aromatic hydrocarbons in atmospheric particulate matter: Molecular characterization and occurrence. **Atmospheric Environment**, v. 44, n. 15, p. 1831–1846, 1 maio 2010.

WANG, J. et al. Characteristics and major sources of carbonaceous aerosols in PM2.5 from Sanya, China. **Science of The Total Environment**, v. 530–531, p. 110–119, 15 out. 2015.

WANG, J. et al. Impact analysis of meteorological variables on PM2.5 pollution in the most polluted cities in China. **Heliyon**, v. 9, n. 7, p. e17609, 1 jul. 2023a.

WANG, J. et al. Impact analysis of meteorological variables on PM2.5 pollution in the most polluted cities in China. **Heliyon**, v. 9, n. 7, p. e17609, 1 jul. 2023b.

WANG, L.; ATKINSON, R.; AREY, J. Formation of 9,10-phenanthrenequinone by atmospheric gas-phase reactions of

phenanthrene. **Atmospheric Environment**, v. 41, n. 10, p. 2025–2035, 1 mar. 2007.

WANG, W. et al. Concentration and photochemistry of PAHs, NPAHs, and OPAHs and toxicity of PM 2.5 during the beijing olympic games. **Environmental Science and Technology**, v. 45, n. 16, p. 6887–6895, 15 ago. 2011.

WANG, Y. et al. The ion chemistry, seasonal cycle, and sources of PM2.5 and TSP aerosol in Shanghai. **Atmospheric Environment**, v. 40, n. 16, p. 2935–2952, 1 maio 2006.

WANG, Y. et al. Sulfate-nitrate-ammonium aerosols over China: Response to 2000-2015 emission changes of sulfur dioxide, nitrogen oxides, and ammonia. **Atmospheric Chemistry and Physics**, v. 13, n. 5, p. 2635–2652, 2013.

WANG, Z. et al. Modeling and analysis of pumping cell of NOx sensor – Part Ⅰ: Main oxygen pumping cell. **Sensors and Actuators B: Chemical**, v. 359, p. 131622, 15 maio 2022a.

WANG, Z. et al. Modeling and analysis of pumping cell of NOx sensor – Part II: NOx pumping cell. **Sensors and Actuators B: Chemical**, v. 373,

p. 132658, 15 dez. 2022b.

WHO. **Air Quality Standards**. Disponível em: <https://www.who.int/tools/air-quality-standards>. Acesso em: 24 mar. 2023a.

WHO. **World Health Organization - global air quality guidelines**. [s.l: s.n.].

WHO. **Air Pollution. World Heal. Organ**. Disponível em: <https://www.who.int/health-topics/air-pollution#tab=tab_1>. Acesso em: 13 dez. 2022a.

WHO. **Ambient (outdoor) air pollution**. Disponível em: <https://www.who.int/news-room/fact-sheets/detail/ambient-(outdoor)-air-quality-and-health>. Acesso em: 2 abr. 2023b.

WHO, W. H. O. **Mercury and health**. Disponível em: <https://www.who.int/news-room/fact-sheets/detail/mercury-and-health>. Acesso em: 21 fev. 2024.

WHO, W. H. O. **Ten chemicals of public health concern**. Disponível em: <https://www.who.int/news-room/photo-story/photo-story-detail/10-chemicals-of-public-health-concern>. Acesso em: 21 fev. 2024.

WIEDINMYER, C. et al. The Fire INventory from NCAR (FINN): A high resolution global model to estimate the emissions from open burning. **Geoscientific Model Development**, v. 4, n. 3, p. 625–641, 2011.

WINDMÖLLER, C. C. et al. Use of a direct mercury analyzer® for mercury speciation in different matrices without sample preparation. **Analytical Methods**, v. 9, n. 14, p. 2159–2167, 6 abr. 2017.

WINGFORS, H. et al. Characterisation and determination of profiles of polycyclic aromatic hydrocarbons in a traffic tunnel in Gothenburg, Sweden. **Atmospheric Environment**, v. 35, n. 36, p. 6361–6369, 1 dez. 2001.

WOOD, E. C. et al. A case study of ozone production, nitrogen oxides, and the radical budget in Mexico City. **Atmospheric Chemistry and Physics**, v. 9, n. 7, p. 2499–2517, 2009.

WOOD, E. C. et al. Investigation of the correlation between odd oxygen and secondary organic aerosol in Mexico City and Houston. **Atmospheric Chemistry and Physics**, v. 10, n. 18, p. 8947–8968, 2010.

WU, Y. et al. The challenge to NOx emission control for heavy-duty diesel vehicles in China. **Atmospheric Chemistry and Physics**, v. 12, n.

19, p. 9365–9379, 2012.

XIAO, H. W. et al. Atmospheric aerosol compositions over the South China Sea: Temporal variability and source apportionment. **Atmospheric Chemistry and Physics**, v. 17, n. 4, p. 3199–3214, 2 mar. 2017.

XIU, G. L. et al. Characterization of size-fractionated particulate mercury in Shanghai ambient air. **Atmospheric Environment**, v. 39, n. 3, p. 419–427, jan. 2005.

XU, H. M. et al. Mercury stable isotope compositions of Chinese urban fine particulates in winter haze days: Implications for Hg sources and transformations. **Chemical Geology**, v. 504, p. 267–275, 20 jan. 2019.

XU, L. et al. Characterization of mercury in atmospheric particulate matter in the southeast coastal cities of China. **Atmospheric Pollution Research**, v. 4, n. 4, p. 454–461, 1 out. 2013.

XU, L.; PENNER, J. E. Global simulations of nitrate and ammonium aerosols and their radiative effects. **Atmospheric Chemistry and Physics**, v. 12, n. 20, p. 9479–9504, 2012.

XU, Q. P. et al. Particulate Size Distribution and Sources Evaluation of n-Alkanes during Long-Term Haze Episode around Chaohu Lake,

Eastern China. **Aerosol and Air Quality Research**, v. 17, n. 8, p. 1975–1984, 2017.

YADAV, S.; TANDON, A.; ATTRI, A. K. Monthly and Seasonal Variations in Aerosol Associated n-alkane Profiles in Relation to Meteorological Parameters in New Delhi, India. **Aerosol and Air Quality Research**, v. 13, n. 1, p. 287–300, 2013a.

YADAV, S.; TANDON, A.; ATTRI, A. K. Characterization of aerosol associated non-polar organic compounds using TD-GC-MS: A four year study from Delhi, India. **Journal of Hazardous Materials**, v. 252–253, p. 29–44, 15 maio 2013b.

YAMASOE, M. A. et al. Chemical composition of aerosol particles from direct emissions of vegetation fires in the Amazon Basin: water-soluble species and trace elements. **Atmospheric Environment**, v. 34, n. 10, p. 1641–1653, 1 jan. 2000.

YANG, J. et al. Characteristics of particulate-bound n-Alkanes indicating sources of PM2.5in Beijing, China. **Atmospheric Chemistry and Physics**, v. 23, n. 5, p. 3015–3029, 7 mar. 2023.

YANG, L. et al. Exposure to Atmospheric Particulate Matter-Bound Polycyclic Aromatic Hydrocarbons and Their Health Effects: A Review.

International Journal of Environmental Research and Public Health 2021, Vol. 18, Page 2177, v. 18, n. 4, p. 2177, 23 fev. 2021.

YANOWITZ, J. et al. Chassis dynamometer study of emissions from 21 in-use heavy-duty diesel vehicles. **Environmental Science and Technology**, v. 33, n. 2, p. 209–216, 15 jan. 1999.

YAO, E.; SONG, Y. Study on Eco-Route Planning Algorithm and Environmental Impact Assessment. **Journal of Intelligent Transportation Systems**, v. 17, n. 1, p. 42–53, 1 jan. 2013.

YAO, Z. et al. Comparison of NOx emissions from China III and China IV in-use diesel trucks based on on-road measurements. **Atmospheric Environment**, v. 123, p. 1–8, 1 dez. 2015.

ZHANG, F. W. et al. Distribution characteristics of particulate mercury in aerosol in coastal city]. **Huan Jing ke Xue= Huanjing Kexue**, v. 31, n. 10, p. 2273–2278, 1 out. 2010.

ZHANG, J. et al. The pollution characterization of black carbon aerosols in the southwest suburb of beijing from 2013 to 2019. **Atmospheric Pollution Research**, v. 14, n. 2, p. 101669, 1 fev. 2023.

ZHANG, L. et al. Size distribution of particulate polycyclic aromatic

hydrocarbons in fresh combustion smoke and ambient air: A review. **Journal of Environmental Sciences**, v. 88, p. 370–384, 1 fev. 2020.

ZHANG, M. et al. Determination and source identification of priority polycyclic aromatic hydrocarbons in PM2.5 in Taiyuan, China. **Atmospheric Research**, v. 178–179, p. 401–414, 1 set. 2016.

ZHANG, Q. et al. Influences of accumulated mileage and technological changes on emissions of regulated pollutants from gasoline passenger vehicles. **Journal of Environmental Sciences**, v. 71, p. 197–206, 1 set. 2018.

ZHANG, S. et al. Can Euro V heavy-duty diesel engines, diesel hybrid and alternative fuel technologies mitigate NOX emissions? New evidence from on-road tests of buses in China. **Applied Energy**, v. 132, p. 118–126, 1 nov. 2014.

ZHANG, X. et al. Black carbon aerosols in urban central China. **JQSRT**, v. 150, p. 3–11, 1 jan. 2015.

ZHANG, Y. et al. Probing into regional O3 and particulate matter pollution in the United States: 2. An examination of formation mechanisms through a process analysis technique and sensitivity study. **Journal of Geophysical Research: Atmospheres**, v. 114, n. D22, 27 nov. 2009.

ZHANG, Y. et al. Spatiotemporal variations and source on black carbon over Chongqing, China: Long-term changes and observational experiments. **Science of The Total Environment**, v. 946, p. 174127, 10 out. 2024.

ZHANG, Y.; TAO, S. Global atmospheric emission inventory of polycyclic aromatic hydrocarbons (PAHs) for 2004. **Atmospheric Environment**, v. 43, n. 4, p. 812–819, 1 fev. 2009.

ZHU, J. et al. Exposure to ambient black carbon and particulate matter during pregnancy in associations with risk of pre-eclampsia: A meta-analysis based on population-based studies. **Environmental Pollution**, v. 343, p. 123230, 15 fev. 2024.

ZHUANG, H. et al. Size distributions of particulate sulfate, nitrate, and ammonium at a coastal site in Hong Kong. **Atmospheric Environment**, v. 33, n. 6, p. 843–853, 1 mar. 1999.

ZIELINSKA, B. et al. Emission rates and comparative chemical composition from selected in-use diesel and gasoline-fueled vehicles. **Journal of the Air & Waste Management Association (1995)**, v. 54, n. 9, p. 1138–1150, 2004.

12. Appendix – Published papers

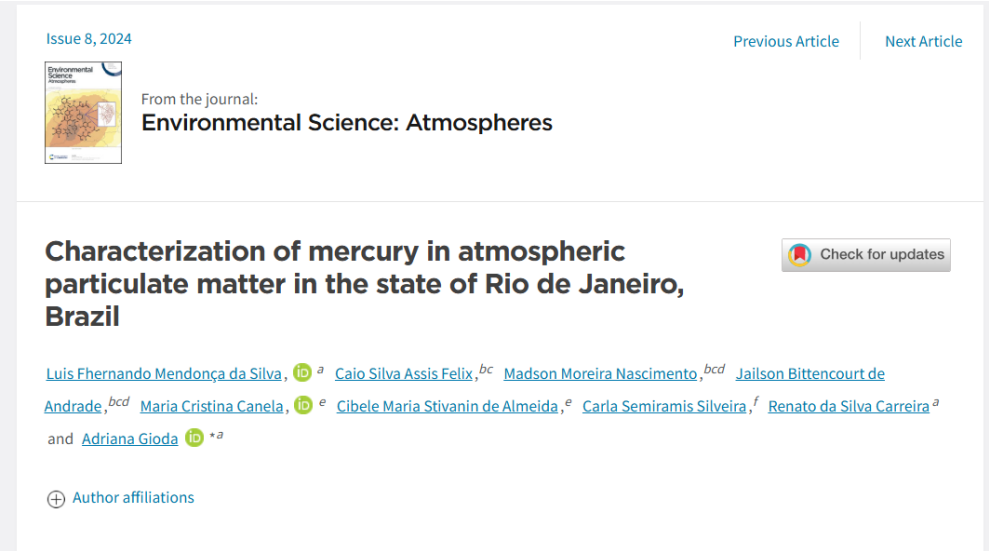

Issue 8, 2024

Previous Article | Next Article

From the journal:
Environmental Science: Atmospheres

Characterization of mercury in atmospheric particulate matter in the state of Rio de Janeiro, Brazil

Check for updates

Luis Fhernando Mendonça da Silva [a], Caio Silva Assis Felix [bc], Madson Moreira Nascimento [bcd], Jailson Bittencourt de Andrade [bcd], Maria Cristina Canela [e], Cibele Maria Stivanin de Almeida [e], Carla Semiramis Silveira [f], Renato da Silva Carreira [a] and Adriana Gioda [*a]

Author affiliations

Figure 12.1. SILVA, L. F. M. DA et al. Characterization of mercury in atmospheric particulate matter in the state of Rio de Janeiro, Brazil. Environmental Science: Atmospheres, v. 4, n. 8, p. 872–878, 8 ago. 2024.

Article

Journal of the Brazilian Chemical Society

https://dx.doi.org/10.21577/0103-5053.20230170

J. Braz. Chem. Soc. **2024**, *35*, 7, e-20230170, 1-7

Real-Time Monitoring of Nitrogen Oxides Emission Factors Using Sensors in the Exhaust Pipes of Heavy Vehicles in the Metropolitan Region of Rio de Janeiro

Luis F. M. Silva,[a] *Alex R. H. De La Cruz,*[a] *André H. M. Nunes*[b] *and Adriana Gioda*[*,a]

[a]*Departamento de Química, Pontifícia Universidade Católica do Rio de Janeiro (PUC-Rio), 22451-900 Rio de Janeiro-RJ, Brazil*

[b]*ZANE-Tecnologia da Informação LTDA, 22451-900 Rio de Janeiro-RJ, Brazil*

The Metropolitan Region of Rio de Janeiro is one of the most populous in Brazil, besides being one of the most important routes for marketing goods through heavy vehicles. This type of vehicle is the main source of nitrogen oxides (NOx) emission into the atmosphere. To assess NOx emission factors, this pilot study used sensors to monitor in real-time the exhaust of 9 trucks from July to September 2022. To the best of our knowledge, this is the first study carried out in the city using low-cost sensors. Although there is legislation to reduce the emission of pollutants from the vehicle fleet, the results showed that 7 out of 9 trucks, exceeded the stipulated limits, reaching 6 g kWh^{-1}. Furthermore, carrying out the maintenance of the engine of one of the vehicles decreased 60% of the NOx emission, even being an old vehicle. Thus, with this data, it was verified that the sensor performed excellently in monitoring NOx, demonstrating robust performance. This pilot study is part of a project that aims to make a long-term study of NOx emissions factors from heavy-duty diesel vehicles using sensors and other parameters.

Keywords: NOx, emission factor, remote sensing, Rio de Janeiro

Figure 12.2. SILVA, L. F. M. et al. Real-Time Monitoring of Nitrogen Oxides Emission Factors Using Sensors in the Exhaust Pipes of Heavy Vehicles in the Metropolitan Region of Rio de Janeiro. Article J. Braz. Chem. Soc, v. 35, p. 1–7, 2024.